MODELLING LOCAL SCOUR AROUND BRIDGE PIERS USING TELEMAC

by

ALAMGIR KABIR

A Dissertation Submitted in Partial Fulfilment of the Requirements for the Degree of Master of Science (MSc) in Engineering

Promoter: A/Professor N P Armitage

Department of Civil Engineering
University of Cape Town

November 2005

Declaration

I, the undersigned, hereby declare that this dissertation contains only my own original work, except where reference is made with acknowledgement to contributions from others. I also declare that this material has not been submitted for any purpose or examination to any other Department or University.

I empower the University of Cape Town (UCT) to reproduce for the purpose of research either the whole or any portion of the contents in any manner whatsoever.

Signature ..... Signed by candidate .....

Alamgir Kabir

Date 26.08.05 .....

Acknowledgements

I consider it a matter of great privilege and rare opportunity to work under the guidance of A/Professor Neil Armitage. His profound knowledge in fluid mechanics and keen interest in applying it to scour problems by means of Computational Fluid Dynamics (CFD) have inspired me during the last two years. Prof. Armitage read this thesis thoroughly and made many helpful comments and constructive criticisms. I am extremely grateful to him for his continuous support, encouragement and professional advice during all phases of my study. I also would like to thank Prof. Paul Samuels, HR Wallingford, UK, for his constructive criticism and suggestions during examining this thesis.

I would like to thank the Department of Civil Engineering, UCT and the Water Research Commission (WRC), South Africa for their financial support. More especially my deepest gratitude is to the peoples of Bangladesh and South Africa for shouldering almost the entire cost of my education.

I would like to thank Professor N Rajaratnam, University of Alberta, Canada for physical modelling data. Thanks to Pierre Lang, SOGREAH Consultants, France, for his valuable advice and on line technical supports on TELEMAC. Also thanks to Florence and Rene for their technical support at the beginning of TELEMAC study.

Thanks to my fellow colleagues Margie, Benjamin, Case and Avinash for their help during my study at UCT. I would like to thank Banda for his valuable advice, company and help in exploring all the nice things in Cape Town. I am also grateful to Ras and Obey for accompanying me.

The support and encouragement of my family members, friends and Halcrow work colleagues/supervisors are gratefully acknowledged. In particular, I like to thank my mother and father for all nice things they have done for me.

My most special thanks are to my beloved wife Munny, who took entire responsibilities of our new born wonderful daughter Moumi on her shoulder during my study at UCT. Her encouragement and support made me possible to cope with all the ups and downs that came with my graduate studies abroad leaving them in Bangladesh.

Abstract

Scour at bridge crossings is a major cause of bridge failure. There are several different types of scour such as general scour, constriction scour and local scour. One of the most serious types is local scour which occurs as a result of vortex formation around bridge piers and abutments (Hoffmans & Verheij, 1997; Raudkivi, 1998; Melville & Coleman, 2000; Richardson & Davis, 2001; Armitage & McGahey, 2003). Local scour is also one of the most difficult to predict accurately. If not adequately designed for, local scour of a riverbed at a bridge pier may become deep enough to undermine the pier foundation and eventually cause the bridge to collapse.

Complete protection against scour is expensive and therefore not a favourable design option. It is generally cheaper to ensure that the foundation lies below the maximum expected scour depth. Traditionally, the maximum scour depth is predicted from empirical equations derived from simple laboratory tests without much regard for local conditions. Alternatively, small-scale hydraulic models, which are laborious and time intensive, are widely used.

In view of the above, increasing attention is being paid to the use of Computational Fluid Dynamics (CFD) based modelling for the prediction of local scour and its opposite, local deposition. The ever-improving capabilities of computers and the increasing availability of powerful and flexible CFD codes have further assisted in this process. This study is a contribution in this direction.

Local scour and deposition form part of the field of sediment transport, which in turn, is part of the field of fluid mechanics. The presence of bridge piers in an alluvial channel alters the natural flow patterns causing channel constriction and steep pressure and velocity gradients, which increases the bed shear stresses and thus sediment transport capability at the channel bed causing bed erosion and deposition (called evolution).

A numerical model is a powerful tool for the determination of the flow characteristics adjacent to the bridge piers and hence the bed evolutions and resulting local scour. In this study, the commercial CFD solver TELEMAC V5.5, which is based on the Finite Element Method, was adapted to simulate the flow conditions in the vicinity of a circular pier and predict the movement of the bed.

The hydrodynamic of the flow field was modelled in two-dimensional (2D) space (TELEMAC-2D) as well as in three-dimensional (3D) space (TELEMAC-3D). The 2D flow field was modelled by solving the shallow water Saint-Venant equations (TELEMAC-2D, 2002) assuming a hydrostatic pressure distribution. These equations were solved by the Fractional Step Method in conjunction with the Method of Characteristics for the velocity components (u and v), however, a conservative scheme with SUPG (Streamline Upwind Petrov Galerkin) was used for the advection of water depth. The 3D flow field was modelled by solving the Navier-Stokes equations (TELEMAC-3D, 1998), approximating the non-hydrostatic pressure distribution using the Fraction Step Method to simulate the 3D flow fields. The two-equation

Standard k-ε model was used for the prediction of the turbulent shear stresses and viscosities with reasonable accuracy for both the 2D and 3D flow fields. These equations were also solved by the Fractional Step Method in conjunction with the Method of Characteristics. These 2D or 3D models were coupled with a sediment transport model SISYPHE to solve the bed evolution equation (SISYPHE, 2004). The bed evolution equation was solved in conjunction with four different sediment transport formulae. Shields incipient motion criterion was used for the prediction of the initiation of sediment particle motion.

One problem, however, is that there is not even general agreement on the best sediment transport formula. Most of sediment transport formulae are based in part on classical sediment transport theory and in part on empirical analysis in laboratory studies. This study selected the well-known sediment transport formulae for bed-load and total load suggested by Meyer-Peter and Muller (1948), Einstein & Brown (1950), Engelund & Hansen (1967) and Van Rijn (1984a). The equilibrium condition, which assumes that erosion flux is equal to deposition flux, was used for bed-load. The coupling between bed-load and suspended load was taken into account by solving the advection-diffusion equation, where sediment fluxes were treated according to Celik & Rodi (1988). The bed roughness was implemented by means of the Chezy coefficient. The bed evolution equation was approximated by the predictor-corrector concepts during solution by GMRES (Generalised Minimum RESidual).

The numerical model was used to simulate the movement of uniform fine non-cohesive sand beds in presence of circular piers and was compared to the physical model data measured by Ahmed (1995). The scour was investigated for clear-water conditions. The numerical model predicted different bed evolution for the different sediment transport formulae. In general, scour initiation took place at the side of the pier, where flow is deflected and accelerated. This agreed with literature (e.g. Ahmed, 1995). The scour hole then deepened at the same location and expanded towards channel boundary. The model did not, however, predict the scour all around the piers as reported by Ahmed (1995). Solution of the bed evolution equation using the Van Rijn (1998a) sediment transport formula predicted the maximum scour depth in the case of both 2D and 3D flow models. This study was, however, not able to identify a preferred formula for the prediction of local scour.

Despite some limitations imposed by TELEMAC V5.5, the results were sufficiently encouraging suggesting that there is potential for the use of numerical modelling to predict local scour given improved software.

Table of contents

4 Development of the local scour model

List of Figures

List of Tables

List of Symbols

Tables	Description	Unit
a	Interface between suspended-load layer and bed-load layer	m
a_1, a_2, a_3	Distance used by Van Rijn (1993) to describe force on particles	m
a_c	MATISSE generated coefficients used to establish velocity vector related to smooth wall	
a_p	Projected area where lift and drag force acts	m^2
A	Compact mass matrix to form linear equations using TELEMAC code	
Al	Parameter describing alignment	
b	Width of pier in general	m
b_1, b_2, b_3	Distance used by Van Rijn (1993) to describe force on particles	m
b_p	Projected frontal width of pier perpendicular to flow	m
B	Coefficient matrix to form linear equations using TELEMAC code	
$\overline{B}_x$, $\overline{B}_y$	Vertical averaged buoyancy terms used to calculate free surface	
c	Specific heat	J/KgK
c_f	Quadratic friction coefficient	
c_k	Constant used to determine P_{kv} for k-ε turbulence model	
c_ε	Constant used to determine $P_{\varepsilon v}$ for k-ε turbulence model	
C	Depth-averaged sediment concentration	Kg/m^3 or m^3/m^3
C'_h	Grain related Chezy's coefficient	$m^{1/2}/s$
$C_{1\varepsilon}$	Constant in transport equations for k-ε turbulence model	
$C_{2\varepsilon}$	Constant in transport equations for k-ε turbulence model	
$C_{3\varepsilon}$	Constant in transport equations for k-ε turbulence model	
C_D	Drag coefficient	
C_{eq}	Near bed concentration	
C_h	Chezy's coefficient	$m^{1/2}/s$
C_k	Universal Kolmogorov constant	
C_L	Lift force	N
C_p	Pressure coefficient	
C_s	Volumetric sediment concentration	m^3/m^3
C_μ	Constant in transport equations for k-ε turbulence model	

d	Diameter of a sediment particle	mm
d_{50}	Median size of the sediment	mm
d_i	Median diameter of any particle size fraction	mm
$\overline{d}$	Mean diameter of sediment particle	mm
d_*	Dimensionless particle diameter	
D	Circular pier diameter	m
D_d	Deposition flux	
e	Magnitude of a vector perpendicular to the wall	
E	Specific energy	J/kg
$E(\kappa)$	Energy spectrum function	
E_e	Erosion flux	
E_{ij}	Deformation tensor	
f	"a function of" read in an equation	
f	Symbol describing unknown variables i.e. u, v, h etc. in TELEMAC system	
f^a	Unknown variables evolved during advection	
f^n	Unknown variables at time $n\Delta t$	
f^{n+1}	Unknown variables at time $(n+1)\Delta t$	
f_r	Frequency of vortex shedding	Hz
f^d	Unknown variables evolved during diffusion	
$\tilde{f}$	Intermediate value of f within same time step during advection	
F_d	Densimetric Froude number	
F_{di}	Inception densimetric Froude number	
F_D	Drag force	N
F_G	Force due to gravity	N
F_L	Lift force	N
F_{Mx}	Source term in Saint Venant equations in x-direction	
F_{My}	Source term in Saint Venant equations in y-direction	
F_R	Resisting force due to particle movement	N
$Fr_b = U/\sqrt{gD}$	Circular pier Froude number	
g	Acceleration of gravity	m/s^2
$\mathbf{g}$	Gravity vector	m/s^2
G	Parameter describing the effect of lateral distribution of flow in approach channel and cross-sectional shape of the approach channel	
h	Depth of water used during simulation	m

h_{prop}	Depth at propagation within same time step	m
h^n *and* h^{n+1}	Depth at time $n\Delta t$ and $(n+1)\Delta t$ respectively	m
$\tilde{h}$	Depth during advection step	m
i	Internal energy of a fluid particle	J
i	Unit vector along x-direction	
I, I_1, I_2	Einstein integral	
j	Unit vector along y-direction	
k	Turbulent kinetic energy	m^2/s^2
k_δ	Kinetic energy at a distance δ from the boundary	m^2/s^2
k^n *and* k^{n+1}	Turbulent kinetic energy at time $n\Delta t$ and $(n+1)\Delta t$ respectively	m^2/s^2
k_s	Roughness height	m
k_{sf}	Form roughness generated by pressure force	m
k_{sg}	Grain roughness generated by skin friction	m
k_T	Coefficient of thermal conductivity	W/m/K
$\tilde{k}$	Turbulent kinetic energy during advection step	m^2/s^2
k	Unit vector along z-direction	
ℓ	Turbulent length scale	μm
L_{ahm}	Length scale for Ahmed (1995) domain	m
L_{tel}	Length scale for TELEMAC domain	m
m	Co-coordinate in the current direction	
M	Mass matrix associated to solve bed evolution equation	
$Mn = u_*/v_{ss}$	Movability number	
Mn_c	Critical Movability Number for incipient sediment motion	
$Mn_{c(\beta,\gamma)}$	Critical Movability Number on a sloped channel bed	
M_o	Overturning moment due to F_D and F_R	N-m
M_R	Resisting moment due to F_L and F_G	N-m
n	Number of time step	
n_p	Bed porosity	%
N_p	Total number of prism	
p	Pressure	N/m^2
p_0	Upstream undisturbed static pressure	N/m^2
p_d	Dynamic pressure	N/m^2
p_h	Hydrostatic pressure	N/m^2
p_i	Percentage of mass of particle size d_i	%
p_x	Static pressure at position x along flow direction	N/m^2

P	Production term due to horizontal mean velocity gradient for k-ε turbulence model	
P_{kv}	Production term due to vertical shear during turbulent kinetic energy for k-ε turbulence model	
$P_{\varepsilon v}$	Production term due to vertical shear during energy dissipation for k-ε turbulence model	
$\mathbf{q}$	Heat flux vector	J/s
q_b	Volumetric bed-load transport	m^2/s
q_t	Volumetric total sediment load transport	m^2/s
q_x	Component of the heat flux vector along x-direction	J
q_y	Component of the heat flux vector along y-direction	J
q_z	Component of the heat flux vector along z-direction	J
Q	Prescribed flow rate	m^3/s
Q_{ahm}	Flow rate given in Ahmed (1995)	m^3/s
$\mathbf{Q_s}$	Sediment transport vector	m^2/s
$\mathbf{Q}_s^n$	Sediment vector at time $n\Delta t$	m^2/s
$\mathbf{Q}_s^{n+\theta}$	Sediment vector at correction step	m^2/s
Q_{ss}	Volumetric suspended sediment load	m^2/s
Q_{tel}	Equivalent flow rate by dimensional analysis	m^3/s
r	Co-ordinate along the axis perpendicular to the flow (transverse or vertical)	
$Re_* = u_* d/\nu$	Particle Reynolds number	
R_{eD}	Pier Reynolds number	
$R_{es} = (u_* k_s)/\nu$	Roughness Reynolds number	
R_h	Hydraulic radius	m
R_{ij}	Reynolds tensor	
R_p	Rouse number	
$s = \rho_s/\rho$	Specific gravity of sediment particle	
S_0	Bed slope	m/m
SF	Multiplying factor applied to the solid transport rate intensity to take account the bed slope	
Sh	Parameter describing shape	
S_i	Source term in energy equations	
$\mathbf{S_M}$	Source term in fluid flow equation	Kg/ms
S_{Mx}, S_{My}, S_{Mz}	Components of the source term along x-, y- and z-directions respectively	Kg/ms

St	Strouhal number	
$\overline{S}_x$, $\overline{S}_y$	Vertical averaged source terms used to calculate free surface	
S_φ	Source term in general transport equation	
t	Time	s
t^*	Dimensionless equilibrium time scale	
t^*_{max}	Maximum dimensionless equilibrium time scale	
t_e	Time required developing equilibrium scour depth	s
T	Temperature	^{0}C/K
T_*	Dimensionless shear stress parameter	
u	Component of velocity along x-direction	m/s
$\mathbf{u}$	Velocity vector	m/s
$\overline{\mathbf{u}}$	Velocity vector similar to $\mathbf{u}$, can be calculated either TELEMAC-2D or TELEMAC-3D	m/s
$\mathbf{u}'$	Fluctuating velocity vector	m/s
u_0	Effective particle velocity near bed	m/s
u_d	Velocity at distance d from channel bed	m/s
u^n *and* u^{n+1}	Velocity along x-direction at time $n\Delta t$ and $(n+1)\Delta t$ respectively	m/s
u'	Component of fluctuating velocity vector along x-direction	m/s
u'_i	Compact notation of u', v' and w'	m/s
$\tilde{u}$	Velocity along x-direction during advection step	m/s
$u_* = \sqrt{\tau_0/\rho}$	Shear velocity	m/s
$\tilde{u}_*$	Bottom friction velocity near wall	m/s
$\sqrt{\overline{u'^2}}$	root-mean-square of the component of $\mathbf{u}'$	
U	Approach mean velocity in x-direction	m/s
U_{ahm}	Undisturbed velocity used by Ahmed (1995)	m/s
U_c	Critical approach velocity for initiation of bed sediment	m/s
U_{tel}	Equivalent undisturbed velocity by dimensional analysis	m/s
$\mathbf{U}$	Mean velocity vector	m/s
v	Component of velocity along y-direction	m/s
v^n *and* v^{n+1}	Velocity along y-direction at time $n\Delta t$ and $(n+1)\Delta t$ respectively	m/s
v_{ss}	Settling velocity of a particle	m/s
v'	Component of fluctuating velocity vector along y-direction	m/s
$\tilde{v}$	Velocity along y-direction during advection step	m/s
ϑ	Turbulent velocity scale	μm/s
V	Component of mean velocity vector at y-direction	m/s
w	Component of velocity along z-direction	m/s

w_w	Moisture content in natural river bed	%
w'	Component of fluctuating velocity vector along z-direction	m/s
$\tilde{w}$	Velocity along z-direction during advection step	m/s
W	Component of mean velocity vector at z-direction	m/s
W_d	The work done by the fluid on moving the particles over a length equal to the bed form length	J/s/m
W_r	The work required elevating the sediment load over a height equal to the bed-form height	J/s/m
X	Unknown vector matrix to form linear equations using TELEMAC code	
X_f	Length scale factor for dimensional analysis	
XKV	Porosity function	
XY	Plane formed by X and Y axis in a Cartesian system	
y	Depth of flow in general	m
y_s	Scour depth	m
y_{se}	Equilibrium scour depth	m
y^+	Dimensionless wall distance	
YZ	Plane formed by Y and Z axis in a Cartesian system	
z	Height above arbitrary datum	m
z	Vertical elevation of domain in TELEMAC system	m
$z^*(I_p)$	Elevation factor for TELEMAC-3D domain	
Z	Free surface elevation	m
Z_f	Bottom elevation	m
$\tilde{Z}_f^{n+1}$	Bed elevation during prediction step	m
α	Angle between leading velocity direction passes through pier and line perpendicular to the surface of pier	Degree
α_a	Direction of solid transport	
α_1	Emperical coefficient used by Van Rijn (1993) for sediment movement	
β	Slope correction factor	
Γ	Diffusion coefficient	
δ	Distance from the boundary to calculate the dissipation k_δ or ε_δ	m
δ_a	Direction of the bottom shear stress	
δ_{ij}	Coronecker delta	
δx	Length of infinitesimal fluid particle along x-direction	μm
δy	Length of infinitesimal fluid particle along y-direction	μm
δz	Length of infinitesimal fluid particle along z-direction	μm

$\Delta=(\rho_s-\rho)/\rho$	Relative submerged density	
$\Delta\rho$	Mass sediment concentration	Kg/m^3
Δt	Time step	s
ε	Energy dissipation	m^2/s^3
$\tilde{\varepsilon}$	Energy dissipation during advection step	m^2/s^3
ε_δ	Energy dissipation at a distance δ from the boundary	m^2/s^3
ε^n *and* ε^{n+1}	Energy dissipation at time $n\Delta t$ and $(n+1)\Delta t$ respectively	m^2/s^3
ε_s	Sediment diffusivity coefficient	
$\varepsilon_{(t)}$	Average turbulent kinematic viscosity	m^2/s
θ	Shield's parameter	
θ_c	Critical Shield's parameter	
θ_d	Implicitation coefficient for diffusion of velocity	
θ_f	Angle between flow and pier length	Degree
θ_h	Implicitation coefficient for depth	
θ_t	Time-related coefficient to express unsteady problems	
θ_u	Implicitation coefficient for velocities	
λ	Wave number (inverse of turbulent length scale)	
κ	Von Karman constant	
μ	Dynamic viscosity due to viscous flow	Ns/m^2
μ_b	Efficiency factor used in Meyer-Peter & Muller (1948) bed load transport formula	
μ_t	Sum of laminar and turbulent viscosity	Ns/m^2
$\mu_{xy(t)}$	Dynamic viscosity due to turbulent flow	Ns/m^2
$\nu=\mu/\rho$	Kinematic viscosity	m^2/s
ν_t	Turbulent kinematic viscosity	m^2/s
η	Kolmogorov length scale	µm
ρ	Density of fluid	Kg/m^3
ρ_s	Density of the sediment	Kg/m^3
σ	Standard deviation	
σ_g	Geometric standard deviation	
τ_0	Bed shear stress	N/m^2
τ_c	Critical bed shear stress	N/m^2
τ_{ji}	Shear stress component acts in the i-direction on a surface with a normal in the j-direction	N/m^2
φ	Any property of the fluid particle	
Φ	Dissipation function	W/m^3

Φ_b	Dimensionless bed sediment load function	
Φ_t	Dimensionless total sediment load function	
Ψ	Function evolved during discretisation in space	
Ψ_i	Basis function evolved during space discretisation to solve bed-evolution equation	
$\omega=\varepsilon/k$	Turbulence frequency	s^{-1}
Ω	Scour potential	
∇	Grad vector operator	
σ_k	Turbulent Prandtl Number for k	
σ_ε	Turbulent Prandtl Number for ε	
ψ	Slope correction factor for Mn_c	

Abbreviations

Abbreviation	Description
1D	One-dimensional
2D	Two-dimensional
3D	Three-dimensional
ASM	Average Stress Model
CFD	Computational Fluid Dynamics
CGSTAB	Stabilised Conjugate Gradient
DNS	Direct Numerical Simulation
DOS	Disk Operating System
GMRES	Generalised Minimum RESidual
HASP	Hardware against Software Piracy
k-ε	A two-equation turbulence model
k-ω	A two-equation turbulence model
LES	Large Eddy Simulation turbulence model
MATISSE	A Pre-processor Module in the TELEMAC system
MS	Micro Soft
MURD	Multidimensional Upwind Residual Distribution
PC	Personal Computer
PSI	Parameter Space Investigation (A numerical scheme)
RAM	Random Access Memory
RANS	Reynolds averaged Navier-Stokes equations
RNG	Re-normalised Group turbulence model
RSM	Reynolds Stress Model
RUBENS	A Post-processor Module in the TELEMAC system
SISYPHE	Sediment transport module in the TELEMAC system
SUPG	Streamline Upwind Petrov Galarkin
TELEMAC	A commercial open channel CFD software
UCT	University of Cape Town
VLES	Very Large Eddy Simulation turbulence model

Chapter 1
Introduction

1.1 The scour problem

Scour at bridge crossings is a major cause of bridge failure. There are several different types of scour such as general scour, constriction scour and local scour. One of the most serious types is local scour which occurs as a result of vortex formation around bridge piers and abutments (Hoffmans & Verheij, 1997; Raudkivi, 1998; Melville & Coleman, 2000; Richardson & Davis, 2001; Armitage & McGahey, 2003). Local scour is also one of the most difficult to predict accurately. If not adequately designed for, local scour of a riverbed at a bridge pier may become deep enough to undermine the pier foundation and eventually cause the bridge to collapse.

According to Chang (1973), 25% of pier failures and 72% of abutment damage of 383 bridge failures in USA were the direct result of local scour. Brice & Blodgett (1978) estimated the damage to bridges in USA of US$100 million per event during the major floods in 1964 and 1972. Shirhole & Holt (1991) reported that 60% of 823 bridge failures in USA since 1950 were associated with the effects of flow hydraulics including both channel-bed scour around bridge foundations and channel instability, which in turn averaged out at 50 to 60 bridges failures per year.

According to Mackey (1990), the expenditure on scour-related bridge damage in New Zealand amounted to about NZ$18 million per year, with more than 70% of this expenditure being related to bridge repairs rather than preventive maintenance or construction of new (replacement) bridges. Melville & Coleman (2000) reported that at least one serious bridge failure each year (on average) can be attributed to scour around the bridge foundations in New Zealand. They describe 31 individual case studies of major bridge failures in New Zealand since 1980.

According to Armitage et al (2005) local scour was observed at 60% of 105 major bridges identified as having suffered scour damage in South Africa. Routine scour damage to provincially-maintained road bridges over rivers in South Africa amounts to approximately R25 million per annum. This cost may however be increased well above R30 million taking into account the extreme flood events. Statistics from other countries are limited but probably show similar trends.

Despite significant concern and ongoing research, bridge failure due to scour is still common. It is believed that this may partially a consequence of inadequacies in both the design criteria adopted for bridges and also the present state of knowledge about some aspects of bridge hydraulics and scouring. This thesis is concerned with the numerical prediction of local scour around bridge piers.

1.2 The objectives of this study

Most studies in the past were concerned with the prediction of the the maximum depth of scour for design purpose using laboratory flume tests (physical modelling). Some key studies are those by Dey et al. (1995), Melville & Raudkivi (1996), Laursen & Johnson (1997), Melville (1997), Ahmed & Rajaratnam (1998), Ettema et al. (1998), Cardoso & Bettess (1999), Barkdoll (2000), Johnson & Hey (2001), Oliveto & Willi (2002), Coleman et al. (2003), Malavasi & Guadagnini (2003) and Chang et al. (2004). Physical modelling is expensive and time intensive, thus many researchers have attempted to use numerical methods to model local scour e.g., Olsen & Melaaen (1993), Kogaki et al. (1997), Olsen & Kjellesvig (1998), Richardson & Panchang (1998), Biglari & Strum (1998), Yen et al. (2001), Kothyari & Raju (2001), Ali & Karim (2002) Chen et al. (2002), Armitage & McGahey (2003), Chrisohoides et al. (2003), Armitage & McGahey (2004), Kimura et al. (2004), Salaheldin et al. (2004) and Yanmaz (2004). Despite such effort, it has become evident that there are no simple design methodologies for the prediction of local scour around bridge piers. Almost all of these numerical studies had limitations.

Numerical modelling can be treated as an approximate tool to deal with local scour around pier. The complex 3D flow fields around piers make it difficult to formulate a numerical model that will predict local scour with the desired accuracy. Moreover, numerical models require very high speed computers to solve the complex set of equations in a suitably discretised computational domain. The 3D numerical computations are more complex and computationally expensive, so for this reason the 2D analyses are often preferred. There is much commercial computer software available for analysing local scour using the 2D or 3D Computational Fluid Dynamics (CFD) codes e.g. the TELEMAC system.

Local scour around piers is a 3D problem, since the scour directly in front of a circular pier is due to vertical downflow. The point of maximum scour is often initiated and deepened at the side of the pier due to increase and change of direction in the flow velocity in the presence of the pier. As design is often concerned solely with the maximum scour depth, a 2D analysis can be used for the prediction of local scour around circular piers.

The principal objective of this study was to explore the capability of the commercial computer code TELEMAC V5.5 for the prediction of local scour around bridge piers. There are two main elements:

1. A detailed literature review on numerical modelling in order to understand the hydrodynamic and sediment transport phenomena in general and their particular application in the TELEMAC system.

2. Simulation of uniform sand bed evolutions i.e. local scour around circular piers in conjunction with existing sediment transport formulae coupling with the 2D or 3D hydrodynamic modelling using TELEMAC V5.5.

1.3 The structure of this thesis

This report is broken into seven chapters, which deal with the following aspects.

Chapter 1 presents a general discussion on the scour problem and the objectives of this thesis.

Chapter 2 reviews the related background literature, which is important for understanding local scour and its numerical modelling. Local scour is the result of the complex interactions between the local flow patterns resulting from the presence of e.g. a pier, and sediment movement on the river bed. Numerical modelling of local scour is thus complex. This chapter discusses three main topics; local scour, sediment transport and their numerical modelling. The chapter commences with the underlying theoretical concepts of local scour around bridge piers. After this, a brief overview on sediment transports and their associated theories is given. Since this study is concerned with numerical modelling, the mathematical descriptions of the flow fields and their modelling have also been presented. This chapter ends with a summary of some of the past numerical studies related to the modelling local scour around piers.

This study was carried out using the CFD code, TELEMAC V5.5, supplied by SOGREAH Consultants, France. **Chapter 3** thus presents different components of the TELEMAC V5.5 and its logical development. This required, inter alia, describing the solution domain, modelling the boundary conditions, choosing the turbulence model, choosing the numerical schemes and solvers and choosing the coupling between hydrodynamic and sediment transport systems.

Chapter 4 focuses on how the local scour model was developed using and manipulating the TELEMAC V5.5 codes. The model was compared with physical modelling data. The chapter starts with the development of the solution domain, followed by the development of 2D or 3D flow fields which were coupled with sediment transport formula to determine the bed evolution. This chapter is closely linked with **Chapter 2** and **Chapter 3**.

Chapter 5 presents the simulation outputs and their analysis. **Chapter 6** presents the conclusions drawn from this study. Recommendations for further studies are given in **Chapter 7.**

Chapter 2
Literature review

2.1 Introduction

This study is concerned with the prediction of local scour around a circular pier using TELEMAC V5.5 mathematical modelling system. TELEMAC V5.5 and the overall model development using it will be presented in Chapter 3 and Chapter 4.

This chapter presents a review of the background conceptual literature, which is important for the understanding of local scour and its modelling. Local scour is the interaction of the complex local flow patterns due to the presence of a pier with the river bed, which in turn initiates sediment movement causing local scour. The chapter thus starts with a description of the local scour around a circular pier followed by a description of fluvial sediment transport. This chapter also presents the mathematical descriptions of the flow in the channels, which are very essential for the modelling of the scouring process. The chapter ends with a presentation of some of the past efforts to model local scour numerically around piers.

2.2 An overview of local scour around piers

The scour around circular pier can be one of two types; general scour and local scour (Hoffmans & Verheij, 1997; Raudkivi, 1998; Melville & Coleman, 2000; Richardson & Davis, 2001; Armitage & McGahey, 2003). General scour happens irrespective of the existence of pier. The presence of bridge piers however alters the local flow and causes local scour.

The following section provides the different engineering aspects related to local scour around a circular pier. The discussions are mostly limited to uniform sediments under clear-water scour conditions, which is the main interest in this study.

2.2.1 Classification of local scour

Local scour may be classified into two categories; clear-water scour and live-bed scour (Hoffmans & Verheij, 1997; Raudkivi, 1998; Melville & Coleman, 2000; Richardson & Davis, 2001; Armitage & McGahey, 2003).

"Clear-water scour" occurs in the absence of general scour. In other words, the flow conditions in the general vicinity of the structure (but not close to the structure) are below the critical conditions for incipient motion. All sediment movement thus occurs directly as a result of the altered flow conditions caused by the presence of the structure.

"Live-bed scour" occurs in the presence of general scour and is superimposed on it. In this case, the flow conditions in the general vicinity of the structure are above the critical conditions for incipient motion. Whilst clear-water scour can theoretically reach static equilibrium, live-bed scour can only reach dynamic equilibrium when the rate of sediment entering the scour

hole equals the rate of sediment leaving it. A further complication is that riverbeds are not generally flat, but usually consist of bed-forms (Van Rijn, 1993; Yang, 1996; Raudkivi, 1998), such as ripples or dunes, that migrate downstream as sediment is eroded from the upstream face and deposited on the downstream face.

A typical plot showing the scour depth versus time for the two types of scour is given in Figure 2-1. It will be noted that the scour hole develops much more rapidly in the case of live-bed scour, but the gross dimensions of the scour hole never reach equilibrium as they are affected by the passage of bed-forms (CUR, 2000; Melville & Coleman, 2000).

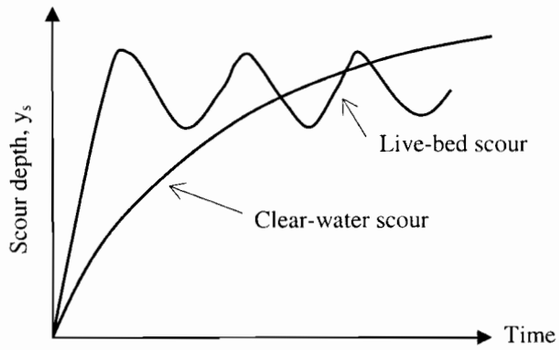

Figure 2-1: Scour depth as a function of time
(After CUR, 2000)

This study is exclusively based on clear-water scour. Not only is it easier to analyse than live-bed scour, it also results in the larger scour hole, which is particularly important from the perspective of engineering design.

2.2.2 Flow field around a circular pier

Hjorth (1975, 1977), Melville (1975) and Dargahi (1990) describe the complex flow field around a circular pier embedded vertically in an erodible bed. Dey et al (1992) further described the complex velocity distributions, which are modified by the development of the scour hole under a clear-water condition. Armitage and McGahey (2003) comprehensively summarised the works of different researchers relating to the flow fields around piers.

2.2.2.1 The flow patterns

Many researchers (e.g. Melville, 1975; Raudkivi & Sutherland, 1981; Dargahi, 1990; Ahmed & Rajaratnam, 1998; Melville & Coleman, 2000; Richardson & Davis, 2001) describe the scouring process around circular piers and caissons. Melville (1975) and Hjorth (1975) outlined the flow pattern in the scour hole development during this process. Raudkivi & Sutherland (1981) and Dargahi (1990) independently verified previous research on flow patterns including Melville (1975) and Hjorth (1975). Ahmed (1995) presented a comprehensive study on the flow patterns around circular pier under different hydraulic regimes. According to Raudkivi (1998) and Melville & Coleman (2000), the local flow field initiates and controls the progress

of local scour pattern due to presence circular pier, which in turn modifies the flow field by continuous dynamic interactions among them. Figure 2-2 illustrates the flow patterns with a scour hole around a circular pier.

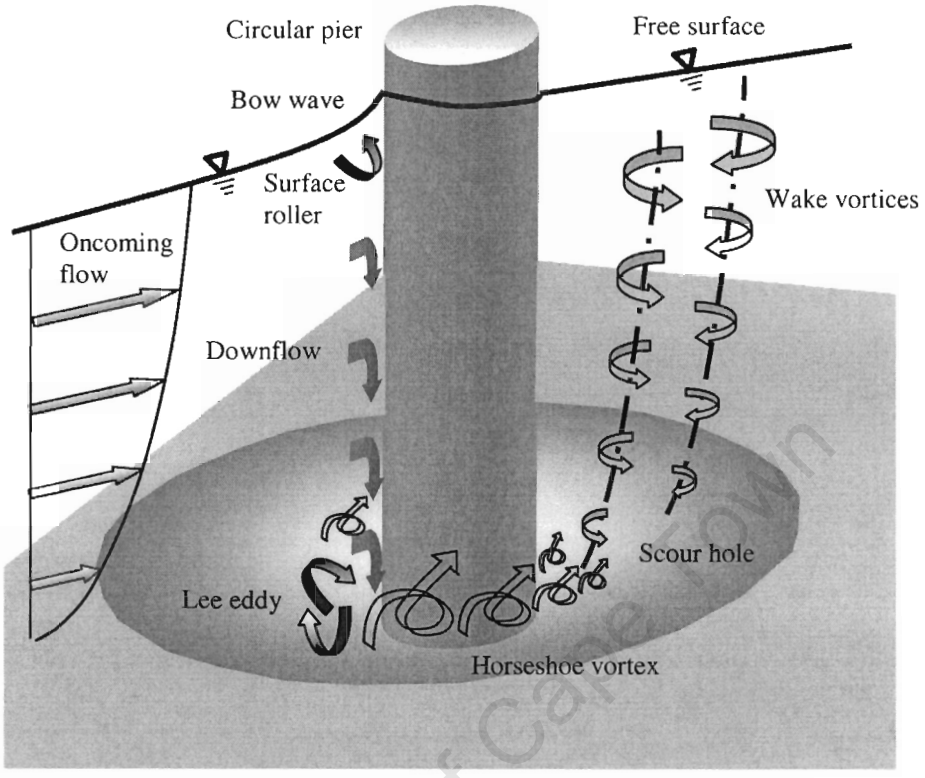

Figure 2-2: Flow and scour pattern around circular pier

Figure 2-2 clearly shows five distinct flow patterns around circular pier; bow wave, downflow, lee eddy, horseshoe vortex and wake. The downflow is immediately upstream of the pier, the horseshoe vortex and lee eddy are at base of the pier, the surface roller is upstream of the pier close to free surface and the wake vortices are downstream of the pier. Each of these flows has significant role in the local scouring process.

2.2.2.2 The bow wave

The presence of the pier blocks a significant part of the flow area and hence the flow decelerates as it approaches the pier. As a consequence, at some distance upstream of the pier, the approach flow separates and spreads around the pier sides. Near the free surface in front of the pier, upward flow forms a circulation called "surface roller" (Melville & Coleman, 2000; Armitage & McGahey, 2003). This surface roller (or bow wave) increases the flow depth at the leading edge of the pier. The bow wave plays a significant role in scouring process during shallow water flows by interfering with the horseshoe vortices.

2.2.2.3 The downflow

The velocity deceleration of the flow on the upstream side of the pier raises the pressure on the leading face, which often termed the "stagnation pressure". This pressure decreases with the square of the velocity of the oncoming flow i.e. it decreases from top to bottom. A "downflow" is thus developed due to the downward negative stagnation pressure gradient of the non-uniform approach flow adjacent to the upstream face of the pier. This downflow impinges on the channel bed like a water jet and is primarily responsible for the initiation of scour at the upstream face of the pier.

The maximum velocity of the downflow in vertical section, according to experimental data by Ettema (1980) and Raudkivi (1986), is situated between 0.05 and 0.02 times the pier breadth, b_p, upstream of the pier, being closer to the pier near the bed than at the surface. The velocity of the downflow also increases in magnitude towards the bed in the vertical section. If no scour is present, the maximum velocity is approximately 40% of the average oncoming velocity, U. This velocity increases to approximately $0.8U$ as the scour depth increases past $2b_p$ (Breusers & Raudkivi, 1991; Raudkivi, 1998).

This relatively high velocity flow, directed at the base of the pier, acts as a sort of water jet that helps to initiate and maintain the scouring process (Armitage & McGahey, 2003). The increased pressure on the leading face of the pier also helps to provide the necessary force for the acceleration of the flow around the sides.

2.2.2.4 The horseshoe vortex

The interaction between the downward flow and the horizontal boundary layer separation close to the riverbed results in the formation of a vortex system (French, 1994; Armitage & McGahey, 2003). The two ends of this vortex system are swept downstream by the flow as they wrap around the pier in the shape of a horseshoe in plan view and hence it is popularly known as the "horseshoe vortex". Once a scour hole begins to form, flow separation at the upstream rim results in the formation of a lee eddy (similar to the ground roller downstream of a dune crest), which rotates in the opposite direction to the surface roller. This lee eddy eventually produces "horseshoe vortex" owing to its distinctive shape. The horseshoe vortex wraps itself around the front half of the pier and extends a few pier diameters downstream on either side before losing its identity and becoming part of the general turbulence.

According to Raudkivi (1998), the vorticity of the horseshoe vortex is quite small and its main role in the scouring process comes about through its interaction with other flow structures. For example, it pushes the maximum downflow velocity within the scour hole closer to the pier. Muzzammil & Gangadhariah (2003) offer a detailed description of the horseshoe vortex including the vortex dimensions, tangential velocity and strength for flows on rigid flat beds, on the solidified scour beds and on mobile sediment beds. Their rigid bed study shows that the mean size of a primary horseshoe vortex is around 20% of the pier diameter (D), while the vortex tangential velocity is approximately 50% of the mean velocity of the approach flow and

relative vortex strength is constant $(\cong 0.1)$ for pier Reynolds number $R_{cD} = \rho UD/\mu$ ranging between 1.0×10^4 and 1.4×10^5.

As the scour hole develops, the horseshoe vortex sinks completely into the scour hole and its mean size increases linearly with the depth of scour and grows until the equilibrium scour hole has been developed. The vortex velocity and strength increase with scour hole development in the initial stages of scouring but decrease in the later stages of scouring (Muzzammil & Gangadhariah, 2003). This vortex significantly affects the scouring process at the base of the bridge piers (Richardson & Panchang, 1998). The downflow and horseshoe vortex together are primarily responsible for the scouring (Melville & Coleman, 2000).

2.2.2.5 The wake votices

Flow separation at the sides of the pier causes the formation of "wake vortices", which alternately separate from the two sides to form a Von Kármán vortex street (Armitage & McGahey, 2003). These vortices are translated downstream by the mean flow and act like vacuum cleaners sucking up sediment from the bed and also transporting sediment entrained by the downflow and horseshoe vortex (Raudkivi, 1998; Melville & Coleman, 2000). The frequency, f_r, of the vortex shedding is indicated by the Strouhal Number, $St = (f_r D/U) \approx 0.2$.

2.2.3 The key parameters affecting local scour

2.2.3.1 The framework for analysis

There are numerous factors affect the local scour including flood-flow transport, bed sediment, bridge geometry and duration of peak flow. It is absolutely necessary to understand and quantify these various factors when estimating/modelling local scour. A brief discussion of some of these parameters is given below. The discussion is restricted to the local scour at un-submerged bridges in straight channels with beds mainly comprising homogeneous uniform non-cohesive sediments, which is the focus of this study. Flow contraction effects are assumed to be absent and are not discussed herein, however, these can be found in Raudkivi (1998), Melville & Coleman (2000), Richardson & Davis (2001) and Leyon (2003).

Melville & Coleman (2000) link the local scour depth y_s to four main groups of dependent parameters: flood flow, bed sediment, bridge geometry and time.

$$y_s = f\left[Flood\,flow(\rho, \nu, U, y, G, g), Bed\,sediment(d_{50}, \sigma_g, \rho_s, U_c), Bridge\,geometry(D, Sh, Al), Time(t)\right] \tag{2.1}$$

where f stands for "a function of", ρ is the density of water, ν is the kinematic viscosity, U is the approach depth-averaged flow velocity, y is the flow depth, G is a parameter describing the effect of the lateral distribution of flow in the approach channel and the cross-sectional shape of the approach channel, g is the gravitational acceleration, d_{50} is the median size of sediment,

σ_g is the geometric standard deviation of the sediment particle size distribution, ρ_s is the sediment density, U_c is the critical mean approach flow velocity for entrainment of bed sediment, D is the diameter of the circular pier, Sh and Al are the parameters describing the shape and alignment of the pier, and t is the time.

Assuming a constant relative density of sediment $(\rho_s - \rho)/\rho$, in the absence of viscous effects, Melville & Coleman (2000) further simplify Equation 2.1 into "dimensionless' form:

$$\frac{y_s}{D} = f\left[\frac{U}{U_c}, \frac{y}{D}, \frac{D}{d_{50}}, \sigma_g, Sh, Al, G, \frac{U}{\sqrt{gD}}, \frac{Ut}{D}\right] \tag{2.2}$$

The first three parameters on the right-hand in Equation 2.2 represent respectively; the flow intensity (U/U_c, which relates the average velocity to the critical velocity for sediment transport on the approach flow bed), the flow shallowness (y/D, depth of flow relative to the diameter of the pier) and the sediment coarseness (D/d_{50}, pier diameter relative to the median diameter of the sediment particles). The last two terms in Equation 2.2 are a pier Froude number ($U/\sqrt{gD}$) based on the pier diameter and a time scale (Ut/D) for the development of scour.

2.2.3.2 The flow intensity

The flow intensity plays vital role at the stage of sediment transport on the approach flow bed. According to Melville & Coleman (2000), clear-water scour conditions occur for both uniform and non-uniform sediments when the flow intensity $U/U_c < 1$, whereas live-bed scour occurs for uniform sediments when $U/U_c > 1$ (Figure 2-3). During clear-water condition, the local scour depth in uniform sediments increases almost linearly with flow intensity to a maximum, known as the "threshold peak", which in turn indicates the "threshold velocity". As the velocity exceeds the threshold velocity, the local scour depth in uniform sediment first decreases and then increases to a second peak known as the "live-bed peak".

According to Breusers et al (1977), the live-bed peak occurs at about the transition flat bed stage of sediment transport on the channel bed and does not exceed the value of the "threshold peak". Based on evidence of numerous experiments, Melville & Coleman (2000) concluded that the maximum local scour occurs under clear-water condition in uniform sediment at the threshold velocity, whereas the live-bed scour depth is largely independent of flow velocity. The threshold peak for non-uniform sediments is lower than the value of threshold peak for uniform sediments. The threshold peak for non-uniform sediments mostly depends on the value of geometric standard deviation σ_g (Raudkivi, 1998; Melville & Coleman, 2000).

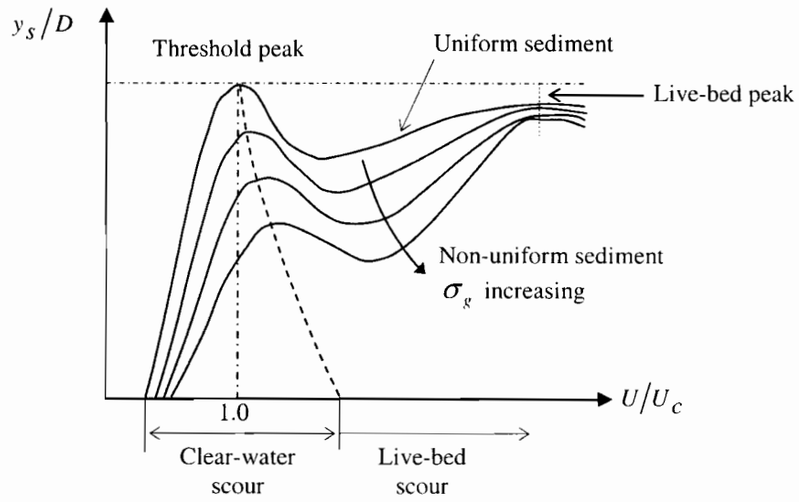

Figure 2-3: Local scour depth variation with flow depth
(After Melville & Coleman, 2000)

2.2.3.3 The flow shallowness

Flow shallowness is important to take account and is defined as the depth of flow in relation to the pier width (y/D). The reciprocal of this ratio (D/y) may be used to classify the pier type as narrow, intermediate or wide.

According to Melville & Coleman (2000), for shallow flow ($D/y > 5$), scour depth increases proportionally with the flow depth y and is independent of foundation size D (scour depth $y_s \propto y$). In this situation, the surface roller becomes more dominant and renders the base vortices (lee eddies and horseshoe vortices) less capable of entraining sediment thus reducing the potential local scour depth. This is because the two upstream vortices (surface roller and base vortices) rotate in opposite directions.

In intermediate depth flows ($0.7 < D/y < 5$), the scour depth depends on both the depth of flow y and the pier diameter D (e.g. scour depth $y_s \propto \sqrt{yD}$). Melville & Coleman (2000) reported that the horseshoe vortexes are still affected by the formation of the surface roller in this region. According to Raudkivi (1986) and Breusers & Raudkivi (1991), the effect of the flow depth y on scour depth vanishes asymptotically with increasing the flow depth and the limiting flow depth is a matter of choice.

In deep flow ($D/y < 0.7$), scour depth increases proportionally with pier diameter D and is independent of flow depth y (e.g. scour depth $y_s \propto D$). In this situation, the strength of the downflow and horseshoe vortex is exclusively related to the diameter of the pier. According to Melville & Coleman (2000), the typical maximum scour depth in uniform bed at a relatively

narrow circular pier is about 2.4 times of the pier diameter, irrespective of the flow depth. Figure 2-4 shows local scour depth variation with flow shallowness.

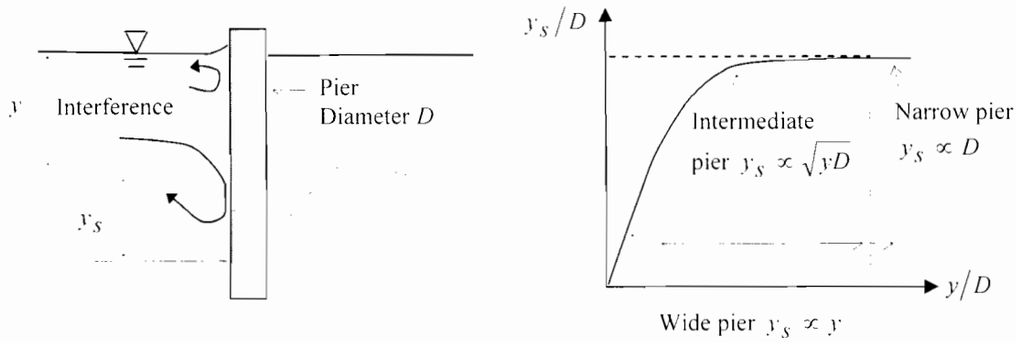

Figure 2-4: Local scour depth variation with flow shallowness
(After Melville & Coleman, 2000)

2.2.3.4 The Sediment coarseness

Ettema (1980) showed that the sediment coarseness of uniform sediments does not contribute further to the development of local scour once $D/d_{50} > 50$ (Figure 2-5).

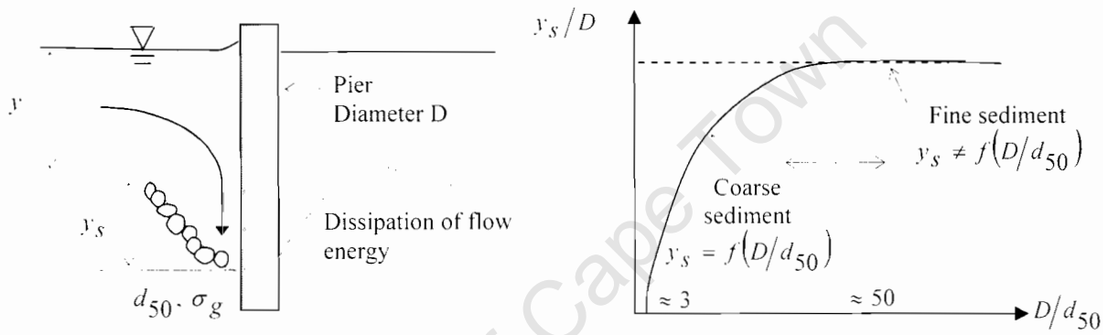

Figure 2-5: Local scour depth variation with sediment coarseness
(After Melville & Coleman, 2000)

According to Melville & Coleman (2000), fine sand ($d_{50} \leq 0.7$) can form ripples under clear-water condition and this limits the scour depth. Ripples can form at sub-threshold conditions with associated sediment transport into the scour hole.

In contrast Ettema (1980) also reported that coarse sediments particles resist the formation of the groove caused by the downflow and impede erosion because they form a porous bed that dissipates some of energy of the downflow. Research indicates that when $D/d_{50} < 50$, individual grains are so large relative to the pier diameter that scour occurs at the sides of the pier due to erosion only (Melville & Coleman, 2000). According to Melville and Sutherland (1988), no significant influence on pier scour is observed when $D/d_{50} \leq 3$ (Figure 2.5).

2.2.3.5 The sediment non-uniformity

Ettema (1976, 1980) carried out intensive laboratory experiments of the effects of sediment non-uniformity on local scour depth under clear-water condition at piers. Chiew (1984) did similar experiments at piers under live-bed conditions. The trend evident from their studies is that there are three distinct phases during the scouring process; the armouring layer formation, the progressive break-up of armouring and the all particle sizes in motion.

Around the threshold condition ($U/U_c \approx 1$), armouring occurs on the approach flow bed and at the base of the scour hole that significantly reduces the development of the scour hole. At high values of U/U_c, when the flow is capable of entraining most grain sizes within the non-uniform sediment, the sediment non-uniformity has only a minor effect on the scour depth. At intermediate values of U/U_c, the effect of σ_g reduces progressively with increasing flow velocity between these limits, as more and more of the grains are transported by the flow.

2.2.3.6 The foundation shape

A variety of different types and shapes of bridge foundation have been studied (Raudkivi & Sutherland, 1981; Ahmed, 1995; Melville & Coleman, 2000). According to Armitage & McGahey (2003), for simplicity, most of the laboratory experiments are based on standard pier shapes such as circular piers. Melville & Coleman (2000) thus suggest a "shape factor" to take account into the effects of bridge pier shape on scour depth. They defined the shape factor as the ratio of the scour depth for a particular pier shape to that for the standard shape. Accordingly the shape factor for uniform circular pier is 1.0 (Melville & Coleman, 2000; Richardson & Davis, 2001).

2.2.3.7 The foundation alignment

Except in the case of circular pier, the alignment of the pier to flow has a significant effect on the local scour depth. Ettema et al (1998) show that the local scour depth increases with increase of flow angle for a rectangular pier because of the large effective frontal width of the pier. Figure 2-6 shows that the effective (or projected) frontal width of pier (b_p) of a rectangular pier for a flow angle θ_f can be written as $b_p = l\sin\theta_f + b\cos\theta_f$. The maximum effective frontal width ($db_p/d\theta_f = 0$) of a rectangular pier with $l/b = 6$ thus occurs at $\theta_f = \tan^{-1}(l/b) = 80.5^0$. The scour depth then (taken into account by a factor, Figure 2-6) is nearly tripled compared to the pier aligned with flow.

In a braided channel, floods may significantly alter the angle of attack on pier, which may further be affected by meandering. Circular pier, a row of circular piers or other shapes with low aspect ratios (length-to-width) are therefore often preferred in braided channels.

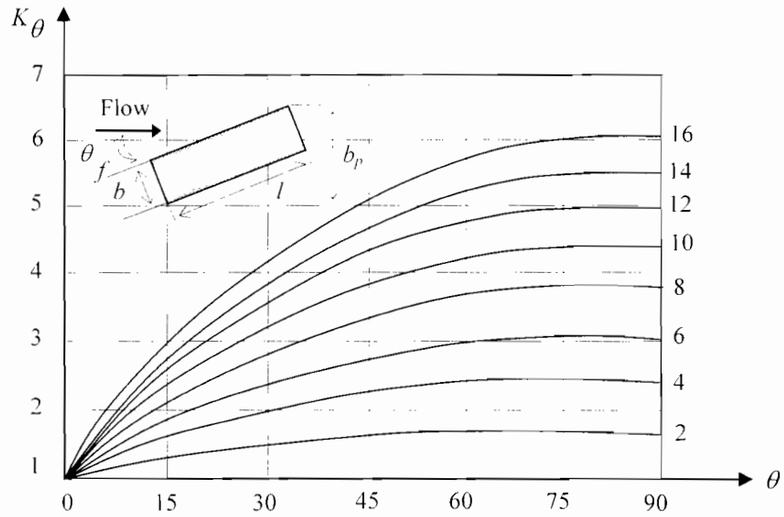

Figure 2-6: Local scour depth variation with pier alignment
(After Melville & Coleman, 2000)

2.2.3.8 The pier Froude number

Most of the scour prediction formulae are based on laboratory model tests, where the model bed material relative to pier size is larger than its scaled counterpart in the field. Accordingly Ettema et al (1998) suggested the pier Froude number $U/\sqrt{gD}$. Flow-field similitude requires preservation of flow patterns such as the pressure heads along the flow paths so that a model pier in the laboratory may be related to a pier in the field. It is obvious that as values of $U/\sqrt{gD}$ become relatively large, implying (for constant U) that D becomes small, the bed becomes rough relative to the pier diameter. As a consequence the scour depth relative to pier width will decrease because of increased boundary roughness and more energy will be dissipated within the scour hole. A narrow pier ($D/y < 0.7$) will therefore induce a smaller value scour relative to pier width (y_s/D) compared to wide pier ($D/y > 5$) in the same flow field. The Ettema et al (1998) data was however insufficient to quantify the influence of pier Froude number on local scour depth at pier. Their data do indicate that using a value for the maximum scour depth at circular piers of $2.4D$ is conservative for all pier diameters larger than about 0.1m (Melville & Coleman, 2000).

2.2.3.9 The time scale

Research shows that the scour depth generally develops asymptotically towards the equilibrium scour depth under clear-water condition. Under live-bed conditions, the equilibrium depth is reached more quickly and thereafter the scour depth oscillates due to the passage of bed features past the pier. The time scale of the clear-water condition is however generally longer than that of the live-bed condition. Chiew & Melville (1996), Melville & Chiew (1999), Chang et al (2004) and Oliveto & Hager (2005) present many laboratory data that suggest the temporal development of local scour at circular piers. According to Melville & Chiew (1999), both the

time required developing the equilibrium scour depth (t_e) and the equilibrium scour depth (y_{se}) are subject to similar influences of flow and sediment properties, as might be expected because they are inherently interdependent. They presented the dimensionless equilibrium time scale ($t^* = Ut_e/D$) with respect to flow intensity (U/U_c), flow shallowness (y/D) and sediment coarseness (D/d_{50}) under steady clear-water condition of uniform sediments (Figure 2-7). The maximum value of t^* is about 25×10^5 (Melville & Coleman, 2000).

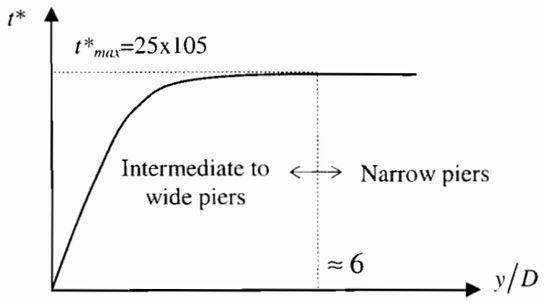

a) Variation of t^* with flow shallowness

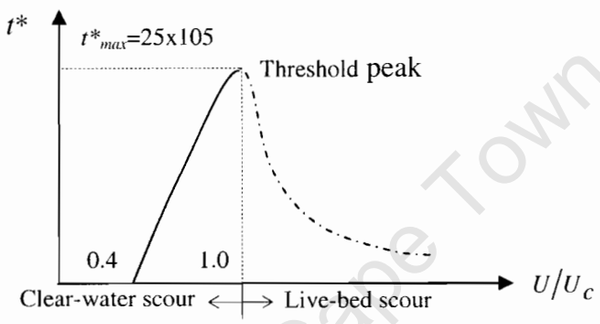

b) Variation of t^* with flow intensity

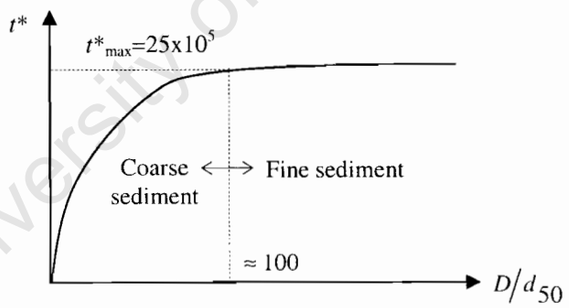

c) Variation of t^* with sediment coarseness

Figure 2-7: Equilibrium time scale variation
(After Melville & Coleman, 2000)

Chang et al (2004) modified the equilibrium time proposed by Melville & Chiew (1999) for non-uniform sediment using a sediment gradation factor. They used a stepwise hydrograph for analysing the temporal scour-depth relationship for unsteady flow conditions in analysing field flood events.

2.2.4 The growth of the local scour hole around a pier

Melville (1975) and Nakagawa & Suzuki (1975) reported that the initial scour-hole development commences near the side of the pier as a result of the tractive force of the accelerated mean flow due to the distortion of the streamlines by the pier. The horseshoe vortex caused due to the downflow then initiates the scour near the leading edge. Following the work by Melville (1975) and Nakagawa & Suzuki (1975), Ettema (1980) reported the development of scour hole progressing in three phases; the initial, the principal and the equilibrium.

In the "initial phase", the scour hole development starts from the flat-bed condition, where sediment transport begins at the sides of the pier and works its way around the circumference to form a shallow scour hole. The eroded material is transported downstream by flow. According to Raudkivi & Sutherland (1981), soon after commencement of scouring, a shallow hole, concentric with the pier, is formed around pier e.g. about $\pm 120^0$ on either side of the centreline (Figure 2-8a) but not in wake region. Ettema (1980) emphasized that the horseshoe vortex plays no important role in this phase.

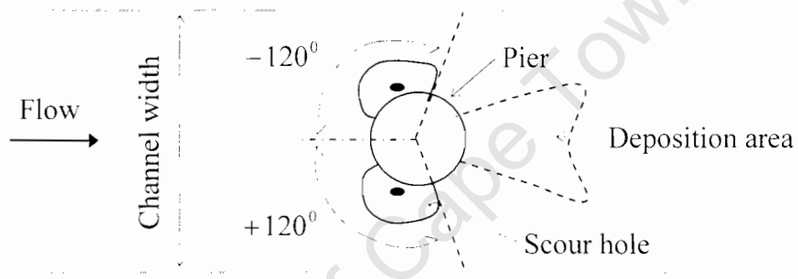

Figure 2-8a: Growth of scour hole around a pier
(Adapted from Raudkivi & Sutherland, 1981)

In the "principal phase", the horseshoe vortex grows rapidly in size and strength and settles into the scour hole resulting in an increase in the strength of the downflow at the leading edge of the cylinder. The downflow acts like a vertical jet eroding a groove in front of the pier. The downflow is then turned 180^0 in the groove, and the resulting upward flow forms the horseshoe vortex that travels up the scour hole slope (Raudkivi & Sutherland, 1981). During this phase, Ettema (1980) observed that erosion occurred in a near flat, narrow strip around the cylinder (extending to $\pm 120^0$) that he called the entrainment zone. The eroded material is carried around the pier by the combined action of accelerating flow and the spiral motion of the horseshoe vortex. The sand in the region around the rim collapses into the groove from time to time in order to return the slope angle to the angle of repose of the bed material. Sand particles in the groove are lifted by the up-flow into the region of the horseshoe vortex where they are either

deposited on the slope or transported into and through the wake region. The hole develops the strength of the horseshoe vortex whilst the downflow weakens until eventually they are no longer able to remove sediment from the entrainment zone.

In the "equilibrium phase", the flow is no longer able to remove sediment for clear water scour or the sediment entering the hole from upstream for live-bed scour balances the sediment removed.

Most other researchers agree on the general process of scour hole development, while differing on some of the details (Raudkivi & Sutherland, 1981; Breusers & Raudkivi, 1991; Ahmed 1995; Raudkivi, 1998; Melville & Coleman, 2000). Generally, for a single cylindrical pier, there is an initial stage during which sediment is removed from the sides of the pier where the flow has been accelerated as predicted by potential flow theory (Ahmed, 1995). At this point, the scour resembles sediment transport on a flat bed. Ettema (1980) and Hjorth (1975) found that the points of initiation of scour occur at roughly $\pm 45^0$ from the leading edge of the pier. Melville (1975) found the maximum shear stress at the unscoured bed at $\pm 100^0$ degrees.

As the scour hole grows, it spreads toward the leading edge of the pier, where the downflow has been established and the horseshoe vortex originates. Shen et al (1969), Chiew (1984) Raudkivi (1998) and Melville & Coleman (2000) identified the downflow as the main cause of local scour and describe the scour hole as an inverted right circular cone with the pier as its axis. The angle that the slope of the hole makes with the vertical is approximately equal to the angle of repose of the sediment. According to Melville (1975), as the hole deepens, the downflow strengthens and the horseshoe vortex grows and descends into the hole. Avalanching of material down the sides of the scour hole occurs once the hole is large enough to contain the horseshoe vortex, causing the hole to widen.

Many researchers (e.g. Nakagawa & Suzuki, 1975; Hjorth, 1977; Ettema, 1980) observed that the actual mobilization and removal of sediment is limited to an area immediately adjacent to the pier at the base of the scour hole. As material slides down the sides of the hole, it is mobilized in this erosion or entrainment zone. Once a sediment particle is put into suspension, it is swept downstream. If the particle is carried high enough by the flow, it may interact with the wake vortices, which in turn can be carried higher into the water column and can be transported and deposited at downstream of the pier. Otherwise, the sediment particle may be swept directly little far behind the pier and enter the relatively calm wake region. Here it will settle out and form the characteristic mound behind the structure. Eventually, the hole becomes deep enough that the strength of the horseshoe vortex and the downflow are weakened and can no longer mobilize and remove sediment from the scour hole.

For clear-water scour, the equilibrium is reached when the combined effect of the temporal mean shear stress, the weight component and turbulent agitation everywhere add up to the local threshold condition of sediment transport (Raudkivi & Sutherland, 1981). In the live bed case, the equilibrium is reached when the amount of sediment removed from scour hole is exactly

equal to that deposited in the hole from upstream. Development of the live-bed scour hole becomes more complicated with the passage of bed forms past the pier (CUR, 2000). Scour is generally less for live-bed condition than clear-water (Melville & Coleman, 2000; May et al, 2002). Live-bed scour also tends to reach equilibrium much faster than clear-water scour – commensurate with the higher sediment transportation capacity of the flow (Armitage & McGahey, 2003).

2.2.5 The shape of the scour hole

Dargahi (1987) schematised the plan section of a fully developed cylindrical pier scour hole into a semi-circle on the upstream side and half of an ellipse (cut along the minor axis) on the downstream side (Armitage & McGahey, 2003). The semi-circle has a radius of about $2b_p$ measured from the centre of the pier, provided that the flow depth is at least $3b_p$. The length of the scour in the downstream direction is in the order of $5b_p$. According to Hoffmans & Verheij (1997) the average upstream slope is approximately equal to the angle of repose, ϕ_r, being a little steeper in the groove close to the pier and a little flatter outside of this. The average downstream slope is about $\phi_r/2$.

The deepest point of the scour hole is usually in the vicinity of the leading face of the pier, but at times it can be found at an angle of up to 60^0 on either side of the front face (Chiew, 1995). According to Melville & Coleman (2000), the scour hole looks like an inverted right circular cone with the pier as its axis and deepest scour at front of the pier (refer to Figure 2-2).

Oliveto & Hager (2005) schematised scour holes with the deepest points at the sides of the pier, which are approximately between $\pm 65^0 - 75^0$ from leading face (Figure 2-8b). Their experiments are based on relatively coarse ($d_{50} = 3.1 - 4.3$ mm) non-uniform ($\sigma_g = 2.15 - 2.35$) field sediment data.

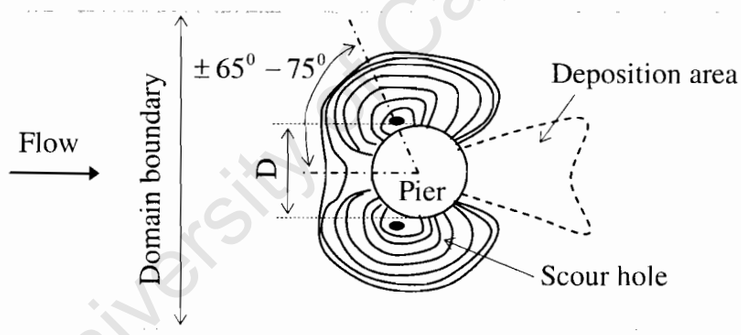

Figure 2-8b: Shape of scour hole and deposition area
(Adapted from Oliveto & Hager, 2005)

2.3 An overview of sediment transport

The previous discussion clearly indicates that scour is the fluvial process due to interaction of hydrodynamic and sediment transport systems. Sediment transport near a pier is thus a complex process and involves the deformation channel in response to scour, deposition and bed forms (in the case of live-bed scour) which strongly affect the bed roughness, energy loss and velocity gradient (Van Rijn, 1993; Yang, 1996; Raudkivi, 1998; Chien & Wan, 1999).

At a bridge site, sediment can be transported in three different modes; bed load, suspended load and wash load (Van Rijn, 1993; Yang, 1996; Raudkivi, 1998). Their relative contribution depends on many factors such as river shape, sediment classification and the hydrology of the river basin. Over the past few decades, a large number of experiments have been carried out in the laboratory, and numerous empirical or semi-empirical formulae have been developed for the initiation of sediment particle movement and its transport in the rivers.

Some of these formulae have been used to determine the potential sediment transport – and hence scour in open channel CFD model. A basic knowledge on sediment transport theory is thus important for understanding the development of the CFD model. This section summarises various engineering aspects related to fluvial sediment transport. The section starts with some of the important physical characteristics of sediment followed by a description of the incipient motion of sediment particles from the bed and estimates of their rate of transport using common formulae.

2.3.1 The physical characteristics of sediment particles

The physical characteristics of the sediment particles have an important role in determining the motion of particles i.e. incipient motion. The sediment particles can be characterised according to their size, shape, uniformity, settling velocity, cohesiveness and angle of repose.

Sediment dimensions cover a large "size" range, which in turn used to classify the sediments (Yang, 1996). Sediment size is commonly determined by sieve analysis. The most common grain size classification is that of the American Geophysical Union, which is based on the approximate diameter of the sediment particles (Armitage & McGahey, 2003). A wide variety of sediment "shapes" are observed in the rivers. Van Rijn (1993) and Yang (1996) present a so-called "shape factor" to take into account the deviation from spherical. Naturally worn quartz particles typically have a shape factor of 0.7.

The distribution of the particle sizes determines the sediment "uniformity". Sieve analysis is undertaken to determine the size of sediments. Sediment uniformity is determined from frequency histograms depicting the percentage of material by mass passing one sieve diameter but retained on one size smaller. Statistical parameters such as the mean, standard deviation, skewness and kurtosis may be determined from this (Van Rijn, 1993; Yang, 1996).

The "median diameter" (d_{50} or d_i) is the diameter that is not exceeded by 50% of the material by mass and is often expressed as:

$$d_{50}(\text{or } d_i) = \frac{d_{15.9} + d_{84.1}}{2} \tag{2.3}$$

The "mean diameter" ($\bar{d}$) is the arithmetic mean of the particle size and can be expressed in terms of the median diameter (d_i) of any particle size fraction and the percentage by mass of that fraction (p_i) as follows:

$$\bar{d} = \frac{\sum p_i d_i}{100} \tag{2.4}$$

The "standard deviation" (σ) is determined using the mean diameter (Equation 2.5). The "geometric standard deviation" (σ_g) is also often used (Equation 2.6), which assumes the particle distribution is normally distributed which is approximately true for finely graded or uniform sand. If σ_g<1.3, the sediment is considered to be uniform, alternatively, if σ_g>1.3, the sediment is considered to be non-uniform (Melville, 1997).

$$\sigma^2 = \frac{\left\{\sum p_i \left(d_i - \bar{d}\right)^2\right\}}{100} \tag{2.5}$$

$$\sigma_g \cong \sqrt{\frac{d_{84.1}}{d_{15.9}}} \cong \frac{d_{84.1}}{d_{50}} \cong \frac{d_{50}}{d_{15.9}} \cong \frac{1}{2}\left(\frac{d_{50}}{d_{15.9}} + \frac{d_{84.1}}{d_{50}}\right) \tag{2.6}$$

The "settling velocity" of a particle – sometimes called the "fall velocity" – is generally defined as the terminal velocity of that fluid particle in an unbounded quiescent body of water. In general, it depends on the size, shape, surface-roughness and density of the particle, and on the density and viscosity of the fluid. The fluid turbulence, particle concentration, and the presence of boundaries can also influence the settling velocity. If the particle is less dense than the fluid, it will have a negative settling velocity – sometimes called a "rise velocity". Raudkivi (1998) presents the settling velocity (v_{ss}) using the drag coefficient C_D.

According to Van Rijn (1993), the settling velocity of non-spherical natural sediment particles of sieve diameter d, specific gravity s, kinematic viscosity ν and acceleration of gravity g can be estimated from:

$$v_{ss} = \frac{(s-1)gd^2}{18\nu} \qquad \text{if } 1 < d \leq 100 \ \mu\text{m} \tag{2.7a}$$

$$v_{ss} = \frac{10\nu}{d}\left[\sqrt{\left(1+\frac{0.01(s-1)gd^3}{18\nu^2}\right)}-1\right] \qquad \text{if } 100 < d \le 1000 \ \mu\text{m} \tag{2.7b}$$

$$v_{ss} = 1.1[(s-1)gd]^{0.5} \qquad \text{if } d > 1000 \ \mu\text{m} \tag{2.7c}$$

Cheng (1997) approximated the settling velocity (v_{ss}) of natural sand particles by defining the "relative submerged density" (Δ) and the "dimensionless particle diameter" (d_*) as:

$$v_{ss} = \frac{\nu\left(\sqrt{25+1.2{d_*}^2}-5\right)^{1.5}}{d} \tag{2.8a}$$

$$d_* = \left(\frac{\Delta g}{\nu^2}\right)^{1/3} d_{50} \tag{2.8b}$$

$$\Delta = \frac{\rho_s - \rho}{\rho} \tag{2.8c}$$

Generally the fall velocity is significantly reduced in higher sediment concentrations. The effect of concentration on settling velocity is known as "hindered settling" (Raudkivi, 1998).

Sediments can be divided mainly into two groups; "cohesive" (i.e. clay, silt) and "non-cohesive" (i.e. sand). The weight of the particles is the dominant force in determining the transportability of non-cohesive sediments. On the other hand, for the cohesive sediments, the physicochemical forces play a major role. The cohesive materials affect the soil properties such that the particle tends to behave as one large coherent mass. Vanoni (1975) describes that once suspended; the cohesive mass breaks up and the particles behave as non-cohesive materials. This study will only be covering non-cohesive sediment types.

The "angle of repose" (ϕ_r) - sometimes called the angle of internal friction- is the maximum side-slope that can be sustained by sediment particles lying on the bottom or sides of a channel before sliding commences. Van Rijn (1993) lists the angle of repose of quartzitic sand sediment; however, ϕ_r for any material other than quartztic sand needs to be determined experimentally.

2.3.2 The forces acting on particles at rest on the bed

In reality a sediment particle in channel bed is surrounded by neighbour particles and rests on the bed before incipient motion. It is obvious that there are three main forces acting on an exposed particle; drag, lift and gravity. Figure 2-9 depicts the different forces act on a sediment particle (inclined bed).

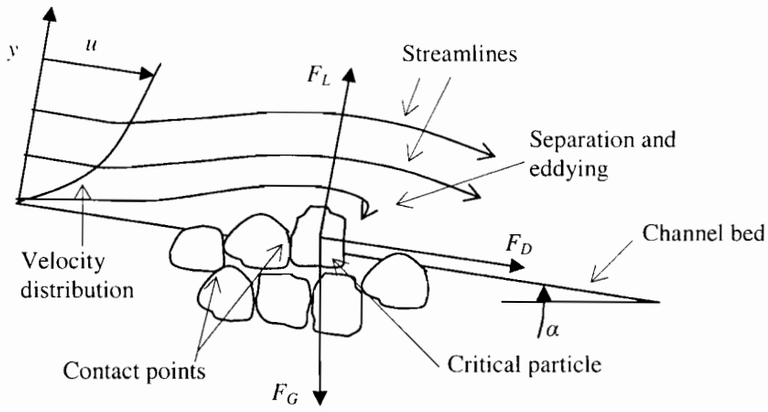

Figure 2-9: Forces on a sediment particle (inclined bed)

The drag F_D and lift F_L force represent the horizontal and vertical components due to the integrated shear stress and pressure forces acting on the particle.

The shear stress at any point on the particle surface acts tangentially to the direction of flow and depends on the local velocity gradient or one of its three dimensional variants (Equation 2.9). The drag due to shear stress is thus often called "surface drag".

$$\tau_{xy} = \left(\mu + \mu_{xy(t)}\right)\left(\frac{\partial u}{\partial y} + \frac{\partial v}{\partial x}\right) \tag{2.9}$$

In Equation 2.9, μ is the coefficient of viscosity due to shear flow and $\mu_{xy(t)}$ is due to the turbulent flow (Section 2.4.6). The pressure force at any point on the particle surface acts normal to the surface and depends on the depth and local velocity in accordance with the Bernoulli Equation. If z is the height above some arbitrary datum, the Bernoulli equation can be written as in Equation 2.10. The pressure $p = \rho g y$ at water depth y can be determined using the hydrostatic conditions.

$$\frac{p}{\rho g} + \frac{u^2}{2g} + z = \text{Constant along the streamline} \tag{2.10}$$

Equation 2.10 clearly indicates that, for a constant datum, increases in velocity lead to a corresponding decrease in the local pressure. This situation is complicated by flow separation, which result in the formation of eddies. According to Armitage & McGahey (2003), these eddies redistribute the pressure more uniformly over the separated surfaces. Van Rijn (1993) shows that the integration of pressure forces over the entire surface of the particle indicates the resultant drag force, which is known as "form drag".

The gravitational force F_G is related to the submerged weight of the critical particle. Despite the absence of fluid motion, there is a net force on the particle and its direction depends on the "buoyancy" effect. The gravitational force acts vertically down if the particle is denser than water and vertically upward if it is not. Van Rijn (1993) describes the gravitational force F_G on a critical particle with a particle diameter d, particle density ρ_s and water density ρ as:

$$F_G = \frac{1}{6}\pi(\rho_s - \rho)gd^3 \tag{2.11}$$

Chien & Wan (1999) describe the drag force F_D and the lift force F_L, using the projected area a_p (which is defined different for drag and lift), drag coefficient C_D, lift coefficient C_L, density of water and effective velocity near the bed particle u_0 as:

$$F_D = C_D a_P \frac{\rho u_0^{\,2}}{2} \tag{2.12}$$

$$F_L = C_L a_P \frac{\rho u_0^{\,2}}{2} \tag{2.13}$$

The presence of channel boundary makes the velocity distribution non-linear. Also the lift force is relatively larger at the boundary particles where the drag forces do not act through the centre of gravity of the particle. According to Saffman (1965), for a viscous flow, the lift force due to the spinning motion is less by an order of magnitude than that due to shear effect and is generally neglected (Colebrook & White, 1937; Van Rijn, 1993).

2.3.3 The role of effective roughness

The definition of the effective roughness height k_s is very important for the simulation. In the case of a mobile bed, it is the sum of the "grain roughness" k_{sg} generated by the skin friction and the "form roughness" k_{sf} generated by the pressure forces acting on the bed.

$$k_s = k_{sg} + k_{sf} \tag{2.14}$$

According to Van Rijn (1993), two approaches can be used to estimate the bed roughness; bed form and grain related parameters (e.g. bed form length, height, steepness and bed material size) or integral parameters (e.g. mean depth, mean velocity).

According to Young et al (1997), the particle at the boundary could form part of a laminar boundary ($Re_s < 5$), a transitional boundary ($5 < Re_s < 70$) or a turbulent boundary ($Re_s > 70$), where Re_s is roughness Reynolds number defined as:

$$Re_s = \frac{u_* k_s}{\nu} \tag{2.15a}$$

where ν is the kinematic viscosity and u_* is the shear velocity, which is defined using the bed shear stress τ_0 and the density of fluid ρ as:

$$u_* = \sqrt{\frac{\tau_0}{\rho}} \tag{2.15b}$$

Colebrook & White (1937) show when Re_s increases beyond 3.5, separation commences behind the top of the particle and a wake is formed. According to Chien & Wan (1999), the form drag becomes then the dominant force.

Other definitions of k_s are (Yang, 1996; SISYPHE, 2004), $k_s = d_{65}$ (Einstein, 1950), $k_s = d_{90}$ (Meyer-Peter & Muller, 1948), $k_s = d_{85}$ (Simons & Richardson, 1966) and $k_s = 3d_{50}$ (SISYPHE, 2004).

The value of k_s significantly decreases for increasing velocities, probably because the bed forms become more rounded or are washed out (Van Rijn, 1993).

2.3.4 The initiation of sediment movement

The initiation of sediment movement may be determined from a consideration of the forces acting on the particles due to drag, lift and gravity (Van Rijn, 1993; Yang, 1996). Van Rijn (1993) describes the initiation of sediment movement using forces acting on the spherical sediment particle on flat bed shown in the Figure 2-10.

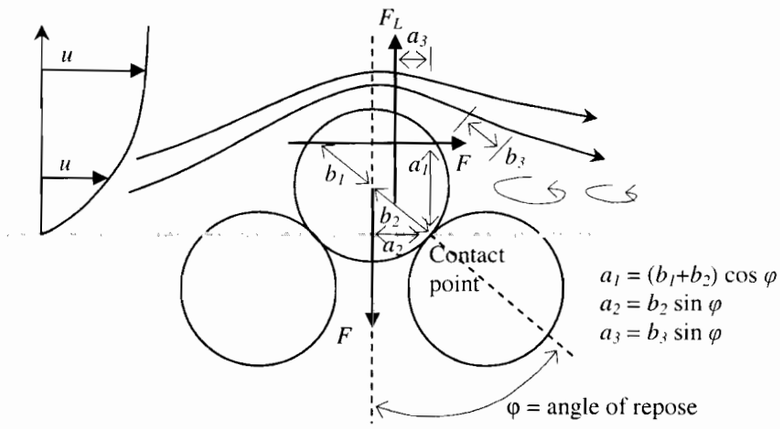

Figure 2-10 Forces on a sediment particle by Van Rijn (1993)

In the derivation, Van Rijn (1993) neglects the ratio of the lift force and the submerged particle weight $(F_L/F_G \cong 0)$. He introduces the empirical coefficient α_1, by which the effects of lift force has been taken into account. The condition of sediment movements therefore yields as:

$$F_D \geq \alpha_1 F_G \tan\varphi, \text{ where } \alpha_1 = \frac{b_2}{b_1 + b_2} \tag{2.16}$$

The value of the empirical coefficient α_1 depends on the local turbulence and hence the Reynolds number (Van Rijn, 1993).

Yang (1996) adds further simplifications and shows the incipient motion of sediment particles satisfies one or more of the three conditions indicated in Equation 2.17 and Figure 2-11.

$$F_L = F_G \tag{2.17a}$$

$$F_D = F_R \tag{2.17b}$$

$$M_O = M_R \tag{2.17c}$$

where F_L is the lift force, F_G is the gravitational force, F_D is the drag force, F_R is the resistance force, M_O is the overturning moment due to F_D and F_R and M_R is the resisting moment due to F_L and F_G.

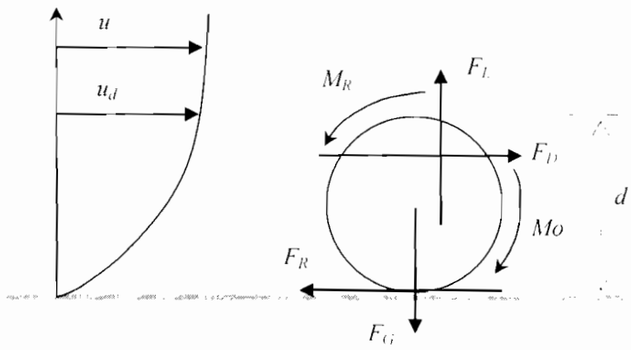

Figure 2-11: Forces on a sediment particle by Yang (1996)

In reality the calculation of the forces acting on a particle is difficult. Many reserchers therefore define the sediment incipient movement criteria using shear stress (Shield, 1936), velocity (Yang, 1973), stream power (Bagnold, 1966; Ackers & White, 1973) or probalility (Gessler, 1970). All of these approaches are reported in Van Rijn (1993), Przedwojski et al (1995), Yang (1996), Chien & Wan (1999) and Raudkivi (1998).

Shields (1936) was one of the first researchers to realise the difficulty of an analytical calculation of the forces acting on a sediment particle. He used dimensional analysis to establish his well-known "Shield diagram" for an incipient motion of a particle using the dimensionless parameters e.g. the particle Reynolds number Re_* (Equation 2.18) and the Shields parameter θ (Equation 2.19).

$$Re_* = \frac{u_* d}{\nu} \tag{2.18}$$

$$\theta = \frac{\tau_0}{(\rho_s - \rho)gd} = \frac{\rho u_*^2}{(\rho_s - \rho)gd} \tag{2.19}$$

where u_* is the shear velocity (Equation 2.15b), d is the particle diameter, ν is the kinematic viscosity, τ_0 is the bed shear stress, ρ_s is the density of sediment, ρ is the density of water and g is the acceleration of gravity. Shields (1936) measured the transport rate at various values of θ at least twice as large as the critical value θ_c and then extrapolated linearly to the point of zero sediment. This indirect method was used to avoid the difficulty of determining the precise condition at which a sediment particle should move. If τ_c is the critical bed shear stress for incipient motion, then critical Shields parameter θ_c is given by (also in Figure 2-12):

$$\theta_c = \frac{\tau_c}{(\rho_s - \rho)gd_{50}} \tag{2.20}$$

Figure 2-12 shows the Shield parameter as a function of the particle Reynolds number. The solid line band indicates the spread of data by Shields, however, most of the published data lie within the dashed lines (Raudkivi, 1998).

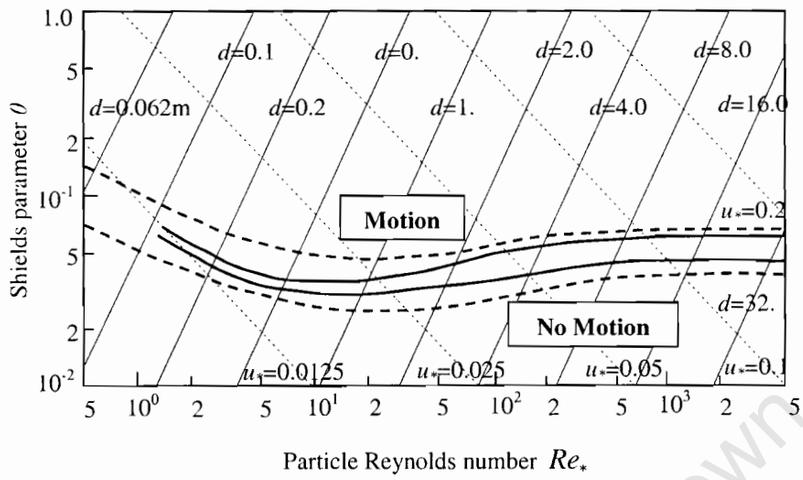

Figure 2-12: Shields parameter with respect to particle Reynolds number
(After Raudkivi, 1998)

Yang (1973) proposed a "dimensionless critical velocity" (U_c/v_{ss}) to describe incipient sediment motion using the particle Reynolds number (Re_*). He showed a "parabolic" and "straight line" variation of (U_c/v_{ss}) in hydraulic smooth $(Re_* < 5)$ and completely rough regime $(Re_* > 70)$. In the transition regime $(5 \le Re_* \le 70)$, both the laminar friction and turbulent friction contributions should be considered. Based on the field data, Yang (1973) however extended the "parabolic" curve for this regime considering the effects of empirical coefficients with respect to Re_*. The Yang (1973) incipient motion criteria curve is shown in Figure 2-13.

It should be noted that Yang (1973) ignored the effect of the flow roughness (y/d) for the transition regime due to data unavailability. Talapatra & Ghosh (1983) and Govers (1987) independently verified the Yang (1973) criteria.

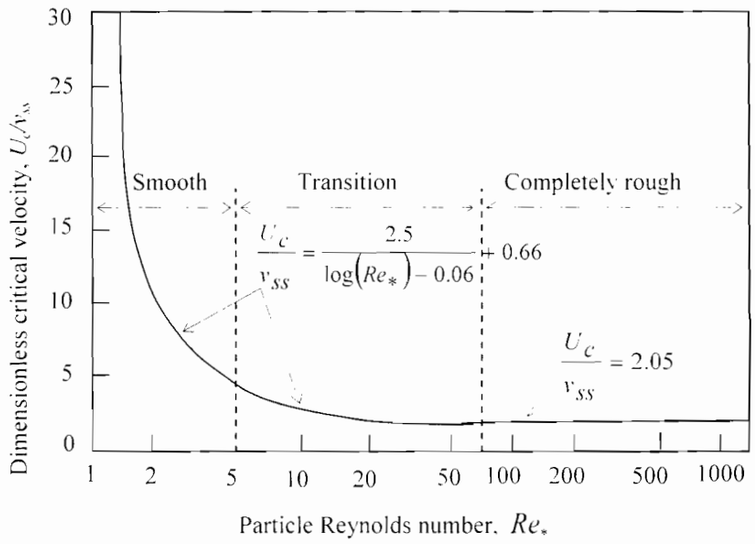

Figure 2-13: Variation of dimensionless critical velocity
(After Yang, 1996)

2.3.5 The means of sediment transport

Once sediment particle movement has been initiated, the particle starts to move. In an alluvial channel, three different types of particle motion are observed (Van Rijn, 1993; Raudkivi, 1998; Chein & Wan, 1999); rolling and/or sliding, salting or hopping and suspension.

In most cases, sediment particle will roll or slide before they will saltate, and they will saltate before they are carried into suspension. The transport of particles by rolling, sliding and salting in the close vicinity of the bed is collectively called "bed load". Another commonly used definition is "contact load", which refers to sediment that is moving continuously in contact with the boundary, i.e. sliding and rolling. Saltation is when the particles hop along following parabolic-type trajectories close to the bed. The "suspended" particles are transported by the upward components of turbulent currents and stay in suspension for an appreciable length of time. According to Yang (1996) sediments are mainly transported via the "suspended load" in most natural rivers whilst the bed load transport is only about 5-25% depending on the bed sediment class.

According to Raudkivi (1998), the concentration of suspended sediment (solid volume or mass per unit water volume or mass) decreases with distance up from the bed. This rate of decrease depends on the fall velocity v_{ss} and the bed-shear velocity u_*, which in turn is used to define the mobility number $Mn = u_*/v_{ss}$. He proposes a rule of thumb for the prediction of different types of transport using mobility number i.e. rolling and/or sliding when $6 > (1/Mn) > 2$, Saltating/hopping when $2 > (1/Mn) > 0.6$ and suspension $0.6 > (1/Mn) > 0$.

Graf & Altinakar (1998) distinguish different types of sediment transport in terms of the water-sediment mixture of gravitational flow depending on the sediment concentration C_s (volume of solid per unit volume of water) or sediment concentration $\Delta\rho$ (mass of solid per unit volume of water). Bed load and suspended load transport are common in a Newtonian mixture (C_s<<1% or $\Delta\rho$<<16 kg/m^3), which is most often encountered in watercourses. In a quasi-Newtonian mixture (C_s<8% or $\Delta\rho$<130 kg/m^3), usually concentrated suspension is observed close to bed. Turbidity currents for example fall into this category. Non-Newtonian mixtures (C_s>8% or $\Delta\rho$>130 kg/m^3) are associated with the hyper-concentrated suspensions experienced with turbidity currents and debris flow.

Classically the sum of "bed-load" and "suspended load" is collectively known as "total load". Depending on source of sediment materials, Raudkivi (1998) further decomposes "total load" into "bed-material load" and "wash load". Generally the wash load consists of materials that are finer than those found in the riverbed and are almost never in contact with the bed. The amount of wash load depends mainly on the supply from the watershed (hydrology), not on the hydraulics of the river.

2.3.6 Non-cohesive sediment transport formula

This study is concerned with the modelling of local scour in uniform non-cohesive sediment using a CFD code. Scour is associated with the initiation of sediment movement and continues by means of sediment transport due to the hydrodynamic forces unless the equilibrium condition is reached. A large number of semi-empirical formulae have been developed to calculate the solid transport rate as a function of various hydrodynamic (e.g. water depth, flow velocity, bottom friction, waves, etc.) and sediment (e.g. d_{50}, d_{90}, relative density, etc.) parameters (Van Rijn, 1993; Przedwojski et al, 1995; Yang, 1996; Chien & Wan, 1999; Raudkivi, 1998; SISYPHE, 2004).

The transport formula may estimate only the "bed load" and/or "suspended load" and/or "total load" (bed and suspended load). The formulae may be grouped together according to their theoretical approach e.g. shear stress, energy slope, probabilistic, stream power, etc (Van Rijn, 1993, Yang, 1996, Chien & Wan, 1999). The formulae used in this study are discussed below. They are all intended for use in the modelling of the transport of uniform median grained sand ($0.5 < d_{50} < 1$ mm).

2.3.6.1 Meyer-Peter and Muller (1948)

The Meyer-Peter and Muller (1948) formula is based on the energy slope approach and is limited to "bed load" transport only. They carried out extensive experimental works in a laboratory flume with a cross-section of 2x2 m^2 and a length of 50m. Uniform bed material as well as particle mixtures were used in the experiments (d = 0.4 to 29 mm, slope S = 0.0004 to 0.02, depth 0.1 to 1.2 m). According to Meyer-Peter and Muller (1948), the bed load transport q_b can be expressed as (Van Rijn, 1993):

$$\Phi_b = \frac{q_b}{\sqrt{(s-1)g{d_{50}}^3}} = 8(\mu_b\theta - 0.047)^{1.5} \tag{2.21}$$

$$\mu_b = \left[\frac{C_b}{C'_b}\right]^{1.5} = \left[\frac{\log(12h/k_s)}{\log(12h/d_{90})}\right]^{1.5} \tag{2.22}$$

where Φ_b is the dimensionless bed sediment load function, θ is the Shields parameter; μ_b is the bed form factor or efficiency factor; $\bar{d}$ is the mean particle diameter; C_b is the Chezy coefficient, C'_b is the grain related Chezy coefficient, k_s is the effective bed roughness and h is the water depth.

The constant value 0.047 can be interpreted as the critical Shields parameter (θ_c), because the experiments considered coarse materials. Meyer-Peter and Muller (1948) found the value of $\bar{d} = \sum p_i d_i$ to be about 1.1 to 1.3 times larger than d_{50} for nearly uniform material. The median particle diameter d_{50} may also be used instead of $\bar{d}$, however, the grain roughness is related to d_{90}. According to Van Rijn (1993), the formula shows that a 25% variation of the particle diameter ($\bar{d}$ = 800 ± 200 μm) results in a 10% variation of the transport rate (q_b = 4.1x10^{-5} ± 0.4x10^{-5} m^2/s). For uniform sands, the grain related Chezy coefficient, C'_b is often approximated in terms of d_{50} using relationship $d_{90} = 3d_{50}$ (SISYPHE, 2004).

It should be noted that the value of Φ_b will be zero if the value of $\mu_b\theta < \theta_c (= 0.047)$. Based on the model validity tests, SISYPHE (2004) recommends using the Meyer-Peter and Muller (1948) formula for the fine to coarse sediments in the range $0.4 < d_{50} < 29.0$ mm.

2.3.6.2 Einstein and Brown (1950)

Einstein (1950) was one of the first researchers to estimate the sediment transport using the concept of probability. Two particular concepts drove him to do so; the difficulties in defining the critical incipient criterion and the need to take into account the turbulent flow fluctuations on sediment transport instead of the forces acting on the sediment particles. As a result, he expressed the probability for the beginning and ceasing of the sediment motion. His experiments highlighted the following points (Yang, 1996):

- There is a steady and intensive exchange of particles between bed material and bed load.
- The movement of bed load is in a series of steps and average of step length is about 100 times the particle diameter.
- The rate of erosion depends on the number and properties of particles in unit area and the probability that the instantaneous hydrodynamic lift force on the particle is large

enough to move it. On the other hand, the rate of deposition per unit bed area depends on the transport rate past a given section, as well as the probability that hydrodynamic load will allow the particle to deposit.

Einstein (1950) approach is based on a stable bed condition i.e. the rate of deposition must be equal to the rate of erosion. Accordingly the number of particles of size d eroded per unit time and unit bed area is calculated using the probability that any given particle will be eroded. At the same time the number of particles, which will be deposited per unit area and unit time, are calculated using the relationship with bed load discharge. He therefore correlates this erosion and deposition taking account into the lift force and submerged weight of the particles in order to get the bed load transport. According to Yang (1996), Einstein (1950) used three different graphical figures to compute the bed load.

Brown (1950) further developed the Einstein (1950) approach taking account into the Shields parameter θ (Equation 2.19) and the dimensionless characteristic sediment diameter d_* (Equation 2.8b) (Yang, 1996; SISYPHE, 2004). Einstein & Brown (1950) thus proposed the following equations for bed load (Equation 2.23):

$$\Phi_b = \frac{q_b}{\sqrt{g(s-1)d_{50}^{\ 3}}} = f_1(d_*) f_2(\theta)$$

$$f_1(d_*) = \left(\frac{2}{3} + \frac{36}{d_*}\right)^{0.5} - \left(\frac{36}{d_*}\right)^{0.5}$$

$$f_2(\theta) = 2.15\exp(-0.391/\theta) \qquad \theta \le 0.2$$

$$f_2(\theta) = 40\theta^3 \qquad \theta > 0.2 \tag{2.23}$$

SISYPHE (2004) recommends using the Einstein & Brown (1950) formula for fine to relatively coarse sediments in the range $0.2 < d_{50} < 3.0$ mm.

2.3.6.3 Engelund and Hansen (1967)

Bagnold (1966) was one of the first researchers to develop a sediment transport function from the stream power concept. Engelund & Hansen (1967) then applied Bagnold's approach and used the similarity principle to obtain their dimensionless total sediment transport load function (Φ_t). The energy-balance concept ($W_r = W_d$) is also considered taking account into the bed-form height and bed-form length. W_r is the work per unit time and width required to elevate the sediment load over a height equal to the bed-form height. W_d is the work per unit time and width done by the fluid on moving the particles over a length equal to the bed form length.

Engelund & Hansen (1967) used 100 sets of flume data combined with a critical Shields parameter of 0.06 (fine sand particles) to establish the relationship between the transport rate

and Shields parameter θ. Their formula calculates the "total load" q_t and can be expressed as (Van Rijn, 1993):

$$q_t = \frac{0.05U^5}{(s-1)^2 g^{0.5} d_{50} C_h^3} \tag{2.24a}$$

where U is the depth averaged velocity, s is the specific density, C_h is the Chezy-coefficient, g is the acceleration of gravity, and d_{50} is the median diameter of sediment particle. Equation 2.24a is the original sediment transport formulation as given by Engelund & Hansen (1967).

In order to achieve consistency with model formulations and bottom friction calculation, SISYPHE (2004) simplifies the original Engelund & Hansen (1967) formula in terms of non-dimensional transport rate Φ_t as:

$$\Phi_t = \frac{q_t}{\sqrt{g(s-1)d_{50}^3}} = 0.05\frac{\theta^{2.5}}{c_f} \tag{2.24b}$$

where the quadratic friction coefficient c_f can be computed using various coefficients given in SISYPHE (2004).

For an alluvial channel, Chollet & Cunge (1980) further modified the Engelund & Hansen (1967) formula in order to account for the effects of sand dune formation using dimensionless skin friction (SISYPHE, 2004). Based on the model validity tests, SISYPHE (2004) recommends using the Engelund & Hansen (1967) formula for fine sediments in the range $0.2 < d_{50} < 1.0$ mm.

2.3.6.4 Van Rijn (1984a)

Van Rijn (1984a) carried out 130 flume experiments with particle diameters, d_{50} ranging from 200 to 2000 μm, water depths larger than 0.1 m and a Froude number smaller than 0.9. The influence of side-wall roughness was eliminated by using the method of Vanoni & Nomicos (1959). He used a bed form factor to eliminate the form roughness caused by the bed form (Van Rijn, 1993). Using the dimensionless characteristics particle diameter d_* (Equation 2.8b) and excess shear stress parameter T_* (Equation 2.25c), the bed load is given as:

$$q_b = 0.053(s-1)^{0.5} g^{0.5} d_{50}^{1.5} T_*^{2.1} d_*^{-0.3} \qquad \text{for } T_* < 3 \tag{2.25a}$$

$$q_b = 0.053(s-1)^{0.5} g^{0.5} d_{50}^{1.5} T_*^{1.5} d_*^{-0.3} \qquad \text{for } T_* \geq 3 \tag{2.25b}$$

$$T_* = \frac{\theta}{\theta_c} - 1 \tag{2.25c}$$

where s is the specific gravity, g is the acceleration of gravity, ν is the kinematic viscosity θ is Shields parameter and θ_c is the critical Shields parameter.

2.4 An overview of numerical modelling

"I have no satisfaction in formulas unless
I feel their numerical magnitude"

- Attributed to Sir William Thomson (1824-1907) by Boyd (2000)

The previous sections have presented the concept of local scour and sediment transport. It is clear that both phenomena are strongly related to the hydrodynamic fields. It is therefore essential to model the hydrodynamic field. Computational Fluid Dynamics (CFD) is a widely used technique to model systems relating fluid flow, heat transfer and associated phenomena such as chemical reactions using computer-based simulation (Anderson, 1995; Versteeg & Malalasekera, 1995). In another words, CFD can be an engineer's attempt to extract the numerical magnitude of complex fluid flow equations (formulas) or material transport formulas by means of simulation using high speed computers. The evolution of CFD has, therefore, been progressing rapidly with the rapid growth of computer technology.

In CFD models, the basic fluid flow and transport equations are mathematically manipulated in order to get approximate solutions of different unknowns. Various techniques have been adopted to solve these equations e.g. Finite Difference (Anderson, 1995), Finite Volume (Versteeg & Malalasekera, 1995), Finite Element (Olsen, 1999; Balden, 2003; BIEF, 2004) and Spectral (Gottlieb & Orszag, 1977; Boyd, 2000; SIAM, 2004).

This section will present some of the mathematical concepts of fundamental fluid flow equations, which are solved using CFD model codes (i.e. TELEMAC system). An overview of the TELEMAC system is presented in Chapter 3. This section commences with brief overview of basic assumptions describing fluid flow followed by their mathematical description. At the end of the section, description on some of the common classical turbulence models is given relevant to this study.

2.4.1 Basic assumptions required for the modelling of fluid flow

Numerous assumptions have to be made to mathematically describe the fluid and related phenomena. These assumptions simplify the complex process into reasonable systems of fluid flow equations and enable their solution.

2.4.1.1 The fluid as a continuum

A fluid particle or a point in fluid may be considered as the smallest possible element of fluid whose macroscopic properties are not influenced by the individual molecules. The behaviour of such a fluid particle can be described in terms of the macroscopic properties; velocity, pressure, density and temperature, together with their space and time derivatives.

According to Pope (2000), the molecular structures of the fluid and its molecular motions may ignored in analyzing fluid flows in macroscopic length scales of say 1 μm and larger. The fluid can thus be regarded as a "continuum" or "continuous media". This concept is useful in defining fluid flow using the "fluid particles" or "infinitesimal fluid elements" (Versteeg & Malalasekera, 1995; Pope, 2000).

2.4.1.2 The coordinate system

It is convenient to adopt a coordinate system (Cartesian or Spherical) to describe the motion of fluids and its property such as density, temperature, pressure and velocity vector. In the interest of simplicity, a 3D Cartesian coordinate system is used here to describe flow phenomena (Figure 2.14).

In a unidirectional flow the x-axis generally is assumed to be a horizontal axis in the dominant direction of flow, whilst the y-axis is often assumed to be in the vertical direction. The z-axis is thus in the transverse direction. In the TELEMAC system, the z-axis is assumed in the vertical direction and y-axis in the transverse direction (TELEMAC-3D, 1998; BIEF, 2004).

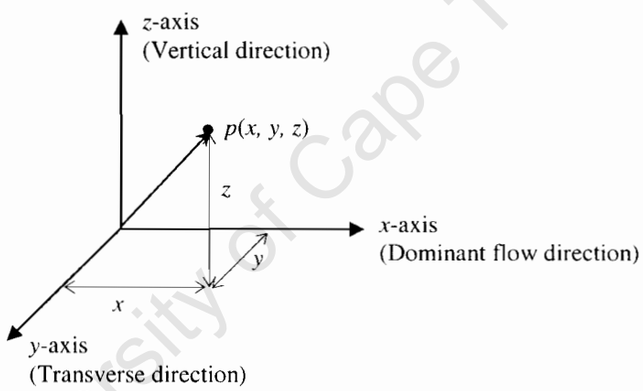

Figure 2.14: The three-dimensional Cartesian coordinate system

2.4.1.3 The velocity vector

The velocity vector can be defined as a function of its positions in Cartesian space (x, y, z) and time (t) and can be expressed as $u(x, y, z, t)$. If i, j and k are the unit vectors along the positive x-direction, y-direction and z-direction respectively, then the velocity vector field in the Cartesian space is given by:

$$\mathbf{u} = u\mathbf{i} + v\mathbf{j} + w\mathbf{k} \tag{2.26}$$

where u, v and w are the component of the velocity along the positive x-direction, y-direction and z-direction respectively.

2.4.1.4 The infinitesimal fluid element

The fluid element is infinitesimal in the same sense as differential calculus or continuum mechanics. It is however large enough to contain a huge number of molecules. For example, a volume as small as 1 $(\mu m)^3$ of water contains some $3x10^{10}$ molecules. An infinitesimal fluid element can be expressed with sides' δx, δy, and δz in view of continuous media (Figure 2.15). Such fluid element may be fixed in space with the fluid moving through it, or alternatively, it may be moving along a streamline with a velocity vector **u** (Anderson, 1995).

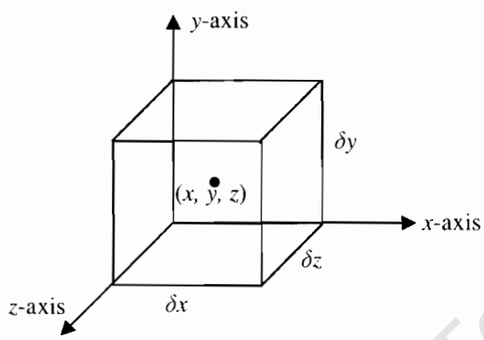

Figure 2-15: The infinitesimal fluid element

The fluid properties e.g. density, pressure, temperature and velocity are assumed to be concentrated at the center of the element at position x(x, y, z). Strictly speaking these properties are function of space and time i.e. $\rho(x, y, z, t)$, $p(x, y, z, t)$, $T(x, y, z, t)$ and u(x, y, z, t). The element under consideration is assumed to be sufficiently small so that the fluid properties at the faces can be expressed sufficiently accurately by the first two terms of a Taylor series expansion.

2.4.1.5 The forces on a fluid element

There are two distinct different types of forces acting on the fluid element (Anderson, 1995; Versteeg & Malalasekera, 1995):

(i) "Body forces" act directly on the volumetric mass of the fluid element. These forces "act at a distance" from the surface; examples are gravitational, centrifugal, coriolis and electromagnetic forces.

(ii) "Surface forces" act directly on the surface of the fluid element. These forces are due to; the pressure distribution imposed by the outside fluid surrounding the fluid element

that acts through normal stresses and the viscous shear distribution imposed by the outside fluid "tugging" or "pushing" on the surface by means of friction.

For simplicity the contributions due to the body forces are frequently lumped together as "source terms" whilst the contributions due to surface forces are considered separately. According to Versteeg & Malalasekera (1995), the state of stress of a fluid element can be defined in terms of pressure and nine viscous stresses components (shear and normal) τ_{ji} acting on a fluid element (or particle). The suffice *i* and *j* indicate that the stress component acts in the *i*-direction on a surface with a normal in the *j*-direction. Figure 2-16 illustrates the viscous stresses.

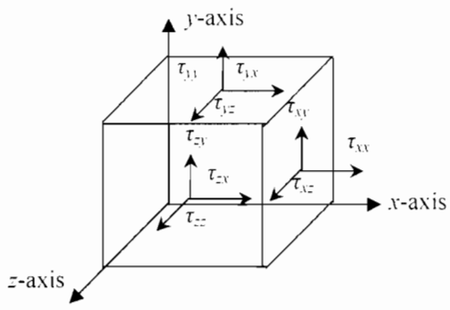

Figure 2-16: Viscous stress components acting on fluid element
(After Versteeg & Malalasekera, 1995)

The viscous stress components τ_{ji} depend on the velocity gradients (for example $\partial u/\partial x$) in the flow. According to Anderson (1995), the viscous normal stresses (such as τ_{xx}) are much smaller than the viscous shear stress and thus these stresses are often neglected in viscous flow analysis.

2.4.1.6 The Eulerian and Lagrangian approach

It is useful to describe that how numerical models deal with fluid motion and its properties. There are two different approaches; Eulerian and Lagrangian (White, 1991; Young et al., 1997; Pope, 2000).

The "Eulerian approach" analyzes the fluid motion through an infinitesimal "fluid element" or finite "control volume" that is fixed in space. This is the more common approach as the interest is usually in the variation of the physical properties (e.g. density, pressure, temperature and velocity) at a fixed point in space rather than those associated with a moving point. In this approach, the governing fluid flow equations are obtained directly from the infinitesimal fluid elements by applying fundamental principles (e.g. continuity, Newton's Second law, First law of thermodynamics) and are expressed in partial differential equation form. The fundamental principles can be applied to the finite control volume, in which the governing fluid flow equations can be obtained directly in integral equation form (Anderson, 1995). The Eulerian

approach gives rise to the so-called "conservative", "conservation" or "divergence" forms of the governing equations of fluid flow (Anderson, 1995; Versteeg & Malalasekera, 1995).

The "Lagrangian approach" tracks the physical properties (e.g. density, pressure, temperature and velocity) of a "fluid particle" as it moves through space by means of a fluid element or control volume or the fluid particle itself. In this approach, the governing fluid flow equations are obtained directly from the infinitesimal fluid element by applying fundamental principles are in partial differential equation form. These principles can also be applied to the finite control volume in order to get the equation either integral equation form or partial differential equation form (Anderson, 1995). The Lagrangian approach gives rise to the so-called "non-conservative", "non-conservation" forms of the governing equations of fluid flow (Anderson, 1995; Versteeg & Malalasekera, 1995).

The Eulerian approach was used in this study.

2.4.1.7 The material derivative

The material derivative is used to describe the changes of properties of a "fluid particle". Any property ϕ of a particle (per unit mass) is usually a function of its position $x(x, y, z)$ and time t. The rate of change of this property ϕ of a particle with respect to time t, $D\phi/Dt$, is called the "material", "particle" (White, 1991), "total", "substantive", "substantial" (Anderson, 1995; Versteeg & Malalasekera, 1995) or "absolute" (Chanson, 1999) derivative. It can be presented mathematically by Eulerian or Lagrangian approach using a Taylor series expansion ignoring the higher-order terms or using the chain rule from differential calculus as:

$$\frac{D\phi}{Dt} = \frac{d\phi}{dt} = \frac{\partial\phi}{\partial t} + \frac{\partial\phi}{\partial x}\frac{dx}{dt} + \frac{\partial\phi}{\partial y}\frac{dy}{dt} + \frac{\partial\phi}{\partial z}\frac{dz}{dt} \tag{2.27}$$

Since a fluid particle follows the streamline path, $dx/dt = u$, $dy/dt = v$ and $dz/dt = w$, and therefore:

$$\frac{D\phi}{Dt} = \frac{d\phi}{dt} = \frac{\partial\phi}{\partial t} + u\frac{\partial\phi}{\partial x} + v\frac{\partial\phi}{\partial y} + w\frac{\partial\phi}{\partial z} = \frac{\partial\phi}{\partial t} + \mathbf{u}\bullet\nabla\phi = \frac{\partial\phi}{\partial t} + \mathbf{u}\bullet grad\phi \tag{2.28}$$

where ∇ is the vector operator, which is also read as "*grad*". According to Anderson (1995), the term $\partial\phi/\partial t$ in Equation 2.28 is called "local derivative", which physically is the time rate of change of any property ϕ at a fixed point (or fluid element). The term $\mathbf{u}\bullet\nabla\phi$ or $\mathbf{u}\bullet grad\phi$ is the "convective derivative", which is physically the time rate of change of any property ϕ due to the movement of the fluid element from one location to another in the flow field where properties are spatially different.

It is important to note that $D\phi/Dt$ indicates the rate of change of a property ϕ per unit mass. This must be multiplied by the density of a fluid ρ to obtain the rate of change of any property ϕ per unit volume. The rate of change of the property ϕ per unit volume of a fluid element is thus given by:

$$\rho\frac{\partial\phi}{\partial t} = \rho\frac{D\phi}{Dt} - \mathbf{u}\bullet\nabla(\rho\phi) \tag{2.29}$$

In other words, the material derivative states that the rate of increase of any property ϕ of a "fluid element" per unit volume is equal to the rate of increase of any property ϕ for a "fluid particle" (moving through the element) per unit volume, minus the net rate of flow of ϕ out of the "fluid element" per unit volume. The momentum and energy equations are derived using material derivative concept (Section s 2.4.3 and 2.4.4).

2.4.2 The mass conservation equation

The mass conservation derives from the concept of continuity in physics and states, *"The rate of increase of mass in fluid element is equal to the net rate of flow of mass into the fluid element."*

Consider an infinitesimal fluid element of sides; *dx*, *dy* and *dz* fixed in space as shown in the Figure 2.17 (Eulerian approach).

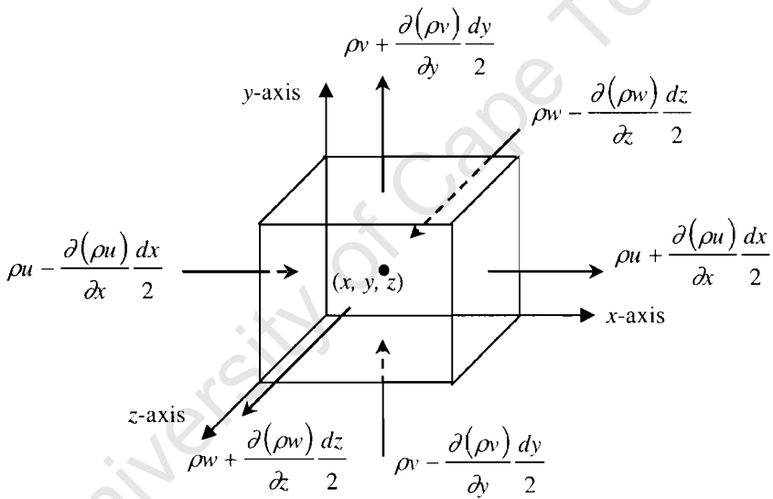

Figure 2.17: Mass flow in and out of fluid element

The rate of increase of mass in fluid element per unit element volume is $\partial\rho/\partial t$. The net rate of flow of mass per unit element volume into the element across its faces (Figure 2-17) can be expressed as; $\partial(\rho u)/\partial x + \partial(\rho v)/\partial y + \partial(\rho w)/\partial z$, where u, v and w is the velocity along x, y and z directions respectively.

In a compressible fluid, the unsteady 3D mass conservation equation can be written as (Anderson, 1995; Versteeg & Malalasekera, 1995):

$$\frac{\partial \rho}{\partial t}+\frac{\partial(\rho u)}{\partial x}+\frac{\partial(\rho v)}{\partial y}+\frac{\partial(\rho w)}{\partial z}=0\text{, or }\frac{\partial \rho}{\partial t}+div(\rho \mathbf{u})=0 \tag{2.30}$$

For an incompressible fluid of constant density ρ, $\partial\rho/\partial t = 0$, Equation 2.30 can therefore be recast as:

$$\frac{\partial u}{\partial x}+\frac{\partial v}{\partial y}+\frac{\partial w}{\partial z}=0\text{, or }div(\mathbf{u})=0 \tag{2.31}$$

2.4.3 The momentum and Navier-Stokes equations

The momentum equation is based on the Newton's second law and states, *"The rate of increase of momentum of fluid particle is equal to the sum of forces on fluid particle."*

Using the concept of material derivative, the rate of increase of x-momentum, y-momentum and z-momentum per unit volume of a fluid particle are given by $\rho(Du/Dt)$, $\rho(Dv/Dt)$, and $\rho(Dw/Dt)$ respectively (Section 2.4.1.7).

Figure 2-18 illustrates only the x-components of the surface forces (using Taylor series neglecting higher-order terms) due to pressure p and the shear stresses τ_{xx}, τ_{yx} and τ_{zx} components. Similar diagrams can be constructed for the y- and z-components of the surface forces.

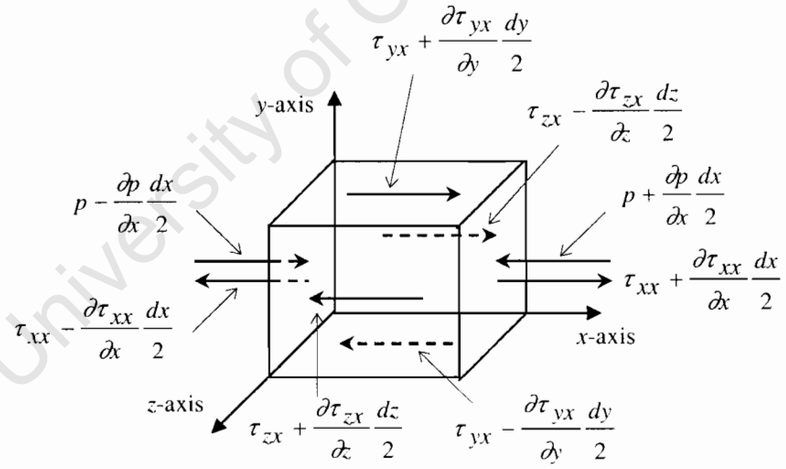

Figure 2-18: The surfaces forces acting on a fluid particle in the x-direction

The body force is described by the vector $\mathbf{S_M}$ lumping together all momentum source terms in a fluid particle per unit volume per unit time. The S_{Mx}, S_{My} and S_{Mz} are the components of $\mathbf{S_M}$ in the x- y- and z-direction respectively.

The resultant surface force in the x-direction per unit volume on a fluid particle can therefore be described as (Versteeg & Malalasekera, 1995):

$$\frac{\partial(-p+\tau_{xx})}{\partial x}+\frac{\partial \tau_{yx}}{\partial y}+\frac{\partial \tau_{zx}}{\partial z} \tag{2.32}$$

The overall effect of the body forces in the x-direction can be included in Equation 2-32 adding source S_{Mx} (x-momentum per unit volume per unit time).

The x-component of the so-called momentum equation can be therefore established by equating the rate of change of x-momentum of the fluid particle equal to the total force in the x-direction on the element due to the surface forces plus the rate of increase of x-momentum due to sources as (Versteeg & Malalasekera, 1995):

$$\rho\frac{Du}{Dt}=\frac{\partial(-p+\tau_{xx})}{\partial t}+\frac{\partial \tau_{yx}}{\partial y}+\frac{\partial \tau_{zx}}{\partial z}+S_{Mx} \tag{2.33a}$$

Similarly, "y-component of the "momentum equation" and "z-component of the "momentum equation" can be derived respectively as:

$$\rho\frac{Dv}{Dt}=\frac{\partial \tau_{xy}}{\partial x}+\frac{\partial(-p+\tau_{yy})}{\partial y}+\frac{\partial \tau_{zy}}{\partial z}+S_{My} \tag{2.33b}$$

$$\rho\frac{Dw}{Dt}=\frac{\partial \tau_{xz}}{\partial x}+\frac{\partial \tau_{yz}}{\partial y}+\frac{\partial(-p+\tau_{zz})}{\partial z}+S_{Mz} \tag{2.33c}$$

The sign associated with pressure p is opposite to that related to normal viscous stress because the usual sign convention assumes the tensile stress to be a positive normal stress. If gravity is the only body force, S_{Mx}, = 0 and S_{My} = 0, whilst $S_{Mz} = \rho\mathbf{g}$ where $\mathbf{g}$ is the gravity vector.

It is clear that the momentum equations contain unknowns the viscous stress τ_{ji}. For simplification, the calculation of these stresses is usually based on a Newtonian fluid, where viscous stresses are proportional to the rates of deformation. Further assumptions are the "incompressibility" and "isotropic" nature of a Newtonian fluid, Schlichting (1979) shows that

the rate of linear deformation of a fluid element has nine components in three dimensions, six of which are independent.

The "Navier-Stokes" equations express these unknown viscous stresses in terms deformation rates and proportionality constants. Taking account mass conservation, the nine viscous components for incompressible fluids can be expressed in terms of dynamic viscosity μ and deformation rate (Versteeg & Malalasekera, 1995):

$$\tau_{xx} = 2\mu\frac{\partial u}{\partial x} \qquad \tau_{yy} = 2\mu\frac{\partial v}{\partial y} \qquad \tau_{zz} = 2\mu\frac{\partial w}{\partial z}$$
$$\tau_{xy} = \tau_{yx} = \mu\left(\frac{\partial u}{\partial y} + \frac{\partial v}{\partial x}\right) \quad \tau_{xz} = \tau_{zx} = \mu\left(\frac{\partial u}{\partial z} + \frac{\partial w}{\partial x}\right) \quad \tau_{yz} = \tau_{zy} = \mu\left(\frac{\partial v}{\partial z} + \frac{\partial w}{\partial y}\right) \tag{2.34}$$

Substituting Equation 2.34 in the momentum equations (Equation 2.33a, 2.33b and 2.33c), a generic fluid flow equation can be recast in indicial notation (White, 1991) and general form (Versteeg & Malalasekera, 1995):

$$\rho\frac{D\mathbf{u}}{Dt} = -\nabla p + \frac{\partial}{\partial x_j}\left[\mu\left(\frac{\partial u_i}{\partial x_j} + \frac{\partial u_j}{\partial x_i}\right)\right] + \mathbf{S}_M \quad \text{- Indicial notation}$$
$$\frac{\partial u}{\partial t} + div(u\mathbf{u}) = -\frac{1}{\rho}\frac{\partial p}{\partial x} + \nu\, div\, grad(u) + S_{Mx}$$
$$\frac{\partial v}{\partial t} + div(v\mathbf{u}) = -\frac{1}{\rho}\frac{\partial p}{\partial x} + \nu\, div\, grad(v) + S_{My} \quad \text{- General form}$$
$$\frac{\partial w}{\partial t} + div(w\mathbf{u}) = -\frac{1}{\rho}\frac{\partial p}{\partial x} + \nu\, div\, grad(w) + S_{Mz}$$
(2.35)

Equation 2.35 is popularly known as the "Navier-Stokes" equations for an incompressible Newtonian fluid in three dimensions (i=1, 2, 3 and j=1, 2, 3). It should be noted that, generally, the kinematic viscosity $\nu = \mu/\rho$ or absolute viscosity μ varies with temperature, pressure and position. In a numerical model, the effective viscosity is generally calculated using a turbulence model (Section 2.4.7.1, Equation 2.60c).

2.4.4 The energy equations

The energy equation is derived from the first law of thermodynamics and states, *"the rate of change of energy of a fluid particle is equal to the rate of heat transfer to the fluid particle plus the rate of work done on the fluid particle"*

Using the concept of material derivative, the rate of increase of energy of a fluid particle per unit volume is given by $\rho(DE/Dt)$ (Section 2.4.1.7).

The rate of the rate of work done on the fluid particle per unit volume in the element due to surface force is equal to the product of the forces and velocity component in the relevant direction of the force divided by the volume of the element. Accordingly the rates of work done due to surface forces acting along x-, y- and z-direction are respectively (Versteeg & Malalasekera, 1995):

$$\frac{\partial[u(-p+\tau_{xx})]}{\partial x}+\frac{\partial(u\tau_{yx})}{\partial y}+\frac{\partial(u\tau_{zx})}{\partial z} \tag{2.36a}$$

$$\frac{\partial(v\tau_{xy})}{\partial x}+\frac{\partial[v(-p+\tau_{yy})]}{\partial y}+\frac{\partial(v\tau_{zy})}{\partial z} \tag{2.36b}$$

$$\frac{\partial(w\tau_{xz})}{\partial x}+\frac{\partial(w\tau_{yz})}{\partial y}+\frac{\partial[w(-p+\tau_{zz})]}{\partial z} \tag{2.36c}$$

Figure 2-19 illustrates the heat transfer into the fluid element, where q_x, q_y and q_z are the components of the heat flux vector **q.**

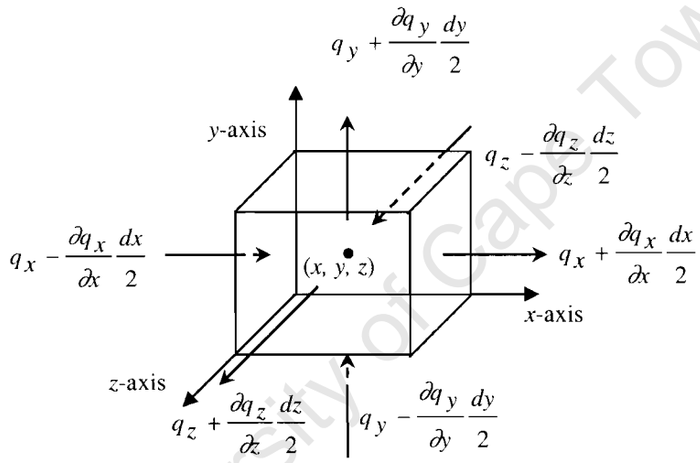

Figure 2-19: The heat transfer to a fluid particle

The total rate of heat added to the fluid particle per unit volume due to heat flow across its boundaries can be derived as (Versteeg & Malalasekera, 1995):

$$-\frac{\partial q_x}{\partial x}-\frac{\partial q_y}{\partial y}-\frac{\partial q_z}{\partial z}=-div\mathbf{q} \tag{2.37}$$

According to the Fourier's law of heat conduction, this relates the heat flux to the local temperature gradient:

$$q_x = -k_T \frac{\partial T}{\partial x}, \qquad q_y = -k_T \frac{\partial T}{\partial y} \qquad q_z = -k_T \frac{\partial T}{\partial z} \tag{2.38}$$

where k_T is the coefficient of thermal conductivity and T is the temperature. Equation 2.38 can be recast to the vector form as:

$$\mathbf{q} = -k_T grad T \tag{2.39}$$

Equations 2.37 and 2.39 can be combined to give the total rate of heat addition to the fluid particle per unit volume due to heat conduction across element boundaries:

$$-div\mathbf{q} = div(k_T grad T) \tag{2.40}$$

If S_E is the energy source term per unit volume per unit time, the energy equation can be represented by:

$$\rho \frac{DE}{Dt} = -div(p\mathbf{u} + \frac{\partial(u\tau_{xx})}{\partial x} + \frac{\partial(u\tau_{yx})}{\partial y} + \frac{\partial(u\tau_{zx})}{\partial z} + \frac{\partial(v\tau_{xy})}{\partial x} + \frac{\partial(v\tau_{yy})}{\partial y} + \frac{\partial(v\tau_{zy})}{\partial z} + \frac{\partial(w\tau_{xz})}{\partial x} + \frac{\partial(w\tau_{yz})}{\partial y} + \frac{\partial(w\tau_{zz})}{\partial z} + div(k_T grad T) + S_E \tag{2.41}$$

The specific energy E is defined as the sum of internal energy i and the kinetic energy $(u^2 + v^2 + w^2)/2$ e.g. $E = i + (u^2 + v^2 + w^2)/2$.

2.4.4.1 The rate of change of kinetic energy equation

It is common practice to extract the changes of the kinetic (mechanical) energy to obtain an equation for internal energy *i* or temperature *T*. The rate of change of kinetic energy of a fluid particle per unit volume of a fluid element can be found by multiplying the *x*-momentum equation by velocity component *u*, the *y*-momentum equation by *v* and *z*-momentum equation by *w* and adding the results together.

The equation of the rate of change of kinetic energy of a fluid particle is (Versteeg & Malalasekera, 1995):

$$\rho\frac{D\left[\frac{1}{2}\left(u^2+v^2+w^2\right)\right]}{Dt} = -\mathbf{u}\bullet grad\, p + u\left(\frac{\partial\tau_{xx}}{\partial x}+\frac{\partial\tau_{yx}}{\partial y}+\frac{\partial\tau_{zx}}{\partial z}\right) + v\left(\frac{\partial\tau_{xy}}{\partial x}+\frac{\partial\tau_{yy}}{\partial y}+\frac{\partial\tau_{zy}}{\partial z}\right)+w\left(\frac{\partial\tau_{xz}}{\partial x}+\frac{\partial\tau_{yz}}{\partial y}+\frac{\partial\tau_{zz}}{\partial z}\right)+\mathbf{u}\bullet S_M \tag{2.42}$$

In other words, the rate of change of the kinetic energy of a fluid particle depends on the energy lost during work done against the pressure gradient plus the energy gained from the work done through the shear gradient plus the work done by the body forces.

2.4.4.2 The rate of change of internal energy and temperature equations

The equation for the rate of change of the internal energy for a fluid particle per unit volume of a fluid element can be derived by subtracting Equation 2.42 from Equation 2.41, defining a new source term $S_i = S_E - \mathbf{u}\bullet\mathbf{S}_M$ and can be written as (Versteeg & Malalasekera, 1995):

$$\rho\frac{Di}{Dt} = -p\, div\mathbf{u} + div(k\, grad\, T) + \tau_{xx}\frac{\partial u}{\partial x}+\tau_{yx}\frac{\partial u}{\partial y}+\tau_{zx}\frac{\partial u}{\partial z} + \tau_{xy}\frac{\partial v}{\partial x}+\tau_{yy}\frac{\partial v}{\partial y}+\tau_{zy}\frac{\partial v}{\partial z}+\tau_{xz}\frac{\partial w}{\partial x}+\tau_{yz}\frac{\partial w}{\partial y}+\tau_{zz}\frac{\partial w}{\partial z}+S_i \tag{2.43}$$

In the case of an incompressible fluid, $i = cT$ and $div\mathbf{u} = 0$, where c is the specific heat of the fluid.

The effects due to viscous stresses in the internal energy Equation 2.43 can be replaced by the "dissipation function", Φ (White, 1991; Versteeg & Malalasekera, 1995). In the other words, using indicial notation:

$$\Phi = \tau_{ji}\frac{\partial u_i}{\partial x_j} \tag{2.44}$$

In the case of incompressible Newtonian fluid, after considerable algebra and the use of shear stress relationship with rate of deformation (Equation 2.34), the Φ can be written as (White, 1991; Versteeg & Malalasekera, 1995):

$$\Phi = \mu_t\left[2\left\{\left(\frac{\partial u}{\partial x}\right)^2+\left(\frac{\partial v}{\partial y}\right)^2+\left(\frac{\partial w}{\partial z}\right)^2\right\}+\left(\frac{\partial u}{\partial y}+\frac{\partial v}{\partial x}\right)^2+\left(\frac{\partial u}{\partial z}+\frac{\partial w}{\partial x}\right)^2+\left(\frac{\partial v}{\partial z}+\frac{\partial w}{\partial y}\right)^2\right] \tag{2.45}$$

where μ_t is the sum of laminar and turbulent viscosities. In indicial notation (White, 1991):

$$\Phi = \mu_t \left(\frac{\partial u_i}{\partial x_j} + \frac{\partial u_j}{\partial x_i} \right) \frac{\partial u_i}{\partial x_j} \tag{2.46}$$

Yang & Song (1979) developed the dissipation function Φ from a consideration of the Reynolds modification of the Navier-Stokes equations of motion for incompressible fluids (section 2.4.7). In the case of gradually varied steady open channel flows for which the Froude number is not too large, they give:

$$\Phi = \frac{1}{2} \rho (\upsilon + \varepsilon_{(t)}) \left(\frac{\partial u_i}{\partial x_j} + \frac{\partial u_j}{\partial x_i} \right)^2 \tag{2.47}$$

Where $\varepsilon_{(t)}$ is the average turbulent kinematic viscosity defined in terms of an average turbulent dynamic viscosity, $\mu_{(t)}$ as:

$$\varepsilon_{(t)} = \frac{\mu_{(t)}}{\rho} \tag{2.48}$$

Noting that the total kinematic viscosity is the sum of the viscous and turbulent kinematic viscosities, it is clearly shown that Equation 2.47 can be rewritten as Equation 2.45 or 2.46 with μ_t representing the total viscosity. Equation 2.43 may now be rewritten in terms of dissipation function Φ as follows:

$$\rho \frac{Di}{Dt} = \Phi + div\,(k_T\, grad\, T) \tag{2.49}$$

The rate of change of the internal energy of a fluid element is obtained by combining Equation 2.29 and Equation 2.49 and can be recast as:

$$\rho \frac{\partial i}{\partial t} = \Phi + div\,(k_T\, grad\, T) - \rho(\mathbf{u} \bullet grad\, i) \tag{2.50a}$$

$$\text{Since } i = cT \text{, therefore, } \rho\frac{\partial i}{\partial t} = \Phi + div\,(k_T\, grad\, T) - \rho(\mathbf{u} \bullet grad\, cT) \tag{2.50b}$$

In other words, for a fixed element, the internal energy can also be transported into or out of the element by the flow of fluid through it. In incompressible fluids, Equation 2.43 can be recast as a rate of change of temperature of fluid particle per unit volume of a fluid element as (Versteeg & Malalasekera, 1995):

$$\rho c\frac{DT}{Dt} = div(k\ grad\, T) + \tau_{xx}\frac{\partial u}{\partial x} + \tau_{yx}\frac{\partial u}{\partial y} + \tau_{zx}\frac{\partial u}{\partial z} + \tau_{xy}\frac{\partial v}{\partial x} + \tau_{yy}\frac{\partial v}{\partial y} + \tau_{zy}\frac{\partial v}{\partial z} + \tau_{xz}\frac{\partial w}{\partial x} + \tau_{yz}\frac{\partial w}{\partial y} + \tau_{zz}\frac{\partial w}{\partial z} + S_i \tag{2.51}$$

2.4.5 The general fluid flow equations

It can be noticed that there are significant commonalities between the various equations derived from fundamental principles of fluid flow i.e. mass conservation, momentum and energy. If ϕ is a general variable, the conservative form of all fluid flow equations, including equations for scalar quantities such as temperature and pollutant concentration etc., can be written in the following form (Versteeg & Malalasekera, 1995):

$$\frac{\partial(\rho\phi)}{\partial t} + div(\rho\phi\mathbf{u}) = div(\Gamma grad\phi) + S_\phi \tag{2.52}$$

where Γ is diffusion coefficient. In words Equation 3.32 states that the sum rate of increase of ϕ of fluid element plus the net rate of flow of ϕ out of fluid element is equal to the sum of the rate of increase of ϕ due to diffusion plus rate of increase of ϕ due to sources.

Equation 2.52 is also known as so-called "differential" or "conservative" form of transport or fluid flow equation (advection-diffusion) for any property ϕ. It clearly highlights the various transport process; the ***rate of change*** term and the ***convective*** term respectively on the left hand side and the ***diffusive*** term and the ***source*** term respectively on the right hand side. In the CFD solution, the convective term is often "hyperbolic" in nature, which is a marching problem without significant dissipation. On the other hand, the diffusive term is "parabolic" in nature, which is a marching problem with significant dissipation (Anderson, 1995; Versteeg & Malalasekera, 1995).

2.4.6 The turbulence and energy spectrum

Turbulence is a complex phenomenon of unsteady and random fluid flow, which occurs at higher Reynolds numbers and is very difficult to model. Flow exhibiting turbulence is often called turbulent flow and has numerous characteristic features (Pope, 2000; Davidson, 2003; Chadwick et al, 2004). Typical examples are boundary layers (French, 1994; Armitage & McGahey, 2003) and the wakes around and after bluff bodies such as cars, aeroplanes, buildings and bridge piers (Versteeg & Malalasekera, 1995; Melville & Coleman, 2000; Davidson, 2003). The coherent structures within a turbulent flow field are frequently termed loosely as turbulent "eddies" (Wilcox, 2000; Yalin & Da Silva, 2001).

Figure 2-20 depicts the velocity in a turbulent flow with respect to time. The magnitude of the fluctuation may be based upon the root-mean-square of the component of $\mathbf{u}'$ i.e. $\sqrt{\overline{u'^2}}$. This measure is often known as the 'intensity of turbulence', which can be expressed as $\sqrt{\overline{u'^2}}/u$ (Versteeg & Malalasekera, 1995; Chadwick et al, 2004). According Van Rijn (1993), the turbulent flow field highly depends on their statistical quantities such as root-mean-square values, amplitude distribution, correlation and spectra.

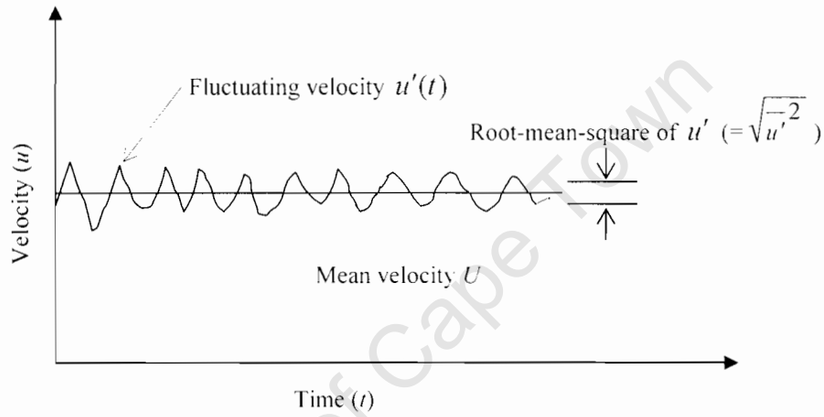

Figure 2-20: A typical point velocity in a turbulent flow
(After Chadwick et al, 2004)

Turbulent flow exhibits rotational flow structures of turbulent eddies (bursts), which have a wide range of length scales. A typical flow domain of dimensions 0.1m x 0.1m x 0.1m with high Reynolds number turbulent flow might contain eddies (bursts) down to scale 10 to 100 μm. According to Versteeg & Malalasekera (1995), in a fully developed turbulent flow, 10^{15} eddies may be present in a 1m x 1m x 1m flow domain. The larger scales are of the order of the flow geometry such as boundary layer thickness. Often a length scale ℓ and a velocity scale ϑ are used to represent the large scale turbulence (Versteeg & Malalasekera, 1995). The "large eddy" Reynolds number $(\ell\vartheta/\nu)$ is calculated using these scales in turbulent flows. The large eddies are dominated by inertia effects, whereas viscous effects are negligible.

The smaller scales (eddies) are themselves stretched strongly by larger eddies and more weakly by the mean flow. As a consequence a "small eddy" gains kinetic energy from a slightly "large eddy" when they interact with them. Such course of action continues in an energy cascade process. As a result small scale eddies are dominated by viscous forces (stresses) and hence viscosity. As work is done against the action of viscous stresses, the energy associated with the eddy motions is finally dissipated and converted into thermal internal energy (Versteeg & Malalasekera, 1995). The dissipation is denoted by ε, which indicates energy loss per unit mass per unit time.

The viscous stresses exist at all scales, however, their magnitude are larger with the smaller eddies. Eddies receiving kinetic energy from slightly larger scales do not give away all of it to the slightly smaller scales; a small fraction is dissipated. Nevertheless it is assumed that most of the energy i.e. 90 % that goes into the large scales is finally dissipated at the smallest (dissipative) scales (Davidson, 2003). The smallest scales where dissipation occurs are called the Kolmogorov scales characterised by the characteristic velocity scale υ, the characteristic length scale η and the characteristic time scale Γ (Pope, 2000).

2.4.6.1 The energy spectrum

The turbulent kinetic energy (per unit mass) can be expressed by summing the kinetic energy due to the three fluctuating velocity components e.g. u' v' and w' (Versteeg & Malalasekera, 1995; Pope, 2001):

$$k = \frac{1}{2}\left(\overline{u'^2} + \overline{v'^2} + \overline{w'^2}\right) = \frac{1}{2}\overline{u_i' u_i'} \tag{2.53}$$

According to Pope (2001) and Wilcox (2000), the energy spectrum function $E(\kappa)$ is a function of the wave number λ. The wave number λ is simply the inverse of turbulent length scales (large or Kolmogorov scales). Davidson (2003) shows that the total turbulent kinetic energy can be obtained by integrating $E(\lambda)d\lambda$ over the whole wave number space:

$$k = \int_0^\infty E(\lambda)d\lambda \tag{2.54}$$

Figure 2-21 illustrates the energy spectrum function $E(\lambda)$ varying with wave number λ. It clearly shows three distinct regions; the energy containing range, the inertial sub-range and the dissipation range.

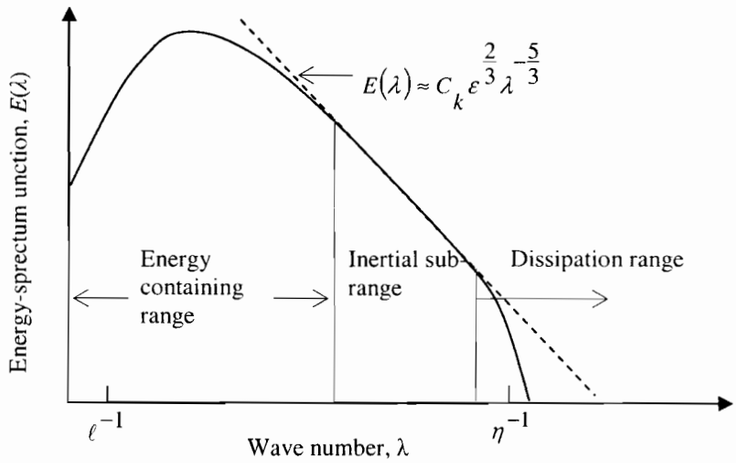

Figure 2-21: Variation of the energy spectrum function
(After Wilcox, 2000)

The "energy-containing range" has large eddies which carry most of the energy by interacting and extracting energy from the mean flow U. The energy of this range is passed onto the slightly smaller eddies at the upper end of the "inertial sub-range". Generally, in this range, the eddy scales are large. According to Davidson (2003), these eddies extract kinetic energy from the mean flow. If the time scale is given by $(=\ell/\vartheta)$, then the velocity gradient may be estimated from:

$$\frac{\partial U}{\partial y} \propto \frac{1}{(\ell/\vartheta)} \tag{2.55}$$

According to Davidson (2003), the "inertial sub-range" can be considered as the main "transport region" in the cascade process, which is the progressive transfer of kinetic energy from larger eddies to smaller eddies. The Reynolds numbers are generally high in this region. The dissipation energy per unit time (ε) is transferred from the large eddies at the lower part of this range to the "dissipation range" at the higher part (Figure 2-21). Eddies in this region are independent of both energy containing eddies and eddies in the dissipation range. The energy spectrum of this range can be expressed as (Pope, 2000; Wilcox, 2000; Davidson, 2003):

$$E(\lambda) = C_k \varepsilon^{\frac{2}{3}} \lambda^{-\frac{5}{3}} \tag{2.56}$$

Equation 2.56 is popularly known as "Kolmogorov spectrum law" (Pope, 2000; Wilcox, 2000), where C_k=1.5 (Pope, 2000) is the universal Kolmogorov constant, ε is the dissipated energy and λ is the wave number. The relationship clearly indicates that for a fully developed

turbulent flow (high Reynolds number), the energy spectra should exhibit a $-5/3$ power decay. This concept is often used in Large Eddy Simulations (LES) and Direct Numerical Simulations (DNS) of turbulent flow (Wilcox, 2000). Further details can be found in Wilcox (2000) and Pope (2000).

The "dissipation range" has smaller eddies and their motion is isotropic. In this range, dissipation occurs and the scales of eddies are described by the Kolmogorov scales. The energy dissipated i.e. ε at the small scales can be estimated using the large length scale ℓ and large velocity scale ϑ as (Pope, 2000; Davidson, 2003):

$$\varepsilon \propto \frac{\vartheta^2}{(\ell/\vartheta)} \propto \frac{\vartheta^3}{\ell} \tag{2.57}$$

2.4.7 Turbulence modelling

Turbulence modelling describes the numerical techniques used to calculate the impact of turbulence on the Navier-Stokes equations (Equation 2.35) or the Reynolds equations (Equation 2.58). The Reynolds equations consider the influence of turbulent fluctuations on the mean flow **U** (with U, V and W are the components along x-, y- and z-directions). In a Cartesian co-ordinate system, these can be derived from instantaneous continuity (i.e. $div\mathbf{U} = 0$) and Navier-Stokes equations (Equation 2.35) for an incompressible flow with constant viscosity.

$$\begin{aligned}
\frac{\partial U}{\partial t} + div(U\mathbf{U}) &= -\frac{1}{\rho}\frac{\partial P}{\partial x} + \nu div\, grad\, U + \left[-\frac{\partial \overline{u'^2}}{\partial x} - \frac{\partial \overline{u'v'}}{\partial y} - \frac{\partial \overline{u'w'}}{\partial z} \right] \\
\frac{\partial V}{\partial t} + div(V\mathbf{U}) &= -\frac{1}{\rho}\frac{\partial P}{\partial y} + \nu div\, grad\, V + \left[-\frac{\partial \overline{u'v'}}{\partial x} - \frac{\partial \overline{v'^2}}{\partial y} - \frac{\partial \overline{v'w'}}{\partial z} \right] \\
\frac{\partial W}{\partial t} + div(W\mathbf{U}) &= -\frac{1}{\rho}\frac{\partial P}{\partial z} + \nu div\, grad\, W + \left[-\frac{\partial \overline{u'w'}}{\partial x} - \frac{\partial \overline{v'w'}}{\partial y} - \frac{\partial \overline{w'^2}}{\partial z} \right]
\end{aligned} \tag{2.58}$$

The main difficulties with turbulence models arise from the non-linear convective term in the Navier-Stokes equations, and much more so from the pressure-gradient term, which is both non-linear and non-local (Pope, 2000).

According to Versteeg & Malalasekera (1995), the close set of Navier-Stokes equations with mass conservation cannot be solved in a foreseeable way economically. Further introduction of the fluctuation terms in the Navier-Stokes equations further complicates the scenario, which is resolved by introducing additional "Reynolds stress" terms given in Equation 2.59.

$$\tau_{xx} = -\rho\overline{u'^2} \qquad \tau_{yy} = -\rho\overline{v'^2} \qquad \tau_{zz} = -\rho\overline{w'^2}$$
$$\tau_{xy} = \tau_{yx} = -\rho\overline{u'v'} \quad \tau_{xz} = \tau_{zx} = -\rho\overline{u'w'} \qquad \tau_{yz} = \tau_{zy} = -\rho\overline{v'w'} \tag{2.59}$$

The complexity of turbulence usually precludes simple formulae for the extra stress and turbulent scalar terms. The challenge in the modelling of turbulence is to develop computational procedure of sufficient accuracy and generality for engineers to predict the Reynolds stresses and the scalar transport terms. Various techniques have been developed over the last few decades. Based on accuracy and computation costs those can be read in order as; Direct Numerical Simulation (DNS), Large or Very Large Eddy Simulation (LES or VLES), Reynolds Stress Model (RSM), Algebraic Stress Model (ASM), k-ω Model, k-ε Model, Mixing Length Model and Constant Viscosity model. Details of those can be found in Versteeg & Malalasekera (1995), Wilcox (2000), Pope (2001) and Hoffman & Johnson (2003). Some of the details of k-ε Model, which was used in this study, are discussed hereafter.

2.4.7.1 The k-ε model

The basic form of k-ε model is developed by manipulating both the Navier-Stokes equations (Equation 2.35) and the Reynolds equations (Equation 2.58 and Equation 2.59) and adding two extra equations for the turbulent kinetic energy and its dissipation (Versteeg & Malalasekera, 1995; Pope, 2000; TELEMAC-2D, 2001). The fundamental concepts of kinetic energy and their dissipation are discussed in the Section 2.4.6.

The two equations obtained cannot be solved economically because of their non-closure nature. Many researchers (Launder & Spalding, 1974; Bradshaw et al, 1981; Yakhot & Orszag, 1986, Shih et al, 1995; Analytis, 2003) have therefore further simplified the form of $k-\varepsilon$ governing equations to yield simple solution techniques. Hrenya et al (1998), Iyer et al (1999), Costa et al (1999), Cheng et al (2003), Salaheldin et al (2004), Wang & Mujumder (2005) report comparative studies of these different $k-\varepsilon$ turbulence models, which show that the $k-\varepsilon$ model has been validated against a wide range of physical data.

Some of the popular $k-\varepsilon$ models adopted in the various CFD software are the "Standard $k-\varepsilon$ model" (Launder & Spalding, 1974; Versteeg & Malalasekera, 1995), the "RNG $k-\varepsilon$ model" (Yakhot & Orszag, 1986; Analytis, 2003) and the "Realizable $k-\varepsilon$ model" (Shih et al, 1995). Among these, the Standard $k-\varepsilon$ model proposed by Launder & Spalding (1974) is popular because of its robustness (Versteeg & Malalasekera, 1995; McGahey, 2001; Salaheldin, 2004).

The TELEMAC system adopts the model originally presented by Launder & Spalding (1974). According to TELEMAC-2D (2001), the vertically averaged k and ε can be expressed as:

$$k = \frac{1}{h}\int_{zf}^{z} \frac{1}{2}\overline{u_i' u_j'}\, dz \quad \text{, where } (i = 1 \text{ to } 3)$$

$$\varepsilon = \frac{1}{h}\int_{zf}^{z} \frac{\nu_t}{2}\overline{\frac{\partial u_i'}{\partial x_j}\frac{\partial u_i'}{\partial x_j}}\, dz \text{, where } (i = 1 \text{ to } 3 \text{ and } j = 1 \text{ to } 3)$$

(2.60a)

The closing is done by the hypothesis of Boussinesq (Versteeg & Malalasekera, 1995), which expresses the Reynolds tensor (R_{ij}) as a function of the mean velocity gradient.

$$R_{ij} = -\overline{u_i' u_j'} = \nu_t\left(\frac{\partial U_i}{\partial x_j} + \frac{\partial U_j}{\partial x_i}\right) - \frac{2}{3}k\delta_{ij} = 2\nu_t E_{ij} - \frac{2}{3}k\delta_{ij}$$

(2.60b)

where $i = 1$ to 2 and $j = 1$ to 2. The last term in Equation 2.60b containing k is neglected (TELEMAC-2D, 2001). This term is an integral part of pressure in the Navier-Stokes equation, which is not considered in the TELEMAC because of simplicity. According to Kolmogorov (Ppoe, 2000), the turbulent viscosity is calculated as:

$$\nu_t = C_\mu \frac{k^2}{\varepsilon}$$

(2.60c)

In TELEMAC, the adaptation of the Standard $k-\varepsilon$ model is an extension of the classical model put forward by Rastogi & Rodi (1978). It should be noted that the vertical integration results in a dissipation term due to non-uniformity of the vertical velocity profile, which does not exist in the classical model. The TELEMAC system solves the following equations:

$$\frac{\partial k}{\partial t} + \mathbf{u}.grad(k) = \frac{1}{h}div\left(h\frac{\nu_t}{\sigma_k}grad\,k\right) + P - \varepsilon + P_{kv}$$

$$\frac{\partial \varepsilon}{\partial t} + \mathbf{u}.grad(\varepsilon) = \frac{1}{h}div\left(h\frac{\nu_t}{\sigma_\varepsilon}grad\,\varepsilon\right) + \frac{\varepsilon}{k}\left(C_{1\varepsilon}P - C_{2\varepsilon}\varepsilon\right) + P_{\varepsilon v}$$

(2.60d)

The first term on the right hand side is the diffusion term, whereas the production terms (always positive) are composed on the one hand of the horizontal mean velocity gradient (Equation 2.61a) and on the other hand of the terms of the vertical shear (Equation 2.61b) (TELEMAC-2D, 2001).

$$P = \nu_t \left(\frac{\partial U_i}{\partial x_j} + \frac{\partial U_j}{\partial x_i} \right) \frac{\partial U_i}{\partial x_j}, \text{ where } i = 1 \text{ to } 2 \text{ and } j = 1 \text{ to } 2$$

(2.61a)

$$P_{kv} = c_k \frac{u_*^3}{h}, \text{where } c_k = \frac{1}{\sqrt{c_f}}$$

$$P_{\varepsilon v} = c_\varepsilon \frac{u_*^4}{h^2}, \text{where } c_\varepsilon = 3.6 \frac{C_{2\varepsilon}\sqrt{C_\mu}}{c_f^{3/4}}$$

(2.61b)

where c_f is the coefficient of friction, u_* is the friction velocity at the bottom, which can also be defined using bed shear stress and the coefficient of friction c_f.

$$u_* = \sqrt{\frac{\tau_0}{\rho}} = \sqrt{c_f \sum u_i^2}$$

(2.62)

The coefficient of friction c_f is calculated using Chezy coefficient C_h (i.e. $c_f = 2g/C_h^2$). This value can be also calculated using the Strickler's, Manning's or Nikuradse's coefficient. The value of c_k and c_ε are determined from the normal flow in the centre of straight channel (TELEMAC-2D, 2001).

All the other dimensionless constants c_μ, σ_k, σ_ε, $c_{1\varepsilon}$ $c_{2\varepsilon}$ are based on classical test cases. A test on the free decrease of turbulence enables finding a value of $c_{2\varepsilon}$ (TELEMAC-2D, 2001). The constant c_μ and $c_{1\varepsilon}$ are determined from the data for a turbulent flow near a solid wall. The constant σ_k and σ_ε have been "optimised" on basis of test case performances. The values of the constants used in the Standard $k-\varepsilon$ model are given in Table 2-1.

Table 2-1: Constants used in the Standard k-ε turbulence model
(After TELEMAC-2D, 2001)

C_μ	$C_{1\varepsilon}$	$C_{2\varepsilon}$	σ_k	σ_ε
0.09	1.44	1.92	1.00	1.3

2.4.8 Bed evolution modelling

The word "bed evolution" indicates the change in the channel bottom topography as a result of scour and deposition. It is a complex process, which strongly depends on the hydrodynamic and sediment transport coupling. SISYPHE (2004) uses the following bottom evolution equation:

$$(1-n_p)\frac{\partial Z_f}{\partial t} + div(\mathbf{Q}_s) = 0 \tag{2.63}$$

where n_p is the bed porosity, Z_f is the bottom elevation (Figure 2.22) and $\mathbf{Q}_s$ is sediment transport (volume) vector per unit width.

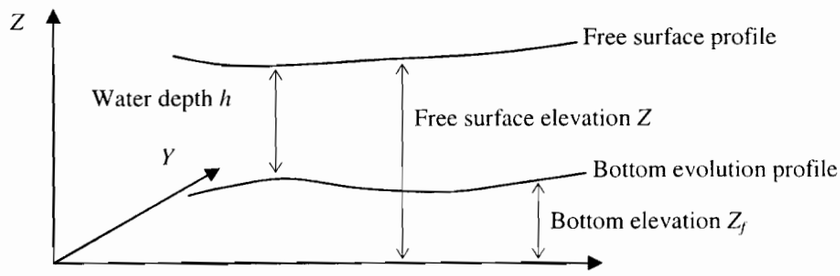

Figure 2-22: Bottom evolution profile

Equation 2.63 links the variation of sediment thickness to the sediment mass balance. It strongly depends on the equilibrium conditions between the sediment bed and the turbulent flow. It assumes that the concentration of sand corresponds to the saturation condition at equilibrium.

In this study the bottom evolution Equation 2.63 is solved using a Finite Element Method in order to get each node of the resolution grid, the bottom evolution and the sediment transport (volume) rate. In order to achieve these objectives, SISYPHE (2004) uses various well-known sand transport formulae.

2.5 Computational modelling of local scour around a pier

The previous sections describe the local scour, sediment transports and their numerical modelling by means of governing equations. This section briefly summarizes some of previous studies of the modelling local scour around a circular pier e.g. Olsen & Melaaen (1993), Olsen & Kjellesvig (1998), Richardson & Panchang (1998), Yen et al. (2001), Ali & Karim (2002), Armitage & McGahey (2003) and Salaheldin et al. (2004). All of these studies are documented in Armitage & McGahey (2003) and Armitage et al (2005).

Olsen & Melaaen (1993) attempted to compute the geometrical shape of a scour hole around a circular pier with the aid of a Finite Volume numerical model. The bed shear stress was used to compute the bed changes assuming a long time step with steady flow. This was iterated over 10 time steps, giving a scour hole shape very similar to what was obtained in a physical model study. The steady Navier-Stokes equations for the 3D flow field on a general non-orthogonal grid were solved at each time step. The *k-ε* turbulence model was used to solve for the Reynolds-stress term. The flow field gave the shear stress on the boundaries, which in turn was used to estimate the sediment concentration for the bed elements. The diffusion-convection

equation for the sediment concentration was then solved, and changes in the bed elevation were calculated from sediment continuity. A new flow field was then determined using the modified bed topology, and the above sequence repeated until the depth of the calculated scour hole was identical to that measured in a separate physical model study. Once the scour depth was correct, the shape of the computed scour hole compared quite well with that measured in the physical model. Neither the CFD nor the physical model tests were however run for an equilibrium scour condition.

Olsen & Kjellesvig (1998) predicted the water flow using the Reynolds-averaged transient Navier-Stokes equations together with the k-ε turbulence model. The location of the water surface was calculated by extrapolating the pressure from the inner cells to the water surface. The pressures in the surface cells were then compared to fixed reference values located on the downstream boundary. If there were any discrepancies between the two values, the water surface was adjusted accordingly. The sediment transport was calculated using the convection-diffusion equation for sediment concentration except for the cells closest to the bed. In these cells, the bed concentration c_{bed} was calculated using a formula presented by Van Rijn (Section 2.3.6.4) with the reference level (a), set to 5% of the water depth. The critical bed shear stress, τ_c, was adjusted for sloping beds using a formula presented by Brooks (1963). The level of the bed was then adjusted for the next time step (100 seconds). The height of the cells was continuously adjusted in proportion to the height difference between the bed and the water surface. The flow field for a stationary solution with a horizontal non-moving bed and water surface appeared to give realistic velocity vector and bed shear stress fields. The same problem was then run with the sediment concentration calculation procedure adjusting the location of the bed and the water surface after each time step. The scour hole and bar developed much as expected although it took an IBM-370 workstation nine weeks to simulate 208 hours of scour hole development. The maximum scour depth was obtained after about 104 hours. The depth was of the same magnitude as those predicted by four different empirical equations.

Olsen & Kjellesvig (1998) used a relatively large grid and time step. As a consequence, the model did not simulate the wake vortices. A coarser grid gave a significantly smaller scour hole that indicated the sensitivity of the analysis to mesh size. The shape of the scour hole was also very sensitive to the angle of repose. Another problem was that the rate of scour development was dependent on the empirical parameters in the Van Rijn equation. It was thus impossible to tell how well the numerical model predicted the development of scour hole without resort to confirmation from some sort of physical modelling.

Encouraged by the work of Olsen & Melaaen (1993), Richardson & Panchang (1998) used FLOW-3D to model the flow field past a circular pier for which physical model results were available. Three steady-state flow conditions were modelled; with the initial flat bed, the intermediate scour hole, and the equilibrium scour hole. The model of Richardson & Panchang (1998) was based on the transient 3D Navier-Stokes equations, which involved very little approximation with the exception of the turbulent closure scheme used to model internal stress. The computations were performed using two different turbulent closure schemes; Prandtl's

mixing length theory and the RNG model. A qualitatively more realistic vector field appeared downstream of the pier using the RNG model, but in general the results of both simulations were largely similar. All of the boundaries were rigid, i.e. no free surface or scour routines were employed. The shape of scour hole was approximated by the frustum of a cone. The computed flow velocities were broadly in agreement with the laboratory observations. Particle tracking showed that sediment movement through the scour holes was also much as expected. Each simulation required approximately 168 hours of CPU time on a desktop SUN workstation.

Yen et al. (2001) developed a morphological model consisting of a 3D flow field model and a scour model to simulate the bed elevation around a circular pier and compared the simulated results with experimental results. They incorporated the large eddy simulation (LES) with Smagorinsky's subgrid-scale (SGS) turbulence model to simulate the flow and bed shear field. The submerged jet flow scouring process was adopted to describe the effect of the downflow on the scouring process in the area in the front of pier. The bed shear stress was calculated using following equation:

$$\tau_{ij} = \mu\left(\frac{\partial \overline{u}_i}{\partial x_j} + \frac{\partial \overline{u}_j}{\partial x_i}\right) \tag{2.64}$$

where μ and $\overline{u}$ are the dynamic fluid viscosity and time-averaged velocity respectively. The computation of the bed shear was carried out with the aid of a Taylor series approximation of the velocity profile as the velocity profile in the region close to pier is not logarithmic. The sediment continuity equation with sediment transport relation was solved imposing open and solid boundary conditions to simulate the evolution of the scour hole. The effect of the local bed slope of the scour hole on the direction of sediment particle motion was incorporated into the model as part of the effective shear stress. The bed-load sediment transport for course bed materials was calculated using the Van Rijn (1986) formula as follows:

$$q_b = 0.053\sqrt{(S_s - 1)g}\,d^{1.5}\frac{T_*^{2.1}}{d_*^{0.3}}, \text{ where } T_* = \frac{\tau_0 - \tau_c}{\tau_c}, d_* = d\left(\frac{\rho^2 S_s' g}{\mu^2}\right)^{1/3}, \; S_s' = S_s - 1 \tag{2.65}$$

where T_* and d_* are the characteristics parameters for excess bed shear stress and particle diameter respectively, q_s is the sediment volume transport rate per unit width, S_s is specific gravity of the sediment, g is the gravitational acceleration, d is the sediment particle diameter, τ_0 is the bed shear stress, τ_c is the critical shear stress and μ is the dynamic viscosity. Experimental data of the scour depth evolution at the pier nose and the scour depth contours around the pier were compared to the numerical results and good agreement was obtained.

Ali & Karim (2002) used FLUENT V4.3 to predict the 3D flow field around a circular cylinder and compared the numerical results to an experimental model. Solutions were obtained for rigid beds and for scour holes of different sizes for different time durations. The numerical results were used to predict the variation of bed shear stress around the cylinder using two different turbulence models – the Standard k-ε and RNG k-ε. Since the shear stresses calculated by FLUENT V4.3 were sensitive to the absolute size of the cells within the solution grid, the cell sizes had to be kept small in order to avoid a grid-dependent solution. The calculated bed shear stresses were then used in the sediment continuity equation to obtain an expression for the variation of scour depth with time. As FLUENT V4.3 could not simulate a free surface, the water surface was modelled by means of a 'rigid-lid' boundary. The asymptotic scour depth was found to depend on three dimensionless numbers; the pile number, the sediment size number and the duration time number. The flow field predicted by FLUENT V4.3 compared favourably with limited available experimental results. The results obtained using the RNG k-ε model were virtually identical to those produced by the Standard k-ε. Good agreement is difficult to obtain in view of the many factors involved that cannot be modelled directly in numerical simulation. For example, FLUENT V4.3 was not capable of modelling the 'turbulent bursts' that are widely observed in the physical phenomena, and are capable of enlarging the scour hole through the removal of sediment from the bed.

Armitage & McGahey (2003) developed Unit Stream Power and Movability Number models for the prediction of local scour in rivers. In their study, CFX V4.3 was used to predict the scour potential upstream of a vertical weir, at an abutment and two piers. The results were then compared to the observed equilibrium scour patterns measured in small-scale laboratory models. The simulations were carried out using relatively coarse meshes to reduce both the CPU time and the size of the data file files that were manipulated in the post-processor where simulation output was analysed. CFX-V4.3 did not contain a free surface modelling routine. Three alternatives were therefore considered for the modelling of the free surface; a symmetry or slip (no shear) boundary, a rigid-lid incorporating an air interface and a moving wall. The moving wall was chosen as it most accurately predicted the turbulent viscosity distribution with depth. The shear stresses were determined principally from velocity gradients in the turbulent flow.

Of the available turbulence models in CFX-V4.3, Armitage & McGahey (2003) found the Standard k-ε and the Low Reynolds Number k-ε models were the best predictions of the turbulent shear stresses for the two- and 3D flow-fields respectively. The QUICK differencing scheme was implemented for the discretisation of velocity and pressure terms, while the HYBRID scheme was employed for solution of the turbulent quantities. Additional FORTRAN subroutines were written to access the basic flow variables and determine, inter alia, velocity gradients, shear velocities and Movability Numbers. A Unit Stream Power or Movability Number higher or lower than the critical value indicated potential for scour or deposition respectively. The scour potential, Ω, was defined as the difference between Movability Number, Mn (Liu, 1957), calculated by the program, and the critical Movability Number $Mn_{c(\beta,\gamma)}$ (adjusted to account for bed-slope where relevant):

$$\Omega = Mn\text{-}Mn_{c(\beta,\gamma)}, \text{ where } Mn = \frac{u_*}{v_{ss}} = f(Re_*),\ Mn_{c(\beta,\gamma)} = \left.\frac{u_*}{v_{ss}}\right|_{\beta,\gamma} = \psi \left.\frac{u_*}{v_{ss}}\right|_0 = \psi Mn_c \tag{2.66}$$

The subscripts (β,γ) and (0)indicate a sloped bed and a horizontal bed respectively. u_*, v_{ss} and ψ are the shear velocity, particle settling velocity and correction factor for bed slope. The scour potential is a measure of the deviation of the boundary from the equilibrium condition. Determination of this equilibrium position could theoretically be computed iteratively with the scour potentials being recalculated after each boundary adjustment. The final solution would be obtained once all scour potentials were close to zero. In CFX-V4.3, however, this could not be automated. Instead of generating new geometries manually for each iteration, Armitage & McGahey (2003) chose simply to compute the scour potential for the initial and final scoured states and compared these with the physical model. Despite the limitations of CFX-V4.3, the agreement between numerical and physical results was sufficiently encouraging to suggest that there was potential for the use of their method for scour prediction.

Salaheldin et al. (2004) used FLUENT V5.0 to model the separated turbulent flow around vertical circular piers in clear water and compared the results with several sets of physical data. The 3D Reynolds-Averaged Navier-Stokes equations for incompressible flow were solved using the Finite Volume technique. The two-phase domain (water in the channel with a region of air on the top) was represented using the Volume of Fluid (VOF) Method coupled with a multiphase formulation solver in order to resolve the variation of the water surface around the pier. The ratio between the initial depths of air to the initial depth of water was set equal to 0.5 or larger to avoid any effect from the boundary condition at the top of the domain on the water flow. Two continuity equations were solved to account for each phase although the momentum and general transport equations were shared by both phases. The size of the cells adjacent to solid boundaries was chosen to satisfy the limits of the wall unit distance $11.225<y^+<30$. At the channel boundaries, the no-slip boundary condition was used to set the velocity to zero there, whilst the wall of the pier were assumed to be a smooth wall. The law-of-the-wall for the mean velocity modified for roughness was utilized to calculate the bottom shear stress.

Salaheldin et al. (2004) used three variants of the k-ε Model; Standard, Renormalization Group (RNG) and the Realizable k-ε model. Despite the high computational effort and time required, the Reynolds Stress Model (RSM) was also used in their study. The RSM was found to give satisfactory estimates for the flow velocity field, shear stress distribution, and water level variation around the pier in the case of flat bottom, and for estimating the velocity field and water level variation in the case of equilibrium scour. The vertical distributions of the streamwise velocity, u, obtained using the Standard k-ε, RNG k-ε and the RSM models were also close to the experimental data. The vertical velocities v however deviated significantly from the experimental data near the bed and near the water surface because of the no-slip boundary condition. It was noticeable that the three k-ε Models, (Standard, RNG and Realizable) overestimated the area in which the computed bed shear stress exceeded the critical

bed shear stress compared to that suggested by the physical data. This overestimation of bottom shear stress may have resulted from the overestimation of the stream wise velocity near bottom with these turbulence models. The pressure coefficient, C_p, was used as a surrogate for the water level variation at the pier. C_p is related to the static pressure as follows:

$$C_p = \frac{p_x - p_0}{0.5\rho U^2} \tag{2.67}$$

where p_x is the local static pressure at position x in the flow direction, p_0 is the upstream undisturbed static pressure, U is the upstream approach velocity and ρ is water density. With the exception of the RSM, the computed pressure coefficients deviated substantially from the physical data. Salaheldin et al. (2004) concluded that the RSM available in FLUENT-V5.0 is an effective tool for predicting the complex flow around bridge piers.

2.6 Summary

This chapter presented the basic concepts of local scour associated with changes in the flow field around a circular pier and its dependency on the key parameters.

The initiation of sediment motion and sediment movement due to transport process are one of the main features of scour and deposition in the fluvial system. The various physical sediment properties, methods of the initiation of sediment motion and the quantification of sediment transport were thus outlined.

The local flow field due to the presence of a pier changes the hydrodynamic variables near the pier, which in turn contributes the movement of particles from bed during the local scouring process. To incorporate all of these phenomena into a numerical model, a rigorous mathematical description was outlined using fundamental concepts of fluid flow; the conservation of mass, momentum and energy respectively. In doing so various assumptions to model fluid flow were also mentioned.

Some of the past key numerical model studies on local scour around a circular pier are presented at the end of this chapter. This chapter is important for understanding the complexity of the local scouring process and the complexities inherent in the numerical modelling of local scour.

Chapter 3
An overview of the TELEMAC system

3.1 Introduction

The TELEMAC system is an integrated numerical modelling tool which consists of a whole processing chain for the calculation of water, solute and sediment motion in the fluvial, coastal, estuarine, lacustrine and groundwater domains. It comprises a "pre-processor" for digitising data and describing the problem, "simulation" programs for calculating numerical magnitude and "post- processors" for displaying and analysing the results.

Electricite de France (EDF) – Laboratoire National d'Hydraulique (LNH) originally developed the program taking into account inter-software communication. It is extensively used, marketed and developed by SOGREAH Consultants, France, in close partnership with EDF-LNH. The TELEMAC system primarily uses the Finite Element theory, which comprises a rigorous theoretical framework and flexibility for describing complex geometries (Hervouet, 2000). The recent development of TELEMAC also includes the Finite Volume theory for the analysis of 2D flow and non-cohesive sediment transport. All of its components are compiled and structured using standard FORTRAN programming.

The University of Cape Town (UCT) received a TELEMAC software licence from SOGREAH Consultants, France, in December 2004 with on-line support. This study began with TELEMAC V5.4, however, UCT received TELEMAC V5.5 in May 2005. All simulations described in this thesis were carried out using TELEMAC V5.5. A list of some alternative codes is given in Appendix C.

The intention of this chapter is to provide a brief description of the various components of the TELEMAC system. The chapter commences with a brief description of TELEMAC structures; the computer environment and FORTRAN programming followed by the detail description of related modules used in this study i.e. MATISSE, TELEMAC-2D, TELEMAC-3D, SISYPHE and RUBENS/POSTEL-3D. Particular attention is given to those aspects which were relevant to this study.

3.2 The structure of the TELEMAC system

The TELEMAC system can be broken into three distinct parts; pre-processing, simulation and post-processing. Each of these contains different modules. The pre-processing includes the grid generation (MATISSE) and grid interface (STBTEL) module. The simulation comprises variety of modules i.e. hydrodynamic (TELEMAC-2D and TELEMAC-3D), sediment transport (SISYPHE and SEDI-3D), wave climate (TOMAWAC), harbour agitation (ARTMIS), water quality (SUBIEF-2D and SUBIEF-3D) and ground water (ESTEL-2D and ESTEL-3D). The post-processing includes RUBENS-2D and POSTEL-3D. This study used MATISSE, TELEMAC-2D, TELEMAC-3D, SISYPHE, RUBENS-2D and POSTEL-3D for the

modelling local scour. Description of the TELEMAC structure is thus limited to these modules and only the relevant features are discussed.

The computational domain is discretised using an unstructured grid of triangular elements, which are generated using MATISSE. The TELEMAC-2D simulation module is designed to simulate 2D hydrodynamic fields, whereas TELEMAC-3D is designed to simulate 3D flow fields. SISYPHE simulates the evolution of channel bottom transporting non-cohesive sediments along with TELEMAC-2D/TELEMAC-3D generated hydrodynamic variables. The post-processor module RUBENS was designed for one or 2D graphics visualisation, therefore an additional interface module POSTEL-3D has been designed to represent the TELEMAC-3D outputs. Figure 3-1 illustrates the different modules of TELEMAC system used in this study.

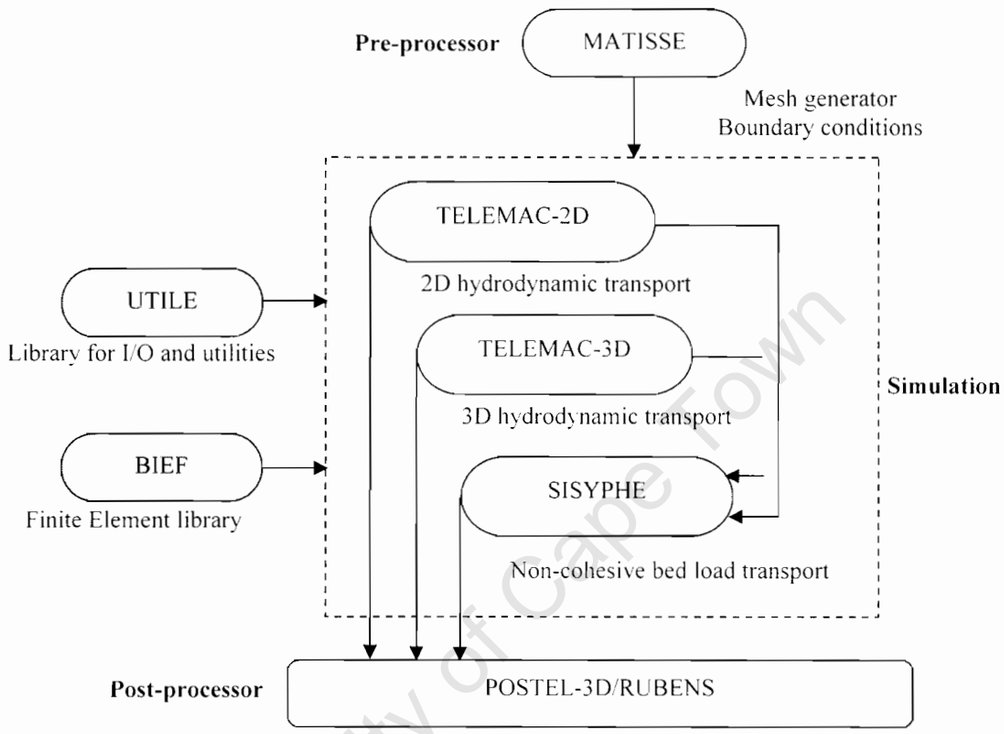

Figure 3-1: Modules of TELEMAC system used to model local scour

A single Finite Element Library called BIEF has been implemented in TELEMAC system to enabling the sharing of the common codes during simulation of different modules. This library has been specially designed for various numerical algorithms to solve the classical fluid mechanics equations. Another library UTILE is used to control input-output (I/O) and utilities during mesh and output file manipulations.

3.3 The computer environment

The main simulation modules are written in FORTRAN-90 codes with no machine-specific language extensions. They can therefore be run on all workstations operating under UNIX, Windows NT or XP and on certain vector computers such as Cray and Fujitsu. The graphics modules (RUBENS and MATISSE) are run on similar computer environments.

The recommended computer hardware for Windows XP or NT should include as a minimum a Pentium IV with 2 GHz CPU (central processing unit) processor, 128 MB RAM (random access memory), and 550 MB free hard disk. During simulation the system also requires Standard Compaq Visual FORTRAN version 6.5 or above. The software is protected using HASP (Hardware Against Software Piracy) keys, therefore, special software for the HASP driver provided with the TELEMAC system needs to be installed. This study used a PC (personal computer) Pentium IV with 3GHz CPU and 2 GB RAM along with 20 GB free hard disk space with a Windows XP operating system.

Originally TELEMAC was developed for the UNIX system and some of the operating features are not well developed for a Windows operating system. SOGREAH Consultants, France, are, however, working to improve this (Lang, 2005). It should be noted that the all TELEMAC modules start up with DOS commands under MS DOS shell windows.

3.4 FORTRAN programming with TELEMAC

The TELEMAC system codes are flexible and can be manipulated by the user using FORTRAN programming. This can be achieved using a single FORTRAN file of different subroutines that access the library BIEF during simulation. This FORTRAN file is compiled and linked automatically to BIEF at the beginning of the simulation to generate an executable program for the desired results. The source code of a number of so-called "user subroutines" is also provided with the TELEMAC system. The following procedures were recommended and followed in the modification of some of the subroutines in this study:

- Pick up the standard version of the user subroutine provided with the TELEMAC system and copy it into the working directory.
- Modify and save each subroutine according to the model requirements using Compaq Visual FORTRAN version 6.0.
- Link up the set of subroutines into a single standard FORTRAN 90 file.

The various TELEMAC system variables were accessed by calling FORTRAN files gathered into a "module" type component (BIEF, 2004). To access TELEMAC-3D code, "USE DECLARATIONS_TELEMAC3D" should be written at the beginning of the subroutine in a FORTRAN file. It is also necessary to add the code "USE BIEF" in the FORTRAN file.

Almost all the arrays used in simulation modules have to be declared in the form of a structure with pointers (BIEF, 2004; Metcalf & Reid, 1990). For example, access to the water depth variable is in the form H%R where the %R indicates that a pointer of real type is being used. If the pointer is of integer type, the %R is replaced by a %I. To avoid having to handle too many %R and %I, a number of aliases have been defined, such as for example the variables NPOIN (total number of points), NELEM (total number of elements), etc. Further details can be found in BIEF (2004).

3.5 The pre-processing module MATISSE

The pre-processing module MATISSE has been designed to generate the mesh in the computational domain and the boundary conditions along the domain boarders in an interactive manner. These are essential for the construction of the model for carrying out the hydrodynamic simulations of containment and sediment transport.

MATISSE builds a mesh of unstructured triangular elements to discretise the computational domain. These elements are used for the solution of the governing hydraulic equations principally through the Finite Element Method. Appropriate mesh construction is of major importance to enable the modelling of the complex water-structure interactions and numerical stability. The followings must be considered during mesh generation:

- The outside contour of the computational domain
- Any island within the domain
- The geometry of the different structures (i.e. bridge piers and abutments)
- The local bathymetry
- Criteria for defining the local densification of nodes. These criteria can be defined either manually or according to external items such as velocity, concentration fields, etc. The bathymetry is always taken into account as a criterion for computing the desired inter-point distance.

MATISSE generates two essential output files; (i) GEOMETRY (mesh file) and (ii) CONLIM (boundary condition file). In order to construct these files, five consecutive steps are implemented:

- Bathymetry
- Geometric lines
- Digital Terrain Model (DEM)
- Mesh
- Boundary conditions

3.5.1 The bathymetry

The bathymetry describes the elevation of the riverbed which in turn helps to define the inter-point distance for the densification of the nodes. The bathymetric data is defined with respect to coordinate systems of various units (SI, CGS and Nautical Miles). These data should be in MATISSE-readable formats namely (MATISSE, 1998); SINUSX (digitised map format ASCII file), SERAFIN (Fortran Real*4 format Binary file), DXF (Drawing Interchange File format file) or XYZ (MS DOS file).

The simple XYZ format was adopted in this study. This was achieved using MS Excel with three columns of data for the x-coordinate, y-coordinate and z-coordinate respectively. The points were uniformly distributed using a 0.1m spacing in both the x- and y- directions. The value of z-coordinate was set to 0.0 (zero) in order to specify flat bed condition.

3.5.2 The geometric lines

The geometric line mode establishes some position limits of the points and segments in the future mesh. These are achieved by creating lines consisting of point sets or simple geometric lines having either "user" or "contour" attributes. Both of these lines consist of successive link segments.

User defined lines are used for defining the constraint lines of the mesh. The constraint line serves as a support for the nodes and segments of mesh. The segment will be linked to a line and may not intersect it. For example the construction of a circular pier within the domain employs user defined lines.

Contour lines construct the mesh support and make up the outside or inside boundary of the domain. They comprise various user defined lines. For example semi-circular or rectangular abutments may be defined at the boundary of the domain using contour lines.

The geometric dimensions of the computational domain were established in this step.

3.5.3 The Digital Terrain Model (DEM)

The Digital Terrain Model (DEM) is the first triangulation attempt of the mesh generation algorithms. It is used to prepare the "density map", i.e. a basic mesh on which a list of criteria and, consequently, the desired inter-node distance are defined. The DEM globally comprises a "bathymetry-geometric lines-density map" providing an optimal size of equilateral triangular elements to ensure the suitable distribution of the unstructured mesh.

Definition of the mesh criteria is an important task in the construction of the mesh. The criteria indicate the dimension of the side of the triangular elements in SI unit i.e. metres (m). These can be imposed or defined in many ways, however, a global constant criterion is normally defined for the entire computational domain. This global constant criterion defines the relatively coarse uniform triangles for the entire domain. After that, a refined new constant mesh criterion is imposed at the area of interest within the global constant criterion region in

order to create a finer mesh. During this process, a liner geometric relationship is imposed at the interface between the global constant criterion and the refined constant criterion in order to get a uniform distribution of the triangles in the mesh. In this study, finer mesh was constructed around the pier.

It is important to mention that a smaller value of the refined constant criterion produces large numbers of elements, which in turn increases the computational time. In the case of pier, an analytical function called "smooth criteria" was adopted to define the mesh between the pier and the boundary. This function enables the construction of finer elements near the pier and larger ones away from the pier, i.e. near the limits of the boundary of the domain. Once the mesh criteria have been defined, they cannot be modified or replaced.

3.5.4 The mesh

The mesh mode generates an unstructured triangular mesh based on the criteria defined in the DEM mode. The preliminary information on the mesh is then inspected considering the following aspects:

- The number of nodes
- The number of triangles
- The number of islands or geometric lines
- The number of fixed points
- The maximum and minimum bathymetric values
- The dimension of the largest and smallest segments
- Maximum cell distortion
- Maximum cell increment

After the preliminary inspection, the quality of mesh is assessed using the post-processor RUBENS, which plots the isovalue graphs of the following quantities in the mesh structures:

- Bathymetry
- Mean length of segments in the triangles (related to the inter-node distance)
- Surface area of the triangles
- Distortion of the triangles
- Smallest angle of the triangles
- Largest angle of the triangles

Generally a uniform distribution of the nodes is desired with near equilateral triangles of different sizes. Such a distribution is important for numerical stability and for reducing computational time.

In general, the MATISSE generated automatic mesh was adequate. The mesh structure can however be amended manually by accessing nodes before generation of the GEOMETRY file (or mesh file). During manual mesh amendment, care must be taken to avoid introducing errors into mesh, especially intersected segments and over-constrained triangle (out of the range of the desired criteria). When the mesh satisfies the specification criteria, a GEOMETRY file of SERAFIN format (TELEMAC-2D, 2002; Appendix 7, pp 1) is generated. This geometry file is linked with TELEMAC hydrodynamic and sediment transport modules during simulation.

The following sections briefly describe the development of the mesh structure mesh used in this study.

3.5.4.1 Two-dimensional (2D) mesh

The 2D mesh consisting of the three-node triangles is constructed using the BIEF_MESH FORTRAN subroutine in the TELEMAC system. Each element is addressed by the local and the global numbering systems and is stored in a geometry file with corresponding X and Y coordinates.

The base functions for the Finite Element analysis (TELEMAC-2D, 2001; BIEF, 2004) are derived for the local elements using local numbers and then a connectivity table is used to transfer the local number to the global numbers in order to solve the entire linear system (BIEF, 2004). Figure 3-2 depicts a single triangular element in a mesh with the local numbering (ascending order in clockwise direction).

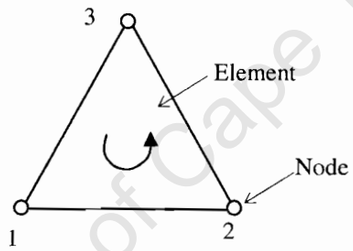

Figure 3-2: 2D triangular element and nodes numbering

3.5.4.2 Three-dimensional (3D) mesh

The 3D mesh consisting of six-node prisms are developed at two stages during 3D simulations in TELEMAC-3D.

1. Firstly, a 2D-mesh is constructed as described in Section 3.5.4.1 consisting of the three-node triangles that cover the whole horizontal domain.
2. Secondly, the same 2D mesh is reproduced along the vertical on a number of curved surfaces known as planes using sigma coordinates (TELEMAC-3D, 1998).

Figure 3-3 illustrates a typical prismatic 3D (3D) element in the mesh.

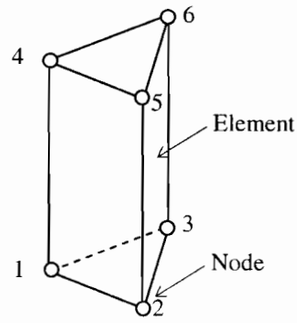

Figure 3-3: 3D prism element and nodes numbering

Like the 2D mesh, the various connectivity tables are generated to link the different nodes of each plane in order to discretise the entire domain.

It should be noted that only the velocity components are computed at each point of the 3D mesh including the bottom and the surface and these are thus 3D variables. The water depth (free surface) and the bottom elevation are computed only once along a vertical using the depth-averaged velocity components and hence these are 2D variables. As a consequence, certain calculations in TELEMAC-3D are the same as those in TELEMAC-2D sharing the same library codes e.g. the calculation of the water depth and the bottom elevation. In essence TELEMAC-2D runs as a part of the TELEMAC-3D simulation for the calculation of these values at each node. Further details are in Section 3.8.

3.5.4.3 Boundary mesh

TELEMAC boundary mesh consists of three-node triangles for the 2D mesh and the six-node prisms for the 3D mesh. The boundary mesh is thus similar in the 2D or 3D mesh except the characteristics of the points associated with the boundary. Unlike 2D meshes, an additional global numbering is assigned to the boundary nodes.

Three types of numbering are therefore associated with the boundary of the domain; (i) the boundary point numbers, (ii) the boundary face numbers, and (iii) the local numbers of the boundary nodes in each of the boundary faces. Additional connectivity tables are generated to link these various numbering systems depending on the character of the boundary conditions e.g. the smooth wall or imposed flow rate or prescribed elevation.

The Figure 3-4 illustrates how these tables address a triangular element. Figure 3-4 indicates a triangle called P1 (TELEMAC addresses P1 as a three-node triangle) designated IELEM situated inbetween 3 nodes with the global numbers NG1, NG2 and NG3.

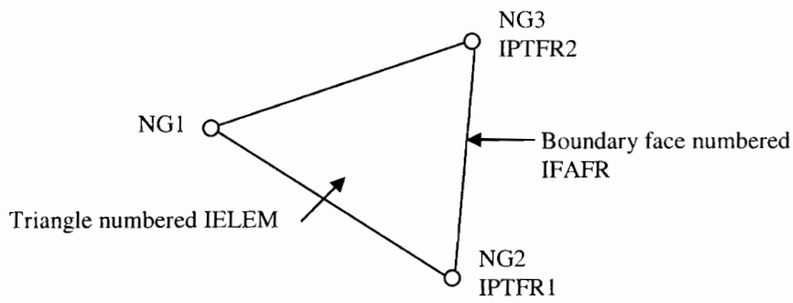

Figure 3-4: Three nodes triangle with boundary face

The face defined by the two points NG2 and NG3 is a boundary face addressing IFPTFR. The nodes NG2 and NG3 are therefore the boundary nodes with the boundary numbers IPTFR1 and IPTFR2. The nodes NG1, NG2 and NG3 have the local numbers 1, 2 and 3 in the triangle. Finally the nodes IPTFR1 and IPTFT2 also have the local numbers 1 and 2 in the boundary face. Further details can be found in BIEF (2004).

During simulation, the governing equations are solved separately at the boundary nodes depending on the imposed boundary conditions e.g. solid boundary or liquid boundary.

3.5.5 The boundary conditions

The final step in MATISSE involves defining the boundary conditions. The boundary types and values at the various nodes of the domain are defined in two ways; as an "entity" and as a "group".

An entity refers to the boundary condition characteristics at an individual node, which comprise so-called type and value related to the unknown variables (water depth, velocity components and tracer). There are six different so-called "types" in MATISSE, which can be chosen to describe the nature of boundary condition; adherence, wave, sliding, free, imposed-flow rate and imposed-values. The "value" indicates the value of the variable in the case when the boundary condition is constant on a time basis. An entity is defined by an entity name. A group is a set of nodes belonging to the particular contour lines. Like an entity, a group is defined by a group name. A group and an entity have to be associated to create a complete boundary condition file. It is therefore clear that three distinct steps have to be followed in order to create a complete boundary condition file:

- defining the required entities
- allocating all the contour line nodes to groups
- linking each group to entity

In this study, a boundary condition CONLIM file of SERAFIN format (TELEMAC-2D, 2002; Appendix 7, pp 1) was created, which was linked to hydrodynamic and sediment transport

modules during simulation. Two types of boundaries were modelled; solid walls and liquid boundaries. The channel sides and the surface of pier were modelled as solid smooth walls. The upstream and the downstream faces were modelled as liquid boundaries. The influence of turbulence on the solid and the liquid boundaries was modelled separately.

The following sections briefly describe the modelling of these boundaries used in this study.

3.5.5.1 Solid boundaries

The solid boundaries are modelled as a solid smooth wall so that no discharge could take place across a boundary and a negligible friction could exert on the boundary. When this boundary character is applied to the nodes, an automatic generated coefficient (a_c) is generated to ensure the gradient proportional to the local velocity as:

$$\frac{\partial u}{\partial e} = a_c u \text{ and } \frac{\partial v}{\partial e} = a_c v \tag{3.1}$$

where e is the magnitude of a vector perpendicular to the wall which is derived for a local logarithmic velocity profile.

3.5.5.2 Liquid boundaries

The flow and the water depth are controlled at the upstream and the downstream respectively. The upstream face is modelled as an open boundary with a prescribed flow rate, whereas the downstream is modelled as an open boundary with a prescribed depth only. In this case TELEMAC requires a velocity profile to initialise the computation of the velocity components. The velocity profile is defined at normal to the upstream boundary and its norm is approximated to a value proportional to the square root of the water depth from bottom. At the downstream face, a constant free surface level is maintained during the simulation. Further details are in Section 4.8.

A sudden introduction of a full discharge can cause computational instability (TELEMAC-2D, 2002). The discharge is therefore progressively increased such as 0.0 to 15.81m^3/s over a model period of half an hour. A liquid boundary condition file has to be created using text editor as an alternative to FORTRAN programming.

3.5.5.3 Boundary conditions for k-ε model

This study uses the Standard k-ε turbulence model. The boundary condition of the k-ε model on the solid smooth walls is modelled by considering the local logarithmic velocity profile. The local turbulence kinetic energy and dissipation is computed assuming that the production due to shear stress equal to the dissipation at a boundary layer distance δ. The calculation of a boundary layer distance δ from the wall is carried out according to TELEMAC-2D (2001, pp 53-54). Equation 3.2 describes the value of kinetic energy k_δ and dissipation ε_δ at a distance δ from the boundary for a water depth h.

$$k_\delta = \frac{u_*^2}{\sqrt{C_\mu}} + \frac{C_{2\varepsilon}}{c_\varepsilon c_f}\tilde{u}_*^2 \tag{3.2a}$$

$$\varepsilon_\delta = \frac{u_*^3}{\kappa\delta} + \frac{1}{\sqrt{c_f}}\frac{\tilde{u}_*^3}{h} \tag{3.2b}$$

where $\kappa = 0.41$ is the von Karman's constant, u_* is the friction velocity and $\tilde{u}_*$ is the bottom friction velocity near wall, the other coefficients in Equation 3.2a and 3.2b are related to the *k*-ε model given in the Section 2.4.7.1. In order to obtain the values of the kinetic energy k_δ and the dissipation ε_δ, Equation 3.3 (for a smooth wall) is solved together with Equation 3.2a and 3.2b using the Iterative Method.

$$\frac{\tilde{u}_*}{u_\delta} = \left[\frac{1}{\kappa}\ln\left(\frac{\tilde{u}_*\delta}{\nu}\right) + 5.5\right]^{-1} \tag{3.3}$$

It will be noted that the model considers $\tilde{u}_*\delta/\nu = 100$ as an initial value, which amounts to a turbulence intensity of 6% (TELEMAC-2D, 2001).

Equation 3.4 calculates the turbulent kinetic energy and dissipation using the standard coefficients for *k*-ε model to initialise the calculations.

$$k = C_{2\varepsilon}\frac{P_{kv}^2}{P_{\varepsilon v}} \text{ and } \varepsilon = P_{kv} \tag{3.4}$$

The value of the standard coefficients for *k*-ε model i.e. $C_{2\varepsilon}$, P_{kv} and $P_{\varepsilon v}$ can be found in Section 2.4.7.1 (Table 2-1 and Equation 2.61b).

The liquid boundary for the *k*-ε model is modelled using the homogeneous Neumann conditions given by TELEMAC-2D (2001):

$$\frac{\partial k}{\partial e} = 0 \text{ and } \frac{\partial \varepsilon}{\partial e} = 0 \tag{3.5}$$

where e is the magnitude of a vector perpendicular to the wall which is derived for a local logarithmic velocity profile.

3.6 An overview of TELEMAC-2D

TELEMAC-2D is the digital simulation module of the TELEMAC system for the solution of 2D Saint-Venant equations at each node of the computational domain. The water depth and the depth-averaged velocity components are the main variables, but the transport of tracers as well as turbulence can be taken into consideration.

The Saint-Venant equations are derived from the Navier-Stokes equations (Equation 2.35) taking account the depth-averaged velocity components in which, however, necessitates certain assumptions and approximations for the non-linear terms. These assumptions and approximations form the limits and are responsible for the restricted domain of validity of the equations (TELEMAC-2D, 2001; BIEF, 2004).

The following equations are simultaneously solved for the modelling of the 2D flow assuming hydrostatic pressure distribution (TELEMAC-2D, 2002).

Continuity equation:

$$\frac{\partial h}{\partial t} + \mathbf{u} \bullet grad\, h + h\, div\, \mathbf{u} = 0 \tag{3.6a}$$

Momentum equation:

$$\frac{\partial u}{\partial t} + \mathbf{u} \bullet grad\, u = \frac{1}{h} div(h\nu_t\, grad\, u) - g\frac{\partial Z}{\partial x} + F_{Mx}$$
$$\frac{\partial v}{\partial t} + \mathbf{u} \bullet grad\, v = \frac{1}{h} div(h\nu_t\, grad\, v) - g\frac{\partial Z}{\partial y} + F_{My} \tag{3.6b}$$

where h is the water depth, u and v are the component of the velocity vector $\mathbf{u}$, Z is the free surface, ν_t is the turbulent viscosity and F_{Mx} and F_{My} are source terms (gravity, bottom friction, etc.).

This study required the solution of the above equations together with the k-ε model (Section 3.9) using the Fractional Step Method (Section 3.11.3) with the Method of Characteristics scheme (Section 3.11.1) for the velocity components (u and v), turbulent kinetic energy k and the dissipation ε. A conservative scheme with SUPG is considered for the advection of depth h solution.

The advection, propagation and diffusion terms in Equations 3.6a, 3.6b and 2.60d are solved separately by TELEMAC-2D at each discretised nodes between the time t^n and the time t^{n+1} (i.e. so-called "time step" Δt).

The following equations are solved by TELEMAC-2D during the advection step:

$$\frac{\tilde{h}-h^n}{\Delta t}+\mathbf{u}\bullet grad(h)=0$$
$$\frac{\tilde{u}-u^n}{\Delta t}+\mathbf{u}\bullet grad(u)=0$$
$$\frac{\tilde{v}-v^n}{\Delta t}+\mathbf{u}\bullet grad(v)=0$$
$$\frac{\tilde{k}-k^n}{\Delta t}+\mathbf{u}\bullet grad(k)=0$$
$$\frac{\tilde{\varepsilon}-\varepsilon^n}{\Delta t}+\mathbf{u}\bullet grad(\varepsilon)=0$$

(3.6c)

The following equations are solved by TELEMAC-2D during the propagation and the diffusion steps:

$$\frac{h^{n+1}-\tilde{h}}{\Delta t}+h\,div(\mathbf{u})=0$$
$$\frac{u^{n+1}-\tilde{u}}{\Delta t}=-g\frac{\partial Z}{\partial x}+\frac{1}{h}div[h\nu_t\ grad(u)]+F_{Mx}$$
$$\frac{v^{n+1}-\tilde{v}}{\Delta t}=-g\frac{\partial Z}{\partial y}+\frac{1}{h}div[h\nu_t\ grad(v)]+F_{My}$$

(3.6d)

The following equations are solved by TELEMAC-2D during the k-ε model solutions:

$$\frac{k^{n+1}-\tilde{k}}{\Delta t}-div[\frac{\nu_t}{\sigma_k}grad(k)]=P+P_{kv}-\varepsilon$$
$$\frac{\varepsilon^{n+1}-\tilde{\varepsilon}}{\Delta t}-div[\frac{\nu_t}{\sigma_\varepsilon}grad(\varepsilon)]=PC_{1\varepsilon}\frac{\varepsilon}{k}+P_{\varepsilon v}-C_{2\varepsilon}\frac{\varepsilon^2}{k}$$

(3.6e)

where $\tilde{u}$, $\tilde{v}$, $\tilde{k}$ and $\tilde{\varepsilon}$ are the intermediate value of u, v, k and ε within same time step during advection. The viscosity ν_t is calculated by the turbulence model using the value of the kinetic energy k and the dissipation ε. The initial value of the kinetic energy k and the dissipation ε are calculated using Equation 3.4. The viscosity was calculated using Equation 2.60c.

$$\nu_t = C_\mu \frac{k^2}{\varepsilon}$$

(2.60c)

The terms F_{Mx} and F_{My} in Equation 3.6d are the source terms. This study neglects all source terms except bottom friction. The values of these source terms due to bottom friction may be given to the model according to the friction law of Chezy, which is originally derived for a uniform flow. Considering the flatbed domain and the non-linear nature of the Chezy's equation, they are modelled as:

$$F_{Mx} = \frac{g}{hC_h^{\,2}} u^{n+1} \sqrt{(u^n)^2 + (v^n)^2}$$
$$F_{My} = \frac{g}{hC_h^{\,2}} v^{n+1} \sqrt{(u^n)^2 + (v^n)^2}$$

(3.6f)

This study considers additional numerical treatment for the solution of the non-linear terms i.e. $h\,div(\mathbf{u})$. This is done by specifying the numerical coefficient for the "implicitation for velocities" and the "implicitation for depth". Equation 3.6g is then solved within the same time step taking account the so-called propagation depth h_{prop}.

$$h\,div(\mathbf{u}) = h_{prop} div[\theta_u \mathbf{u}^{n+1} + (1-\theta_u)\mathbf{u}^n]$$
$$h_{prop} = \theta_h h^{n+1} + (1-\theta_h)h^n$$

(3.6g)

where θ_u is the implicitation for velocity and θ_h is the implicitation for the depth.

The diffusion term is treated similarly using the coefficients for the "option for diffusion velocities". The diffusion term is approximated (Equation 3.6h) and solved defining the value of the "implicitation for diffusion of velocity" θ_d.

$$div[\nu_t\, grad(u)] = div[\nu_t grad\{\theta_d u^{n+1} + (1-\theta_d)u^n\}]$$

(3.6h)

Finally the change of depth δh is calculated during the solution of the terms $-g(\partial Z/\partial x)$ and $-g(\partial Z/\partial y)$. This is approximated by solving Equation 3.6i.

$$-g\, grad(Z) = -g\theta_h grad(\delta h) - g\, grad(h_n + Z_f)$$

(3.6i)

At the each time step, the change of water depth is added to the initial depth in order to obtain the free surface and it is continued accordingly for the successive time steps.

It should be noted that the Saint-Venant equations for two-dimensions assume negligible vertical velocity. This is linked to a condition of hydrostaticity neglecting the vertical accelerations. As a consequence TELEMAC-2D may under-predict the flow field in front of pier, where downflow is dominant due to stagnation pressure.

3.7 An overview of TELEMAC-3D

TELEMAC-3D is a 3D computational code that describes the 3D velocity field (u, v, w) and the water depth or free surface measured from the bed. Like TELEMAC-2D, the transport of tracers as well as turbulence can be taken into consideration. It is important to note that TELEMAC-3D shares the same library codes as in TELEMAC-2D in order to calculate the water depth or the free surface. TELEMAC-3D default solves the 3D hydrodynamic equations with the following fundamental assumptions (TELEMAC-3D, 1998):

- The Navier-Stokes equations with free surface changing in time
- Negligible density variation in the mass conservation equation
- Hydrostatic pressure distribution
- Boussinesq approximation for momentum

The following 3D equations are solved by TELEMAC-3D (Hervouet & Jankowski, 2000).

The continuity:

$$\frac{\partial u}{\partial x}+\frac{\partial v}{\partial y}+\frac{\partial w}{\partial z}=0 \tag{2.31}$$

The Navier-Stokes (Momentum):

$$\frac{\partial u}{\partial t}+\mathbf{u}\bullet grad\, u=\frac{1}{\rho}\frac{\partial P}{\partial x}+div\left(\nu_t\, grad\, u\right)+F_{Mx}$$
$$\frac{\partial v}{\partial t}+\mathbf{u}\bullet grad\, v=\frac{1}{\rho}\frac{\partial P}{\partial y}+div\left(\nu_t\, grad\, v\right)+F_{My} \tag{2.35}$$

The hydrostatic pressure:

$$p=\rho g\left(Z-z\right)+\rho g\int_z^s\frac{\Delta\rho}{\rho}dz \tag{3.7}$$

where u, v, and w are the component of the velocity vector **u**, Z is the free surface, z is the vertical elevation, ν_t is the turbulent viscosity, ρ is the density of the water and F_{Mx} and F_{My} are source terms. The second term at right hand side in Equation 3.7 takes into account the bouyancy effects due to temperature or salinity.

It should be noticed that the momentum equation, which contains the w-component is not included in the TELEMAC-3D default option. In this case, the vertical velocity component is deduced from the continuity equation (Equation 2.31). This approach is valid only when the vertical velocity remains small within assumption of hydrostatic pressure variation. The latest versions of TELEMAC V5.5 do however provide codes to deal with non-hydrostatic pressure distributions.

For non-hydrostatic pressure distributions, the Navier-Stokes equations (Equation 2.35) are solved by decomposing the total pressure p into the hydrostatic pressure p_h and the hydrodynamic pressure p_d so that:

$$p = p_h + p_d \tag{3.8a}$$

Like TELEMAC-2D, the equations are solved for the advection, diffusion and the source terms (friction only) separately. The Poisson Pressure Equation (PPE), followed by the velocity projection, is solved in order to get a divergence-free velocity field for the calculation of the hydrodynamic variables on pressure (Hervouet & Jankowski, 2000).

The full Navier-Stokes equations (Equation 3.8b) are then solved by first approximating the hydrostatic pressure. The velocity vector $\tilde{\mathbf{u}}$ is linked to the hydrostatic pressure, whose components are $\tilde{u}$, $\tilde{v}$ and $\tilde{w}$ in the x-, y- and z-directions respectively.

$$\begin{aligned}
\frac{\partial \tilde{u}}{\partial t} + \tilde{\mathbf{u}} grad(\tilde{u}) &= -\frac{1}{\rho}\frac{\partial p_h}{\partial x} + div(\nu_t grad\,\tilde{u}) + F_{Mx} \\
\frac{\partial \tilde{u}}{\partial t} + \tilde{\mathbf{u}} grad(\tilde{u}) &= -\frac{1}{\rho}\frac{\partial p_h}{\partial x} + div(\nu_t grad\,\tilde{u}) + F_{My} \\
\frac{\partial \tilde{w}}{\partial t} + \tilde{\mathbf{u}} grad(\tilde{w}) &= -\frac{1}{\rho}\frac{\partial p_h}{\partial z} + div(\nu_t grad\,\tilde{w}) - \frac{\Delta\rho}{\rho}
\end{aligned} \tag{3.8b}$$

The hydrodynamic pressure is then taken account through the continuity equation using the velocity field predicted during the solution of Equation 3.8b. Equation 3.8c is then solved at each time step (Δt) for a divergence free velocity field.

$$\nabla^2(p_d) = \frac{\rho}{\Delta t} div(\tilde{\mathbf{u}})$$

(3.8c)

Finally, the velocity field is established by projecting the $\tilde{\mathbf{u}}$ field which is related to the hydrostatic pressure distribution and the hydrodynamic pressure gradient as:

$$\mathbf{u} = \tilde{\mathbf{u}} - \frac{\Delta t}{\rho} \nabla(p_d)$$

(3.8d)

The hydrostatic pressure gradient is added as a source term in the advection-diffusion step and only the dynamic pressure is used in the PPE step. As a consequence, Equation 3.8d tends to become trivial when a flow is nearly hydrostatic (Hervouet & Jankowski, 2000).

Like TELEMAC-2D, the *k-ε* model is used to calculate the viscosity ν_t, however, the *k-ε* equations are solved for the vertical and for the horizontal planes separately. Calculation of the change of the water depth is done in the same manner as for TELEMAC-2D. It should be noted that during solving equations using TELEMAC-3D, TELEMAC-2D module is automatically activated for the solution of the water depth and the free surface.

3.7.1 The establishment of vertical coordinates in the mesh

There are various ways to establish the vertical coordinates of the nodes in the mesh during TELEMAC-3D simulations (TELEMAC-3D, 1998). This study established the vertical coordinates using the generalized sigma transformation by modifying the user FORTRAN subroutines called "CONDIM" in the TELEMAC V5.5 (Appendix A). This transformation adjusts the mesh to correct for the change of bottom topography. According to Hervouet & Jankowski (2000), sigma grids can tolerate much smaller levels of horizontal viscosity and diffusivity in order to get computational accuracy. More details on the sigma transformation can be found in TELEMAC-3D (1998) and Mellor et al (2002).

The following factors are needed for the sigma-transformation:

- The total number of prisms, N_p
- The total number of horizontal planes, N_p+1
- The bottom elevation on the vertical of point *IPOIN3*, $Z_f(IPOIN3)$
- The free surface elevation on the vertical of point *IPOIN3*, $Z_s(IPOIN3)$

It is obvious that for a total number of N_p prisms, the 2D mesh needs to be repeated in N_p+1 planes in 3D domain. The position of each of the planes I_p is then defined by a single coordinate $z^*(I_p)$. The value of $z^*(I_p)$ is different for each plane and might vary between 0.0 and

1.0. I_p indicates the number of planes from 1 to N_p+1. The parameter $z^*(I_p)$ is increased strictly with the increase of the index I_p so that:

$$\begin{aligned} z^*(1) &= 0.0 && \text{defines the bottom} \\ z^*(N_p+1) &= 1.0 && \text{defines the surface} \end{aligned} \tag{3.9a}$$

The parameter $z^*(I_p)$ determines the elevation of prism in metres at the same horizontal position as the bathymetry of the I_p plane. Every point of that plane has to be the same elevation. No plane cuts another; whilst the bottom and the free surface are fixed at each time step. A minimal water depth *HMIN* is calculated in TELEMAC-3D simulation for each time step. An additional relationship, given in Equation 3.9b, is then applied during the mesh transformation to ensure the correct distance between two consecutive planes e.g. $HMIN / N_p$.

$$Z(IPOIN3) = \min\left\{\max\left[Z_f(IPOIN2) + \frac{I_p - 1}{N_p} HMIN, z^*(I_p)\right], Z(IPOIN2) - \frac{N_p - I_p + 1}{N_p} HMIN\right\} \tag{3.9b}$$

where $Z_f(IPOIN2)$ is the bottom elevation on the vertical of point *IPOIN3* and $Z(IPOIN2)$ is the free surface elevation on the vertical of point *IPOIN3*. $Z(IPOIN3)$ is the distance between two planes in 3D prismatic mesh. In this condition (Equation 3.9b) the prisms in 3D mesh are degenerated with a $HMIN / N_p$ depth.

The generalised sigma transformation code is coupled with the "hydrostatic inconsistency filter". This is mainly to avoid inconsistencies, which might occur on prisms, when one of the nodes of a lower layer has an elevation higher than one of the nodes of a higher layer. This would introduce major numerical instabilities during computation. Any inconsistency due to the diffusion and the bouyancy terms within the prisms is set to "zero". The 3D mesh is biased in the vertical section so that there are more layers close to the bottom.

3.8 Free surface modelling in the TELEMAC system

The TELEMAC-2D and TELEMAC-3D approaches to computing the free surface are the same. They calculate the water depth by integrating the pressure-continuity terms in the vertical direction (TELEMAC-3D, 1998). After calculating the water depth, the free surface is adjusted at each node taking account the bottom bathymetry and bed evolution. The continuity equation is then integrated between the bottom elevation and the free surface. Using Leibnitz's rule (TELEMAC-2D, 2001) the following equations are derived and solved for water depth and free surface at each time step assuming no bottom outfall in the domain.

$$\frac{\partial h}{\partial t}+\frac{\partial \overline{u}h}{\partial x}+\frac{\partial \overline{v}h}{\partial y}=0 \quad \text{or} \quad \frac{\partial h}{\partial t}+h\,div(\overline{\mathbf{u}})=0 \tag{3.10}$$

$$\frac{\partial \overline{u}}{\partial x}=-g\frac{\partial Z}{\partial x}+\overline{B}_x+\overline{S}_x$$
$$\frac{\partial \overline{v}}{\partial y}=-g\frac{\partial Z}{\partial y}+\overline{B}_y+\overline{S}_y \tag{3.11}$$

where $\overline{u}$ and $\overline{v}$ are the velocity components in horizontal palne, Z is the free surface, $\overline{B}_x$ and $\overline{B}_y$ are the vertically-averaged buoyancy terms (coriolis, etc.) in the x- and y-direction respectively and $\overline{S}_x$ and $\overline{S}_y$ are the other vertically averaged source terms (friction, etc.).

Equation 3.10 is similar to the continuity equation given in Equation 2.30 - replacing water density ρ by water depth h (which ensures perfect mass conservation). According to Hervouet & Jankowski (2000), this equation was thoroughly studied before implementation in TELEMAC-2D. As the velocities are known, the problem is linear and the divergence term in the equation can be treated to ensure perfect mass conservation. Once the new free surface elevation is known, the mesh is updated using σ-transformation and a new time step can then be performed.

The overscored letters (e.g. $\overline{u}$, $\overline{v}$ $\overline{B}_x$, $\overline{B}_y$, $\overline{S}_x$ and $\overline{S}_y$) in Equations 3.10 and 3.11 indicate the corresponding vertically integrated 3D variables computed by TELEMAC-3D (the value of which may be different from the value computed by TELEMAC-2D independently).

After calculating water depth (h) and the free surface elevation (Z), a simple mathematical relationship is maintained for the new bottom elevation (Z_f) i.e. $Z = h + Z_f$. During the sediment transport process, the value bottom evolution ΔZ_f is calculated and vertical coordinated are adjusted accordingly.

3.9 Turbulence modelling in the TELEMAC system

TELEMAC-2D and TELEMAC-3D generally use different turbulence model algorithms - although some of these are common for both modules including.

- Constant viscosity (TELEMAC-2D/TELEMAC-3D)
- Elder (TELEMAC-2D)
- Mixing length (TELEMAC-3D)
- Standard k-ε (TELEMAC-2D/TELEMAC-3D)
- k-ω (TELEMAC-3D)

Details on these models can be found in TELEMAC-3D (1998) and TELEMAC-2D (2002). In this study only the Standard k-ε model was used. Equations 2.61a and 2.61b are solved by a Fractional Step Method (Section 3.11.3), with convection of the turbulent variables being processed at the same time as the hydrodynamic variables, with the other terms relating to the diffusion and production/dissipation of the turbulent values being a single step. The following equations are solved during the k-ε model solutions:

$$\frac{k^{n+1}-\widetilde{k}}{\Delta t} - div[\frac{\nu_t}{\sigma_k} grad(k)] = P + P_{kv} - \varepsilon$$
$$\frac{\varepsilon^{n+1}-\widetilde{\varepsilon}}{\Delta t} - div[\frac{\nu_t}{\sigma_\varepsilon} grad(\varepsilon)] = PC_{1\varepsilon}\frac{\varepsilon}{k} + P_{\varepsilon v} - C_{2\varepsilon}\frac{\varepsilon^2}{k} \qquad (3.6e)$$

where $\widetilde{k}$ and $\widetilde{\varepsilon}$ are the intermediate value of k and ε within same time step during advection. The viscosity ν_t was calculated by the turbulence model using the value of the kinetic energy k and the dissipation ε. The initial value of the kinetic energy k and the dissipation ε are calculated using Equation 3.4. The viscosity was calculated using Equation 2.60c.

$$\nu_t = C_\mu \frac{k^2}{\varepsilon} \qquad (2.60c)$$

In general a finer mesh is required to solve the Standard k-ε model equations than, say, the Constant viscosity or Mixing Length models. Although it is more accurate than these models, it is also computationally more expensive.

3.10 An overview of SISYPHE

SISYPHE is a digital simulation module for non-cohesive sediment transport and bed evolution. It uses empirical formulae which may be expressed as functions of various hydrodynamic and sediment parameters. The bottom evolution equation is then solved using either a Finite Element or Finite Volume Method. This module cannot calculate the flow field independently, therefore the hydrodynamic variables are either imposed in the model using FORTRAN programming or exchanging result files (hydrodynamic and sediment transport) by coupling TELEMAC-2D/TELEMAC-3D and SISYPHE. The following bottom evolution equation (Equation 2.63) is solved at each node point in order to calculate the change of sediment thickness using mass balance:

$$(1-n_p)\frac{\partial Z_f}{\partial t} + div(\mathbf{Q}_s) = 0 \qquad (2.63)$$

where n_p is the bed porosity, Z_f is the bottom elevation (Figure 2.22) and $\mathbf{Q}_s$ is the sediment transport (volume) vector per unit width.

The following sediment transport formulae are programmed in SISYPHE for the calculation of sediment transport (volume) vector per unit width $\mathbf{Q}_s$ (SISYPHE, 2004).

- Meyer-Peter & Muller (1948)
- Einstein & Brown (1950)
- Engelund & Hansen (1967)
- Bijker (1968)
- Bailard (1981)
- Van Rijn (1984a)
- Dibajnia & Watanabe (1992)
- Hunziker (1995)
- Soulsby & Van Rijn (1997)

Description of these formulae can be found in relevant references mentioned above or Van Rijn (1993), Yang (1996) and SISYPHE (2004). For simplicity, SISYPHE (2004) considers all of these formulae in terms of the Shields parameter θ. This study used the Meyer-Peter & Muller (1948), Einstein & Brown (1950), Engelun & Hansen (1967) and Van Rijn (1984a) formulae. Details are in Section 2.3.6.

3.10.1 Coupling between bed-load and suspended load

The bed evolution Equation 2.63 is valid for only the bed-load transport assuming local equilibrium. Equation 2.63 is coupled with a transport-diffusion equation (Equation 3.13a) in order to consider the suspended sand concentration in non-equilibrium conditions.

$$\frac{\partial C}{\partial t}+U\frac{\partial C}{\partial x}+V\frac{\partial C}{\partial y}=\frac{1}{h}\left[\frac{\partial}{\partial x}\left(h\varepsilon_s\frac{\partial C}{\partial x}\right)+\frac{\partial}{\partial y}\left(h\varepsilon_s\frac{\partial C}{\partial y}\right)\right]+\frac{(E_e-D_d)_{z=a}}{h} \tag{3.13a}$$

where h is the water depth, U and V are the depth-averaged flow velocities in the x- and y-directions, C is the depth-averaged sediment concentration, ε_s is the sediment diffusivity coefficient. E_e - D_d is the net erosion minus the deposition flux of the sediment, which was calculated at the interface between the suspended-load layer and the bed-load layer ($z=a$). The erosion (E_e) and deposition (D_d) fluxes between the suspended load and their effect on the bed evolution are calculated using various semi-empirical expressions.

For uniform flat beds, the bed-load layer thickness is assumed to be proportional to the grain size d_{50}. For the rippled beds, it is proportional to the bed roughness k_s. The interface layer thickness between the bed-load and the suspended load i.e. $z = a$ is therefore determined according to SISYPHE (2004) as:

$$a = \max(2d_{50}, k_s) \tag{3.13b}$$

It should be noted that the passive scalar hypothesis is only valid for a dilute suspension i.e. when the sediment velocity is equal to the mean flow velocity without the effect of the vertical settling velocity.

The bottom evolution Equation 2.63 is modified in order to take into account the erosion and the deposition flux calculated from Equation 3.13a:

$$(1 - n_p)\frac{\partial Z_f}{\partial t} + div(\mathbf{Q}_s) + (E_e - D_d)_{z=a} = 0 \tag{3.13c}$$

Equation 3.13c clearly shows that when the erosion flux is equal to the deposition flux e.g. $(E_e - D_d)_{z=a} = 0$, there is equilibrium and the equation simplifies to Equation 2.63.

The choice of units of concentrations can be either in kg/m^3 for the mass concentration or dimensionless for the volume concentration. In order to avoid inconsistencies in the units of Equations 3.13a and Equation 3.13c, the volume concentration was used in this study.

The erosion and deposition term $(E_e - D_d)_{z=a}$ in Equations 3.13a and 3.13c is further approximated according to Celik & Rodi (1988), which is relevant for non-cohesive sediments. They considered the equilibrium volume concentration, the near bed concentration and the settling velocity to express the mathematical relationship for the prediction of the erosion and deposition fluxes (SISYPHE, 2004):

$$(E_e - D_d)_{z=a} = v_{ss}(C_{eq} - C_{z=a}) \tag{3.13d}$$

where v_{ss} is the settling velocity, C_{eq} is the near-bed concentration and $C_{z=a}$ is the near bed concentration calculated at $z=a$.

The Zyserman & Fredsoe (1994) formulation is used to calculate the near-bed concentration C_{eq}, which is expressed in terms of the critical Shields parameter θ_c and the Shields parameter θ taking account the bottom friction.

$$C_{eq} = \frac{0.331(\theta - \theta_c)^{1.75}}{1 + 0.72(\theta - \theta_c)^{1.75}} \tag{3.13e}$$

The near bed concentration is calculated as a function of the mean velocity U and the depth-averaged concentration C as:

$$C_{z=a} = \frac{UC}{u_*} \frac{\kappa}{I} \left[\frac{1 - a/h}{a/h} \right]^{R_p} \tag{3.13f}$$

$$I = I_1 \log(30h/k_s) + I_2$$

$$I_1 = \int_{a/h} \left(\frac{1-u}{u} \right)^{R_p} du \text{ and } I_2 = \int_{a/h} \left(\frac{1-u}{u} \right)^{R_p} \log(u) du \tag{3.13g}$$

$$R_p = \frac{v_{ss}}{\kappa u_*} \tag{3.13h}$$

where κ is the von Karman constant, u_* is the shear velocity, a is the interface layer between bed load and suspended load, h is the water depth, u is the velocity in the leading direction, $k_s = 2d_{50}$ is the bed roughness height, R_p is the Rouse number and I, I_1 and I_2 are the so-called Einstein integrals (SISYPHE, 2004).

The suspended sediment transport rate (q_s) is calculated by integrating the product of the Rouse concentration profile $c(z)$ and the logarithmic velocity profile $u(z)$ (SISYPHE, 2004):

$$q_s = \int_a^{z_1} u(z)c(z)dz \tag{3.13i}$$

3.10.2 The bed slope effect

Most of the time incipient sediment motion criteria – and hence sediment transport – is described for flat bed (horizontal) channel conditions. In reality streambeds are rarely flat and the particles normally lie on a slope. The effect of a slopping bottom is to increase the sand transport rate in the down-slope direction, and to reduce it up-slope. This is particularly so for sediment movement where scour and deposition is taking place.

This study considered a correction factor to both the magnitude and the direction of the solid transport rate before solving the bed evolution Equation 2.63. The correction method is based on Koch & Flokstra (1981).

The solid transport rate intensity is multiplied by a factor SF to take into account the change of the vertical coordinates and the horizontal coordinates along the current direction.

$$SF = 1 - \beta \frac{\partial Z_f}{\partial m} \tag{3.13j}$$

where m is the co-coordinate in the current direction and β is an empirical constant that varies between 0.6 and 1.3.

The correction factor due to the change of solid transport direction is applied considering the direction of solid transport (α_a) and the direction of the bottom shear stress (δ_a) in relation to the flow direction. If r is the co-ordinate along the axis perpendicular to the flow (transverse or vertical) then the change in direction of the solid transport is taken account using Equation 3.13k.

$$\tan \alpha_a = \tan \delta_a - \beta \frac{\partial Z_f}{\partial r} \tag{3.13k}$$

The value of empirical constant $\beta = 1.3$ is used in accordance with SISYPHE (2004). The effect of bed slope is then similar to adding diffusion term in the bed evolution equation. This value might tend to smooth the results and reduce the instabilities. This formulation however does not include the effect of friction angle and is only applicable for a gentle slope.

3.11 Numerical techniques used by the TELEMAC system

There are a large number of numerical techniques implemented in the TELEMAC system. These techniques are used to get numerical solutions of the various different equations. This section will briefly discuss the commonly used numerical techniques such as the numerical schemes, solvers and numerical algorithms.

3.11.1 The numerical schemes

In TELEMAC system, different numerical schemes or techniques are implemented for the solution of the governing fluid flow equations with the desired accuracy. Details of those can be found in TELEMAC-3D (1998), TELEMAC-2D (2001), TELEMAC-2D (2002), SISYPHE (2004) and BIEF (2004). Some of common features are discussed below.

In TELEMAC-2D, the common numerical schemes are:

(i) Method of Characteristics

(ii) Centred semi implicit scheme + SUPG

(iii) Conservative scheme + SUPG

(iv) PSI scheme

Different schemes can be chosen for different variables (e.g. velocity, depth, tracer and k-ε) during simulations. The Conservative scheme + SUPG (Streamline Upwind Petrov Galerkin) is valid only for advection of depth. Advection of the k-ε model can only be done with the Method of Characteristics. The stability of a PSI scheme is conditioned by ensuring a Courant number lower than 1.0. TELEMAC-2D (2002) suggests using the Method of Characteristics for solving all variables. Depending on the scheme used, mass-conservation can be improved using so-called sub-iterations within same time step. It should be noted that the TELEMAC-2D time discretisation is so-called semi-implicit (TELEMAC-2D, 2001). This implies that the time related weighting parameters e.g. θ_h and θ_u (Section 3.6) should not be less than 0.5.

The schemes related to SUPG are further configured depending on which types of upwind scheme give stable solutions; (i) no upwind scheme, (ii) upwind scheme with the classic SUPG method and (iii) upwind scheme with the modified SUPG method. In principle, option (ii) is more stable when Courant number is less than 1.0 and option (iii) is more stable otherwise.

When solving the linearized system $AX = B$ (Equation 3.14), TELEMAC-2D offers the possibility of mass-lumping on the mass matrices.

$$A = \begin{bmatrix} AM1 & BM1 & BM2 \\ CM1 & AM2 & 0 \\ CM2 & 0 & AM3 \end{bmatrix},\ X = \begin{bmatrix} \delta h \\ u \\ v \end{bmatrix},\ B = \begin{bmatrix} CV1 \\ CV2 \\ CV3 \end{bmatrix} \tag{3.14}$$

where *AM1*, *AM2*, *AM3*, *BM1*, *BM2*, *CM1* and *CM2* are the regular block matrices and *CV1*, *CV2* and *CV3* are the right hand side terms of known values. The values in each block matrices are the combination of matrices consisting of the mass matrices, the diffusion matrices, matrices related to the "gradient and divergence" (in continuity and momentum equations), matrices related to the k-ε and the friction matrices (TELEMAC-2D, 2001; pp 71-74).

This mass-lamping technique brings some or the entire matrix on the diagonal, and enables computation times to be considerably shortened (TELEMAC-3D, 1998; Hervouet & Jankowski, 2000).

The TELEMAC-3D formulation is more complex than that of TELEMAC-2D and SISYPHE. For simplicity TELEMAC-3D solves water depth using same library codes as in TELEMAC-2D. The schemes for advection of depth during TELEMAC-3D simulation are considered separately and these are:

(i) Method of Characteristics

(ii) Explicit + SUPG

(iii) Hybrid scheme (characteristics + SUPG)

(iv) Conservative scheme

It should be noted that the conservation scheme in TELEMAC-3D is similar in TELEMAC-2D except for SUPG option. This constraint is specific in TELEMAC-3D to improve the mass-conservation without sub-iterations (TELEMAC-3D, 1998).

As far as schemes with 3D variables are concerned (all variables except the water depth), the following possibilities are available in TELEMAC-3D:

(i) Method of Characteristics

(ii) Centred semi-implicit scheme + SUPG decentring

(iii) Hybrid scheme (characteristics + centred explicit)

(iv) Explicit scheme + MURD-N scheme

(v) Explicit scheme + MURD-PSI scheme

Despite slightly more computational time, TELEMAC-3D (1998) recommends scheme (iv) and (v) for tracers to overcome oscillations in the solution. It strongly recommends scheme (i) for the velocity components and the k-ε model. Depending on the scheme used, mass-conservation may be improved by running sub-iterations within a time step. Like TELEMAC-2D, TELEMAC-3D schemes also allow mass-lumping on the mass matrices in order to reduce computational time.

Unlike TELEMAC-2D (2002) and TELEMAC-3D (1998), SISYPHE (2004) only uses the SUPG scheme including Method of Characteristics and PSI scheme.

It should be noted that the scheme for activation of diffusion is only implicit in TELEMAC-2D, TELEMAC-3D and SISYPHE.

3.11.2 The solver and accuracy

During solving the linear system, the original equations can be replaced by the generalised wave equation obtained by eliminating the velocity from the continuity equation using a value obtained from the momentum equation. This technique increases the calculation speed but has the disadvantage of artificially smoothing the results. This is a user choice; the TELEMAC-3D default code solves the original equations. The wave equation option is particularly recommended for steady-state calculations.

The solver is used for solving the systems of equations. The choice of solver is the same in TELEMAC-2D, TELEMAC-3D and SISYPHE. Seven different solvers are available in the TELEMAC system. These are:

(i) Conjugate gradient

(ii) Conjugate residual

(iii) Conjugate gradient on normal equation

(iv) Minimum error

(v) Square conjugate gradient

(vi) CGSTAB (stabilised conjugate gradient)

(vii) GMRES (Generalised Minimum RESidual)

All these methods are iterative for the solution of the linear system $AX = B$. Starting with an estimate X^0, they construct a series of vectors X^m that converge towards the exact solution of the system provided of course that A has the required properties. Details can be found in BIEF (2004).

In TELEMAC-2D and SISYPHE simulation, GMRES method is the most economical. The GMRES method with a Krylov space dimension equal to 2 or 3 seems to fit most cases, however, the optimum value of this parameter generally increases with the mesh size (TELEMAC-2D, 2002; BIEF, 2004). According to TELEMAC-3D (1998), GMRES appears to be highly effective in many cases. Severe oscillations were however observed using GMRES during the modelling of local scour in this study. Conjugate gradient and conjugate gradient on normal equation were found slightly stable compared to GMRES.

Iterative Method requires the specification of the required accuracy that is to be achieved during the solution process. The maximum numbers of iterations are also defined to prevent the computations from excessive looping if the required accuracy is not achieved. Higher accuracy requires more computational time. The time step, mesh size, solver and accuracy are the crucial parameters in dealing with numerical stability.

According to TELEMAC-3D (1998), when solving a system of equations by a Conjugate Gradient Method, convergence can often be hastened by means of so-called preconditioning (TELEMAC-3D, 1998; TELEMAC-2D, 2002; BIEF, 2004). The various possibilities are:

(i) Diagonal preconditioning

(ii) Diagonal preconditioning with condensed matrix

(iii) Diagonal preconditioning with possibility for the diagonal to have nil or negative value

(iv) Crout's preconditioning per element

(v) Diagonal preconditioning and crout's preconditioning per element

(vi) Diagonal preconditioning with condensed matrix and crout's preconditioning per element

In general option (i) is recommended, however, if solution requires more iterations, option (iv) is preferred for numerical stability.

3.11.3 The solution algorithm

The fundamental concepts of the solution algorithms are similar in TELEMAC-2D, TELEMAC-3D and SISYPHE. The solution algorithms depend on the consideration of the numerical schemes. If the Method of Characteristics is chosen, the equations are treated in two steps using the Method of Fractional Steps:

(i) First step: the advection terms corresponding to transport of the physical variables h, u, v and w and in the alternative k and ε are treated taking account the hyperbolic character of the equations.

(ii) Second step; the remaining equations are treated i.e. propagation, diffusion, source terms and advection terms when there is no recourse to the Method of Characteristics. This stage is solved by the Finite Element Method discretisation of time that allows the elimination of non-linearity of the equations. Discretisation of space transforms the continuous equations into a linear discrete system where the values of h, u, v, and w at the nodes are the unknown variables. The system is solved by the Conjugate Gradient Method or GMRES.

In the Fractional Step Method, with space time discretised, the unknowns are located at multiples of the given time step Δt such that $t^n = t^0 + n\Delta t$. The derivative with respect to time of a function f is discretised as:

$$\frac{\partial f}{\partial t} = \frac{f^{n+1} - f^n}{\Delta t} \tag{3.15a}$$

where f represents unknown variable h, u, v, w, k, and ε. Starting from the initial solution f^0 at time t^0, the solution is obtained successive iterations (time steps) by finding first f^1 then f^2, etc. Within the time step, this method consists of finding f^{n+1}, starting from f^n, and passing through intermediate steps for variables h, u, v, w, k, and ε and such that:

$$\text{First } \frac{\tilde{f} - f^n}{\Delta t} + advection\ \ terms = 0 \text{ and then } \frac{f^{n+1} - \tilde{f}}{\Delta t} + other\ \ terms = 0 \tag{3.15b}$$

where $\tilde{f}$ is the intermediate value of f within same time step during advection. The approximation in time will be of order one because certain advection terms are not discretised at $t^n + \Delta t/2$. Detail can be found in TELEMAC-2D (2001).

When the Method of Characteristics is not considered, the complete set of equations is solved for propagation-diffusion-source terms. This is performed by:

- Discretisation in time
- Discretisation in space

Generally speaking the "discretisation in time", called semi-implication, cannot be strictly applied. This is because the Fourier analysis of the Semi-implicit Method does not take into account non-linearity or the boundary conditions. A safety margin is thus provided in the TELEMAC system by expressing a function f as; $f = \theta_t f^{n-1} + (1-\theta_t) f^n$, with $\theta_t > 0.5$ while always remaining close to this value (minimum 0.5) or up to 1. Details can be found in TELEMAC-2D (2001).

In "discretisation in space", the functions f will be evaluated only at the discretisation points (node points at mesh) by decomposing into the base functions as (TELEMAC-2D, 2001):

$$f = \sum_{i=1}^{n} f_i \psi_i \tag{3.15c}$$

where n is the number of discrete points, f_i is the value of the function f at point i and ψ_i is the function associated with that point. Each of these base functions is associated to a degree of freedom. This function evaluates to 1 at this point and to 0 at all other points. Within the element the function is interpolated from the values at the nodes of discretisation. The interpolation functions are within a reference element, which has corresponding domain element linked by isoparametric geometrical transformation.

The reference elements are three node triangles in TELEMAC-2D or SISYPHE and six node prisms in TELEMAC-3D simulation. The base functions of these elements are determined using isoparametric transformation with linear interpolations. This is because isoparametric transformation in triangles with linear interpolation can be easily inverted. Details can be found in TELEMAC-2D (2001) and BIEF (2004).

"In TELEMAC-3D", the general numerical solution techniques consist of the activation of three steps: the advection step, the diffusion step and the free-surface-continuity-pressure step (propagation step) as:

$$\frac{\partial f}{\partial t} = \frac{f^{n+1} - f^{d}}{\Delta t} + \frac{f^{d} - f^{a}}{\Delta t} + \frac{f^{a} - f^{n}}{\Delta t}$$

(3.15d)

The advection step $\frac{f^{a} - f^{n}}{\Delta t} + \mathbf{u} \bullet grad(f) = 0$ can be solved depending on the chosen option and its hyperbolic character e.g. by the Method of Characteristics, by the Streamline Upwind Petrov Galerkin (SUPG) or by the distributive schemes such as PSI scheme.

The diffusion step $\frac{f^{d} - f^{a}}{\Delta t} - div(\nu_t \, grad\, f) = 0$, which is parabolic in character, can be solved by the implicit scheme. Generally speaking the performance of this step is dependent on the value of the implication coefficients (time weighting function), which ranges between 0.5 and 1.0. The default value in TELEMAC-3D (1998) is 0.55; however, often value 1.0 is suggested in order to get smooth solution and convergence.

In the free-surface-continuity-pressure step (or propagation step), Equation 3.10 is solved. The conservative scheme is often preferred to ensure improved mass-conservation with sub-iterations (TELEMAC-3D, 1998).

"In SISYPHE", using the Finite Element theory, Equation 2.63 is approximated by the predictor-corrector concepts split up into three steps; prediction, correction and final (SISYPHE, 2004).

$$(1 - n_p)\frac{\partial Z_f}{\partial t} + div(\mathbf{Q}_s) = 0$$

(2.63)

In the "prediction step", Equation 2.63 is approximated by applying the associated mass matrices and the base functions derived for each node of the discretised domain. This step is used to assess the bottom depth at time $(n+1)\Delta t$:

$$M\tilde{Z}_f^{\,n+1} = MZ_f^{\,n} - \Delta t \cdot \int_{\Omega} div\left(\mathbf{Q}_s^{\,n}\right) \cdot \Psi_i \cdot d\Omega$$

(3.16a)

where $Z_f^{\,n}$ is the bottom depth at the time $n\Delta t$, Δt is the time step, $\tilde{Z}_f^{\,n+1}$ is the assessment of the bottom depth at time $(n+1)\Delta t$, M is the mass matrix and Ψ_i is the base function derived from discretised element nodes during isoparametric transformation (BIEF, 2004). The value $\mathbf{Q}_s^{\,n}$ is calculated using the given sediment transport formula (Section 2.3.6) and hydrodynamic variables imposed by TELEMAC-2D or TELEMAC-3D.

In the "correction step", the sediment transport is computed and verified using the first assessment of the bottom elevation carried out in the "prediction step" using θ_t time weighting factor at the time $(n+1)\Delta t$.

$$\mathbf{Q_s}^{n+1} = \theta_t \mathbf{Q}_s{}^{n}\left(\tilde{Z}_f{}^{n+1}\right) + (1-\theta_t)\mathbf{Q}_s{}^{n} \tag{3.16b}$$

The value $\mathbf{Q}_s{}^{n}$ and $\mathbf{Q}_s{}^{n+1}$ is computed using the Semi-explicit Method with SUPG (upwind schemes, Section 3.11.1) for a default value of $\theta_t = 0.5$.

In the "final step", the following Equation 3.17c is solved for the bed evolution taking account the bed porosity n_p.

$$(1-n_p)\frac{\partial Z_f}{\partial t} = -div\left(\mathbf{Q_s}^{n+1}\right) \tag{3.16c}$$

3.12 Post-processing module RUBENS

RUBENS in the TELEMAC system is a one-dimensional (1D) or 2D graphics visualisation module to process and manipulate simulation output data. RUBENS cannot handle TELEMAC-3D output; therefore, an interface module POSTEL-3D is required. The POSTEL-3D code enables the results of TELEMAC-3D to be displayed simply and quickly by RUBENS. Details can be found in POSTEL-3D (1998) and RUBENS (1998). Some of the features of RUBENS are:

- Domain geometry and grid display
- Isovalue curves and coloured areas
- Line and shaded contour plots
- Current line and trajectories
- Space and time dependent profiles
- 2D and 3D profiles with its perspectives
- Vector fields

All the graphical representations of simulation results of this study were carried out using RUBENS and POSTEL-3D.

3.13 Summary

The TELEMAC system was described. This chapter is essential background material for understanding Chapter 4, where the adaptation of TELEMAC V5.5 for the purpose of modelling local scour around bridge piers is described. Particular emphasis was given to the features which were used in this study.

- MATISSE constructs the density map driven triangular mesh in 2D space. The mesh generation is user friendly. The 2D mesh needs to be reproduced along the vertical on a number of curved surfaces to construct the 3D prismatic mesh during TELEMAC-3D simulation. The sigma transformation coupling with the hydrostatic inconsistency filter may be useful to adjust the 3D mesh during bottom evolution. Care and judgement has to be applied to the fixing of liquid boundaries and meshing of the entire domain.
- TELEMAC-2D solves the Saint-Venant equations for the depth-averaged velocity components and water depth. TELEMAC-3D solves the Navier-Stokes equations for 3D velocity components using either hydrostatic or non-hydrostatic pressure distribution. During TELEMAC-3D simulation, TELEMAC-2D is automatically activated for the calculation of the water depth or free surface.
- The TELEMAC system offers four different turbulence models including the Standard k-ε model. This study used the k-ε model.
- SISYPHE solves the bed evolution equation using various sediment transport formulae from the existing literature e.g. Meyer-Peter & Muller (1948), Einstein & Brown (1950), Engelund & Hansen (1967) and Van Rijn (19984a). This study focuses on the channel bottom evolution using these four formulae rather than computing the rate of sediment transport.
- A large number of numerical techniques are implemented in the TELEMAC system. These techniques are used to compute numerical solutions of the various different equations. This section discusses the commonly used numerical techniques e.g. numerical schemes, solvers and solution algorithms which are relevant to this study.

Chapter 4
Development of the local scour model

4.1 Introduction

This study is concerned with the prediction of local scour around a circular bridge pier using the TELEMAC numerical modelling system. For simplicity, non-cohesive uniform quartzitic sand was used as a bed material and the circular pier was embedded vertically into the bed. The flow field was modelled in 2D and 3D flow using TELEMAC-2D and TELEMAC-3D respectively. In 2D, the Saint-Venant equations were solved whereas the Navier-Stokes equations were solved in 3D. Turbulence was modelled using the two-equation Standard k-ε turbulence model. The bed evolution equation was solved using four different sediment transport formulae. The hydrodynamic models (TELEMAC-2D or TELEMAC-3D) were coupled with the sediment transport equations in SISYPHE in order to simulate the deformation of the bed as result of scour and deposition around the piers.

The model was initially developed using TELEMAC V5.4. After receiving TELEMAC V5.5 from the supplier SOGREAH Consultants, France, the later version was used to develop the model. The software supplier assisted with online technical support during this investigation.

The original intention was to validate the model against reliable physical model data, however, reliable detail physical model data was difficult to obtain. In the end, the physical model data of Ahmed (1995) was used. He investigated the flow fields and scour around cylindrical piers for mobile bed arrangements using a Prandtl tube for the definition of the velocity profile and the bed shear stress in the plane of symmetry.

The purpose of this chapter is to describe the way TELEMAC was manipulated to develop the local scour model, which was then verified against the scour results given in Ahmed (1995). A description of the model development is provided including the adaptation of the different physical and numerical parameters essential for numerical modelling. The simulation results are presented and discussed in Chapter 5.

4.2 A brief description of the Ahmed (1995) model data

4.2.1 General description

Ahmed's (1995) model experiments were conducted in a straight rectangular flume 18.4 m long, 1.22 m wide and 0.67 m deep at the University of Alberta, Canada. For water flow, he used a pumping system of maximum capacity 0.072 m^3/s (72 l/s). The discharge was measured by a 200 mm diameter Foxboro magnetic flow meter using a Fluke 8000A digital multimeter display. The header tank was 2.44 m long and 1.8m wide, and had smooth semi-circular contractions from the sidewalls and the floor into flumes.

A weir of masonry brick was used to dissipate the turbulence caused by the delivery pipe. Then the water was guided through a flow straightener consisting of a number of 1 m long pipes with a diameter of 100mm. 50 mm thick mattresses of synthetic hair-like material were placed both upstream and downstream of the flow straightener to also help suppress the surface waves and turbulence.

A wooden frame 0.165 m high and 10 m long was constructed on the flume bed and was covered with a 15 mm thick layer of sand having the desired diameter. At the upstream end of the wooden frame, a 1:14.5 ramp covered with rough sand paper was constructed to provide the smooth transition of water depth. A 0.78 m by 0.78m sediment recess was constructed in the wooden frame at a distance of 7.5 m from the start of sand bed. The cylinder of the desired diameter was placed vertically inside the centre of the sediment recess. The size of the recess was sufficient for containing the scour hole. Figure 4-1 shows the Ahmed (1995) experimental apparatus.

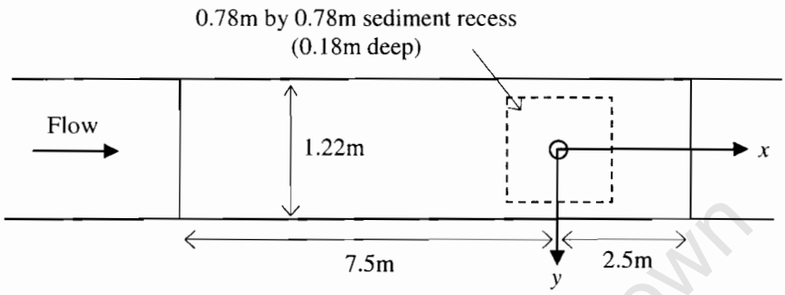

Figure 4-1: Ahmed (1995) experimental domain

4.2.2 Physical parameters in Ahmed (1995)

Two types of physical parameters were given in Ahmed (1995): one is related to the sediment characteristics and the other is related to the characteristics of undisturbed flows. The sediment properties are shown in the Table 4.1.

Table 4-1: Sediment characteristics in Ahmed (1995)

Properties	Value
Median diameter d_{50} (mm)	0.88
$d_{15.9}$ (mm)	1.11
$d_{84.1}$ (mm)	0.75
Geometric standard deviation, σ_g	1.22
Specific gravity, s	2.65
Angle of repose, ϕ_r (degree)	28
Critical shear stress, τ_c (Pa)	0.420

The properties of sand were derived from the grain size distributions. The median diameter of sand 0.88 mm was calculated using Equation 2.3 in the Ahmed (1995) study. The geometric

standard deviation of fine sand was 1.22 (Equation 2.6), which essentially indicates uniform sediment particles (Melville, 1997).

Ahmed (1995) determined the characteristics of the fully developed undisturbed flow by measuring the velocity profile. Pitot-static tubes were used to measure the velocity when the direction of flow was known i.e. the undisturbed 2D flow on the centre line of the flume without the cylinder in place. A set of yaw and pitch probes was used when the flow directions were unknown in the vicinity of the cylinder. A data acquisition system, run on a Macintosh FX II computer, was used to log the velocity at points of interest. The velocity at each point was computed as the arithmetic average of 2000 samples. The log-law equations were then used to establish the velocity profiles. Based on an analysis of his measured velocity profile, Ahmed (1995) derived the various other parameters related to the undisturbed flow. These and other relevant parameters are given in Table 4-2, which were used in this study. Further details can be found in Ahmed (1995).

Table 4-2: Undisturbed flow characteristics in Ahmed (1995)

Characteristics	Value
Nature of bed	Sand (see Table 4-1)
Channel width (m)	1.22
Water depth, h (m)	0.182
Discharge, Q (m^3/s)	0.05
Average velocity, U (m/s)	0.2252
Froude Number, $Fr = U/\sqrt{gh}$	0.1685
Bed shear stress, τ_0 (Pa)	0.1931
Shear ratio (τ_0 / τ_c)	0.46
Shear velocity, $u_* = \sqrt{\tau_0/\rho}$ (m/s)	0.013897
Nature of turbulent flow	Transitional
Particle Reynolds number ($Re_* = d_{50}u_*/\nu$)	12
Roughness Reynolds number ($Re_s = k_s u_*/\nu$)	35
Roughness height, k_s (mm)	2.65
k_s / d_{50}	3.01

4.2.3 Scour depth and scour profiles in Ahmed (1995)

The scour profiles in the upstream, at the downstream and on the lateral side of the cylinder were measured using a Vernier point gauge. The smallest division on the scale was 1 mm, thus the nominal uncertainty in measurement on a flat bed was 0.5 mm at a 95% confidence level. According to Ahmed (1995), the uncertainty in the depth measurement inside the scour hole with inclined bed was also estimated to be 1 mm. Since the scour depth at any level was calculated as the difference between these two measurements, the uncertainty in scour depth was about 1.12 mm as determined using the procedure described in Kline & McClintock (1953). Ahmed (1995) measurement points were spaced 5 mm apart for measuring the

upstream and lateral scour profiles. A spacing of 5 mm was also generally used for the downstream scour profiles, except when the bed level variation was small then a larger spacing (10-20 mm) was used. The measurement of a single profile took about 5 to 15 minutes depending on its length, and the middle point of the time period was taken as the representative measurement time of that profile. The scour profiles were taken many times during the mobile bed runs.

Ahmed (1995) only reports on scour profiles for mobile bed run reference A3M (Ahmed, 1995; pp 285-288). This study was thus aimed to model this using TELEMAC V5.5. The diameter of the cylinder during A3M run was 0.064 m. Figure 4-2, Figure 4-3 and Figure 4-4 depict the Ahmed (1995) scour profiles at the upstream, laterally and downstream of the pier respectively.

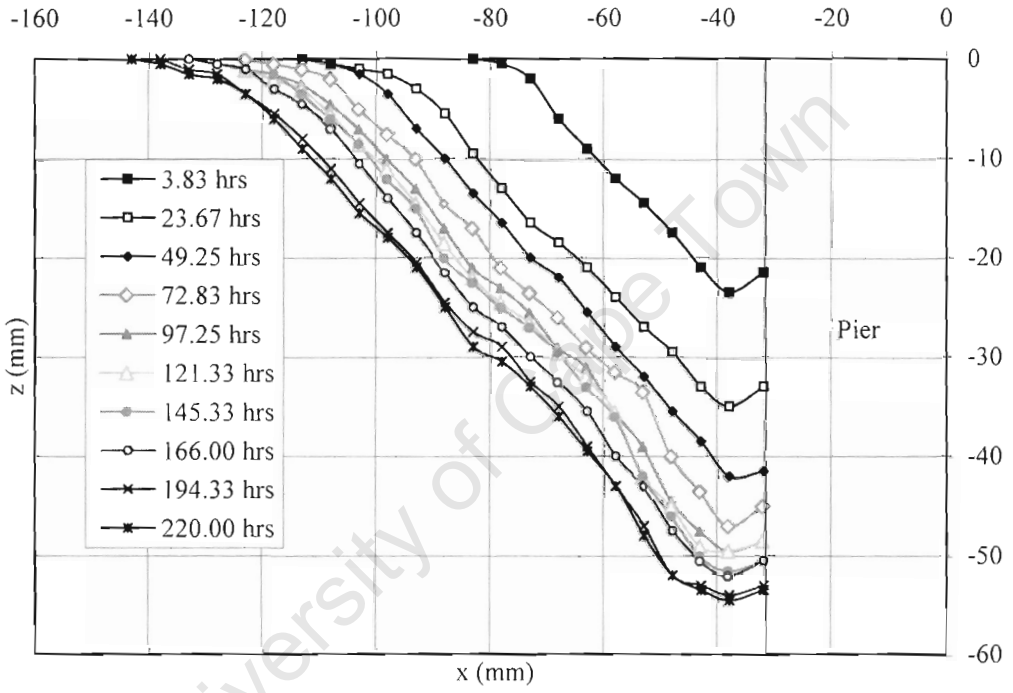

Figure 4-2: Ahmed (1995) scour profiles at upstream of the pier

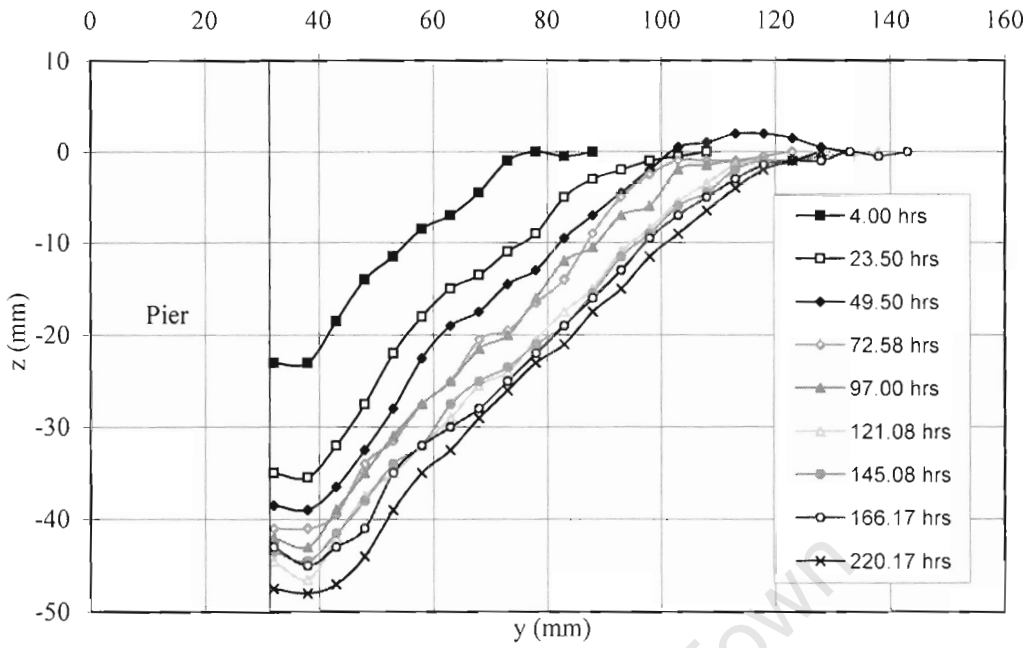

Figure 4-3: Ahmed (1995) lateral scour profiles

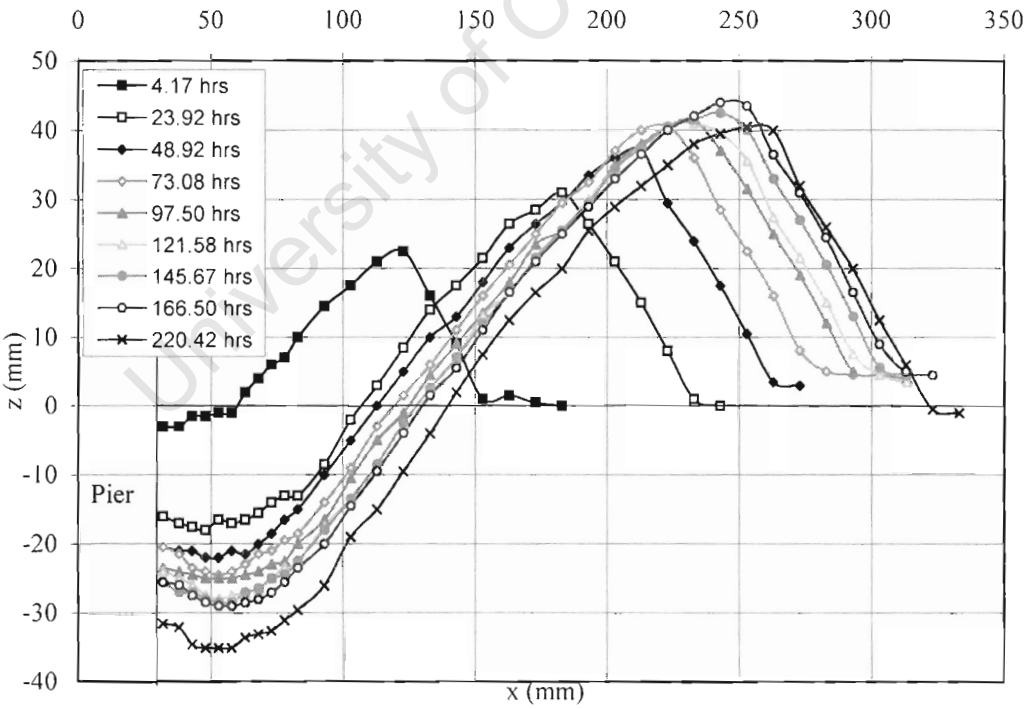

Figure 4-4: Ahmed (1995) scour profiles downstream of the pier

4.3 Dimensional analysis to modify key parameters

At the very beginning of this study, it was found that TELEMAC V5.5 was computationally uneconomical or numerically unstable for the solution of a small geometrical domain such as the flume dimensions given in Ahmed (1995). The TELEMAC system is designed for large domains and actual field data (Lang, 2005). Before describing the domain discretisation, it would therefore be useful to describe the dimensional analysis, which was used to model Ahmed (1995) data at the relatively larger scale for the TELEMAC simulations. Care was taken to select the optimum dimensions of the domain in order to avoid the need for unnecessary points resulting in a longer computational time. A length scale factor X_f of 0.1 was selected based on the following definition:

$$X_f = \frac{L_{ahm}}{L_{tel}} = 0.1 \tag{4.1}$$

where L_{ahm} is the length scale representing the Ahmed (1995) domain and L_{tel} is the length scale for the TELEMAC simulations.

It should be noted that, apart from the domain dimensions, some of the other key parameters such as the prescribed flow rate (discharge) also had to be adjusted. The value of the discharge for the TELEMAC domain was calculated using Froude number (Equation 4.2) and Continuity (Equation 4.3) similarity:

$$\frac{U_{ahm}}{\sqrt{g_{ahm} L_{ahm}}} = \frac{U_{tel}}{\sqrt{g_{tel} L_{tel}}}, \text{ which can be recast as } \frac{U_{ahm}}{U_{tel}} = \sqrt{\frac{L_{ahm}}{L_{tel}}} = X_f^{0.5} \tag{4.2}$$

$$\frac{Q_{ahm}}{Q_{tel}} = \frac{A_{ahm} U_{ahm}}{A_{tel} U_{tel}}, \text{ which can be recast as } \frac{Q_{ahm}}{Q_{tel}} = \left(\frac{L_{ahm}}{L_{tel}}\right)^2 \sqrt{\frac{L_{ahm}}{L_{tel}}} = X_f^{2.5} \tag{4.3}$$

Using Equations 4.1 to 4.3, the channel width, depth of flow, flow rate were calculated as 12.2 m, 1.82 m and 15.81 m^3/s respectively.

Other parameters in the TELEMAC system also had to be adjusted e.g. the Chezy's coefficient used to calculate the bed shear stress. SISYPHE (2004) calculates bed shear stress τ_0 using the depth-averaged velocity, the density of water ρ and the quadratic friction coefficient c_f. TELEMAC uses the Chezy's coefficient C_h to calculate the quadratic friction coefficient c_f.

Using Equation 4.4 and 4.5 and the parameters given in Ahmed (1995) (Table 4-2), the Chezy's coefficient C_h was calculated and found to be 50.0 $m^{1/2}/s$.

$$\tau_0 = \frac{1}{2} c_f \rho U^2 \tag{4.4}$$

$$c_f = \frac{2g}{C_h^2} \tag{4.5}$$

This study assumes negligible channel bottom slope e.g. flat channel bed. The effect of the change of flow geometry on the sediment particle size and hence on the critical shear stress was also neglected.

4.4 Determination of the physical input parameters

The basic model input parameters were the initial water depth h, the prescribed flow rate Q, the median diameter d_{50}, the Chezy's friction coefficient C_h, the settling velocity v_{ss}, the critical Shields parameter θ_c and the bed porosity n_p.

The initial water depth h and the prescribed flow rate Q given in Ahmed (1995) were adjusted using Equation 4.1 and Equation 4.3 as 1.82 m and 15.81 m^3/s respectively. The median diameter of sediment particles d_{50} was taken to be 0.88 mm as indicated in Table 4-1.

The Chezy friction coefficient C_h determined and found to be 50.0 $m^{1/2}/s$ (Section 4.3). This was used for the treatment of the source terms added to the governing fluid flow equations (Equation 4.16d) during simulations. This coefficient was used for the prediction of the vertical shear during turbulent energy production (Equation 2.61b). Also in the sediment transport simulation, the friction coefficient was used to calculate the bed shear stress and the bed roughness (Equations 4.4 and 4.5).

The settling velocity v_{ss} was used to model the suspension on particles and their transport during scour and deposition process. The Cheng (1997) equation (Equation 2.8) was used to determine the settling velocity (v_{ss}) using the relative submerged density Δ and the dimensionless particle diameter d_*. The settling velocity was calculated and found to be 0.1m/s.

$$v_{ss} = \frac{v\left(\sqrt{25 + 1.2 d_*^2} - 5\right)^{1.5}}{d}, \text{ where } \Delta = \frac{\rho_s - \rho}{\rho} \text{ and } d_* = \left(\frac{\Delta g}{v^2}\right)^{1/3} d \tag{2.8}$$

The critical Shields parameter θ_c was given to the model as the incipient sediment motion criterion (Equation 2.20). This parameter was also used to quantify the sediment transport during the local scouring process. This parameter was calculated using the associated parameters given in Table 4-1, Table 4-2 and Equation 2.20 and found to be 0.029.

The porosity n_p was given to the model to take into account the effect of the porous nature of the bed material during simulation. The porosity was calculated assuming a dense uniform sand bed with a 15% moisture content (Das, 2002) and found to be 28.0%:

$$n_p = \frac{w_w s}{1 + w_w s} \tag{4.6}$$

where w_w is the moisture content and s is the specific gravity. The model actually uses a porosity function (*XKV*), defined as (SISYPHE, 2004):

$$XKV = \frac{1}{1 - n_p} \tag{4.7}$$

This value was calculated and found to be 1.4.

4.4.1 Criteria used for clear-water scour

Clear-water scour occurs when no sediment is supplied from the approach channel to the scoured region; in other words, the particles along the bed upstream of the scour region are at rest. This study investigated the condition of clear-water scour.

Three critical conditions for clear-water scour were used; the critical shear stress (Shields, 1936), the critical velocity (Yang, 1973) and the inception densimetric Froude number (Hager & Oliveto, 2002). The conditions for clear-water scour may be defined as follows:

$$\theta < \theta_c \tag{4.8a}$$

$$U < U_c \tag{4.8b}$$

$$F_d < F_{di} \tag{4.8c}$$

where θ and θ_c are the Shields parameter and the critical Shields parameter respectively, U and U_c are the average mean velocity and the critical velocity respectively, and F_d and F_{di} are

the densimetric particle Froude number and the inception densimetric particle Froude number respectively.

Shields (1936) relation has been the subject of intense criticism from e.g. Yang (1973) and Hager & Oliveto (2002), but is commonly used for the inception of sediment transport. Equation 4.8a was therefore used as a first criterion to satisfy clear-water condition upstream of the pier. The value of θ and θ_c were calculated using Equation 2.19 and Equation 2.20 respectively.

For Equation 4.8b, the critical velocity was calculated and verified according to Yang (1973) (in Yang, 1996) using the dimensionless critical velocity (U_c/v_s) and the particle Reynolds number (Re_*). Details are in Section 2.3.4 (Figure 2-13).

The condition given in Equation 4.8c was calculated and verified according to Hager & Oliveto (2002). Their criterion was based on the median sediment diameter d_{50}, mean velocity U and hydraulic radius R_h. The main advantage of their approach is that the equations are free from bed shear stress and thus shear velocity, which are often difficult to measure. The value of F_d and F_{di} were calculated and verified as (Hager & Oliveto, 2002):

$$F_d = \frac{U}{\sqrt{(s-1)gd_{50}}} \tag{4.8d}$$

$$F_{di} = 2.33 d_*^{-0.25}\left(\frac{R_h}{d_{50}}\right)^{1/6} \qquad d_* \le 10 \tag{4.8e}$$

$$F_{di} = 1.08 d_*^{1/12}\left(\frac{R_h}{d_{50}}\right)^{1/6} \qquad 10 < d_* < 150 \tag{4.8f}$$

$$F_{di} = 1.65\left(\frac{R_h}{d_{50}}\right)^{1/6} \qquad d_* \ge 150 \tag{4.8g}$$

$$d_* = \left(\frac{(s-1)g}{v^2}\right)^{1/3} d_{50} \tag{2.8b}$$

where R_h is the hydraulic radius and s is the specific gravity.

All these conditions were found sufficient to ensure that there was no sediment transport upstream of the pier used in this study.

4.5 Development of computational domain

Once the physical model dimensions (Ahmed, 1995) described in Section 4.2.1 and Section 4.2.2 had been transformed into a much larger computational model using dimensional analysis (Section 4.3), the domain was then discretised mathematically to form the computational mesh. The mesh consisted of triangles with nodes at each apex where the flow equations were to be solved. During this procedure care had to be taken to minimise the numerical truncation errors in order to save computational time.

Following the work reported by McGahey (2001), Ali & Karim (2002), Armitage & McGahey (2003) and Salaheldin et al (2004), the locations of the upstream and the downstream boundary were modelled with extreme care. The upstream boundary was located at a distance of $62D$ from the upstream face of the pier, whilst the downstream boundary was located at a distance $23D$ from the downstream face of the pier. D is the pier diameter, which was found to be 0.64 m. A greater upstream distance was specified to ensure that errors in the upstream boundary conditions were "smoothed out" to the point that they did not impact on the flow conditions at the pier.

The physical dimensions of the computational domain used in this investigation are shown in Figure 4-5.

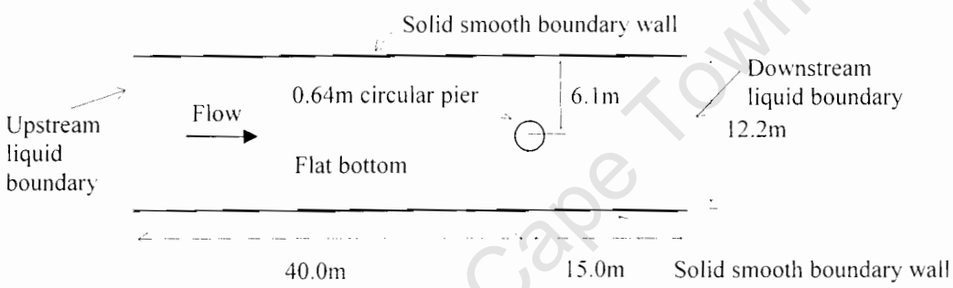

Figure 4-5: Physical dimensions of computational domain

The computational domain (Figure 4-5) was discretised by means of the density map driven optimal unstructured triangular mesh. This was suitable for the Finite Element codes implemented in the TELEMAC system. The bathymetric data consisting of the Cartesian coordinates (X, Y and Z) were developed using MS Excel. These data were defined uniformly along the XY plane with a spacing 1.0 m at each direction. The vertical coordinates Z of all points were initially set at 0.0 m in order to get a flat bottom in the domain. The Excel file containing the bathymetric points was transformed to a MS DOS file and imported into MATISSE. The bathymetric data were then used to calculate the local inter-node distance as a function of physical and mathematical densification criteria for the construction of the mesh.

The solid smooth boundary walls at the sides and the liquid boundaries at the upstream and the downstream were used to form a "close" computational domain. The lines representing such boundaries were defined using the contour lines to support the mesh (Section 3.5.2). The

character of the points on boundary such as solid or liquid was defined during the development of the boundary conditions after constructing the mesh.

The pier was constructed by means of the "user" attributes (Section 3.5.2), which consist of a series of points linked together to form a constrained line segment. These constrained lines formed a circular shape and serve as a support for the nodes and the segments of a mesh. All points on the segments forming the circular pier were defined as hard points and the circular line itself was defined as the "contour" line for a smooth wall.

Once the domain geometric features were outlined, the criteria values were then imposed to prepare the "density map" in order to get an optimal size of the equilateral triangular elements (Section 3.5.3). It was important to establish a finer mesh around the pier and a relatively coarser mesh at the domain boundaries to save the computational time without compromising numerical accuracy. This was done using an analytical function called "smooth criteria". A lower value of criteria was imposed for the circular pier line segments (say 0.01m) and higher value (say 1.0m) was imposed at the domain closed boundary line segments. One of the main intensions of refining the mesh was to increase the time steps to reduce the computational time. A finer mesh constructed around the pier than at the boundaries in the domain. A linear distribution was maintained at the interface region between the finer and coarser mesh to avoid excessive mesh distortion. The mesh was thoroughly checked (Section 3.5.4) before generation of a geometric file for the TELEMAC simulations. Figure 4-6 illustrates the final discretised computational 2D domain used in this investigation.

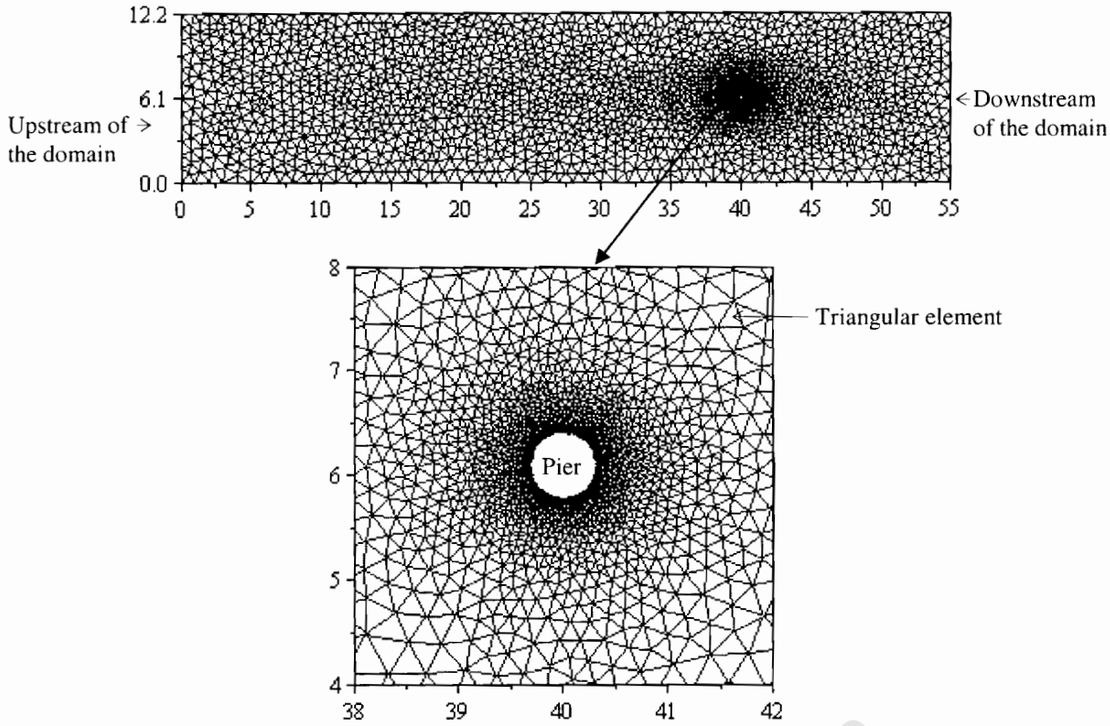

Figure 4-6: Two-dimensional (2D) triangular mesh

The 2D mesh (Figure 4-6) was reproduced along the vertical in 10 planes for the TELEMAC-3D simulations. Figure 4-7 illustrates a typical prismatic mesh used in this study.

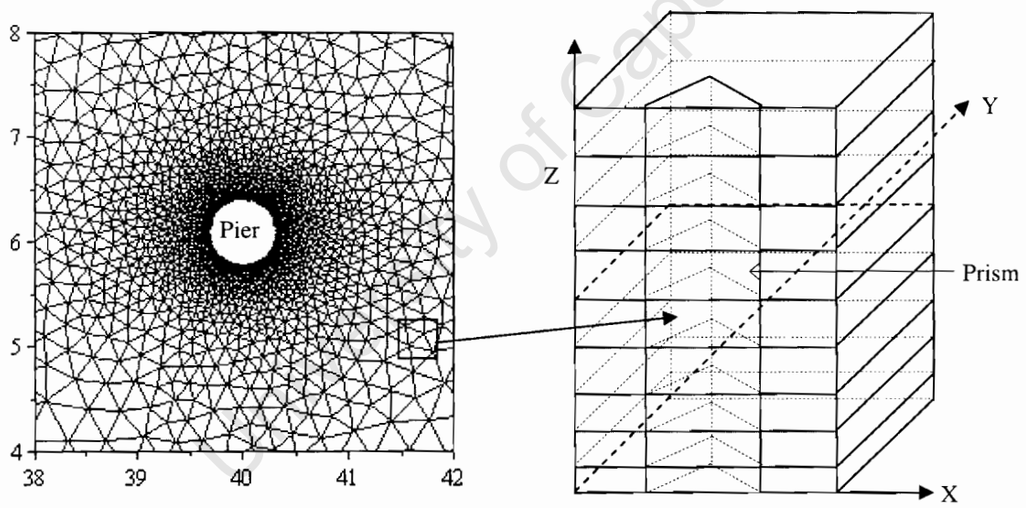

(a) 2D Triangular Mesh (b) 3D Prismatic Mesh

Figure 4-7: Three-dimensional (3D) prismatic mesh

The 3D mesh was refined near the channel bottom by modifying the CONDIM FORTRAN subroutine (Appendix A). The vertical coordinates of a 3D mesh were established using the generalised sigma transformation (Section 3.7.1) during simulation. This system was adopted for the adjustment of mesh during change of bottom topography to smooth the solution.

4.6 Modelling of the two-dimensional (2D) flow field

The Saint-Venant equations (continuity and momentum) were solved simultaneously in conjunction with the Standard k-ε model in order to model the 2D flow field. TELEMAC-2D default option suggests using the Constant Viscosity model for turbulence. This study used Standard k-ε model in line with the work of McGahey (2001), Ali & Karim (2002), Armitage & McGahey (2003), Salaheldin et al (2004).

The inlet boundary condition was fixed at a constant elevation, which was set at 1.82 m. Since the sudden introduction of a full discharge can cause computational instability, the discharge was progressively increased from 0.0 to 15.81m^3/s over a model period of half an hour.

A velocity profile was given to the model to initialise the calculation at the upstream liquid boundary. The TELEMAC-2D default assumption is that the velocity vectors are normal to the boundary. The velocity profile then multiplied by an automatically generated constant to obtain the desired flow rate. Since the TELEMAC-2D default assumes a constant velocity profile along the boundary, the default velocity profile was changed to approximate the Ahmed (1995) (pp 94) velocity profile taking account into the depth-averaged velocity. The velocity vector was defined normal to the boundary and its norm was approximated to a value proportional to the square root of the water depth from bottom. The model approximation of the velocity profile was within 1.7% of Ahmed (1995). Further details are discussed in Section 4.8. At the downstream face, a constant free surface level (e.g. 1.82 m) was maintained during the simulations.

A local logarithmic velocity profile embedded in the TELEMAC-2D system was used at the region of solid boundaries e.g. the pier. The turbulence near the pier was calculated using Equations 3.2a, 3.2b and 3.3 (Section 3.5.5.3). The model assumed the initial value of the turbulent kinetic energy k and dissipation ε using Equation 3.4.

Equations 3.6a, 3.6b and 2.60d were solved by the Fractional Step Method (Section 3.11.3) using the Method of Characteristics scheme (Section 3.11.1) for the velocity components (u and v), the turbulent kinetic energy k and the dissipation ε in the turbulence model. A conservative scheme with SUPG was used for the advection of depth h solution.

The different terms in Equations 3.1a, 3.1b and 2.60d e.g. advection term, diffusion and source terms were solved separately at each discretised nodes between the time t^n and the time t^{n+1} (i.e. Δt). The set of Equations 3.6c and 3.6d were solved in the advection and the propagation and diffusion steps respectively. The viscosity was given to the Momentum

Equation 3.6b by solving Equations 3.6e and 2.60c using the GMRES (Generalised Minimum Residual) solver with accuracy $1x10^{-6}$.

The terms F_{Mx} and F_{My} in Equation 3.6d are the source terms. The TELEMAC-2D default neglects all source terms. This study also neglected all source terms except for bottom friction. The values of those source terms due to bottom friction were determined by activating the codes relating to the friction law of Chezy. Using the flatbed domain and the non-linear nature of the Chezy's equation, TELEMAC-2D solves Equation 4.9 for the source terms F_{Mx} and F_{My}.

$$F_{Mx} = \frac{g}{hC_h^{\,2}} u^{n+1}\sqrt{(u^n)^2 + (v^n)^2}$$
$$F_{My} = \frac{g}{hC_h^{\,2}} v^{n+1}\sqrt{(u^n)^2 + (v^n)^2} \qquad (4.9)$$

This study used the momentum equation to eliminate the velocity in the continuity equation for mass conservation by changing the TELEMAC-2D default value which uses depth-velocity coupling during solving the linear system. This was done to smoothen the solutions and to reduce the computational time (Lang, 2005).

An additional numerical treatment was used for the solution of the non-linear terms i.e. $h\,div(\mathbf{u})$ and for the diffusion term i.e. $div[\nu_t\, grad(u)]$. This was done by specifying the numerical implicitation coefficient related to the velocity and depth (Equation 3.6g) and diffusion of velocity (Equation 3.6h). This study initially uses the implicitation coefficient according to the TELEMAC-2D default value e.g. 0.55, 0.55 and 1.0 for velocity, depth and diffusion of velocity respectively. The implicitation coefficients for velocity and depth were however changed to 1.0 in order to smooth the solutions. One sub-iteration for non-linearity, recommended in TELEMAC-2D, was used to update the velocity field in order to produce a semi-implicitation of the advective terms for a given time step. Activation of this code uses the velocity field of the previous time step during the solution of mass-conservation. This technique improves the solution of the non-linear terms.

The change of depth δh was calculated during the treatment of the terms $-g(\partial Z/\partial x)$ and $-g(\partial Z/\partial y)$ in Equation 3.6i. At each time step, the change of water depth was added to the initial depth in order to obtain the free surface and this continued accordingly for the successive time steps. The free surface was modelled solving Equation 3.10 together with Equation 3.11.

TELEMAC-2D generates a set of known and unknown variables using the Finite Element procedure. These variables were stored in a linear form (Equation 3.14) with edge-based matrix storage by changing the TELEMAC-2D default. The TELEMAC-2D default suggests using classic storage (TELEMAC-2D, 2002). This study found however that the edge-based storage

was computationally faster than classic storage. During the matrix storage, the TELEMAC-2D defaults related to mass-lumping on velocity and depth were further changed to bring the mass matrix onto the diagonal. This technique was found to increase the computational speed without compromising numerical stability.

Finally, the velocity components and free surface were calculated by solving the linear system using the GMRES (Generalised Minimum Residual) solver with $1x10^{-5}$ accuracy. It should be noted that the TELEMAC default normally uses the conjugate gradient solver. This study found GMRES was computationally faster and numerically stable.

4.7 Modelling of the three-dimensional (3D) flow field

The TELEMAC-3D default solves the Navier-Stokes equations by approximating a hydrostatic pressure distribution (Section 3.7). This approach is only applicable in the situation where the vertical velocity components are negligible. In the case of the flow field upstream of the pier, the magnitude of the vertical velocity component can be 40%-80% of the average oncoming velocity (Raudkivi, 1998). The downflow in upstream of the pier is also related to the stagnation pressure, which decreases from the top to the bottom (Section 2.2.2.2) and thus the pressure distribution is not hydrostatic. In view of these, this study used the option for solving the Navier-Stokes equations (Equation 2.35) by approximating the non-hydrostatic pressure distribution using the Fractional Step Method in order to get the 3D flow fields. In this solution the total pressure p is the sum of the hydrostatic pressure p_h and the hydrodynamic pressure p_d.

Like TELEMAC-2D, the equations were solved for the advection, diffusion and the source terms (friction only) separately. The Poisson Pressure Equation (PPE), followed by the velocity projection, were solved in order to get a divergence-free velocity field (Hervouet & Jankowski, 2000) for the calculation of the hydrodynamic variables on pressure (Equations 3.8a to 3.8d). The hydrostatic pressure gradient was added as a source term in the advection-diffusion step and only the dynamic pressure was used in the PPE step. As a consequence, this step tends to become trivial when a flow was nearly hydrostatic.

The initial model conditions, velocity profile, source term and the model of turbulence were prescribed in a similar manner as TELEMAC-2D simulations (Section 4.6). The turbulence was however modelled separately for the horizontal and vertical directions. Calculation of the change of the water depth was carried out in the same manner as for the TELEMAC-2D simulations. It should be noted that during solving the flow equations using TELEMAC-3D, the TELEMAC-2D module was automatically activated for solving the water depth and the free surface.

The mesh was readjusted at each time step during the change of water depth by activating the sigma transformation. This system was adopted to smooth the solutions of the bottom topography. The generalised sigma transformation code was coupled with the code related the hydrostatic inconsistency filter (Section 3.7.1).

During simulation, TELEMAC-3D was found to be numerically sensitive to the selection of the different numerical parameters i.e. the time step, numerical scheme, preconditioning and solver (Sections 3.11.1 and 3.11.2). One of the primary reasons might be the small-scale computational domain. There were no guidelines in the TELEMAC-3D (1998) documentation for the selection of the time step during 3D flow simulations. It also became evident that the TELEMAC-3D codes coupling with SISYPHE had not been properly tested and validated for Windows operated computers. It is possible that this study was the first attempt to doing so (Lang, 2005). Moreover the University of Cape Town had no local support for TELEMAC during this investigation. As a consequence, a series of TELEMAC-3D models were developed using the various different numerical options in order to find a stable and computationally economical solution. This attempt commenced with the default values. Some of the default values were however found to be unstable for the modelling of local scour around circular pier. The final selected numerical parameters are given in Appendix B.

TELEMAC-3D model uses the implicitation coefficient to treat the non-linear terms in the momentum equations using the TELEMAC-3D default value e.g. 0.55, 1.0 and 1.0 for the velocity, depth and diffusion of velocity respectively. Surprisingly, unlike TELEMAC-2D, the TELEMAC-3D default value classic matrix storage was found more effective compared with edge-based storage. Like TELEMAC-2D, the mass-lumping techniques were found to be an effective way of condensing the mass matrix onto the diagonal.

Unlike TELEMAC-2D, the GMRES solver was found to be unstable when solving the equations in 3D flow. The Conjugate Gradient solver, a default in TELEMAC-3D, was also found to be unstable in this study. The Conjugate Gradient on Normal Equation solver was found to be reasonably stable in the solution of the liner system for propagation, vertical velocity, diffusion of velocities and k-ε. The Poisson Pressure Equation (PPE) followed by the velocity projection was solved using the Squared Conjugate Gradient solver.

In general this study found that using TELEMAC-3D with internal coupling to SISYPHE in a Windows operated environment was computationally very expensive, numerically sensitive, and to some extent unstable.

4.8 Model calibration

After defining all the physical and numerical parameters and numerical schemes relating to the hydrodynamic fields, TELEMAC-2D and TELEMAC-3D were calibrated against reliable data provided by the supplier (SOGREAH Consultants, France) before coupling with the sediment transport module (SISYPHE). Particular attention was given to prediction of the depth-averaged velocity. This was because the depth-averaged velocity is used by TELEMAC for the calculation of the bed shear stress.

The hydrodynamic models (TELEMAC-2D and TELEMAC-3D) were then run for two situations; with the pier and without the pier in the domain. In both cases the models were run

for an actual 4.0 hrs to ensure the full flow condition. The velocity field was then examined against the measured values provided by Ahmed (1995).

Without the pier in position, a very small magnitude of transverse velocity was observed in the vicinity where pier needed to be placed. The magnitude of the longitudinal velocity along the flow direction was however very close to the measured depth-averaged velocity with only a 1.7% discrepancy (Figure 4-8).

With the pier in position, the velocity along the centre of the channel near the pier was reduced to almost zero. This was to be expected as a result of the presence of pier. The TELEMAC-2D values seemed to be closer to the measured value than the TELEMAC-3D values (Figure 4-8).

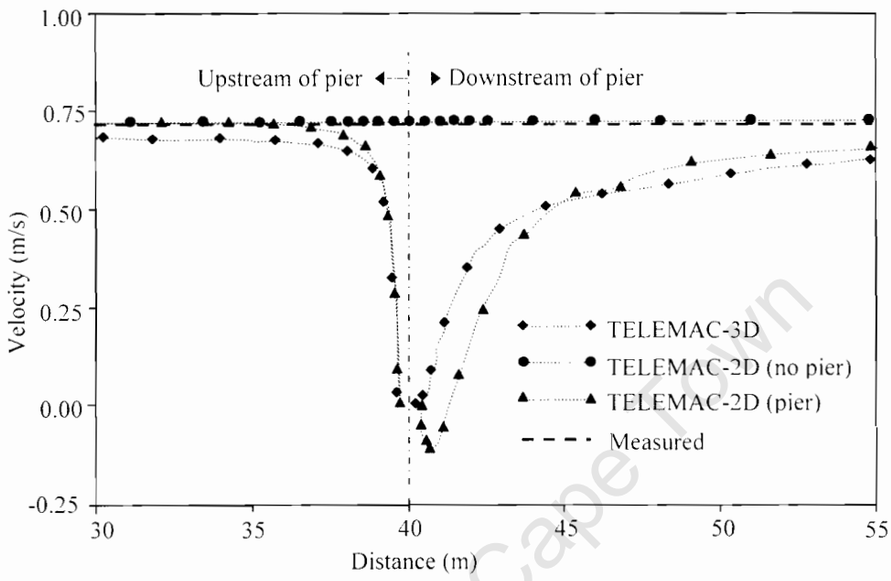

Figure 4-8: Velocity distribution along flow direction (centreline of the pier)

The TELEMAC-2D values managed to capture the eddy circulation downstream the pier. Figure 4-8 clearly shows the negative velocity downstream the pier which indicated the direction of the flow was in the upstream direction.

It should be noted that this study could not independently calibrate the sediment transport module SISYPHE due to the lack of suitable sediment transport data.

4.9 Selection of sediment transport formulae

Once the hydrodynamic modules (TELEMAC-2D and TELEMAC-3D) were calibrated, they could be coupled with the sediment transport module (SISYPHE). In SISYPHE, the bed evolution equation is solved in conjunction with sediment transport formula which need to be selected. The sediment transport process in the open channel is complex, thus the selection

criteria has a significant role in the development of the numerical model. The selection of sediment transport formulae may be one of the major limitations in verifying the scour depths reported in Ahmed (1995).

In this study, the selection of the sediment transport formulae was entirely based on the literature review and the physical characteristics of the sediment particles reported in Ahmed (1995). Four different sediment transport formulae embedded in SISYPHE were used; the Meyer-Peter and Muller (1948), the Einstein & Brown (1950), the Engelund & Hansen (1967) and the Van Rijn (1984a). Details of these formulae are in Section 2.3.6.1, Section 2.3.6.2, Section 2.3.6.3 and the Section 2.6.3.4 respectively.

All of these formulae are reported to be sensitive to the magnitude of the hydrodynamic flow fields. According to SISYPHE (2004), an increase of the current velocity by 10% will result an increase of transport by over 30% (Meyer-Peter and Muller, 1948), 60% (Engelund & Hansen, 1967) and almost 80% (Einstein-Brown, 1950). The accuracy of the hydrodynamic model has a significant impact on the sediment transport modelling.

The validity range of three of the sand transport formulae programmed in SISYPHE V5.4 is given in Table 4-3.

Table 4-3: Validation of sand transport formula
(After SISYPHE, 2004)

Sand transport formula	Meyer-Peter and Muller (1948)	Einstein-Brown (1950)	Engelund & Hansen (1967)
Mode of transport	Bed load	Bed load	Total load
Gravel ($d_{50} > 1\,\text{mm}$) Medium-grained sand ($0.5 \le d_{50} \le 1\,\text{mm}$) Fine sand ($d_{50} < 0.5\,\text{mm}$)	$d_{50} > 1$	$0.2 \le d_{50} \le 3$	$0.2 \le d_{50} \le 4$
Rippled bottoms	YES	YES	YES
Low bed-load flows	YES	YES	NO
High bed-load flows	YES	YES	YES

According to Van Rijn (1993), his bed load formulae (Van Rijn, 1984a) can accurately predict the bed load transport taking account the bed roughness. He made a comparison with various different formulae and criticised the Meyer-Peter and Muller (1948) and the Engelund & Hansen (1967) for yielding poor results in calculating the sediment transport in the rivers of rough beds.

This study attempted to verify the bed evolution programmed in SISYPHE using all of these four formulae in turn for the prediction of the bed deformation and hence the local scour. For simplicity, all of these formulae were programmed in SISYPHE using the Shields parameter θ (Equations 2.21, 2.23, 2.24b, 2.25).

4.10 Coupling between sediment transport and hydrodynamic modules

Solving the bed evolution equation in SISYPHE requires the hydrodynamic variables. This was given to SISYPHE by coupling it with TELEMAC-2D or TELEMAC-3D. The SISYPHE, TELEMAC-2D and TELEMAC-3D codes were stored in separate libraries. An interface code had to be therefore activated to make a link between the hydrodynamic (TELEMAC-2D or TELEMAC-3D) and sediment transport module (SISYPHE).

In the TELEMAC system, there are two procedures to couple the hydrodynamic and the sediment transport modules; imposing the value using subroutines, or exchanging data files and shared memory during simulation. The later is faster and more economical because the data can be exchanged between the two modules by sharing the memories without read and write files. This procedure is called the internal coupling.

This study used internal coupling activating the codes by means of the hydrodynamic and the sediment transport parameter files (Appendix B). This study may be the first attempt to make the internal coupling between TELEMAC-3D and SISYPHE under Windows (Lang, 2005).

4.11 Modelling of bed evolution

Once the sediment transport formula had been selected, the bed evolution equation (Equation 2.63, in Section 2.4.8) was solved in conjunction with this sediment transport formula for the prediction of the deformed bed around the circular pier using the codes in the SISYPHE module. The scalar transport rates were transformed to 2D fluxes by assuming that the transport direction was parallel to the depth-averaged flow directions

All of the sediment transport formulae used in this study calculate bed-load except for Engelund & Hansen (1967). Their formula calculates the total load. The coupling between the bed-load and the suspended load was modelled solving the advection-diffusion equation (Equation 3.13a, in Section 3.10.1). SISYPHE default codes were used to approximate the erosion and deposition fluxes according to Celik & Rodi (1988). SISYPHE also uses the Zyserman & Fredsoe (1994) formulation for the calculation of the near-bed concentration C_{eq} for the critical Shields parameter θ_c and the Shields parameter θ taking account the bottom friction. The model calculates the Shields parameter at each time step using the predicted bed shear stress and the physical properties of the sand.

This study applied a slope correction factor to both the magnitude and direction of the solid transport rate before solving the bed evolution Equation 2.63. The correction method was based on Koch & Flokstra (1981). Details on slope correction are discussed in Section 3.10.2. Following the recommendation of SISYPHE (2004), an empirical constant $\beta = 1.3$ was given to the model after changing the SISYPHE default to take account into the slope correction factor by solving Equations 3.13j and 3.13k.

The technique of mass-lumping was used to diagonalize the mass-matrix in order to smooth the solutions. This technique was also found to be effective in reducing the computational time. Using the Finite Element assumptions, Equation 2.63 was approximated by the predictor-corrector concept (Equations 3.16a, 3.16b and 3.16c), which were solved using the GMRES (Generalised Minimum Residual) solver with $1x10^{-5}$ accuracy.

4.12 Activation of various codes

The TELEMAC simulations require the writing of various parameter files for the activation of the various codes stored in the BIEF library (Section 3.2). These are text files created by a text editor, which in effect represents the control panel of the computation.

Considerable care had to be taken during the development of these parameter files. These files reflect the complete model containing the commands for the geometric, boundary conditions, physical parameters, numerical parameters and schemes for the solution. The rules, for the development of the hydrodynamic and the sediment transport parameter files are similar. These can be found in the TELEMAC-2D (2002, pp 9-11), TELEMAC-3D (1998, pp 11-12) and SISYPHE (2004, pp 47-49). A typical example of these files is given in Appendix B.

Three different parameter files were developed for the simulations; two were for the hydrodynamic e.g. TELEMAC-2D or TELEMAC-3D, and the other was for sediment transport e.g. SISYPHE. The internal coupling was assigned by specifying the SISYPHE parameter file in a hydrodynamic parameter file e.g. in the TELEMAC-2D or TELEMAC-3D parameter files.

4.13 Description of model runs

Six models were developed and simulated as shown in the Table 4-4. The simulation for model runs T2D1, T2D2, T2D3 and T2D4 were performed for the 2D flow fields coupling between TELEMAC-2D and SISYPHE. The physical and numerical parameters were the same for each run. Different sediment transport formulae were, however, used for the solution of the bed evolution equation to obtain the scour bed. Simulation periods of 221 hrs (9 days 5 hrs) were modelled using similar hydraulic and numerical parameters along with the Meyer-Peter and Muller (1948), Einstein-Brown (1950), Engelund & Hansen (1967) and the Van Rijn (1984) sediment transport formula respectively. The maximum scour and the development of the scour profile with time were the major interest of these simulations. The computational time was found to be slightly different for each model run with an average computer time of 20 hrs.

Table 4-4: List of the simulated model runs

Expt. No	Mean Sand Diameter d_{50} (m)	Chezy's constant	Coupling modules	Sediment transport formula	Pier Diameter D (m)	Dis-charge Q (m^3/s)	Water depth h (m)	Average flow U (m/s)	Flow Intensity U/U_c	Flow Shallow-ness h/D	Sediment Coarse-ness D/d_{50}	Comments
T2D1	0.00088	50	TELEMAC-2D & SISYPHE	Meyer-Peter and Muller (1948)	0.64	15.81	1.82	0.712	0.723	2.844	727	Flat bed, scour profile, long time
T2D2	0.00088	50	TELEMAC-2D & SISYPHE	Einstein & Brown (1950)	0.64	15.81	1.82	0.712	0.723	2.844	727	Flat bed, scour profile, long time
T2D3	0.00088	50	TELEMAC-2D & SISYPHE	Engelund & Hansen (1967)	0.64	15.81	1.82	0.712	0.723	2.844	727	Flat bed, scour profile, long time
T2D4	0.00088	50	TELEMAC-2D & SISYPHE	Van Rijn (1984a)	0.64	15.81	1.82	0.712	0.723	2.844	727	Flat bed, scour profile, long time
T3D1	0.00088	50	TELEMAC-3D & SISYPHE	Van Rijn (1984a)	0.64	15.81	1.82	0.712	0.723	2.844	727	Flat bed, scour profile, short time
T3D2	0.00088	50	TELEMAC-3D & SISYPHE	Van Rijn (1984a)	0.64	15.81	1.82	0.712	0.723	2.844	727	Scour bed, vertical flow field, short time

The simulation for model run T3D1 was performed by applying the 3D flow field coupling between TELEMAC-3D and SISYPHE. The computational domain was developed by layering 10 sets of identical 2D meshes in the vertical direction. During the development of the 3D flow field, the TELEMAC-3D was found to be very sensitive to the small computational domain. Moreover the TELEMAC-3D was found to be completely unstable for a long run i.e. 221 hrs. The common modelling response is to reduce the time step, however, no general guidelines and/or technical supports were available to assist in the choice of time step. As a consequence a series of model were run with different combination of time steps and numerical schemes. Unfortunately the model showed severe numerical oscillations even for small time steps like 0.01s. It should be noted that reducing the time step increased the computational time significantly. Despite numerous trail runs, the model run T3D1 only completed 5 hrs of simulation with a time step of 0.1s. The computational time was 177 hrs (7day 9 hrs 20min).

The model run T3D2 was developed to analyse the 3D flow field. It only simulated 1 hrs of scour development. The output of the TELEMAC simulations were stored and saved separately for the hydrodynamic and the sediment transport simulations. During the post processing stage, the scour bed predicted by the SISYPHE could not be merged with the 3D hydrodynamic flow field. As a consequence, the horseshoe vortex and wake around the scour profile could not be identified. T3D2 model did, however, capture the vertical down flow, horseshoe vortex and wake on the scour bed during the scouring process. This model was run for a short period in order to avoid the huge computer time.

Ahmed (1995) gives scour profiles on the centreline of the pier and at a 900 angle through centre of the pier. This study therefore had to incorporate the shape of scour bed inbetween the profiles.

4.14 Final methodology

The final methodology for setting up the TELEMAC system for the modelling of local scour is given in Figure 4-9.

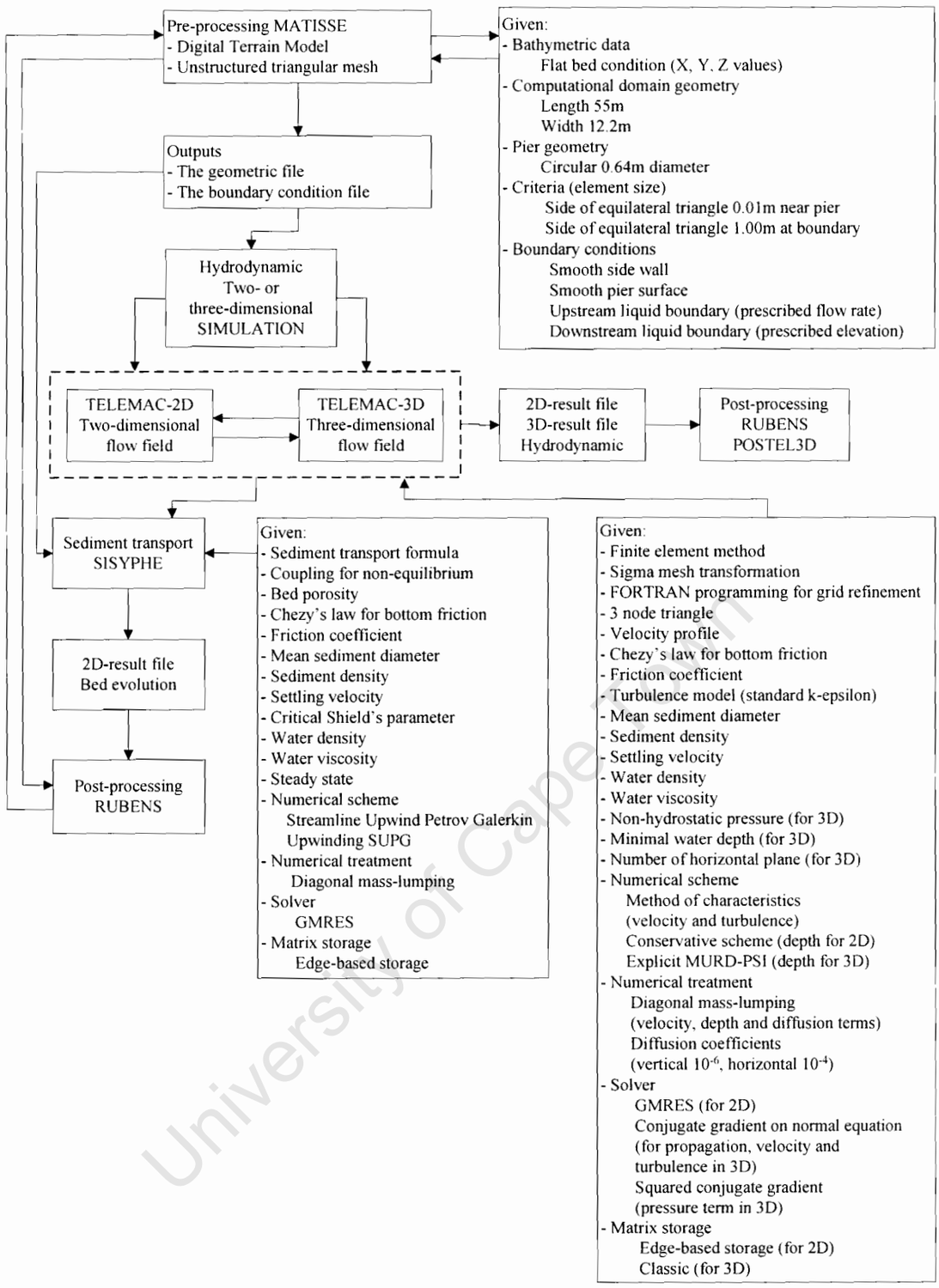

Figure 4-9: Methodology for modelling local scour in TELEMAC

4.15 Summary

This chapter presented the overall development of the model used to simulate the deformation of the uniform sand bed around a circular pier for the prediction of clear-water local scour using TELEMAC V5.5. This chapter should be read in conjunction with Chapter 2 and Chapter 3.

- The model was tested against the Ahmed (1995) physical model. A brief description of his model and physical parameters was therefore given. TELEMAC V5.5 was found to be sensitive for the solution of a small geometric domain such as the flume dimensions employed by Ahmed (1995). The scaling using Froude number and Continuity similarity was thus carried out to model the Ahmed (1995) data at a larger scale for the TELEMAC simulations. Three critical conditions for clear-water scour were used; the critical shear stress (Shields, 1936), the critical velocity (Yang, 1973) and the inception densimetric Froude number (Hager & Oliveto, 2002).

- The computational domain was discretised by means of the density map driven optimal unstructured triangular mesh. The domain geometric features were outlined using user and contour line attributes. Upstream and downstream liquid boundaries were modelled with extreme care. A finer 2D mesh was constructed around the pier than at the boundaries in the domain. The 3D prismatic mesh was developed by reproducing the 2D mesh along the vertical in 10 planes for the TELEMAC-3D simulation.

- The Saint-Venant equations were solved simultaneously together with the Standard k-ε turbulence model in order to model the 2D flow field. The source term was determined using the friction law of Chezy. These equations were solved by the Fractional Step Method using the Method of Characteristics and a conservative scheme with SUPG. GMRES solver was used for the solution of the linear system. The Navier-Stokes equations were solved by approximating the non-hydrostatic pressure distribution using the Fractional Step Method in order to model the 3D flow field. The Conjugate Gradient on Normal Equation and Squared Conjugate Gradient solver were used for the solution of 3D flow.

- The hydrodynamic models (TELEMAC-2D or TELEMAC-3D) were calibrated before coupling them to the sediment transport module (SISYPHE). An internal coupling method was used for the coupling between hydrodynamic and sediment transport for the solution of the bed evolution equation. The bed evolution equation was solved using four different sediment transport formulae given by the Meyer-Peter and Muller (1948), the Einstein & Brown (1950), the Engelund & Hansen (1967) and the Van Rijn (1984a). The coupling between the bed-load and the suspended load was modelled using the advection-diffusion equation. The bed slope correction was applied according to the Koch & Flokstra (1981). GMRES solver was used for the solution of the linear system using predictor-corrector concept.

- The details of the various model runs were summarised. The final methodology for local scour modelling using TELEMAC V5.5 was presented in the form of a flow chart.

Chapter 5
Results, analyses and discussion

5.1 Introduction

In this chapter, the results obtained from all of the simulations are presented. This is followed by analyses and discussion of the results.

The model simulation results are presented using a 3D Cartesian coordinate system (X, Y and Z) describing the computational domain. The XY plane is the plan section represents a vertical cross-section, whereas the YZ plane represents a vertical cross-section. The origin (X=0, Y=0 and Z=0) is the upstream right hand corner.

The domain extended 55.0m by 12.2m in the x- and y-directions respectively. Before simulation, the z-coordinates of the bottom points were set to zero to specify an initial flat bottom. The initial water depth was prescribed as 1.82m. The centre of the circular pier was placed at X=40.0 and Y=6.1. The XY plan view and XZ cross-section are shown in the Figure 5-1.

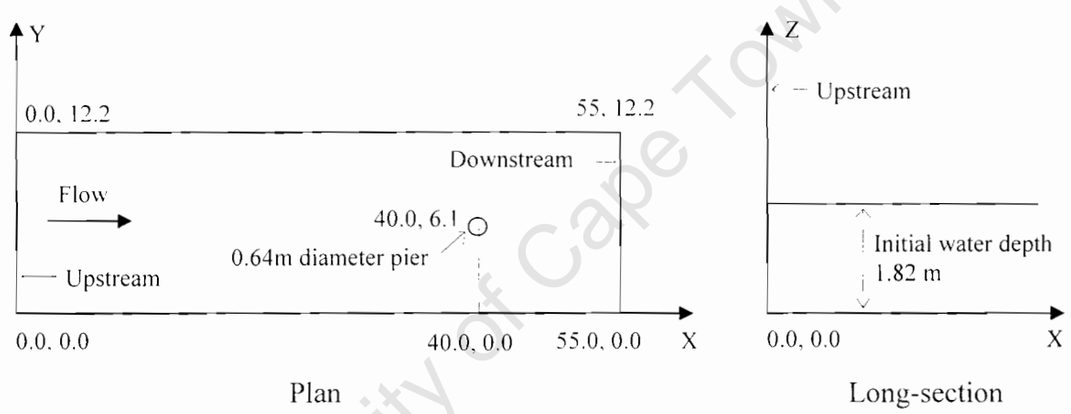

Figure 5-1: The computational domain in the Cartesian coordinate system

The various scour profiles are specified at the clockwise angle α (Figure 5-2) with $\alpha = 0^0$ oriented in the upstream direction.

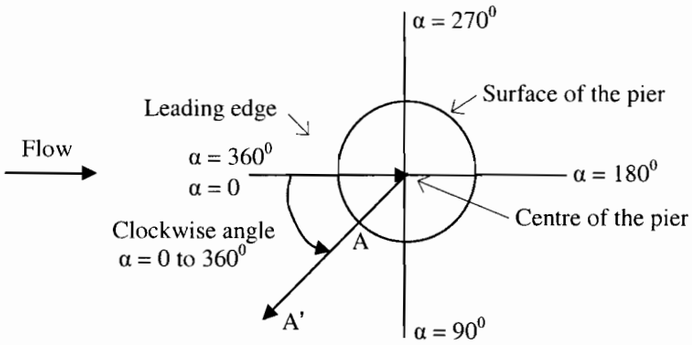

Figure 5-2: Direction of cross-section

As described in Chapter 4, the domain discretisation, the boundary conditions and the numerical and physical parameters were the same for model runs T2D1, T2D2, T2D3 and T2D4. The only difference was the sediment transport formula. The model run T3D1 was developed to compare the 4hrs scour profile given in Ahmed (1995). The 3D flow fields were analysed using the T3D2 run. All model runs were based on the domain geometry of fine unstructured 2D triangular grids near the pier (Figure 5-3).

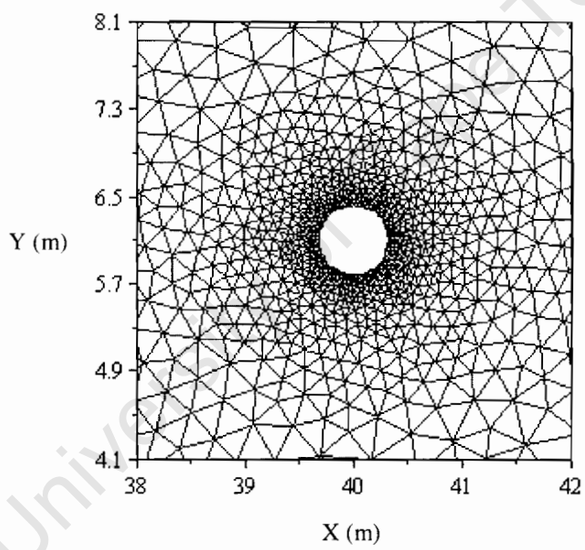

Figure 5-3: Triangular mesh around pier

5.2 Simulation of flow fields

5.2.1 Depth-averaged velocity in the horizontal plan

The discharge was applied to the model progressively over a period of half an hour of the model time to develop the flow pattern smoothly without numerical disturbance. The velocity distributions were plotted in the horizontal plane to investigate the overall flow patterns in plan view. Similar flow patterns were observed for all the simulations and were all symmetrical about the pier. Typical flow patterns showing the velocity components u and v along the x- and y- directions at time t=24 hrs for the T2D4 simulation are shown in Figure 5-4.

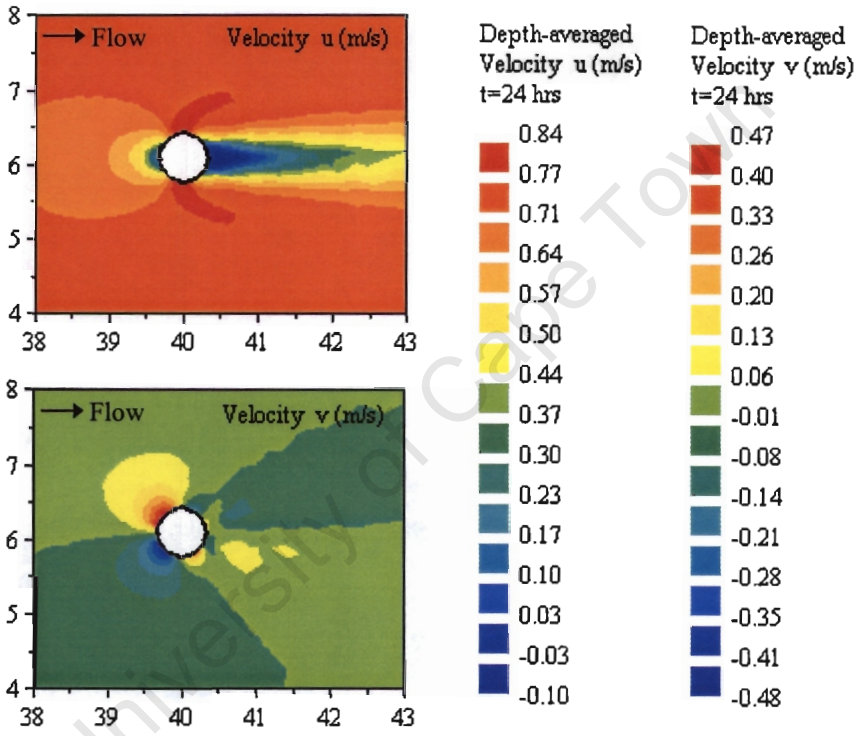

Figure 5-4: Flow patterns in simulation T2D4

In all the simulations, the overall flow patterns were similar to those observed by Ahmed (1995), Melville & Coleman (2000) and Chadwick et al (2004). A typical comparison of the depth-averaged velocity components for runs T2D4 and T3D1 is made in Figure 5-5a and 5-5b to show the similarities and differences between 2D and 3D simulations.

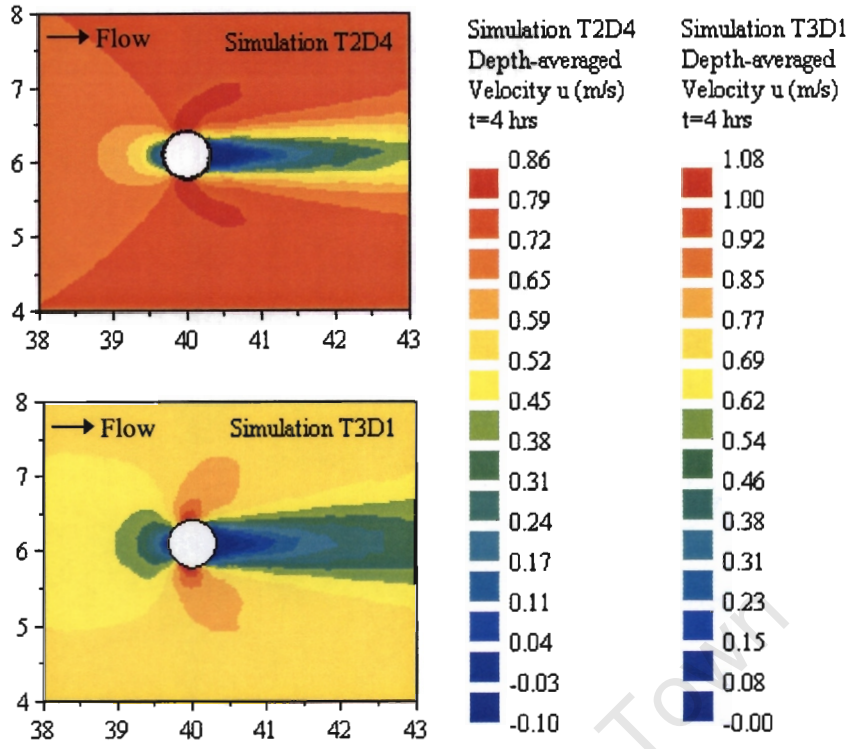

(a) Depth-averaged velocity component *u*

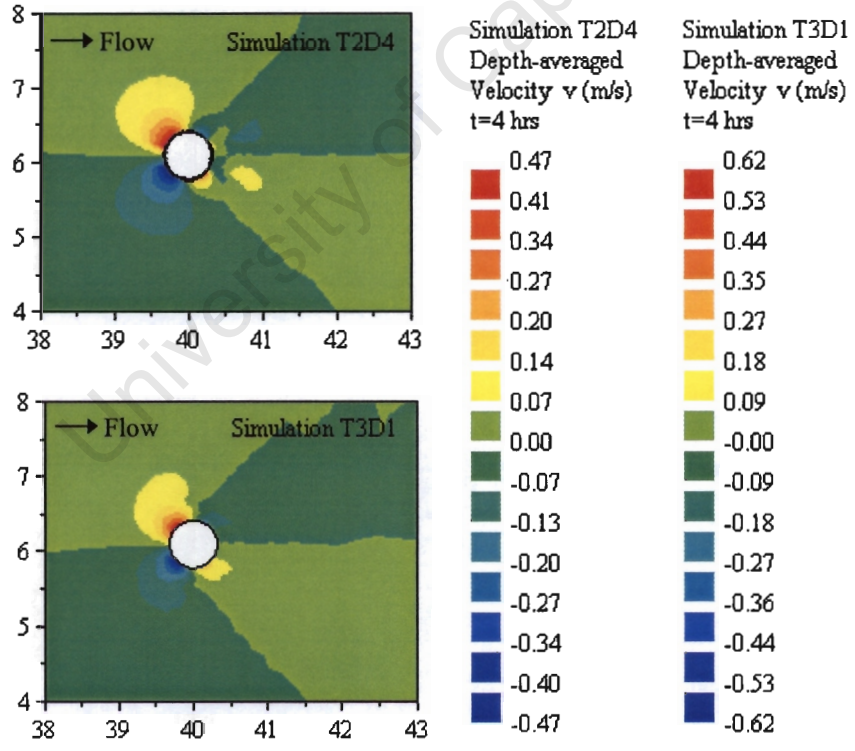

(b) Depth-averaged velocity component *v*

Figure 5-5: Depth-averaged velocity components by TELEMAC-2D and TELEMAC-3D

The depth-averaged velocity distribution was found to be similar during calibration runs using TELEMAC-2D and TELEMAC-3D (Figure 4-8). During simulation, the depth-averaged velocity distribution was found to be slightly different. Figure 5-5 shows that for a similar mesh and boundary conditions, the T3D1 calculated higher depth-averaged velocities than T2D4. One of the reasons might be that the grid size was refined during T3D1 simulation. It could be that TELEMAC-3D simulations are sensitive to the grid size. It should be noted that the minimum length of a triangle formed the mesh at calibration stage was 0.1m, however, the triangles of minimum side length 0.01m near the pier was used during simulation. Unfortunately the TELEMAC-3D simulations had to be prematurely terminated due to numerical problems described in the Section 4.7. The comparison between the depth-averaged velocity components are therefore given only for the time t=4 hrs.

During the T2D4 simulation, it was noted that the magnitude of the velocity components at t = 24 hrs (Figure 5-4) were less than that of the velocity components at t= 4 hrs (Figure 5-5a & 5-5b). This trend was also observed in the other simulations. This is not a surprise because the scour hole accommodated a certain amount of flow as it deepened with time which was in turn contributed to the reduction of average velocity. This phenomenon agrees with Raudkivi & Sutherland (1981), Ahmed (1995) and Melville & Coleman (2000).

One of the major limitations with the post-processor RUBENS is that the velocity distribution is only presented in plan which does not reveal the way in which the flow pattern varies between channel bottom and free surface at a particular location. A further limitation with TELEMAC is that the sediment transport module SISYPHE calculates the bed shear stress using the depth-averaged velocity. Since the bed shear stress is one of the main inputs to the sediment transport formulae, there is a danger that inaccuracies will be introduced in the vicinity of the scour hole.

5.2.2 The deflected flow fields

When flow approaches a pier, the velocity u reduces and the velocity v increases as the fluid is deflected around at the side of the pier. Both TELEMAC-2D and TELEMAC-3D models captured these phenomena (Figure 5-6). The model captured this phenomenon at both the bed level as well as higher in the water column.

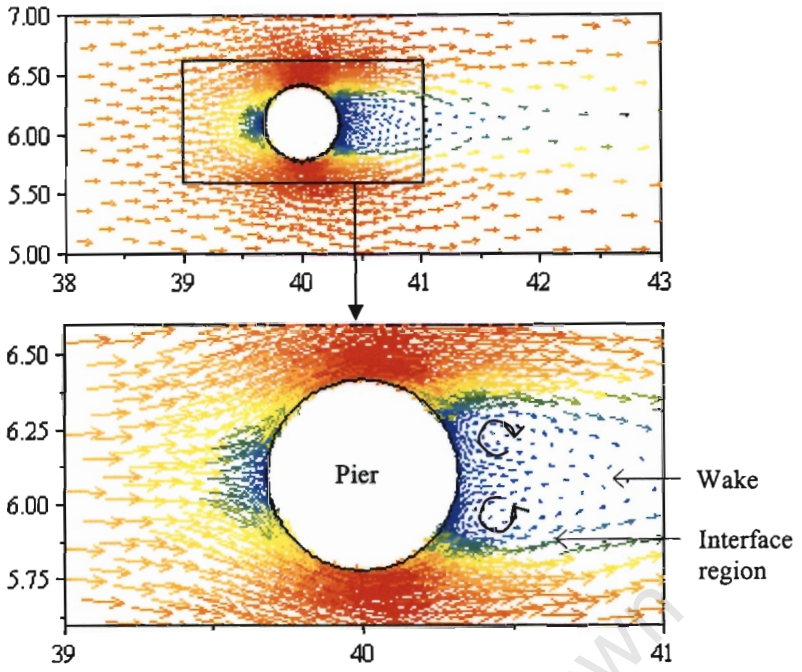

Figure 5-6: The deflected depth-averaged flow field

The accelerated flow was observed at the side of the pier in all simulations. The model results clearly showed that the velocity was increasing after the flow passed the side of the pier. The wake behind the pier disturbed the mean velocity in the interface regions. The wake region is a recirculation zone that contributes little to the net transport of fluid in the downstream direction. As a consequence, the flow adjacent to the wake tends to accelerate in order to transport the extra fluid. The model simulations clearly captured the wake behind the pier, which resembled those reported in Melville & Coleman (2000) (Figure 2-2). The magnitude of the velocity in the wake region was small, however, the velocity fluctuation was large due to the turbulent eddy motions. Ahmed (1995) reported a similar wake field in his observations. Unfortunately he could not measure the velocity components due to their large variation and lack adequate apparatus. TELEMAC-2D could not predict wake up the water column. This was modelled by TELEMAC-3D run T3D2.

5.2.3 The downflow, horseshoe vortex and wake

TELEMAC-2D V5.5 cannot predict the downflow and the horseshoe vortex in front of the pier. TELEMAC-3D V5.5 is however capable of capturing the circulation of the flow field near pier. During post processing stage, it was realised that RUBENS could not merge the scour profile, which was determined by the SISYPHE, with the hydrodynamic field in order to represent the velocity vector fields predicted by TELEMAC-3D. The run T3D2, which was developed for a scoured bottom bathymetry, was thus used to show the downflow and the horseshoe vortex in front of the pier in the scour hole (Figure 5-7).

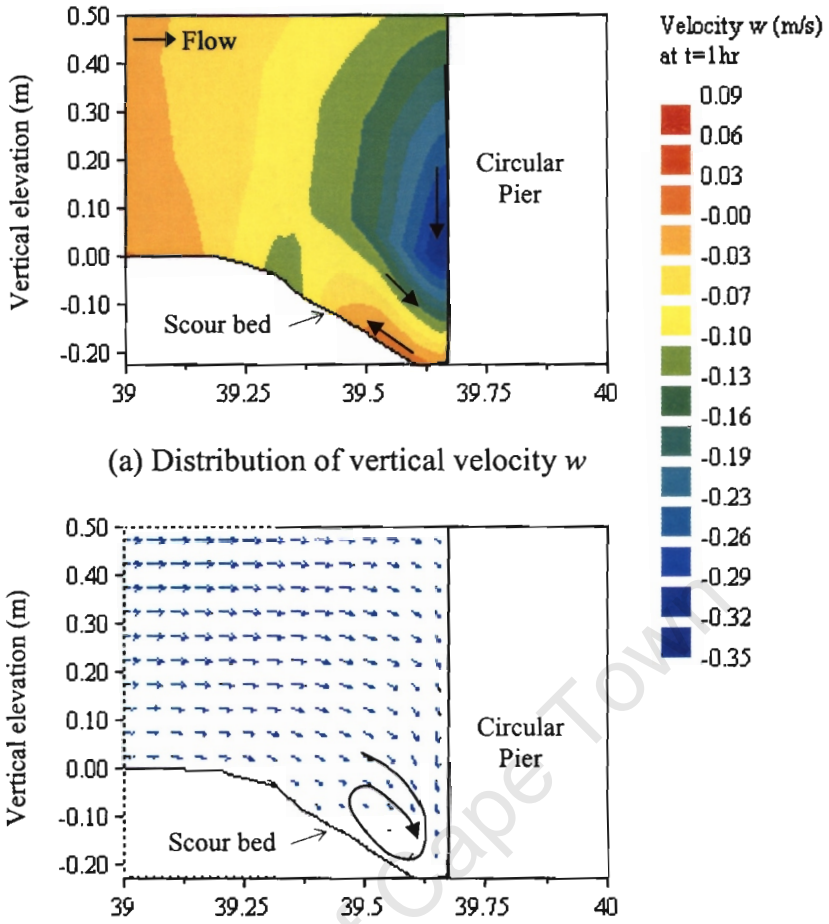

(a) Distribution of vertical velocity *w*

(b) Horseshoe vortex near scour hole

Figure 5-7: Downflow and horseshoe vortex

T3D1 and T3D2 revealed that as the flow approaches the pier, it is deflected in the downward direction towards the scour hole. The deflection was most prominent at a height of $0.1h$ (h is the water depth) from the original bed level. The flow velocity vectors depend on the shape of the scour hole.

TELEMAC-3D V5.5 cannot predict the stagnation pressure distribution in front of the pier. It was therefore difficult to correlate the relationship between the downflow and the stagnation pressure. The results clearly however showed that the downflow was affected by the bed and horseshoe vortices (Figure 5-7b). The maximum magnitude of downflow for 1.0 hr simulation was found to be 50% of the undisturbed depth-averaged velocity. The position of the maximum downflow was just above the original bed level (Figure 5-7a). This was in agreement with Ahemd (1995) and Raudkivi (1998).

The downflow and the scouring caused by it in front of the pier bear many similarities to an impinging jet (Melville & Coleman, 2000) and the corresponding scouring. There are, however, some fundamental differences, which prevent application of the analyses of jets to the downflow (Rajaratnam, 1976). The jet is formed inside the nozzle and after existing, diffuses as

it entrains ambient fluid and forms a shear layer (Ahmed, 1995). The pressure driven downflow is more complex as it develops around the curved surface of the circular pier. It therefore forms and diffuses at the same time. Moreover, unlike the inert fluid around a jet, the approach flow carries both mass and momentum into the downflow. The contribution of the downflow is one of the major causes progressing the scour in front of a pier.

It is extremely difficult to visualise and measure the downflow during physical modelling. It is much easier to analyse the downflow and the horseshoe vortices using CFD.

TELEMAC-3D requires a very fine grid to capture the downflow. It was found that the small prism height (i.e. below 10cm) caused severe numerical instability and a high computational time for convergence. One of the limitations of this study was that the contribution of the downflow to the sediment transport module for the prediction of scour in the front of pier was not properly revealed. The situation was made worse due to lack of adequate TELEMAC documentation and technical support during the period of this investigation.

Figure 5.6 showed the wake predicted by TELEMAC-2D and represented on the horizontal plane. The wake behind the pier was also investigated during T3D2 simulation. The velocity distribution was found to be chaotic with large variation in magnitude (Figure 5-8). This agrees with Dargahi (1990), Ahmed & Rajaratnam (1998) and Melville & Coleman (2000).

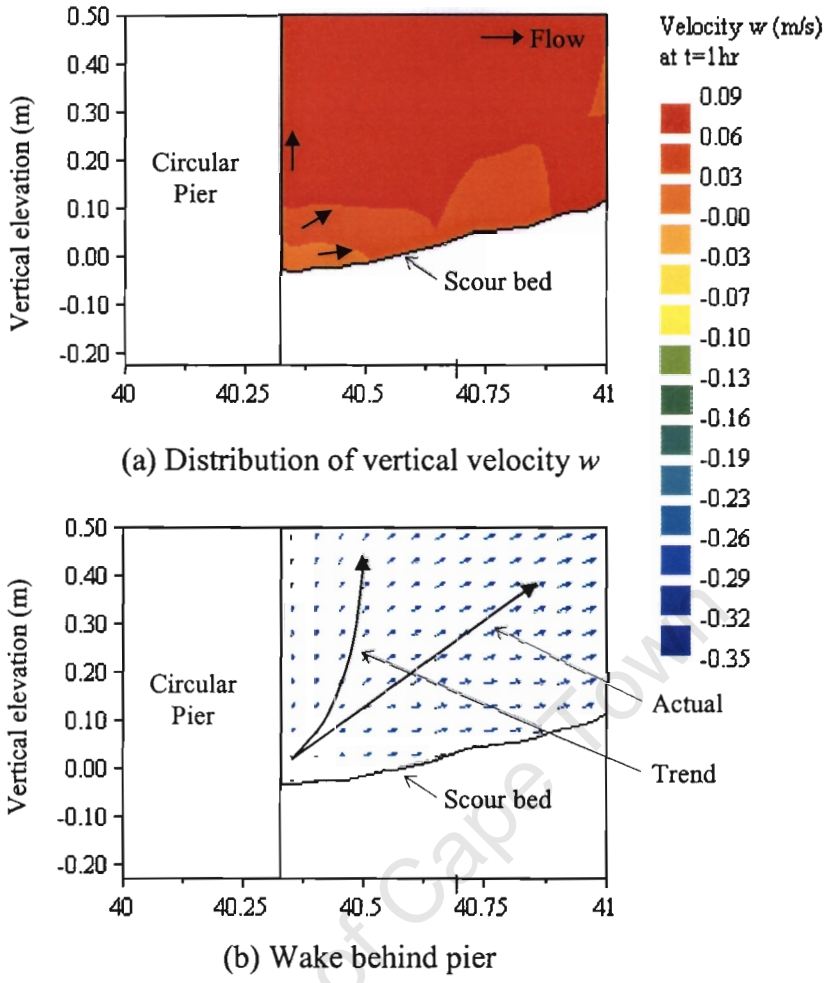

Figure 5-8: Wake behind the pier

The flow travelled up with very low magnitude from the bed level to the free surface at downstream of the pier. The velocity increased progressively upwards to a certain height after which it became almost constant (Figure 5-8a).

The role of the wake vortices is the main cause of scour behind the pier as they act like vacuum cleaners. In theory the wake carries the scoured sediment immediately behind the pier and deposits at downstream. T2D1 showed some scattered deposition behind the pier (Figure 5-9). In general however, TELEMAC V5.5 was not capable of predicting much deposition immediately behind the pier. The TELEMAC-2D runs showed more deposition than the TELEMAC-3D runs.

5.3 Bed evolution and scour depth

5.3.1 T2D1 (TELEMAC-2D with Meyer-Peter & Muller formula)

In T2D1, the bed evolution and the scour depth were predicted by solving the bed evolution equation in conjunction with the sediment transport formula given by Meyer-Peter and Muller (1948). The model was simulated for 9 days 5 hrs in the prototype to observe the ability of the model capability to predict the scour topography around the pier in line with Ahmed (1995). The actual computational time was 17hr 3min 18s.

The bed scouring was initiated next to the pier wall at the location *A* at α=45^0 and α=315^0 (Figure 5.9), which agreed with Ahmed (1995). The scoured sediment was immediately deposited downstream of the pier at location *B* at α=135^0 and α=225^0. The scour continued to deepen in this region where the flow is accelerated. The model was however unable to predict the scour further downstream of A, where the divergence of the shear vector and pressure gradient were assumed to be highest. Moreover the model could not predict the scour in front of the pier. As a consequence the T2D1 simulation could not predict the scour hole pattern as reported in Ahmed (1995). A typical scour and deposition pattern predicted by the model run T2D1 is shown in Figure 5-9.

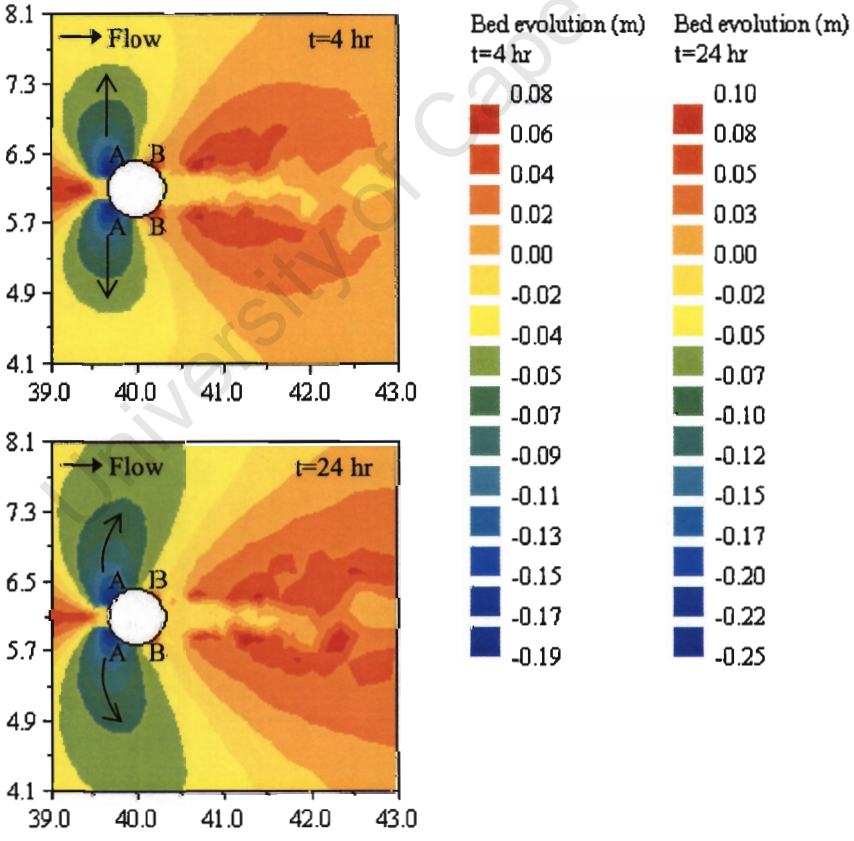

Figure 5-9: Scour and deposition pattern in simulation T2D1

Initially the scour holes that developed at the both sides of the pier (Figure 5-9) extended towards the side walls of the channel. As the scour progressed, the scour hole was gradually skewed in the downstream direction. The velocity inbetween the side walls and the pier was generally higher than the approach velocity to accommodate the obstructed flow due to presence of pier. This was also true for the downstream region where the wake disturbance was prominent in the flow field. This is one cause of the scour inbetween the pier and the side walls.

The scour rate was very high at first few hours during the model run (Figure 5-10). Ahmed (1995) also reported similar trend in his study. In the simulation, the predicted scour rates decreased at each progressive time step. The model reached equilibrium stage at about t=25.0 hrs. According to Ahmed (1995), the actual scour continued up to t=220 hrs.

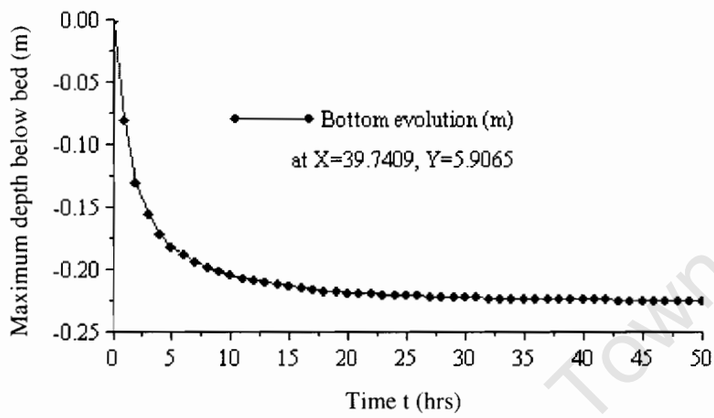

Figure 5-10: Variation of scour depth with time in simulation T2D1

The use of the Meyer-Peter and Muller (1948) formula was found to under-predict the scour around the pier compared with Ahmed (1995). The model simulation T2D1 did not even capture the deposition behind the pier according to Ahmed (1995). The efficiency factor μ_b used in the Meyer-Peter and Muller (1948) formula has a significant role in the transport of sediment from the bed (Section 2.3.6.1). Mathematical analysis suggests that the increase of water depth significantly reduces the value of this efficiency factor. During the scouring process, the hole deepened and the water depth was increased. As a consequence, the efficiency factor reduced and this would have reduced the sediment transport.

SISYPHE V5.5 considers the transport rate zero when the product of efficiency factor and Shields parameter is less than 0.047 (i.e. $q_b = 0$, when $\mu_b\theta < 0.047$. Traditionally the Meyer-Peter and Muller (1948) interpreted the value 0.047 as equivalent to the critical Shields parameter, which was mainly for coarse sediment particles. The model considered the value 0.029 as the critical Shields parameter based on the fine sand particle size given in Ahmed (1995). The sensitivity of the Meyer-Peter and Muller (1948) formula and TELEMAC code on critical Shields parameter was not investigated during this study.

5.3.2 T2D2 (TELEMAC-2D with Einstein & Brown formula)

In T2D2, the bed evolution and the scour depth were predicted using the Einstein & Brown (1950) formula. The model was simulated for 9 days 5 hrs in the prototype. The actual computational time was 15hr 3min 26s.

The scouring was initiated along the pier surface exactly at location *A* at α=45^0 and α=315^0 (Figure 5.11). Like T2D1, the scoured sediment was deposited downstream of the pier at location *B* at α=135^0 and α=225^0. A typical scour and deposition pattern predicted by the model run T2D2 is shown in Figure 5-11.

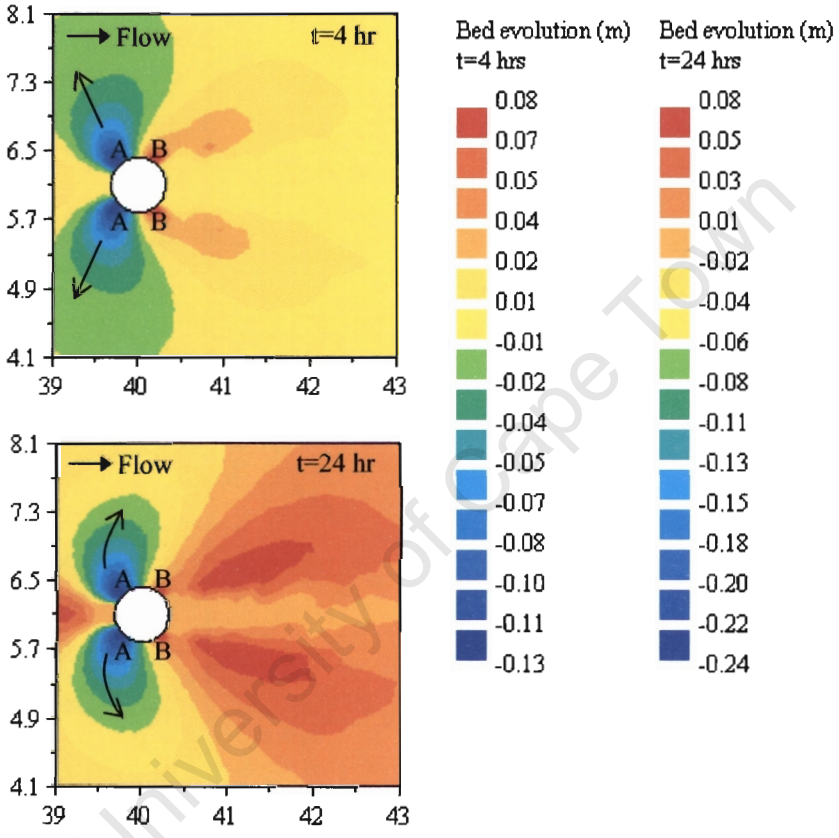

Figure 5-11: Scour and deposition pattern in simulation T2D2

The scour continued to deepen at the region of accelerated flow. The deposition mostly took place at the interface between wake and main currents. The model could not predict the scour in front and behind the pier. The T2D2 model simulation of scour around pier was not the same as in Ahmed (1995).

The model initially predicted higher scour rate compared to that after t=5.0hrs (Figure 5-12). The model also initially under-estimated the scour depth compared to T2D1. The model however calculated a greater scour depth at *t*=24 hrs than T2D1. The model was found to be under-predict the scour around the pier. Unlike T2D1, the deposition at downstream of the pier

was different. Most of the deposition took place at the interface region between the wake and the main flow (Figure 5-11).

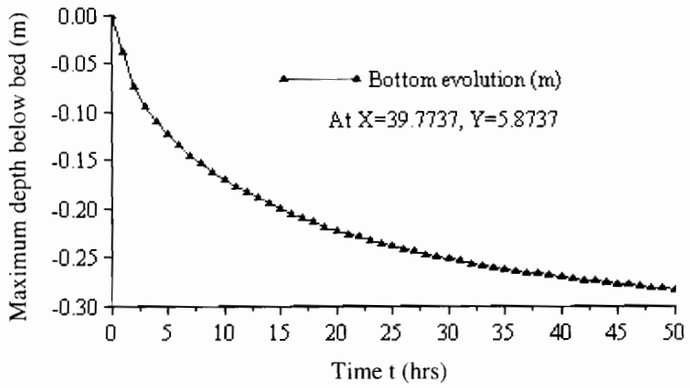

Figure 5-12: Variation of scour depth with time in simulation T2D2

The probability approach, on which the Einstein & Brown (1950) formula is based, considers a stable bed condition i.e. the rate of erosion must be equal to the rate of deposition. SISYPHE has an algorithm to carry sediment particles along the mean velocity direction. As a result most of the sediment particles settled and deposited in the region where the main flow was impacted by the wake.

5.3.3 T2D3 (TELEMAC-2D with Engelund & Hansen formula)

In T2D3, the Engelund & Hansen (1967) formula was used. The model was simulated for 9 days 5 hrs in the prototype with an actual computational time of 15hr 32min 3s.

Like T2D1 and T2D2, the scouring was initiated along the pier surface around location *A* at $\alpha=45^0$ and $\alpha=315^0$ (Figure 5.13) and sediment was deposited further downstream of the pier at location *B* at $\alpha=135^0$ and $\alpha=225^0$. The scour continued to deepen in the regions where it had initiated. Like T2D2, the deposition was mostly took place at the interface between the wake and the main currents. The model could not predict the scour in front and behind the pier. The T2D3 model prediction of scour around pier was not same as in Ahmed (1995). A typical scour and deposition pattern predicted by the model run T2D3 is shown in Figure 5-13.

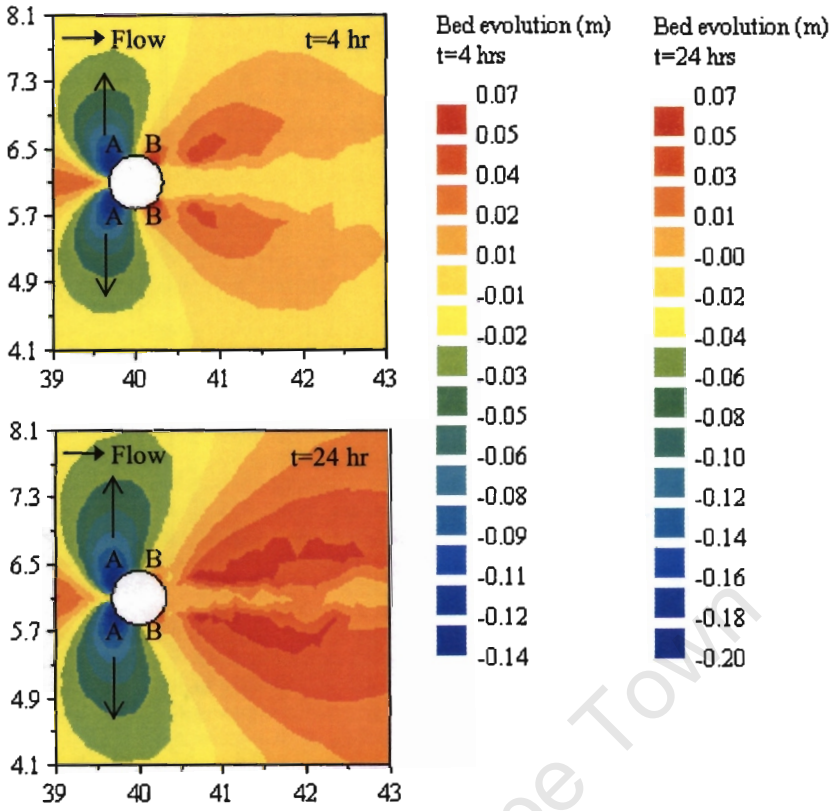

Figure 5-13: Scour and deposition pattern in simulation T2D3

The T2D3 model prediction of scour rate was similar to those in Model T2D1. The prediction of scour rate was very high during first 2 hrs (Figure 5-14). The prediction of scour rate however became very slow after t=20 hrs. The model under-estimated the scour depth compared to T2D1, T2D2 and Ahmed (1995).

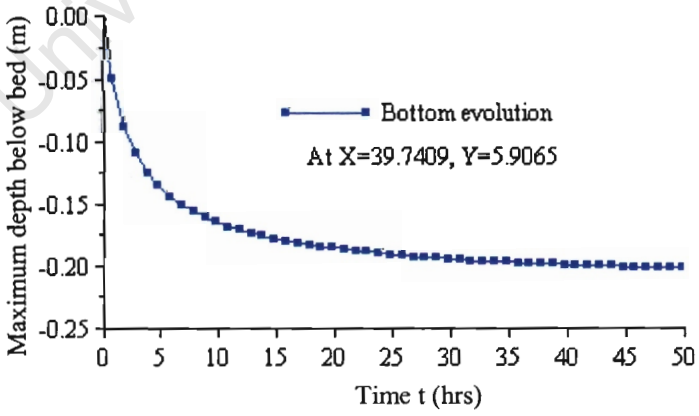

Figure 5-14: Variation of scour depth with time in simulation T2D3

5.3.4 T2D4 (TELEMAC-2D with Van Rijn formula)

In T2D4, the Van Rijn (1984a) formula was used. The model was simulated for 9 days 5 hrs in the prototype with an actual computational time of 33hr 26min 34s.

Like previous simulations, the scouring commenced next to the pier wall at location *A* at α=45^0 and α=315^0 (Figure 5.15). The eroded sediment was deposited at further downstream of the pier at location *B* at α=135^0 and α=225^0. The scour deepened in the same regions where it been initiated. The scour hole initially propagated along the channel side walls. The hole later skewed the downstream along with depth-averaged flow directions inbetween the pier and channel side walls.

Like T2D2 and T2D3, the deposition mostly took place at the interface between the wake and the main currents. The model could not predict the scour in front and behind the pier. The T2D4 model prediction of scour around pier was not same as in Ahmed (1995). A typical scour and deposition pattern predicted by T2D4 is shown in Figure 5-15.

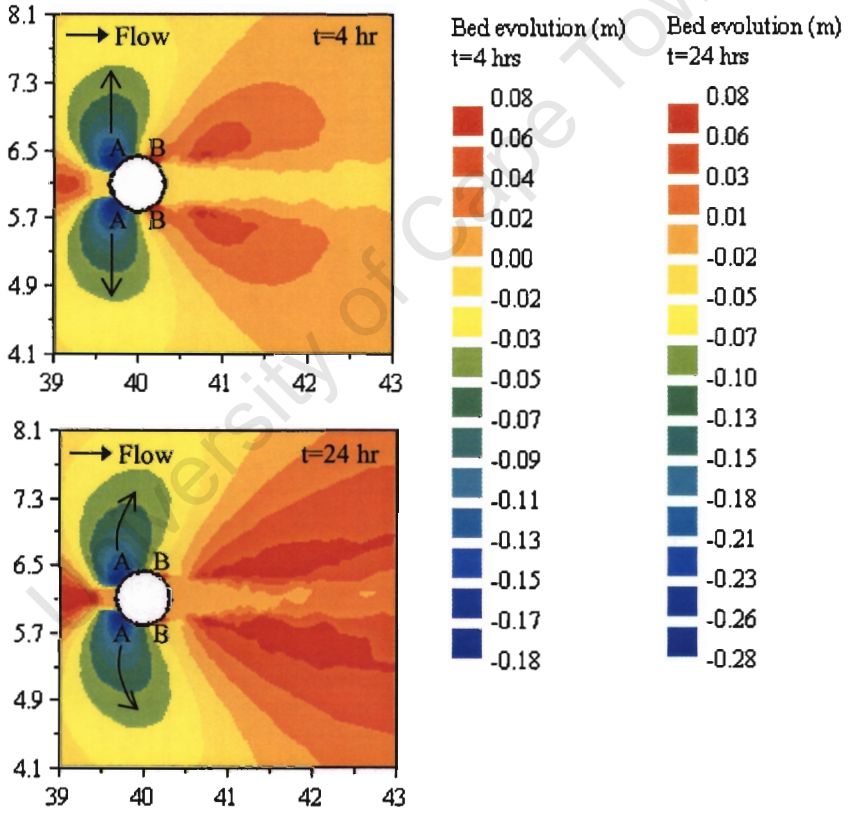

Figure 5-15: Scour and deposition pattern in simulation T2D4

The T2D4 model prediction of the scour rate was similar to those in the model T2D1 and T2D3. The prediction of the scour rate was very high during first 5 hrs (Figure 5-16). The prediction scour rate however became slow after *t*=30 hrs.

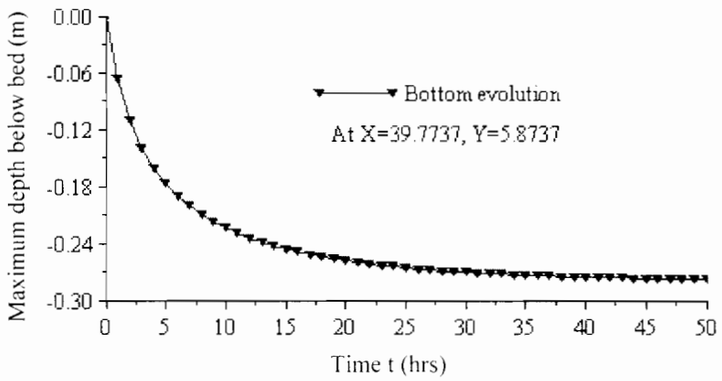

Figure 5-16: Variation of scour depth with time in simulation T2D4

The model T2D4 was found to estimate a greater depth than simulations T2D1, T2D2 and T2D3.

5.3.5 T3D1 (TELEMAC-3D with Van Rijn formula)

In T3D1, TELEMAC-3D was coupled with the Van Rijn (1984a) formula. The 2D mesh was repeated 10 times in the vertical direction in order to build the 3D prismatic mesh. The model was simulated for 5 hrs in the prototype. The actual computational time was 177hr 19min 5s. This model was found to be computationally very expensive.

Despite the 3D simulation, the model did not give better results than the 2D simulations except for the prediction of a greater scour depth at the lateral of the pier. Like the 2D simulations, the scour also commenced along the pier walls around location *A* at $\alpha=45^0$ and $\alpha=315^0$ (Figure 5.17). The scour and deposition pattern was also similar to those in 2D models. Eroded sediment was deposited downstream of the pier at location *B* at $\alpha=135^0$ and $\alpha=225^0$.

The scour deepened in the same region where it had initiated. The deposition took place at the interface between the wake and the main currents. Despite predicting the vertical downflow and the wake (Section 5.2.3), the model could not predict the scour in front and behind the pier. It seems that SISYPHE is not capable of taking account the effect of downflow and wake during the prediction of bed evolution. The overall model prediction of the scour around pier was not the same as in Ahmed (1995). A typical scour and deposition pattern predicted by T3D1 is shown in Figure 5-17.

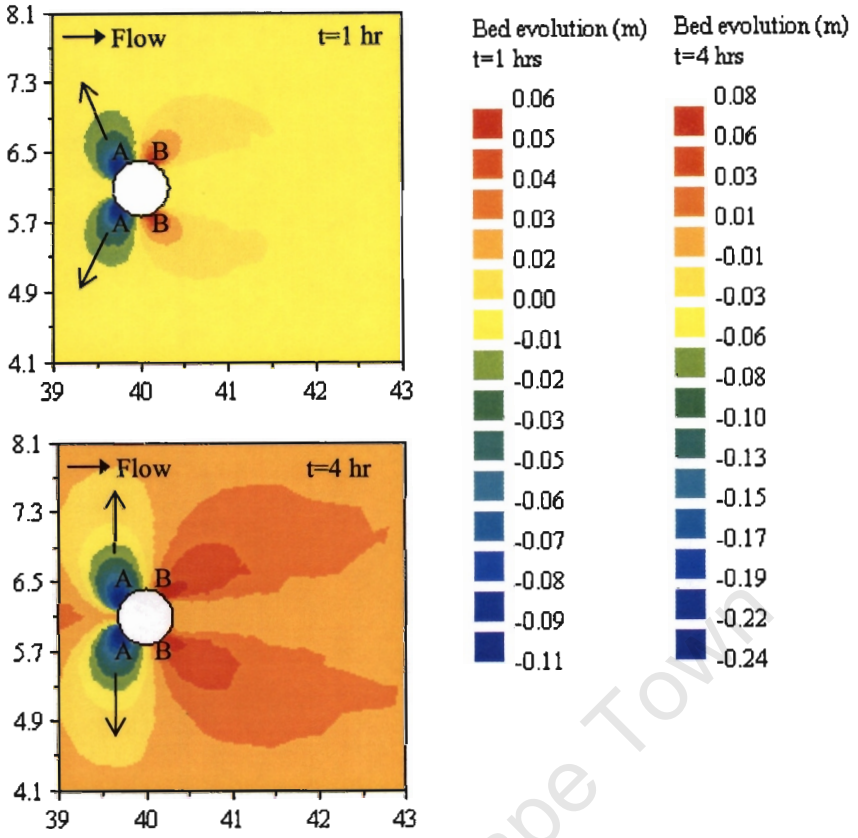

Figure 5-17: Scour and deposition pattern in simulation T3D1

The T3D1 model prediction of scour rate was found to be similar to the T2D2 (Figure 5-18).

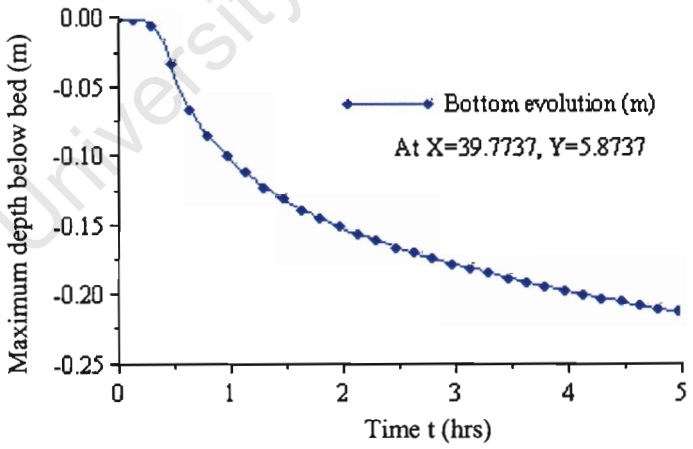

Figure 5-18: Variation of scour depth with time in simulation T3D1

The maximum scour depth at t=4.0 hrs was very close to the value reported in Ahmed (1995). This was not unexpected because the 3D model predicted a greater depth averaged velocity

than the 2D model. The depth-averaged velocity is the main factor in the determination of the bed-shear stress and Shields parameter - thus – local scour.

5.3.6 Comparison of the scour profiles

The predicted scour topography around the pier was however deviated from that measured by Ahmed (1995). In particular, the scour in front and behind the pier was not captured. The model generally predicted the scour at the side of the pier, where it deepened and expanded along the main flow directions. An attempt was thus made to compare the scour profiles along the line *AA*' at α=45^0 (Figure 5.2), where scour was normally deepened.

Unfortunately Ahmed (1995), did not outlined the scour profile at the line *AA*' at α=45^0. This study therefore assumed a uniform scour topography between the profiles at upstream and lateral of the pier measured by Ahmed (1995). These two profiles were therefore interpolated in order to get the intermediate profile along the line *AA*' at α=45^0.

Figure 5-19a and 5-19b give comparisons of the scour profiles for the TELEMAC-2D simulations and Ahmed (1995), whilst Figure 5-20 shows the profiles for T2D4, T3D1 and Ahmed (1995).

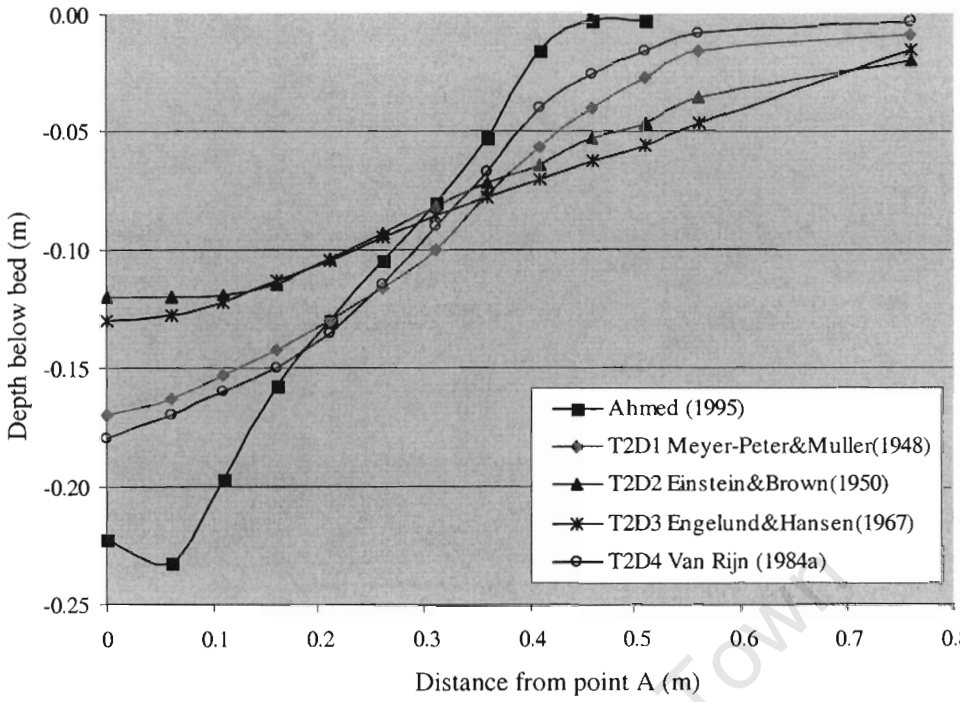

(a) at t= 4 hrs

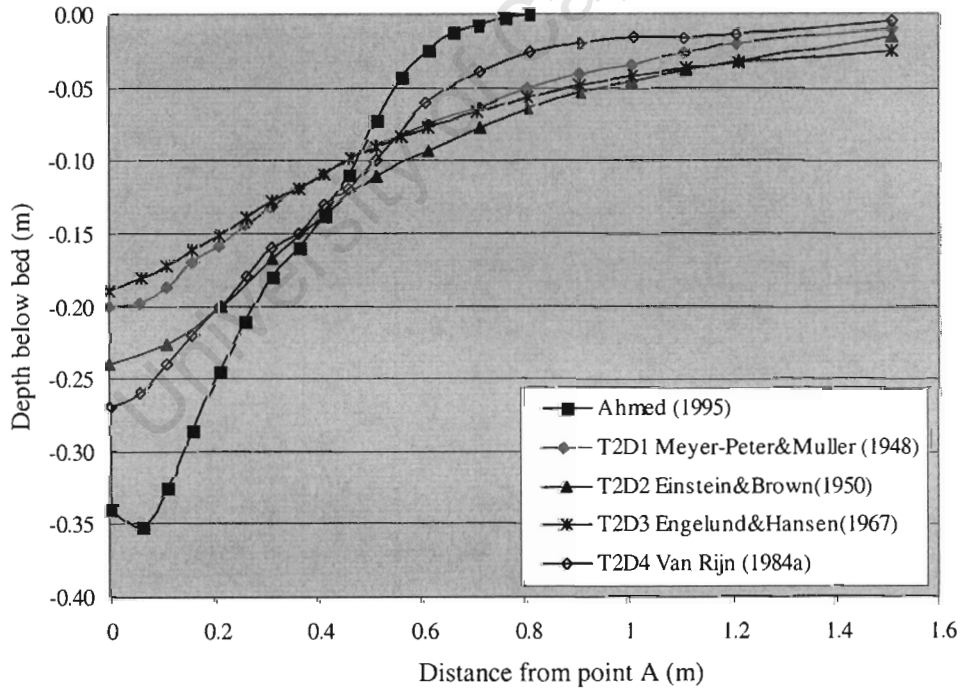

(b) at t= 24 hrs

Figure 5-19: Comparison of scour profiles at α=45^0 (TELEMAC-2D and Ahmed, 1995)

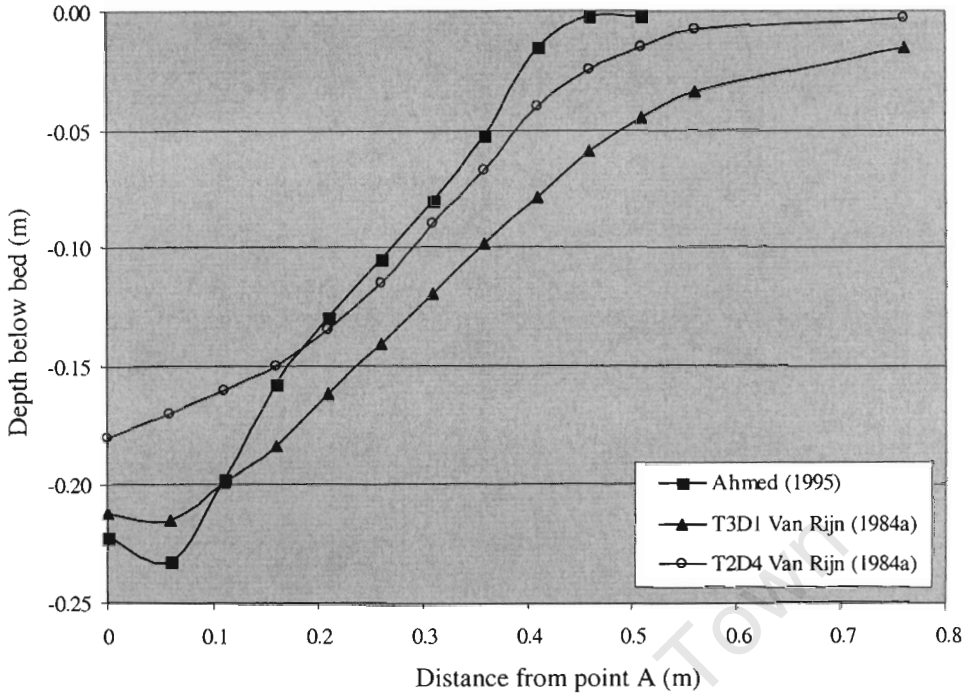

Figure 5-20: Comparison of scour profiles at $\alpha=45^0$ (T2D4, T3D1 and Ahmed, 1995)

Figure 5-19 shows that the model simulations did not agree with Ahmed (1995) as they all under-predicted the maximum scour depth close to pier. T2D2 estimated a lower scour at t=4 hrs, on the other hand T2D3 predicted a lower scour at t=24 hrs. T2D4 was found to predict the maximum scour depth at t=4 hrs and t=24 hr. All model runs estimated a larger scour hole extending towards the boundary than Ahmed (1995). A possible reason might be that the model bed evolution prediction was very sensitive to the depth-averaged velocity and the direction of sediment movement.

Figure 5-20 shows that the T3D1 prediction of maximum scour depth was very close to Ahmed (1995). The extent of the scour hole was however larger and it over-predicted the scour far from pier compared with T2D4 and Ahmed (1995). The T2D4 (Figure 5-19) prediction was very close to Ahmed (1995) far from the pier but did not agree close to the pier. The T3D1 (Figure 5-20) results were however the opposite. In this case, the model predicted more scour depth close to the pier and over-predicted the scour far from the pier.

5.4 Limitations

This study had many limitations, mainly because of the constraints put by the inadequate documentation supplied with TELEMAC V5.5. All comments on the program codes were written in French, as was the TELEMAC formulation documentation. Moreover, much of

documentation was not accessible during the study period. The author's inability to read and write French made it hard for him to understand the various linkages between codes.

The contribution of the downflow to the sediment transport module (SISYPHE) for the prediction of scour in the front of pier was not properly revealed. Moreover, SISYPHE module could not be calibrated independently due to lack of suitable sediment transport data.

The sensitivity of the sand transport estimates to the hydrodynamic variables including the current velocity and the friction coefficient was not thoroughly studied due to time constraints.

One serious shortcoming of this study was the use of sediment size that has not been rescaled from that of Ahmed (1995) experiments but the velocities and depths were larger during simulations.

5.5 General discussion

Most research on local scour around bridge piers is based on experiments in laboratory flumes. These experiments are often time intensive and laborious. Numerical prediction also has constraints but can be treated as easy design solution. The present study is a contribution in this direction. This study was probably the first attempt to model local scour around a circular pier using TELEMAC coupled with SISYPHE under a Windows operating system (Lang, 2005).

The 2D and 3D flow field were modelled using TELEMAC V5.5 code. These were coupled to SISYPHE V5.5 (sediment transport module in the TELEMAC system) for the prediction of the local scour. Four well-known sediment transport formulae were independently tested for the prediction of local scour in this study.

Analysis of the flow field revealed the performance of 2D and 3D model and their effect on local scour. The 2D or 3D model predicted the maximum scour next to the pier wall at location A at $\alpha=45^0$ and $\alpha=315^0$ (Figure 5-2). The prediction of local scour differed depending on the sediment transport formulae used. The study was however not able to identify the best sediment transport formula for the prediction of local scour around a circular pier.

TELEMAC V5.5 was found to model the hydrodynamic field fairly accurately. TELEMAC coupling with SISYPHE put some constraints on use of the sediment transport formulae – thus – the prediction of scour depth around the pier was found to vary and to some extent was under-predicted compared with Ahmed (1995). TELEMAC V5.5 may not be able to take into account the contribution of the downflow, horseshoe vortex and wake in the bed evolution process.

Chapter 6
Conclusions

Local scour and deposition around bridge piers is a result of the complex interaction of many physical factors related to hydrodynamics and sediment transport. The numerical modelling of local scour is therefore not easy. This study was an attempt to model local scour using the commercial CFD codes TELEMAC V5.5. This investigation can be treated as an alternative to laborious physical modelling. This study found that:

- TELEMAC V5.5 is not suitable for a small-scale computational domain e.g. laboratory flume. This made comparison with the laboratory data very difficult. The Froude and Continuity similarity had to be used to scale the computational domain.

- The 2D mesh generation is user-friendly. TELEMAC did not, however, allow the generation of the 3D mesh in the pre-processing stage. The accuracy of the results is dependent on the fineness of mesh. The study generated a mesh consisting of equilateral triangular elements, whose length ranges from 0.01m around the pier to 1.0m at the channel sidewalls using MATISSE. The 2D mesh was reproduced along the vertical in 10 planes for the 3D flow simulations. TELEMAC does not allow the inspection of the 3D mesh before simulation. The Sigma 3D mesh transformation was found to be effective for the adjustment of mesh automatically during the scouring process.

- The upstream and downstream liquid boundaries had to be placed a sufficient distance from the pier location in order to avoid the numerical disturbance around the pier locations. The discharge has to be progressively increased over a model period of half an hour. A constant depth had to be maintained at the downstream liquid boundary. The model had to be calibrated against measured data. During calibration, this study found only a 1.7% discrepancy of the depth-averaged velocity measured by Ahmed (1995).

- The selection of time step is one of the crucial numerical parameters for the convergence of the Saint Venant (TELEMAC-2D) and Navier-Stokes (TELEMAC-3D) equations. This study used the value of time step 1.0s and 0.1s for 2D and 3D simulation respectively.

- In TELEMAC-2D, a Conservative scheme along with SUPG was found to be effective for the solution of the advection of water depth, whereas the Method of Characteristics was found to be efficient to solve the advection of velocity components and k-ε terms. The GMRES solver was found to be efficient for the convergence with a 1.0×10^{-6} accuracy. Computational time was found to be different for different model runs with an average between 16 hrs and 22 hrs depending on the mesh.

- The 3D simulation is more complex than the 2D model in terms of the mesh management and numerical schemes. The solution of the Navier-Stokes equations with the non-hydrostatic pressure distribution using the Fractional Step Method was found to be stable for the simulation of the 3D flow. The Conjugate Gradient on Normal Equation and Squared Conjugate Gradient solver were found to be efficient for the solution of the 3D model equations.

- The 2D or 3D flow was coupled with a two-equation Standard k-ε model and was found to be reasonable against physical model data. The model predicted the down flow, horseshoe vortex in front and the wake behind the pier.

- The scour depth was predicted by solving the bed evolution equation in conjunction with four different sediment transport formulae i.e. Meyer-Peter and Muller (1948), Einstein-Brown (1950), Engelund & Hansen (1967) and Van Rijn (1984a) in SISYPHE. Internal coupling between TELEMAC-SISYPHE was found to be efficient to transfer the hydrodynamic variables to the bed evolution equation. TELEMAC-3D coupled to SISYPHE predicted a greater scour depth near pier than the TELEMAC-2D simulation and was computationally expensive. There have been very few attempts in the past to model local scour with different sediment transport formulae. The Shields approach was used for the initiation of sediment movement. Its critical value had to be calculated carefully.

- The simulation showed different model responses with the different sediment transport formulae. The prediction of scour depth also varied for different sediment transport formulae. Van Rijn (1984a) was found to predict the maximum scour depth near the pier. This study was not intended to identify the best sediment transport formula for the prediction of local scour around a circular pier.

- The initiation of scour took place next to the pier wall inbetween the upstream and lateral side of the pier where flow was deflected and accelerated. The scour hole was deepened at the same location and was found to expand towards channel sidewalls. The model did not predict the scour topography all around the piers as described in literature i.e. Ahmed (1995). This study was probably the first attempt to model local scour around a circular pier using TELEMAC coupled with SISYPHE under a Windows operating system (Lang, 2005).

- An important constraint on this study was the limited English language documentation on TELEMAC V5.5. Despite some limitations imposed by TELEMAC V5.5, the results were sufficiently encouraging to suggest that there is potential for the use of numerical modelling to predict local scour given in improved codes and faster machines.

Chapter 7
Recommendations for future work

Numerical prediction of local scour around bridge piers in open channel flow is a possible alternative to time-consuming laboratory experiments. With limitations, the present study gives an indication of the potential to model local scour using the commercial TELEMAC system. Further research in the following areas is required:

- Exploring the use of a more limited region upstream of the pier to speed up the computation with the mesh dependency of the solutions to ensure the grid size is fine enough.

- The model physical parameters were mainly based on one set of data taken from Ahmed (1995), which was determined from laboratory flume experiments. A sensitivity analysis of the hydrodynamic fields to different physical and numerical parameters should be thoroughly studied. Similar sensitivity analyses should be performed for the sediment transport and bed evolutions with the sensitivity of the results to sediment size and properties.

- As the TELEMAC system was found to be sensitive to flume dimensions, it is recommended that the model should be verified against field data. The model should also be calibrated using measured field data before simulation of local scour. Recoding the TELEMAC data input and results presentation to enable validation of the software against laboratory data.

- The sediment transport formulae such as Meyer-Peter and Muller (1948), Einstein-Brown (1950), Engelund & Hansen (1967) and Van Rijn (1984a) did not consider the effect of the presence of piers. It is recommended that the suitability of existing sediment transport formula taking into account the influence of pier should be examined thoroughly. A similar study can be performed for the use of the other incipient motion criteria except the Shields parameter. The link between hydrodynamic and sediment transport modules should be investigated properly. Examination of the use of a constant value of the Chezy coefficient and its compatibility with the alluvial resistance implied by the sediment transport formulae.

- It is recommended that a better sediment transport algorithm, that will more accurately predict the effect of the downflow, horseshoe vortex and wake, needs to be developed. "Stability" constraints of TELEMAC-3D need to be identified.

- Increased CPU that would increase the solver speed and hence the accuracy would help to reduce the computational time. Increased computing power i.e. RAM would also enhance the computing efficiency so that limitations on mesh refinement and the size of the flow domain would be lifted.

References

Ahmed F (1995), "Flow and erosion around bridge piers" PhD thesis, Department of Civil Engineering, University of Alberta, Canada

Ahmed F & Rajaratnam N (1998), "Flow around bridge piers." *J. Hydr. Engrg.* ASCE, Vol. 124, Issue 3, pp 288-300

Ali KMH & Karim O (2002), "Simulation of flow around piers." *J. Hydr. Res.,* Vol. 40, No. 2, pp 161-174

Analytis GT (2003), "Implementation of the renormalization group (RNG) k–ε turbulence model in GOTHIC/6.lb: solution methods and assessment", *Annals of Nuclear Energy*, Vol. 30, Issue 3, pp 349-387

Anderson, DAJ (1995), *Computational fluid dynamics: the basics with applications,* McGraw-Hill, Inc. USA

Armitage N & McGahey C (2003), "A unit stream power model for the prediction of local scour in rivers", Report No 1098/1/03, Water Research Commission, South Africa

Armitage N & McGahey C (2004), "Scour prediction using the mobility number criteria for incipient motion." *Proceedings of the second International conference on fluvial hydraulics,* River Flow 2004, Vol.1, pp 511-519

Armitage N, Cunningham M & Kabir A (2005), "Local scour in rivers", Report No 565, Water Research Commission, South Africa

Bagnold RA (1966), "An approach to the sediment transport problem from general physics", US Geological Survey Professional Paper 422-J

Bailard J (1981), "An energatics total load transport model for a plane slopping beach", *Journal of Geographic Science*, 86, C11, pp 10938-10954, In SISYPHE (2004)

Balden V (2003), "Introduction to Finite Elements-AMU502z/MEC563z", CERECAM, The University of Cape Town, South Africa

Barkdoll BB (2000), "Time scale for local scour at bridge piers.", *J. Hydr. Engrg.* ASCE, Vol. 126, Issue 10, pp 793-795

BIEF (2004), "Programming with BIEF V5.4" -edited by Hervouet JM, TELEMAC Modelling System, SOGREAH Consultants, France

Biglari B & Sturm TW (1998), "Numerical modelling of flow around bridge abutments in compound channels." *J. Hydr. Engrg. ASCE*, Vol. 124, Issue 2, pp 156-164

Bijkar EW (1968), "Mechanics of sediment transport by the combination of currents and waves", 23rd Int. Conf. on Coastal Engineering, pp 147-173, In SISYPHE (2004)

Boyd JP (2000), *Chebycheb and Fourier Spectral Method*, 2nd Edition, DOVER publications, Mineola, New York, USA

Bradshaw P, Cebeci T & Whitelaw JH (1981), *Engineering calculation methods for turbulent flow,* Academic Press, London

Breusers HNC, Nicollet G & Shen HW (1977), "Local scour around cylindrical piers", *J. Hydr. Res.* IAHR, Vol. 15, No. 3, pp 211-252

Breusers HNC & Raudkivi AJ (1991), *Scouring*, IAHR Hydraulic Structures Design Manual 2, AA Beklahama

Brice JC & Boldgett JC (1978), "Countermeasures for hydraulic problems at bridges", Vols 1 and 2, Federal Highway Administration, US Department of Transportation, Washington DC, USA

Brooks NH (1963), Discussion of "boundary shear stresses in curved trapezoidal channels", by AT Ippen & PA Drinker, *J. Hydr. Div.* ASCE, Vol. 89, Issue HY3, pp 327-333

Brown CB (1950), "Sediment transportation", *Engineering Hydraulics*-edited H Rouse, John Wiley, New York

Cardoso AH & Bettess R (1999), "Effects of Time and Channel Geometry on Scour at Bridge Abutments." *J. Hydr. Engrg.* ASCE, Vol. 125, Issue 4, pp 387-398

Celik I & Rodi W (1988), "Modelling suspended sediment: transport in non-equilibrium situation", *J. Hydr. Engrg.* ASCE, Vol. 114, Issue 10

Chadwick A, Morfett J & Borthwick M (2004), *Hydraulics in Civil and Environmental Engineering*, Spon Press, London, UK

Chang FFM (1973), "A statistical summary of the cause and cost of bridge failures", Federal Highway Administration, US Department of Transportation, Washington DC, USA

Chang WY, Lai JS & Yen CL (2004), "Evolution of Scour Depth at Circular Bridge Piers." *J. Hydr. Engrg.* ASCE, Vol. 130, Issue 9, pp 905-918

Chanson H (1999), *The hydraulics of open channel flow*, Arnold

Chen, Q, Dai, G & Liu, H (2002), "Volume of fluid model for turbulence numerical simulation of stepped spillway overflow." *J. Hydr. Engrg. ASCE*, Vol. 128, Issue 7, pp 683-688

Cheng NS (1997), "Simplified settling velocity formula for sediment particle" *J. Hydr. Engrg.* ASCE, Vol. 123, Issue 2, pp 149-152

Cheng Y, Lien FS, Yee E & Sinclair R (2003), "A comparison of large Eddy simulations with a standard k–ε Reynolds-averaged Navier–Stokes model for the prediction of a fully developed turbulent flow over a matrix of cubes", *Journal of Wind Engineering and Industrial Aerodynamics*, Vol. 91, Issue 11, pp 1301-1328

Chiew YM (1984), "Local scour at bridge piers", Report No 355, School of Engineering, The University of Auckland, Auckland, New Zealand

Chiew YM (1995), "Mechanics of riprap failure at bridge piers" *J. Hydr. Div.*, ASCE, Vol. 121, No 9, pp 635-643

Chiew YM & Melville BW (1996), "Temporal development of local scour depth at bridge piers", North American Water and Environment Congress, ASCE, June 1996, California, USA

Chien N & Wan Z (1999), *Mechanics of sediment transport*, ASCE Press

Chollet JP & Cunge JA (1980), "New interpretation of some head loss flow velocity relationship for deformable bed", *J. Hydr. Engrg.*, ASCE, Vol. 17, No 1

Chrisohoides, A, Sotiropoulos, F & Sturm, TW (2003), "Coherent structures in flat-bed abutment flow: computational fluid dynamics simulations and experiments." *J. Hydr. Engrg. ASCE*, Vol. 124, Issue 3, pp 177-186

Colebrook CF & White CM (1937), "Experiments with fluid friction in roughened pipes" *Proc. Roy. Soc. London,* Vol A161, pp 367-381

Coleman SE, Lauchlan CS & Melville BW (2003), "Clear-water scour development at bridge abutments." *J. Hydr. Res.*, Vol. 41, No 5, pp 521-531

Costa JJ, Oliveira LA & Blay D (1999), "Test of several versions for the k–ε type turbulence modelling of internal mixed convection flows", *International Journal of Heat and Mass Transfer,* Vol. 42, Issue 23, pp 4391-4409

CUR (2000), "Manual on the use of rock in hydraulic engineering", AA Balkema, Rotterdam, Netherland

Dargahi B (1987), "Flow field and local scouring around a cylinder", Bulletin TITRA-VBI-137, Department of Hydraulic Engineering, Royal Institute of Technology, Stockholm, Sweden

Dargahi B (1990) "Controlling mechanism of local scour" *J. Hydr. Engrg.* ASCE, Vol. 116, Issue 10, pp 1197-1214

Das BM (2002), *Principles of geotechnical engineering*, 5th Edition, Brooks Cole, Thomson Learning

Davidson L (2003), "An introduction to turbulence models", Publication No. 97/2, Department of Thermo and Fluid Dynamics, Chalmers University of Technology, Göteborg, Sweden

Dey SB, Sujit KS & Sastry GLN (1992a), "Clear water scour at circular pier, part I: Flow model", Proc. 8th Congr. Of Asian and Pacific Div of IAHR, Pune, India, III (C), pp 69-80

Dey SB, Sujit KS & Sastry GLN (1992a), "Clear water scour at circular pier, part II: Flow model", Proc. 8th Congr. Of Asian and Pacific Div of IAHR, Pune, India, III (C), pp 81-90

Dey SB, Sujit KS & Ghandikota LN (1995) "Clear water scour at circular piers: a model." *J. Hydr. Engrg.* ASCE, Vol. 121, Issue 12, pp 869-876

Dibajnia M & Watanabe A (1992), "Sheet flow under non-linear waves and currents", *Proc. of the Int. Conf. on Coast Eng.*, pp 2015-2029, In SISYPHE (2004)

Eisntein HA (1950), "The bed-load function for sediment transportation in open channel flows" Technical Bulletin No. 1026, Department of Agriculture, Washington DC, USA

Engelund F & Hansen E (1967), "A monograph on sediment transport in alluvial streams", University of Denmark, Copenhagen, Denmark

Ettema R (1976), "Influence of bed material gradation on local scour", School of Engineering Report No 124, University of Auckland, New Zealand

Ettema R (1980), "Scour at bridge piers", School of Engineering Report No 216, University of Auckland, New Zealand

Ettema R, Mostafa EA, Melville BW & Yassin AA (1998) "Local scour at skewed piers." *J. Hydr. Engrg.* ASCE, Vol. 124, Issue 7, pp 756-763

French RH (1994), *Open-Channel Hydraulics*, International Edition, McGraw-Hill Inc.

Gessler J (1970), "Self-stabilising tendencies of alluvial channels" *Journal of the Waters and Harbours Division.* ASCE, Vol. 96, No. WW2, pp 235-249

Gottlieb D & Orszag SA (1977), *Numerical Analysis of Spectral Methods: Theory and Applications*, Society for Industrial and Applied Mathematics (SIAM), Philadelphia, USA

Govers G (1987), "Initiation of motion in overland flows", *Sedimentology*, No 34, pp 1157-1164

Graf WH & Altinakar MS (1998), *Fluvial hydraulics flow and transport processes in channels of simple geometry,* John Wiley & Sons, UK

Hager WH & Oliveto G (2002), "Shields entrainment criteria in bridge hydraulics", *J. Hydr. Engrg.* ASCE, Vol. 128, Issue 5, pp 538-542

Hervouet JM & Jankowski J (2000), "Comparing numerical simulations of free surface flows using non-hydrostatic Navier-Stokes equations and Boussinesq equations" *Hydroinformatics*, Iowa Institute of Hydraulic Research, Iowa City.

Hervouet JM (2003), "TOMAWAC software for finite element sea state modelling", Release 5.2, Theoretical note, Report EDF – LNHE HP-75/02/065/A, In SISYPHE (2004)

Hrenya C, Miller S, Mallo T & Sinclair J (1998), "Miller Comparison of low Reynolds number k–ε turbulence models in predicting heat transfer rates for pipe flow", *International Journal of Heat and Mass Transfer,* Vol. 41, Issue 11, pp 1543-1547

Hjorth P (1975), "Studies on the Nature of Local Scour." Dept. of Water Resource Engineering, Lund Inst of Tech., Bulletin Series A, No. 46

Hjorth P (1977), "A Stochastic Model of Progressive Scour." Hydraulic Problems Solved by Stochastic Methods, Ed. P. Hjorth, L. Jonsson, and P. Larsen, Water Resources Publications, Fort Collins, CO, 1977, pp. 365-383.

Hoffman GJCM & Verheij HJ (1997), *Scour manual*, AA Balkema, Rotterdam, Netherland

Hoffman J & Jhonson C (2003), "Adaptive DNS/LES: a new agenda in CFD." CIMS, New York University, USA

Hunziker RP (1995), "Fraktionsweiser Geschuebetransport" PhD thesis, ETH Zurich, Switzerland, In SISYPHE (2004)

Iyer GR & Yavuzkurt S (1999), "Comparison of low Reynolds number k–ε models in simulation of momentum and heat transport under high free stream turbulence", *International Journal of Heat and Mass Transfer*, Vol. 42, Issue 4, pp 723-737

Johnson PA & Hey RD (2001), "Aggradation at bridges", *J. Hydr. Engrg.* ASCE, Vol. 127, Issue 2, pp 154-157

Kimura, I, Hosoda, T, Onda, S & Tominaga, A (2004), "Computation of 3D turbulent flow structures around submerged spur dikes under various hydraulic conditions." *Proc. 2nd International Conference on Fluvial Hydraulics,* River Flow 2004, Vol. 1, pp 543-553

Kline SJ & McClintock FA (1953), "Describing uncertainties in single-sample experiments", Mech. Engrg, ASME, Vol. 75, pp 3-8, In Ahmed (1995)

Koch FG & Flokstra C (1981), "Bed level computations for curved alluvial channels", XIXth Congress of the International Association for Hydraulic Research, New Delhi, India

Kogaki, T, Kobayashi, T & Taiguchi, N (1997), "Large eddy simulation of flow around a rectangular cylinder." *J. Fluid Dynamics Research*, Vol. 20, Issue 1-6, pp 11-24

Kothyari, UC & Raju, KGR (2001), "Scour around spur dikes and bridge abutments." *J. Hydr. Res.*, Vol. 39, No. 4, pp 367-374

Lang P (2005), "Personal e-mail communication", SOGREAH Consultants, France

Launder, BE & Spalding BD (1974), "The numerical computation of turbulent flows", *Comput. Methods Appl. Mech. Eng.,* Vol. 33, pp 269-289

Laursen EM & Johnson PA (1997), "Modeling uncertainty in prediction of pier scour." *J. Hydr. Engrg.* ASCE, Vol. 123, Issue 9, pp 822-823

Lyons S (2003), "An investigation into the initiation of local scouring around long contractions", MSc Thesis, Department of Civil Engineering, The University of Cape Town, South Africa

Macky GH (1990), "Survey of road expenditure due to scour", Report CR 90.09, DSIR Hydrology Centre, Chirstchurch, New Zealand, 52pp

MATISSE (1998), "User Manual", MATISSE V1.0, TELEMAC Modelling System, SOGREAH Consultants, France

Malavasi S & Guadagnini A (2003), "Hydrodynamic loading on river bridges", *J. Hydr. Engrg.* ASCE, Vol. 129, Issue 11, pp 854-861

May RWP, Ackers JC & Kirby AM (2002), "Manual on scour at bridges and other hydraulic structures", CIRIA C551, London, UK

Mellor G, Häkkinen S, Ezer T & Patchen R (2002), "A Generalization of a sigma coordinate ocean model and an inter-comparison of model vertical grids", In *Ocean Forecasting: Conceptual Basis and Applications*, by Pinardi N & Woods J (Eds.), Springer, Berlin, pp 55-72

Melville BW (1975), "Local Scour at Bridge Sites", University of Auckland, School of Engineering, Auckland, New Zealand, Rep. No. 117

Melville BW & Sutherland AJ (1988), "Design method for local scour at bridge piers" *J. Hydr. Engrg.* ASCE, Vol. 114, Issue 10, pp 1210-1226

Melville BW & Raudkivi AJ (1996), "Effects of foundation geometry on bridge pier scour." *J. Hydr. Engrg.* ASCE, Vol. 122, Issue 4, pp 203-209

Melville BW (1997), "Pier and abutment scour: integrated approach." *J. Hydr. Engrg.* ASCE, Vol. 123, Issue 2, pp 125-136

Melville BW & Chiew YM (1999), "Time scale for local scour at bridge piers", *J. Hydr. Engrg.* ASCE, Vol. 125, Issue 1, pp 59-65

Melville BW & Coleman SE (2000), *Bridge Scour*, Water Resources Publications, LLC, Colorado, USA

Metcalf M & Reid J (1990), *FORTRAN 90 explained*, Oxford Science Publication, UK

Meyer-Peter PE & Muller R (1948), "Formulas for bed load transport" *Proc. 3rd International Association for Hydraulic Research*, Stockholm, Sweden, pp 39-64

Midgely M (2000), "Sediment movement around piers in open channel flow", BSc Thesis, the University of Cape Town, South Africa

Muzzammmil M & Gangadhariah T (2003), "The mean characteristics of horseshoe vortex at a cylindrical pier", *J. Hydr. Res.* IAHR, Vol. 41, No 3, pp 285-297

Nagagawa H. & Suzuki K (1975), "An Application of Stochastic Model of Sediment Motion to Local Scour Around a Bridge Pier." *Proceedings 16th International Association for Hydraulic Research Congress,* Sao Paulo, Brazil, Vol. 2, pp. 228-235.

Oliveto GH & Hager WH (2002), "Temporal evolution of clear-water pier and abutment scour." *J. Hydr. Engrg.* ASCE, Vol. 128, Issue 9, p811-820

Oliveto GH & Hager WH (2005), "Further results to time-dependent local scour at bridge elements" *J. Hydr. Engrg.* ASCE, Vol. 131, Issue 2, pp 97-106

Olsen NRB & Melaaen MC (1993), "Three dimensional calculation of scour around cylinders." *J. Hydr. Engrg.* ASCE, Vol. 119, No. 9, pp 1048-1054

Olsen NRB & Kjellesvig, HM (1998), "Three dimensional numerical flow modelling for estimation of maximum local scour depth." *J. Hydr. Res.*, Vol. 36, No. 4, pp 579-590

Olsen NRB (1999), "CFD in Hydraulic and Sedimentation engineering", Department of Hydraulic and Environmental Engineering, The Norwegian University of Science and Technology, Report Ref ISBN 82 7598-041-0

Pope SB (2000), *Turbulent Flows, Cambridge University Press*, Cambridge, UK

Przedwojski B, Blazejewski R & Pilarczyk KW (1995), *River training techniques fundamentals, design and applications,* A.A. Balkem, Rotterdam, Brookfield, Netherlands

Rajaratnam N (1976), Turbulent jets, Elsevier, 304pp – in Ahmed (1995)

Rastogi AK & Rodi W (1978), "Prediction of heat and mass transfer in open channels", *J. Hydr. Div.* ASCE, Issue HY3, pp 397-420

Raudkivi AJ & Sutherland AJ (1981), "Scour at bridge crossings", Road Research Unit Bulletin 54, National Roads Board, Wellington, New Zealand

Raudkivi AJ (1986), "Functional trends of scour at bridge piers", *J. Hydr. Engrg.* ASCE, Vol. 112, Issue 1, pp 1-13

Raudkivi AJ (1998), *Loose boundary hydraulics*, AA Balkema, Rotterdam, Netherland

Richardson, JE & Panchang, VG (1998), "Three-dimensional simulation of scour-inducing flow at bridge piers." *J. Hydr. Engrg. ASCE,* Vol. 124, Issue 5, pp 530-540

Richardson EV & Davis SR (2001), "Evaluating scour at bridges", Fourth Edition, HEC 18, US department of Transportation, USA

RUBENS (1998), "User Manual", RUBENS V4.1, TELEMAC Modelling System, SOGREAH Consultants, France

Saffman PG (1968), "The lift on a small sphere in a slow shear flow", *J. Fluid Mechanics*, Vol. 22, In Van Rijn (1993)

Salaheldin TM, Imran J & Chaudhry, MH (2004), "Numerical modelling of three-dimensional flow field around circular piers" *J. Hydr. Engrg.* ASCE, Vol. 130, Issue 2, pp 91-100

Schlichting H (1979), *Boundary layer theory*, 7th edition, McGraw-Hill

Shen HW, Schneider VR & Karaki SS (1969), "Local scour around bridge piers", *J. Hydr. Div.* ASCE, Vol. 95, Issue HY6, pp 1919-1940

Shields A (1936), "Application of similarity principles and turbulence research to bed load movement", California Institute of Technology, Pasadena (translated from German)

Shirhole AM & Holt RC (1991), "Planning for a comprehensive bridge safety program", Transportation Research Board 1290, National Research Council, Washington DC, USA, Vol. 1, pp 39-50

SIAM (2004), "New perspectives for spectral and high-order methods", Society for Industrial and Applied Mathematics, *SIAM News*, Vol. 37, No. 1

Simon BD & Richardson EV (1966), "Resistance to flow in alluvial channels" US Geology Survey Professional Paper 422-J

SISYPHE (2004), "User Manual" Sediment transport, SISYPHE V5.4, TELEMAC Modelling System, SOGREAH Consultants, France

Soulsby R (1997), *Dynamics of marine sand*, Thomas Thelford, In SISYPHE (2004)

Talapatra SC & Ghosh (1983), "Incipient motion criteria for flow over a mobile bed sill", Proceeding of the 2nd International Symposium on River Sedimentation, Nanjing, China

TELEMAC-3D (1998), "User Manual" TELEMAC-3D V2.2, TELEMAC Modelling System, SOGREAH Consultants, France

TELEMAC-2D (2001), "Principle note" TELEMAC-2D V3.0, TELEMAC Modelling System, SOGREAH Consultants, France

TELEMAC-2D (2002), "User Manual" TELEMAC-2D V5.2, TELEMAC Modelling System, SOGREAH Consultants, France

Unger J & Hager W (2005), "Spatial and temporal scour features of circular bridge piers", VAW ETH-Zentrum, CH-8092 Zurich, Switzerland – Unpublished

Van Rijn LC (1984a), "Sediment transport, Part I: Bed load transport", *J Hydr. Enggr. ASCE*, vol. 110, No. 10.

Van Rijn LC (1993), *Principles of sediment transport in rivers, estuaries and coastal seas*, Aqua Publications, Amsterdam, Netherlands

Vanoni VA (1975)-editor, *Sedimentation Engineering*, ASCE Press

Vanoni VA & Nomicos GN (1959), "Resistance properties of sediment-laden streams", *J. Hydr. Div.* ASCE, Vol. 85, Issue HY5, pp 77-107

Versteeg, HK & Malalasekera, W (1995), *An introduction to Computational Fluid Dynamics*, Addison Wesley Longman Limited, Harlow, Essex, UK

Wang SJ & Mujumdar AS (2005), "A comparative study of five low Reynolds number k–ε models for impingement heat transfer", *Applied Thermal Engineering*, Vol. 25, Issue 1, pp 31-44

White FM (1991), Viscous Fluid Flow, McGraw-Hill Book Co. Singapore

Wilcox DC (2000), *Turbulence modelling for CFD*, DCW Industries, California, USA

Yakhot V & Orszag SA (1986), "Renormalization Group Analysis of Turbulence: I. Basic Theory", *Journal of Scientific Computing*, Vol. 1, No. 1, pp1-51

Yalin MS & Da Silva AMF (2001), *Fluvial processes*, IAHR, Delft, Netherlands

Yang CT (1973), "Incipient motion and sediment transport" *J. Hydr. Div.* ASCE, Vol. 99, Issue HY10, pp 1679-1704

Yang CT & Song CCS (1979), "Theory of minimum rate of energy dissipation", *J. Hydr. Div.* ASCE, Vol. 105, Issue HY7, pp 769-784

Yang CT (1996), *Sediment transport: theory and practice*, McGraw-Hill Inc. New York, USA

Yanmaz, AM (2004), "A reliable model for bridge abutment scour", *Turkish J. Eng. Env. Sci.*, Vol.28, pp 67-83

Yen, CL, Lai, JS & Chang, WY (2001), "Modelling of 3D flow and scour around circular piers." *Proc. Natl. Sci. Counc.*, ROC(A), Vol.25, No. 1, pp 17-26

Young DF, Bruce RM & Theodore HO (1997), *A brief introduction to fluid mechanics*, John Wiley & Sons, Inc. New York

Zyserman JA & Fredsoe J (1994), "Data analysis of bed concentration of suspended sediment" *J. Hydr. Engrg.* ASCE, Vol. 120, Issue 9, pp 1021-1042

Appendix A

A typical FORTRAN Program

```
!                                      **********************
                                         SUBROUTINE CONDIM
!                                      **********************
     & ( AT )
!
!    Source     : SOGREAH Consultants, France
!    Edited for: Mesh refinement at bottom
!    Fonction:
!    Initialisation des tableaux des grandeurs physiques
!---------------------------------------------------------------------
!    Function:
!    Initialisation of velocity, depth and tracers
!---------------------------------------------------------------------
!    Sous-programme appele par : telemac-3d
!    Sous-programmes appeles : ov , (calcot)
     USE BIEF
     USE DECLARATIONS_TELEMAC
     USE DECLARATIONS_TELEMAC3D
     IMPLICIT NONE
     INTEGER LNG,LU
     COMMON/INFO/LNG,LU
!---------------------------------------------------------------------
     DOUBLE PRECISION, INTENT(OUT) :: AT
!---------------------------------------------------------------------
     INTEGER IPLAN, I,J
!    Time origin
     AT  = 0.D0
!    Initialisation of h, the water depth
     IF(.NOT.SUIT2) THEN
     IF(CDTINI(1:10).EQ.'COTE NULLE'.OR.
    *  CDTINI(1:14).EQ.'ZERO ELEVATION') THEN
      CALL OS( 'X=C     ' ,X=H,C=0.D0)
      CALL OV( 'X=X-Y   ' , H%R(1) , Z , Z , 0.D0 , NPOIN2 )
     ELSEIF(CDTINI(1:14).EQ.'COTE CONSTANTE'.OR.
    *      CDTINI(1:18).EQ.'CONSTANT ELEVATION') THEN
      CALL OS( 'X=C     ' ,X=H,C=COTINI)
      CALL OV( 'X=X-Y   ' , H%R(1) , Z , Z , 0.D0 , NPOIN2 )
     ELSEIF(CDTINI(1:13).EQ.'HAUTEUR NULLE'.OR.
    *      CDTINI(1:10).EQ.'ZERO DEPTH') THEN
      CALL OS( 'X=C     ' ,X=H,C=0.D0)
```

```
      ELSEIF(CDTINI(1:17).EQ.'HAUTEUR CONSTANTE'.OR.
     *       CDTINI(1:14).EQ.'CONSTANT DEPTH') THEN
        CALL OS( 'X=C     ' ,X=H,C=HAUTIN)
      ELSEIF(CDTINI(1:13).EQ.'PARTICULIERES'.OR.
     *       CDTINI(1:10).EQ.'PARTICULAR'.OR.
     *       CDTINI(1:07).EQ.'SPECIAL') THEN
!     Zone a modifier
!     For special initial conditions on depth, program here
        IF(LNG.EQ.1) WRITE(LU,10)
        IF(LNG.EQ.2) WRITE(LU,11)
10      FORMAT(1X,'CONDIM : AVEC DES CONDITIONS INITIALES PARTICULIERES'
     *       ,/,1X,'        VOUS DEVEZ MODIFIER CONDIM')
11      FORMAT(1X,'CONDIM : WITH SPECIAL INITIAL CONDITIONS'
     *       ,/,1X,'        YOU HAVE TO MODIFY CONDIM')
        CALL PLANTE(1)
        STOP
!     End of special initial conditions
!     Fin de la zone a modifier
      ELSE
        IF(LNG.EQ.1) THEN
        WRITE(LU,*) 'CONDIM : CONDITION INITIALE NON PREVUE : ',CDTINI
        ENDIF
        IF(LNG.EQ.2) THEN
        WRITE(LU,*) 'CONDIM: INITIAL CONDITION UNKNOWN: ',CDTINI
        ENDIF
        STOP
      ENDIF
      ELSE
        IF(LNG.EQ.1) WRITE(LU,*) 'HAUTEUR LUE DANS LE FICHIER BINAIRE 1'
        IF(LNG.EQ.2) WRITE(LU,*) 'DEPTH IS READ IN THE BINARY FILE 1'
      ENDIF
!     Clipping of h
      DO I=1,NPOIN2
        H%R(I)=MAX(H%R(I),HMIN)
      ENDDO
      CALL OS ('X=Y     ',X=HN,Y=H)
!     Initialisation of the reference plane for double sigma
!     Transformation
!     Default action below, based of plane number.
      IF(NPLINT.GE.2) THEN
        CALL OV( 'X=C     ' , Z((NPLINT-1)*NPOIN2+1 : NPLINT*NPOIN2),
     *           Z, Z, COTINT , NPOIN2)
      ENDIF
!     Initialisation of zstar, vertical coordinate
```

```
!   In sigma transformation
!   Case without reference plane
!   One must have :
!       * ZSTAR%R(1)    = 0.D0 ( BOTTOM PLANE )
!       * ZSTAR%R(NPLAN) = 1.D0 ( FREE SURFACE PLANE )
!       AND FOR ALL I BETWEEN 1 AND NPLAN-1
!       * ZSTAR%R(I) < ZSTAR%R(I+1)
!   Case with reference plane
!   One must have :
!       * ZSTAR%R(1)     = -1.D0 ( BOTTOM PLANE )
!       * ZSTAR%R(NPLINT) =  0.D0 ( REFERENCE PLANE )
!       * ZSTAR%R(NPLAN)  =  1.D0 ( FREE SURFACE PLANE )
!       AND FOR ALL I BETWEEN 1 AND NPLAN-1
!       * ZSTAR%R(I) < ZSTAR%R(I+1)
!   Standard is: evenly spaced planes
!   If no reference plane : nplint = 1
!   Transf is key-word "mesh transformation"
    IF(TRANSF.EQ.2) THEN
     WRITE(LU,*)
     IF(LNG.EQ.1) THEN
      WRITE(LU,*) 'AVEC TRANSFORMATION DU MAILLAGE = 2'
      WRITE(LU,*) 'DONNER DANS CONDIM LES VALEURS DE ZSTAR'
     ENDIF
     IF(LNG.EQ.2) THEN
              ZSTAR%R(1)=0.0
              ZSTAR%R(2)=0.05
              ZSTAR%R(3)=0.1
              ZSTAR%R(4)=0.2
              ZSTAR%R(5)=0.3
              ZSTAR%R(6)=0.47
              ZSTAR%R(7)=0.63
              ZSTAR%R(8)=0.8
              ZSTAR%R(9)=0.9
              ZSTAR%R(10)=1.0
      WRITE(LU,*) 'WITH MESH TRANSFORMATION = 2'
      WRITE(LU,*) 'GIVE THE VALUES OF ZSTAR IN CONDIM'
    ENDIF
!    Example with 3 planes
!    ZSTAR%R(1)=0.D0
!    ZSTAR%R(2)=0.3D0
!    ZSTAR%R(3)=1.D0
    ELSEIF(TRANSF.EQ.3) THEN
     IF(NPLINT.GE.2) THEN
      DO IPLAN = 1,NPLINT-1
```

```
        ZSTAR%R(IPLAN) = DBLE(IPLAN-NPLINT)/DBLE(NPLINT-1)
       ENDDO
      ENDIF
      DO IPLAN = NPLINT,NPLAN
       ZSTAR%R(IPLAN) = DBLE(IPLAN-NPLINT)/DBLE(NPLAN-NPLINT)
      ENDDO
     ELSEIF(TRANSF.EQ.4) THEN
      WRITE(LU,*)
      IF(LNG.EQ.1) THEN
       WRITE(LU,*) 'AVEC TRANSFORMATION DU MAILLAGE = 4'
       WRITE(LU,*) 'DONNER DANS CONDIM LES VALEURS DE ZSTAR'
       WRITE(LU,*) 'COTES REELLES SOOUHAITEES DES PLANS'
      ENDIF
      IF(LNG.EQ.2) THEN
       WRITE(LU,*) 'WITH MESH TRANSFORMATION = 4'
       WRITE(LU,*) 'GIVE THE VALUES OF ZSTAR IN CONDIM'
       WRITE(LU,*) 'REAL ELEVATION OF PLANES'
      ENDIF
      WRITE(LU,*)
      CALL PLANTE(1)
      STOP
!     Example with 4 planes
!     ZSTAR%R(1)=-10.D0
!     ZSTAR%R(2)=-9.D0
!     ZSTAR%R(3)=-8.D0
!     ZSTAR%R(4)=-7.D0
     ELSE
!     Sigma transformation and other cases
      DO IPLAN = 1,NPLAN
       ZSTAR%R(IPLAN) = DBLE(IPLAN-1)/DBLE(NPLAN-1)
      ENDDO
     ENDIF
!    Computation of elevations
!    If it is a continuation, will be done after calling 'suite'
     IF(DEBU) CALL CALCOT(Z,H%R(1))
!    Initialisation of velocities
     IF(SUIT2) THEN
      DO I=1,NPLAN
       DO J=1,NPOIN2
        U%R((I-1)*NPOIN2+J)=U2D%R(J)
        V%R((I-1)*NPOIN2+J)=V2D%R(J)
       ENDDO
      ENDDO
     ELSE
```

```
      CALL OS( 'X=C     ' , X=U , C=0.D0 )
      CALL OS( 'X=C     ' , X=V , C=0.D0 )
    ENDIF
    CALL OS( 'X=C     ' , X=W , C=0.D0 )
!   Tracers initialization
    IF(NTRAC.GT.0) THEN
     DO I=1,NTRAC
      CALL OS( 'X=C     ', X=TA%ADR(I)%P, C=TRAC0(I))
     ENDDO
    ENDIF
!  Initialisation du modele k-epsilon (facultatif)
!  Si vous le faites, indiquez akep = .false.
    AKEP=.TRUE.
!   IF(ITURBV.EQ.3) THEN
!     HERE INITIALISE K AND EPSILON
!     AKEP = .FALSE.
!   ENDIF
! Initialize the hydrodynamic pressure field to 0.0
! (projection2: it may be appropriate to solve a poisson equation for dp
    IF(NONHYD) THEN
     CALL OS('X=C     ',X=DP,C=0.D0)
       WRITE (LU,*) 'CONDIM: DYNAMIC PRESSURE INITIALISED TO ZERO'
     CALL PHSTAT
   *      (PH%R(1),DELTAR%R(1),Z, T3_01%R(1), T3_02%R(1), RHO0, GRAV,
   *                NPOIN3, NPOIN2, NPLAN, PRIVE )
!!!      WRITE (LU,*) 'CONDIM: HYDROSTATIC PRESSURE INITIALISED.'
    ENDIF
    RETURN
    END
```

Appendix B

Typical parameter files

/ TELEMAC-2D: Hydrodynamic parameter file

```
/*************************************************************************************
/ TELEMAC-2D Version 5.5 - 2005
/ Model T2D4 run – developed by Alamgir Kabir
/ Two-dimensional (2D) flow field
/*************************************************************************************
/Files
BOUNDARY CONDITIONS FILE  : './cli1b'
GEOMETRY FILE             : './geo1b'
LIQUID BOUNDARIES FILE    : './liquide1b.txt'
RESULTS FILE              : './resu2d1t.slf'
/*************************************************************************************
/ Internal coupling with SISYPHE
COUPLING WITH             : 'INTER-SISYPHE'
COUPLING PERIOD           : 1.
SISYPHE STEERING FILE  : './cas2d1s.txt'
/*************************************************************************************
/Tilte of the Project
TITLE : 'TELEMAC-2D - AhmedAM3-Kabir'
/ Run Time and Variable Print Out
VARIABLES FOR GRAPHIC PRINTOUTS  : 'U,V,M,S,B,H,Q,F,K,E'
TIME STEP                        : 1.
MASS-BALANCE                     : YES
DURATION                         : 799200
GRAPHIC PRINTOUT PERIOD          : 3600
LISTING PRINTOUT PERIOD          : 1800
/*************************************************************************************
/Initial conditions
INITIAL CONDITIONS     : 'CONSTANT ELEVATION'
INITIAL ELEVATION      :  1.82
/*************************************************************************************
/Bottom Friction
LAW OF BOTTOM FRICTION   :  2
FRICTION COEFFICIENT     :  50.
/Initial Downstream & Upstream Condition
PRESCRIBED ELEVATIONS    :  1.82;0
PRESCRIBED FLOWRATES     :  0;15.81
VELOCITY PROFILES        :  4
/*************************************************************************************
/General Numerical Parameter
```

```
EQUATIONS                          : 'SAINT-VENANT EF'
DISCRETIZATIONS IN SPACE           : 11;11;11;11
ADVECTION                          : YES
ADVECTION OF H                     : YES
ADVECTION OF U AND V               : YES
ADVECTION OF K AND EPSILON         : YES
PROPAGATION                        : YES
DIFFUSION OF VELOCITY              : YES
/Numerical Schemes
TYPE OF ADVECTION                                    : 1;5;1;1
NUMBER OF SUB-ITERATIONS FOR NON-LINEARITIES : 1
SUPG OPTION                                          : 2
IMPLICITATION FOR DEPTH                        : 1.0
IMPLICITATION FOR VELOCITY                     : 1.0
IMPLICITATION FOR DIFFUSION OF VELOCITY    : 1.0
MASS-LUMPING ON H                  : 1
MASS-LUMPING ON VELOCITY           : 1
/Solving the Linear System
TREATMENT OF THE LINEAR SYSTEM     : 2
SOLVER                                         : 7
SOLVER OPTION                                  : 3
SOLVER ACCURACY                                : 1.E-5
OPTION FOR THE DIFFUSION OF VELOCITIES     : 2
TURBULENCE MODEL                                 : 3
TURBULENCE MODEL FOR SOLID BOUNDARIES      : 1
SOLVER FOR K-EPSILON MODEL                     : 7
OPTION FOR THE SOLVER FOR K-EPSILON MODEL  : 3
ACCURACY OF EPSILON                            : 1.E-6
ACCURACY OF K                                  : 1.E-6
/PRECONDITIONING FOR K-EPSILON MODEL           : 2
VELOCITY DIFFUSIVITY                           : 1.E-6
MAXIMUM NUMBER OF ITERATIONS FOR K AND EPSILON     : 200
MAXIMUM NUMBER OF ITERATIONS FOR SOLVER            : 300
INFORMATION ABOUT SOLVER           : YES
INFORMATION ABOUT K-EPSILON MODEL  : YES
/Other Parameters
MATRIX STORAGE     : 3
/
&FIN
```

/TELEMAC-3D hydrodynamic model parameter file

```
/*************************************************************************
/TELEMAC-3D Version 5.5 - 2005
/Model T3D1 run – developed by Alamgir Kabir
/Three-dimensional (3D) flow field
/*************************************************************************
/Input-output files
GEOMETRY FILE                    = './geo1a'
BOUNDARY CONDITIONS FILE         = './cli1a'
LIQUID BOUNDARIES FILE           = './liquide1a.txt'
FORTRAN FILE                     = './princi3d.f'
NUMBER OF HORIZONTAL LEVELS      = 10
3D RESULT FILE                   = './cas1aout3D.slf'
VARIABLES FOR 3D GRAPHIC PRINTOUTS = 'U,V,W,K,E,Z'
2D RESULT FILE                   = './cas1aout2D.slf'
VARIABLES FOR 2D GRAPHIC PRINTOUTS = 'U,V,M,H,S,B,F,US,EF'
MASS-BALANCE                                                    = YES
INFORMATION ABOUT MASS-BALANCE FOR EACH LISTING PRINTOUT = YES
TITLE = 'SISYPHE & TELEMAC-3D coupling verifying Ahmeds model'
TIME STEP                        = 0.1
NUMBER OF TIME STEPS             = 180000
GRAPHIC PRINTOUT PERIOD          = 600
LISTING PRINTOUT PERIOD          = 300
RATIO OF 3D AND 2D TIME STEPS    = 10
/*************************************************************************
/Internal coupling with sisyphe
COUPLING WITH                    = 'INTER-SISYPHE'
SISYPHE STEERING FILE            = './cas1as.txt'
/*************************************************************************
/***Initial conditions***
INITIAL CONDITIONS   = 'CONSTANT DEPTH'
INITIAL DEPTH        = 1.82
/***Downstream & Upstream Condition***
PRESCRIBED ELEVATIONS    = 1.82;0
PRESCRIBED FLOWRATES     = 0;15.81
/*************************************************************************
/Physical parameters
/Water
DENSITY FOR STANDARD VALUE   = 1000
GRAVITY ACCELERATION         = 9.81
MINIMAL VALUE FOR DEPTH      = 1.E-2
/Sediment
CONSTANT SEDIMENT SETTLING VELOCITY  = 0.1
DENSITY LAW                          = 0
```

```
DENSITY OF THE SEDIMENT                    = 2650.0
MEAN DIAMETER OF THE SEDIMENT              = 0.00088
/Friction
LAW OF BOTTOM FRICTION                     = 2
FRICTION COEFFICIENT FOR THE BOTTOM        = 50.
/*************************************************************************
/Numerical options
/Transport terms
PROPAGATION STEP    = YES
ADVECTION STEP      = YES
DIFFUSION STEP      = YES
/Pressure term
NON-HYDROSTATIC VERSION                    = YES
HYDROSTATIC INCONSISTENCY FILTER           = YES
OPTION FOR THE HYDROSTATIC STEP            = 1
/Scheme for advection
SCHEME FOR ADVECTION OF DEPTH              = 5
SCHEME FOR ADVECTION OF VELOCITIES         = 1
SCHEME FOR ADVECTION OF K-EPSILON          = 1
/Scheme for diffusion
SCHEME FOR DIFFUSION OF VELOCITIES         = 1
SCHEME FOR DIFFUSION OF K-EPSILON          = 1
IMPLICITATION FOR DEPTH                    = 0.55
IMPLICITATION FOR DIFFUSION                = 1.0
IMPLICITATION FOR VELOCITIES               = 1.0
/Solver
SOLVER FOR PROPAGATION                     = 3
SOLVER FOR VERTICAL VELOCITY               = 3
SOLVER FOR DIFFUSION OF K-EPSILON          = 3
SOLVER FOR DIFFUSION OF VELOCITIES         = 3
SOLVER FOR PPE                             = 5
SOLVER FOR PROJECTION                      = 5
/Preconditioning
PRECONDITIONING FOR PROPAGATION            = 2
PRECONDITIONING FOR VERTICAL VELOCITY      = 2
PRECONDITIONING FOR DIFFUSION OF K-EPSILON = 7
PRECONDITIONING FOR DIFFUSION OF VELOCITIES = 7
PRECONDITIONING FOR PPE                    = 7
PRECONDITIONING FOR PROJECTION             = 7
/
MASS-LUMPING FOR DEPTH          = 1
MASS-LUMPING FOR VELOCITIES     = 1
/Solver accuracy
ACCURACY FOR DIFFUSION OF K-EPSILON        = 1.E-6
```

```
ACCURACY FOR DIFFUSION OF VELOCITIES    = 1.E-5
ACCURACY FOR PPE                        = 1.E-4
ACCURACY FOR PROJECTION                 = 1.E-6
ACCURACY FOR PROPAGATION                = 1.E-6
ACCURACY FOR VERTICAL VELOCITY          = 1.E-6
/Iterations
MAXIMUM NUMBER OF ITERATIONS FOR PROPAGATION                    = 400
MAXIMUM NUMBER OF ITERATIONS FOR VERTICAL VELOCITY              = 200
MAXIMUM NUMBER OF ITERATIONS FOR DIFFUSION OF K-EPSILON         = 200
MAXIMUM NUMBER OF ITERATIONS FOR DIFFUSION OF VELOCITIES        = 200
MAXIMUM NUMBER OF ITERATIONS FOR PPE                            = 200
MAXIMUM NUMBER OF ITERATIONS FOR PROJECTION                     = 200
NUMBER OF SUB ITERATIONS FOR NON LINEARITIES                    = 1
/Different coefficients
COEFFICIENT FOR VERTICAL DIFFUSION OF VELOCITIES        = 1.E-6
COEFFICIENT FOR HORIZONTAL DIFFUSION OF VELOCITIES      = 1.E-4
/Turbulence model
HORIZONTAL TURBULENCE MODEL                             = 3
VERTICAL TURBULENCE MODEL                               = 3
TURBULENCE MODEL FOR THE BOTTOM                         = 2
TURBULENCE MODEL FOR LATERAL SOLID BOUNDARIES           = 1
INFLUENCE OF TURBULENCE ON SETTLING VELOCITY            = YES
/Matrix
MATRIX STORAGE                  = 1
/Other options
INITIAL GUESS FOR DEPTH         = 1
CONSISTENT PROJECTION           = YES
MESH TRANSFORMATION             = 1
/
&FIN
```

/SISYPHE: Sediment transport parameter file

```
/*************************************************************************************
/SISYPHE Version 5.5 - 2005
/Model T2D4 run – developed by Alamgir Kabir
/Bottom evolution of the channel bed
/*************************************************************************************
/Input-output files
GEOMETRY FILE                 : './geo1b'
BOUNDARY CONDITIONS FILE  : './cli1b'
RESULTS FILE                  : './resu1bs.slf'
/*************************************************************************************
/Time & output
TITLE : 'AhmedA3M-Kabir'
VARIABLES FOR GRAPHIC PRINTOUTS   = 'U,V,S,B,E,F,H,M,N,P'
MASS-BALANCE                      = YES
TIME STEP                         = 1.
NUMBER OF TIME STEPS              = 799200
GRAPHIC PRINTOUT PERIOD           = 3600
LISTING PRINTOUT PERIOD           = 1800
/*************************************************************************************
/Morphodynamic Model
BED LOAD                                  = YES
BED-LOAD TRANSPORT FORMULA                = 7
COEFFICIENT FUNCTION OF THE POROSITY      = 1.4
/Sediment and Fluid Properties
MEAN DIAMETER OF THE SEDIMENT     = 0.00088
D90                               = 0.0033
SEDIMENT DENSITY                  = 2650.
WATER DENSITY                     = 1000.
WATER VISCOSITY                   = 1.E-6
SETTLING VELOCITIES               = 0.1
/Channel Bed parameters
LAW OF BOTTOM FRICTION      = 2
FRICTION COEFFICIENT        = 50.
SHIELDS PARAMETER           = 0.029
BETA                        = 1.3
/Erosion & Deposition fluxes
FORMULATION FOR DEPOSITION AND EROSION = 2
OPTION FOR THE DISPERSION              = 1
DISPERSION ALONG THE FLOW              = 1.E-3
DISPERSION ACROSS THE FLOW             = 1.E-3
/*************************************************************************************
/For the suspension solid
SUSPENSION                                = YES
```

```
SOLVER FOR SUSPENSION                    = 7
SOLVER OPTION FOR SUSPENSION             = 3
SOLVER ACCURACY FOR SUSPENSION           = 1.E-8
MAXIMUM NUMBER OF ITERATIONS FOR SOLVER FOR SUSPENSION = 50
TETA SUSPENSION                          = 0.5
PRECONDITIONING FOR SUSPENSION           = 2
/*************************************************************************************
/Numerical options
TYPE OF ADVECTION          = 2
TETA                       = 0.5
SUPG OPTION                = 2
MASS-LUMPING               = YES
MATRIX STORAGE             = 3
STEADY CASE                = YES
NUMBER OF SUB-ITERATIONS   = 5
SOLVER                     = 7
SOLVER OPTION              = 3
SOLVER ACCURACY            = 1.E-5
CRITICAL EVOLUTION RATIO   = 10.0
/
&FIN
```

Appendix C

Available CFD codes that could be used to solve scour and deposition around a circular pier

The data given in Appendix C was obtained by the authors from the relevant suppliers and/or their websites and refer to the situation as at September 2004.

C.1: Delft3D

Main Module	:	FLOW (Hydrodynamic), SED (Sediment transport), MOR (Morphology) and WAVE (Waves)
Supplier	:	Delft Hydraulics, Netherlands
Initial price	:	Typical package (FLOW, SED, MOR and WAVE with pre- and post-processing QUICKIN, RGFGRID and GPP) is EUR 6,500 for the university. Commercial price varies; however, typical package is approximately EUR 13,000.
Annual license fees	:	EUR 3,250 for the university including the online helpdesk, bug fixing and the version updates
Computer platform	:	Both UNIX (HP, SGI & SUN), Windows (95, 98, 2000, NT4) and LINUX. 1GHz CPU, 1GB RAM and 10GB free hard disk are preferable for Windows.
Code & Flexibility	:	Finite Difference or Finite Volume. Programming language FORTRAN 90, C/C^{++}, Not flexible to incorporate additional subroutine.
Support	:	Online technical and general supports are available in web http://www.wldelft.nl/soft/d3d/intro/index.html
Capabilities	:	Three coordinate systems (rectangular, curvilinear and spherical) In FLOW, Solves the Navier-Stokes equations for the shallow water approximation, Four turbulence model options: k-ε, k-L, algebraic and constant model, Advection-diffusion solver, Bed shear stress estimates using the quadratic Chezy, Manning or the White-Colebrook formulation In SED, deals the cohesive and the non-cohesive sediments separately, uses embedded existing sediment transport formulae i.e. Engelund & Hansen (1967), deals with erosion & deposition, critical shear stress, particle fractions, hindered settling, burial & digging, etc. In MOR, uses quasi-three dimensional approach, bed-load and equilibrium suspended load, bed slope effect, etc.
Main user	:	Universities, Consultants, public and private organisations

C.2: MIKE 3

Main Module	:	HD (Hydrodynamic), MT (Sediment transport), AD (Advection-dispersion)
Supplier	:	Danish Hydraulic Institute (DHI), Denmark
Initial price	:	Typical package MIKE 3 ELP (HD, MT and AD) with pre- and post-processing PP is EUR 13,900 for the university (maximum 10,000 number water points). Commercial price varies; however, typical package is approximately EUR 37,500 for multiple grids.
Annual license fees	:	10% of the initial price for the university including the online helpdesk, bug fixing and the version updates
Computer platform	:	Windows (95, 98, 2000, NT4), 500MHz P IV CPU, 256MB RAM and 20GB free hard disk are minimum requirement.
Code & Flexibility	:	Finite Difference. Programming language FORTRAN 90, C/C^{++}, Not flexible to incorporate additional subroutine.
Support	:	Online technical and general supports are available in web http://dhisoftware.com/mike3/support/
Capabilities	:	In HD, Solves the Reynolds-averaged Navier-Stokes equations to decompose the flow in mean and turbulent fluctuation, Five available turbulence model: constant eddy viscosity, Smagorinsky subgrid scale, *k*, *k*-ε, and mixed Smagorinsky/*k*-ε, Advection-diffusion solver In SED, deals the cohesive and non-cohesive sediments using multi-fraction and multi-layer mode, uses the embedded existing sediment transport formulae i.e. Van Rijn (1984), deals erosion & deposition, critical shear stress with liquefaction, particle fractions, hindered settling, burial & digging, etc.
Main user	:	Universities, Consultants, public and private organisations

C.3: FLUENT

Main Module	:	FLUENT 6 (General purpose)
Supplier	:	Fluent Europe Ltd., UK
Initial price	:	A wide variety of pricing structures ranging from one stand-alone license to a multiple network license with a special discount for the academic institutions.
Annual license fees	:	The initial and annual license fees are same
Computer platform	:	UNIX (HP, SUN, LINUX, IBM, SGI), Windows (2000, NT, XP), 500MHz P IV CPU, 512 MB RAM and 20GB free hard disk are minimum requirement.
Code & Flexibility	:	Finite Volume. Programming language C^{++}, Flexible to incorporate additional subroutine.
Support	:	Online technical and general supports are available in web http://www.fluent.com/worldwide/europe/about/index.htm
Capabilities	:	The complete mesh flexibility with the solution-based mesh adaptation, the dynamic mesh capability for modelling the flow around the moving bodies, parallel computing option for solving the complicated problems more quickly with unstructured mesh Solves the Navier-Stokes equations with wide range of turbulence model i.e. three variety of k-ε, second order closure Reynolds Stress (RSM), and large eddy simulation (LES) Special free surface treatment algorithm i.e. volume of fluid (VOF), Eulerian and mixture multiphase algorithm.
Main user	:	Diverse, University of Cape Town extensively uses FLUENT

C.4: CFX

Main Module	:	CFX 5 (General purpose)
Supplier	:	AEA Technology, UK
Initial price	:	A wide variety of pricing structures ranging from one stand-alone license to a multiple network license with a special discount for the academic institutions.
Annual license fees	:	The initial and annual license fees are almost same
Computer platform	:	UNIX (HP, SUN, LINUX, IBM, SGI), Windows (2000, NT, XP)
Code & Flexibility	:	Finite Volume. Programming language FORTRAN, Highly flexible to incorporate additional subroutine.
Support	:	Online technical and general supports are available in web http://www.ansys.com/products
Capabilities	:	Generates unstructured meshing, solution on any mixture of tetrahedral, hexahedral, prism and/or pyramid elements, generalised grid interface, import and connect multiple meshes from independent sources, Solution-based mesh adoption, moving and deforming mesh, mesh morphing from prescribed surface or volume movement, explicit volume mesh movement via user FORTRAN Solves the Navier-Stokes equations with wide range of turbulence model i.e. variety of k-ε, k-ω, RSM, detached eddy simulation (DES) and large eddy simulation (LES) Free Surface modelling includes compressive discretisation, homogenous or inter-phase transfer models and surface tension.
Main user	:	Diverse

C.5: Flo++

Main Module	:	Flo++ V3.08 (General purpose)
Supplier	:	Softflow cc, South Africa
Initial price	:	R 12,100 for the universities and the commercial price is almost double.
Annual license fees	:	The initial and annual license fees are same
Computer platform	:	Windows (2000, NT, XP), P IV CPU, 256 MB RAM and 65 MB free hard disk
Code & Flexibility	:	Finite Volume. Programming language C^{++}, Highly flexible to incorporate additional subroutine.
Support	:	Online technical and general supports are available in web http://www.softflo.com
Capabilities	:	Global and local Cartesian and cylindrical co-ordinate systems, manual or automatic creation of vertices, cells and boundary cells using the hexahedral or the prism cells, multi-dimensional interpolation routines for grid points, unstructured local mesh refinement and embedding to locally enhance the accuracy of solutions, arbitrary mesh coupling, couple any two meshes by simply projecting one surface onto the other. It can also generate moving meshes. Solves the Navier-Stokes equations for the incompressible to highly compressible transonic, steady and unsteady flow. Two-fluid with the free surface capability but lacks a proper surface tension model.
Main user	:	SASOL, DENEL (South Africa)

C.6: Flow-3D

Main Module	:	Flow-3D (General purpose)
Supplier	:	Flow Science Inc., USA
Initial price	:	US$ 11,000 for the universities and the commercial price is almost four times.
Annual license fees	:	The initial and annual license fees are same
Computer platform	:	Windows (2000, NT, XP), P IV 1GH CPU, 512 MB RAM and 100 MB free hard disk
Code & Flexibility	:	Finite Volume. Programming language FORTRAN and C^{++}, Highly flexible to incorporate additional subroutine.
Support	:	Online technical and general supports are available in web http://www.flow3d.com
Capabilities	:	Structured finite difference grid, multi-block girding with the embedded and linked blocks Solves the Navier-Stokes equations with wide choice of turbulence model i.e. Prandtl mixing length, k-ε, large eddy simulation (LES) Free surface of complex flow field using the volume of fluid (VOF) or TruVOF methods.
Main user	:	Industry, university and research groups

C.7: TABS

Main Module	:	RMA 10 (Multi-dimensional hydrodynamic) and SED 2D (sediment transport)
Supplier	:	Boss International, USA
Initial price	:	Typical package (RMA 10 & SED 2D) is US$ 3,500 for the universities and commercial price is almost double.
Annual license fees	:	The initial and annual license fees are same
Computer platform	:	Windows (98, 2000, NT, XP), P IV 700 MH CPU, 128 MB RAM and 10 MB free hard disk
Code & Flexibility	:	Finite Element. Programming language FORTRAN, Not flexible to incorporate additional subroutine.
Support	:	Online technical and general supports are available in web http://www.bossintl.com
Capabilities	:	Unstructured mesh, a capacity to include one-dimensional, depth-averaged, laterally averaged and three-dimensional elements within a single mesh as appropriate. Solves the Navier-Stokes equations with the Reynolds stress form turbulence model.
Main user	:	San Francisco Bay (US), Galveston Bay (US), Sydney coastal waters and Illawarra (Australia) and Hong Kong coastal waters (China)

C.8: CCHE3D

Main Module	:	CCHE3D (hydrodynamic and sediment transport)
Supplier	:	National Centre for Computational Hydro-science and Engineering, The University of Mississippi
Initial price	:	US$ 4,000 for the universities and the commercial price is US$ 10,000
Annual license fees	:	The initial and annual license fees are same
Computer platform	:	UNIX, LINUX and Windows (98, 2000, NT, XP), P IV 700 MH CPU, 256 MB RAM and 10 MB free hard disk
Code & Flexibility	:	Mixed Finite Element and Finite Volume, so called Efficient Element Method, Programming language FORTRAN 90, Flexible to incorporate additional subroutine.
Support	:	Online technical and general supports are available in web http://ncche.olemiss.edu/
Capabilities	:	Basic cubic element with twenty-seven nodes. Both hydrostatic and dynamic pressure of the flow can be simulated depending on the nature of the problem. Staggered grid is used for the pressure solution. The velocity correction method is adopted to compute the dynamic pressure and enforce the mass conservation. Solves the Navier-Stokes equations with variety of turbulence model i.e. eddy viscosity, mixing length, k-ε. The kinematics equation for the free surface is solved for the free surface.
Main user	:	University and research organisation